Corrosion inhibition of steel in acidic media using bio-waste extract: Experimental and theoretical consideration

Thesis submitted in partial fulfilment of the requirements for the degree of

DOCTOR OF PHILOSOPHY

by

Abhradip Pal

(Roll No.: 146107038)

Department of Chemical Engineering

Indian Institute of Technology Guwahati

Guwahati–781039, Assam, India

January 2023

TH-3102_146107038

TH-3102_146107038

Corrosion inhibition of steel in acidic media using bio-waste extract: Experimental and theoretical consideration

Abhradip Pal

TH-3102_146107038

TH-3102_146107038

Dedicated
To
My Parents and Teachers

TH-3102_146107038

TH-3102_146107038

DEPARTMENT OF CHEMICAL ENGINEERING

INDIAN INSTITUTE OF TECHNOLOGY GUWAHATI

STATEMENT

I do hereby declare that the content embodied in this thesis entitled "**CORROSION INHIBITION OF STEEL IN ACIDIC MEDIA USING BIO-WASTE EXTRACT: EXPERIMENTAL AND THEORETICAL CONSIDERATION"** is the result of investigations carried out by me at Department of Chemical Engineering, Indian Institute of Technology Guwahati, Guwahati, India, under the guidance of Prof. Chandan Das. In keeping with the general practice of reporting scientific observations, due acknowledgements have been made wherever the work described is based on the findings of other investigators.

Date: Abhradip Pal

TH-3102_146107038

TH-3102_146107038

DEPARTMENT OF CHEMICAL ENGINEERING

INDIAN INSTITUTE OF TECHNOLOGY GUWAHATI

CERTIFICATE

This is to certify that the thesis entitled **"CORROSION INHIBITION OF STEEL IN ACIDIC MEDIA USING BIO-WASTE EXTRACT: EXPERIMENTAL AND THEORETICAL CONSIDERATION"** submitted by **Mr. Abhradip Pal (Roll No.: 146107038)**, a research scholar in the Department of Chemical Engineering, Indian Institute of Technology Guwahati, for the award of the degree of Doctor of Philosophy, is a record of the original research work carried out by him under my supervision and guidance. The thesis has fulfilled all requirements as per the regulations of the institute and in my opinion has reached the standard needed for submission. The work documented in this thesis have not been submitted to any other University or Institute for the award of any degree.

Prof. Chandan Das

Professor

Department of Chemical Engineering

Indian Institute of Technology Guwahati

Guwahati - 781039, Assam, India.

Date:

TH-3102_146107038

TH-3102_146107038

Acknowledgements

I consider myself blessed to have an incredible journey of Ph.D. at Indian Institute of Technology Guwahati (IIT Guwahati). This was all made possible by the guidance, motivation and love of a lot of people who hold immense value in my life.

First and foremost, I would like to express my deepest gratitude to my supervisor Professor Chandan Das, for his continuous support during my Ph.D. studies and research, for his patience and motivation, and for imparting his immense knowledge. Also, I would like to thank Prof. Das for giving me this golden opportunity to work in his laboratory and take care of all the facilities to carry out my research. His guidance helped me throughout the time of my research and my writing of this thesis. His suggestions, encouragement and support were crucial to the completion of my Ph.D. thesis. Without his precious support, it would not be possible to complete this research. I am grateful for his advice, great ideas and scientific discussions, which are part of this thesis. Being a part of the Water Treatment Lab is an invaluable learning experience for me both scientifically and personally. The tremendous support, valuable suggestions, and encouragement are the main factors behind shaping my thesis work.

I would also like to extend my gratitude to the members of my Doctoral Committee, Prof. Vaibhav V. Goud (Chairman), and Dr. Amit Kumar of the Department of Chemical Engineering, and Prof. Sukhomay Pal of the Department of Mechanical Engineering, for their valuable suggestions throughout this journey. Also, I want to extend my thanks to the members of the comprehensive examination committee, Prof. Saswati Chakraborty, Prof. Pranab K. Ghosh, and Dr. Amit Kumar, for their constructive evaluation. I want to thank the present and former Heads of the Department, Prof. Bishnupada Mandal, Prof. Anugrah Singh, and Prof. Kaustubha Mohanty other faculty members, for their support and guidance. Also, I want to thank the technical and non-technical staff of our department for helping me in numerous ways and making my life easy in the department. I would also like to express my gratitude to Prof. Animes Kr. Golder for supporting me in my research work. I want to

TH-3102_146107038

acknowledge the Department of Mechanical Engineering for providing the infrastructure needed for my research work. I would also like to acknowledge the Central Instrumentation Facility (CIF), IIT Guwahati, and Guwahati Biotech Park for providing high-end instruments to execute some of the experiments.

I earnestly thank my seniors, juniors, interns, and labmates—Dr. Sujoy Bose, Dr. Amit Baran Das, Dr. Arijit Das, Dr. Kibrom Alebel Gebru, Dr. Abhishek Shukla, Dr. Sushma Chakraborty, Dr. Kulbhushan Samal, Dr. Aritra Das, Mr. Gunolla Nagendra Prasad, Mr. Anil Kumar, Mr. Ajay Kumar Shakya, Mr. Bharat Bhushan, Mrs. Aswani K Viswanath, —for providing a collaborative research environment. I sincerely appreciate the help, guidance, and love received from all of them.

I want to thank all the individuals who supported me throughout my time at this institute and contributed significantly to the outcome of this dissertation; their time and effort are greatly appreciated. I am immensely thankful to all these people and others who have made my stay in Guwahati a memorable and enjoyable journey. I thank them all for being there for me always and for providing an amicable work environment.

I would like to give my special thanks to the team members of the group "১৩ পার্বণ Tero Parbon, IIT Guwahati", "LUBDHAK" (Bengali performing arts group), Advaya (PG cultural fest of IITG), which kept me active and happy in many ways during my stay in IITG.

My next thanks go to my alma mater, IIT Guwahati, which gave me an opportunity to embark on this delicate endeavour of learning with ample facilities and with an equally enchanting bounty of nature which I experienced throughout the Northeast of India. I am so overwhelmed by the beauty of this campus that I have no words to describe it.

Next, I would like to thank the funding agencies that provided me with the financial support to conduct my research. I am grateful to the Ministry of Education (formerly Ministry of Human Resource Development (MHRD) for the fellowship during my Ph.D. studies and North Eastern Electric Power Corporation Limited, India (grant numbers xCLESPNNEEO00673xxCD002) for fund support.

TH-3102_146107038

"Friendship is beyond all relations of flesh and blood, because it is less material."—John Evelyn

I have been very fortunate to have some great friends; they are more likely to be my family. I would love to thank Atanu, Mitali, Dibyajyoti, Anirban, Arunangshu, Ardhendu, Vinay, Rakhee, Anuma, Nibedita, Rajendra, Mandar Da, Tumpa di, Suman, Biplab, Niladri, Daisy, Shyam, Prince, Swagata, Shounak, Hamish, Swapnali mam for their support, care, and love.

Finally, and most importantly, I would like to remember my parents and family for their never-ending love, support, and patience. It is their numerous personal sacrifices that have enabled me to reach this juncture in life. Simple thanks is not enough to convey my deep respect and gratitude towards my family.

Thanks to the Lord, the Almighty, for showering Her/His/Its grace on me at every step.

Abhradip Pal

TH-3102_146107038

TH-3102_146107038

Abstract

Corrosion is a chemical process that happens when a material, most commonly a metal, interacts with its environment. Metal or metal alloys are oxidized and converted into oxides or hydroxides, which are more stable and are known as rust, during this process. Metal corrodes as a result of a sequence of electrochemical (oxidation and reduction) processes. Corrosion is caused by a variety of factors, including environmental factors. The presence of water determines the two fundamental types of corrosion: dry and wet. Wet rust is more dangerous and may be seen all around us. Corrosion causes industries to shut down, resulting in human and financial losses as well as physical destruction. According to estimations, corrosion has a negative impact on a nation's GDP of 2-4%. India loses between 5-7% of its GDP annually, a survey claims. One of the biggest problems facing the modern industry is the corrosion of metallic materials. The US incurs a $450 billion yearly expenditure due to metal corrosion. According to a forecast, employing the available knowledge and technology might cut down on 40% of corrosion-related costs. For economic and environmental reasons, the effects of corrosion are largely considered. It also has a negative impact on energy, materials, the environment, and human health.

However, there are approaches that exist to mitigate corrosion, like design improvement, change of materials, and change of potential, etc. The application of corrosion inhibitors is the most effective one. Both organic and inorganic inhibitors are widely used. But there is increased concern about the toxicity, biodegradability, and bioaccumulation of corrosion inhibitors discharged into the environment. As a result, the development of green corrosion inhibitors is attracting the interest of a wide range of industrialists and scientists. These inhibitors are biodegradable, free of heavy metals

TH-3102_146107038

and other hazardous substances, and cost-effective. Concurrently, the rising volume of agricultural and food waste from many sources has undoubtedly been a subject of worry. Thus, the valorization of various biomaterials and agricultural by-products or wastes and food wastes is drawing attention to improving the economic sustainability of agricultural companies since these by-products and wastes include numerous important bio-active substances with diverse uses.

Hence this thesis focuses on finding green corrosion inhibitors from various biowastes, such as solid waste from tea factories (food-industrial waste), purple rice bran (agro-byproduct), banana flower bract, and onion peel (kitchen waste). The corrosion inhibition efficiency was determined in acidic media (HCl and H_2SO_4) on boiler-quality steel. The main objectives were (a) Extraction and characterization of green corrosion inhibitors, (b) Electrochemical kinetic study of inhibitors using potentiodynamic polarization on boiler quality study in acidic media to find out their corrosion rate and corrosion current, (c) Study on inhibition mechanism using electrochemical impedance spectroscopy, (d) Adsorption kinetics to find the type of adsorption, (e) Theoretical studies of inhibitory molecules identified in the extract. The entire work of this thesis has been divided into four major chapters as follows:

(a) Corrosion inhibition by extract of solid waste from tea factory (industrial waste)

This chapter discusses the findings and analysis related to the utilization of solid waste from the tea industry as a source of an eco-friendly inhibitor." Liquid chromatography-mass spectroscopy was used to characterize the solid tea waste extract (STWE). After incorporating 500 mg L^{-1} of tea waste extract, the maximal inhibitory efficacy in terms of charge transfer resistance was determined to be 90%. The corrosion

TH-3102_146107038

current (i_{corr}) was found the minimum, 25.29 µA cm^{-2} at 500 mg L^{-1} of STWE. The charge-transfer resistance (R_{ct}) was found 89.72 Ωcm^{-2} and 923.40 Ωcm^{-2} in the absence and presence of 500 mg L^{-1} STWE, respectively. The corrosion current (i_{corr}) was found the minimum, 25.29 µA cm^{-2} at 500 mg L^{-1} of STWE. The formation of a protective barrier on the metal electrolyte interface mainly caused the inhibition. This barrier was formed by the adsorption of the phenolic compounds present in the STWE, which was confirmed by FESEM, EDX, and AFM study. Among the identified compounds, caffeine had a lower energy gap (ΔE) of 4.976 eV.

(b) Corrosion inhibition by extract of purple rice bran (agro by-product)

This chapter discusses the effectiveness of purple rice bran extract, an agricultural by-product rich in antioxidants, at inhibiting corrosion. HPLC was used to characterize the inhibitor after it was conventionally extracted from purple rice bran. This indicated the existence of two key substances called cyaniding-3-glucoside (C3G) and peonidin-3-glucoside (P3G). This purple rice bran extract (PRBE) was used to test its inhibitory efficacy as a green corrosion inhibitor on boiler quality (BQ) steel in 1 (M) HCl and 0.5 (M) H_2SO_4. In the presence of 200 mg L^{-1} of PRBE in HCl and H_2SO_4, the highest efficiency was 91.13% and 87.43%, respectively. After testing several adsorption isotherm models, the Langmuir isotherm was determined to be the best-fitting model, indicating both physical and chemical spontaneous adsorption of PRBE on the BQ surface. Both electrochemical and adsorption experiments revealed that the PRBE is a mixed-type inhibitor.

(c) Corrosion inhibition by extract of banana flower bract (kitchen waste)

This chapter describes the results and discussion of the corrosion inhibition efficacy of a kitchen waste, banana flower bract, which was utilized to minimize the corrosion of boiler grade (BQ) industrially used steel in HCl and H_2SO_4acidic

TH-3102_146107038

environments. By using the gravimetric method, potentiodynamic polarization method, and electrochemical impedance spectroscopy method at room temperature (25 ± 2° C), the anti-corrosive capabilities of banana flower bract extract (BBE) were evaluated. After adding a maximum concentration of 200 mg L^{-1}, the studies showed that banana bract extract (BBE) had maximum inhibitory efficiencies of 90.84 % (1 M HCl) and 90.61% (0.5 M H_2SO_4). The value of K_{ads} (30.74 L g^{-1} in HCl and 28.28 L g^{-1} in H_2SO_4) and $\Delta G°_{ads}$ (-25.62 kJ mol^{-1} in HCl and -25.41 kJ mol^{-1} in H_2SO_4) has also supported thermodynamic favorability of the adsorption. According to the density functional theory study, P3G has a smaller energy gap than C3G, which helps better adsorption and has a more significant inhibitory impact.

(d) Corrosion inhibition by extract of onion peel (kitchen waste)

The results of corrosion inhibition of boiler grade (BQ) steel by onion waste are addressed in this chapter. The extract from onion peel was characterized using LC-MS and the traditional extraction technique. The effectiveness of onion peel extract (OPE) as a green corrosion inhibitor was investigated. From the electrochemical impedance spectroscopy studies, the maximum inhibition efficiencies of 91.30% and 90.71 % were found at 200 mg L^{-1} in 1 (M) HCl and 0.5 (M) H_2SO_4, respectively. The charge-transfer resistance (R_{ct}) was found as 89.72 Ωcm^2 and 85.08 Ω cm^2 in 1 (M) HCl and 0.5 (M) H_2SO_4 media without incorporating inhibitor. Whereas with OPE (200 mg L^{-1}) R_{ct} was increased in both HCl (1031.80 Ωcm^2) and H_2SO_4 media (916.18 Ωcm^2). According to FESEM, EDX, and AFM experiments, the formation of a protective layer on the BQ steel by OPE greatly reduced the rate of corrosion. Quantum chemistry calculations found that quercetin had a lower energy gap in the aqueous phase than in the gaseous phase, resulting in more effective inhibitory action.

TH-3102_146107038

In summary, this Ph.D. thesis affirms that inexpensive, environmentally beneficial Bio-waste extracts can replace traditional, expensive, and harmful inhibitors because of their exceptional effectiveness in preventing steel corrosion in acidic conditions. The collected data are expected to be used as the basis for future studies into creating or discovering a new corrosion inhibitor that is both commercially and environmentally feasible.

भारतीय प्रौद्योगिकी संस्थान गुवाहाटी • Indian Institute of Technology Guwahati •

TH-3102_146107038

TH-3102_146107038

Table of Contents

TH-3102_146107038

TH-3102_146107038

TH-3102_146107038

TH-3102_146107038

TH-3102_146107038

TH-3102_146107038

List of Tables

TH-3102_146107038

TH-3102_146107038

List of Figures

TH-3102_146107038

TH-3102_146107038

TH-3102_146107038

TH-3102_146107038

TH-3102_146107038

TH-3102_146107038

Nomenclature

Abbreviation

Symbol	Abbreviation
AFM	Atomic force microscopy
BBE	Banana flower bract extract
CPE	Constant phase element
EDX	Energy Dispersive X-ray
EIS	Electrochemical impedance spectroscopy
FESEM	Field Emission Scanning Electron Microscopy
FMO	Frontier molecular orbital
HOMO	Highest occupied molecular orbital
LC-MS	Liquid chromatography-mass spectroscopy
LUMO	Lowest unoccupied molecular orbitals
OPE	Onion peel extract
PDP	Potentiodynamic polarization test
PRBE	Purple rice bran extract
STWE	Solid tea waste extract

Notations

Symbol	Nomenclature
A	Effective area (cm^2)
A	Electron affinity (eV)
b_a	Anodic slope (V $decade^{-1}$)
b_c	Cathodic slope (V $decade^{-1}$)
C_{dl}	Capacitance of the effective layer (µF cm^{-2})
Cr	Corrosion rate having a unit of (mmpy)
C_{water}	Concentration of water (g L^{-1})
E	Applied potential (V)
E_{corr}	Corrosion potential (V)

TH-3102_146107038

Symbol	Nomenclature
E_{HOMO}	Energy of the highest occupied molecular orbital (eV)
E_{LUMO}	Energy of the lowest unoccupied molecular orbitals (eV)
E_f	Fermi level
f^+	Fukui index for nucleophilic attack
f^-	Fukui index for electrophilic attack
f^2	Fukui index as dual descriptor
i	Measured current density (µA cm^{-2})
i_{corr}	Corrosion current density (µA cm^{-2})
i_{corr}^{o}	Corrosion current density in the absence of PRBE (µA cm^{-2})
i_{corr}^{in}	Corrosion current density in the presence of PRBE (µA cm^{-2})
I	Ionization potential (eV)
K_{ads}	Adsorption equilibrium constant (L g^{-1})
n	Phase shift
R	Universal gas constant (8.314 J mol^{-1} K^{-1})
R^2	Linear regression coefficient
R_S	Solution resistance (Ω cm^2)
R_{ct}	Charge-transfer resistance (Ω cm^2)
R_{ct}^{i}	Charge transfer resistance in the presence of PRBE (Ω cm^2)
R_{ct}^{0}	Charge transfer resistance in the absence of PRBE (Ω cm^2)
t	Exposure time (h)
W	Weight loss (g)
w_o	Weight loss of the BQ coupon in the absence of PRBE (g)
w_i	Weight loss of the BQ coupon in the presence of PRBE (g)
Y_0	Amplitude comparable to capacitance or modulus of CPE (µMho cm^{-2})
Z_{CPE}	Impedance of the CPE (Ω cm^2)
ΔG_{ads}°	Standard Gibbs free energy (kJ mol^{-1})
ΔN	Fraction of electron transferable from inhibitor to iron (eV)
ΔE	Energy gap between LUMO and HOMO (eV)
η	Global hardness (eV)
θ	Surface coverage
μ	Dipole moment

TH-3102_146107038

Symbol	Nomenclature
$\mu_{CR}\%$	Corrosion inhibition efficiency
$\mu_{R_{ct}}\%$	Inhibition efficiency calculated from R_{ct}^{in} and R_{ct}^{0}
$\mu_{P}\%$	Inhibition efficiency calculated from I_{corr}^{o} and I_{corr}^{in}
ρ	Density of the BQ (g cm^{-3})
σ	Softness (eV^{-1})
χ	Electronegativity (eV)
ω	Angular frequency (rad sec^{-1})

TH-3102_146107038

TH-3102_146107038

1

Introduction and literature review

TH-3102_146107038

TH-3102_146107038

Introduction and literature review

This chapter provides a quick overview of the conventional non eco-friedly corrosion inhibitor and the need for green corrosion inhibitors. Besides, The basic science and the mechanism of corrosion phenomena are discussed along with its types. The current scenario on the adversity of corrosion globally are depicted. State-of-the-art focuses on some recent advances and experimental efforts to overcome corrosion. Some recent efforts on use of natural extracts as corrosion inhibitors are also mentioned. Following that, the issue of rising bio-waste from different agro-food sectors, which gave the research direction are elaborated. Finally, the goals and structure of the thesis are summarised.

TH-3102_146107038

1.1 Background study

1.1.1 Definition of corrosion

Corrosion is a chemical reaction that occurs between a substance, most often a metal, and its surroundings. The environment is comprised of anything in the vicinity of the substance that comes into touch with it. The term corrosion comes from the Latin word "*corrosus*" which literally translates as to be consumed or eaten away. Corrosion may be characterized in a variety of ways, some of which are quite restrictive and specialized to a particular kind of corrosion. Generally speaking, corrosion is the degradation of a metal that occurs as a result of interaction between metal and the surrounding environment. For example, marine corrosion of pier pilings refers to the fact that the steel piling corrodes as a result of its reactivity with the surrounding environment. It is impossible to characterize the corrosion behavior of a material unless the environment to which the substance is exposed has been recognized beforehand. It is helpful to distinguish between natural and unnatural combinations in the corrosion process.

In this process, metal or metal alloys are oxidized and transformed into oxides or hydroxides, which are more stable and known as rust. During the corrosion process, metal goes through a series of electrochemical (oxidation and reduction) reactions and eventually deteriorates. In oxidation, the metal loses electrons, and in reduction, surrounding oxidants gain those electrons. These two reactions (redox) occur simultaneously in the corrosion process (Fig. 1.1**).** The area of the metal where the oxidation occurs is called the anodic area, and the metal and gas or liquid, wherever electrons are gained, is called the cathodic area as shown in Fig. 1.1**.**

TH-3102_146107038

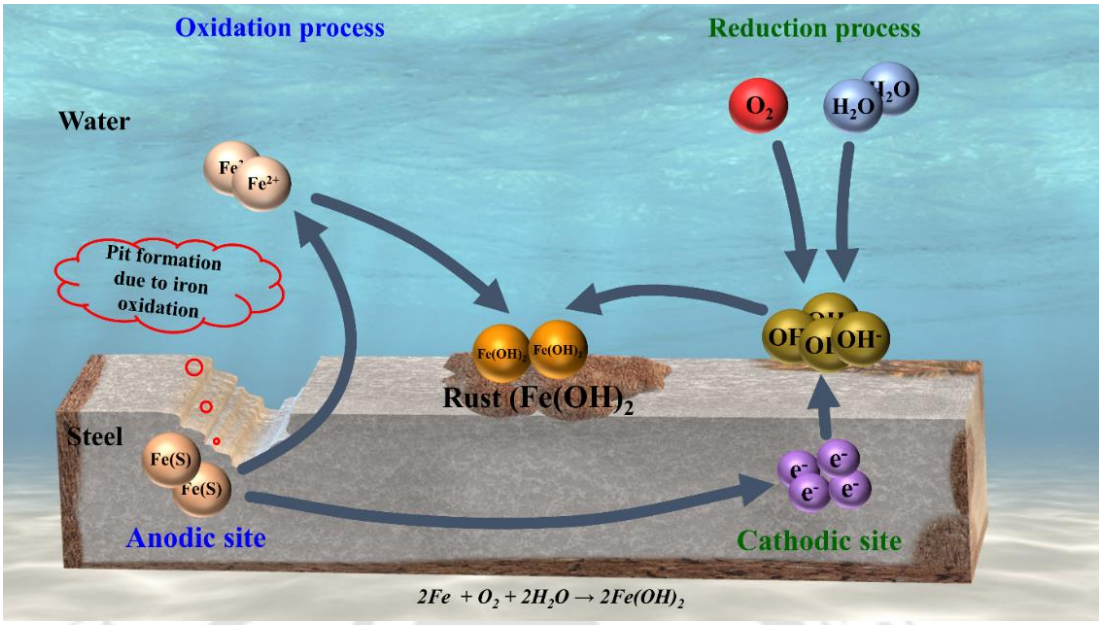

Fig. 1.1 Corrosion mechanism of steel in a water system.

There are several reasons and environmental variables that cause corrosion to occur. Dry and wet corrosion are two basic classifications depending on the presence of water. Dry corrosion occurs when air interacts with metal in the absence of liquid. Atmospheric gases like oxygen, hydrogen, hydrogen sulfide, and nitrogen support dry corrosion as well as halogens and inorganic fluids. Generally, dry corrosion is less harmful than wet corrosion, yet it is temperature sensitive. Wet corrosion happens when liquid is present. The differences in the rate of dry corrosion vary from metal to metal due to the mechanisms involved in it. Wet corrosion is more detrimental and can be observed commonly everywhere around us. Industries are shut down due to corrosion, causing human and financial losses and property devastation. The mechanism of wet corrosion differs from dry corrosion and mostly depends on the environment and the material. Wet corrosion in the presence of water or moisture on the steel surface is a major concern for all.

TH-3102_146107038

1.1.2 Electrochemical reactions of aqueous corrosion

Aqueous corrosion involves two half-reactions named as oxidation and reduction, along with the charge flow (electron). The reaction, which involves the release of electrons, is called an anodic reaction (oxidation process), and the reaction, which involves the release of electrons, is known as a cathodic reaction (reduction process). The area where the metal is oxidized is considered an anode, and where the reduction occurs is considered a cathode (Fig. 1.1**)**.

In an aquatic environment, the corrosion process starts with the dissociation of H_2O molecules into hydrogen (H^+) and hydroxyl (OH^-) ions.

$$H_2O \rightarrow H^+ + OH^- \quad \textbf{1.1}$$

When a metal is immersed in this solution, electrostatic charge differences at the metal-liquid interface will lead to surface ionizations, and the neutral metal is oxidized at the anodic zone.

$$M \rightarrow M^{n+} + ne^- \quad \textbf{1.2}$$

This is the reaction that leads to the corrosion process. The subsequent cathodic reactions depend on the nature of the environment. The oxidation depends on the oxidation state. For example, during the corrosion of iron, oxidized iron ions can be further oxidized as follows:

$$Fe \rightarrow Fe^{2+} + 2e^- \quad \textbf{1.3}$$

$$Fe^{2+} \rightarrow Fe^{3+} + 2e^- \quad \textbf{1.4}$$

When it comes to the cathodic reaction, there are a number of possible reactions depending on the environment. One of the essential practical factors in the natural aquatic environment is pH and dissolved oxygen.

TH-3102_146107038

1.1.2.1 Neutral or alkaline medium

In a neutral or alkaline aquatic environment, when dissolved O_2 is present, oxygen is reduced as follows:

$$O_2 + 2H_2O + 4e^- \rightarrow 4OH^- \ (O_2 \text{ present}) \quad \textbf{1.5}$$

In the absence of dissolved oxygen, the water molecules can be directly reduced to hydroxyl ions as a primary cathodic reaction.

$$2H_2O + 4e^- \rightarrow H_2 + 2OH^- \ (O_2 \text{ absent}) \quad \textbf{1.6}$$

1.1.2.2 Acidic medium

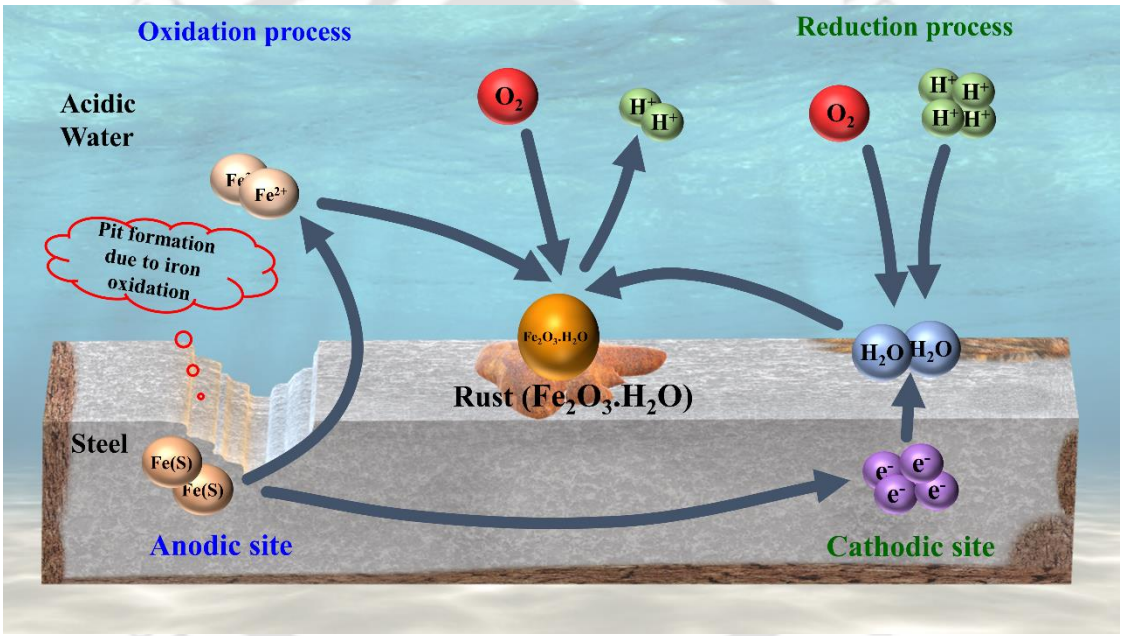

Fig. 1.2 Corrosion mechanism of steel in an acidic environment

In an acidic medium or low pH **(Fig. 1.2)** where the hydrogen ion (H^+) concentration is high, the primary reactions are as follows depending upon the presence of dissolved O_2 in media:

$$O_2 + 4H^+ + 4e^- \rightarrow 2H_2O \ (O_2 \text{ present}) \quad \textbf{1.7}$$

$$2H^+ + 2e^- \rightarrow H_2 \ (O_2 \text{ absent}) \quad \textbf{1.8}$$

TH-3102_146107038

At the cathodic area, the positively charged iron is reduced by interacting with negatively charged hydroxyl ions to form rusts.

$Fe^{2+} + 2OH^- \rightarrow Fe(OH)_2$ **1.9**

$Fe^{3+} + 3OH^- \rightarrow Fe(OH)_3$ **1.10**

So overall, combining Eq. 1.3 and 1.5**,** the overall reaction for wet corrosion in the presence of oxygen and neutral media, which commonly occurs around us, are as follows:

$2Fe + O_2 + 2H_2O \rightarrow 2Fe(OH)_2$ **1.11**

$4Fe(OH)_2 + 2H_2O + O_2 \rightarrow 4Fe(OH)_3$ **1.12**

In the case of acidic media, the overall reaction follows a different path which can be portrayed by combining Eq. 1.3 and 1.7**.**

$2Fe + O_2 + 4H^+ \longrightarrow 2Fe^{2+} + 2H_2O$ **1.13**

The produced Fe^{2+} ion from the anodic reaction is further oxidized by adsorbed oxygen and forms hydrated oxide containing Fe^{3+}. The reaction is as follows:

$4Fe^{2+} + O_2 + (2+4x)H_2O \rightarrow 2Fe_2O_3 \cdot xH_2O + 4H^+$ **1.14**

1.1.3 Types of corrosion

1.1.3.1 Uniform corrosion

This type of corrosion develops as pits of very small diameter, in the order of a micrometer, and results in a uniform and continuous decrease in thickness over the entire surface area of the metal. The rate of uniform corrosion can be easily determined by measuring the mass loss or the quantity of released hydrogen. The schematic of the uniform corrosion is shown in Fig. 1.3 (a).

TH-3102_146107038

1.1.3.2 Galvanic corrosion

When two dissimilar metals are in direct contact with a conducting liquid, experience shows that one of the two may corrode. The other metal will not corrode. This corrosion is different in its kind and intensity from the one that would occur if they were placed separately in the same liquid. The schematic of the galvanic corrosion is shown in **Fig. 1.3 (b).**

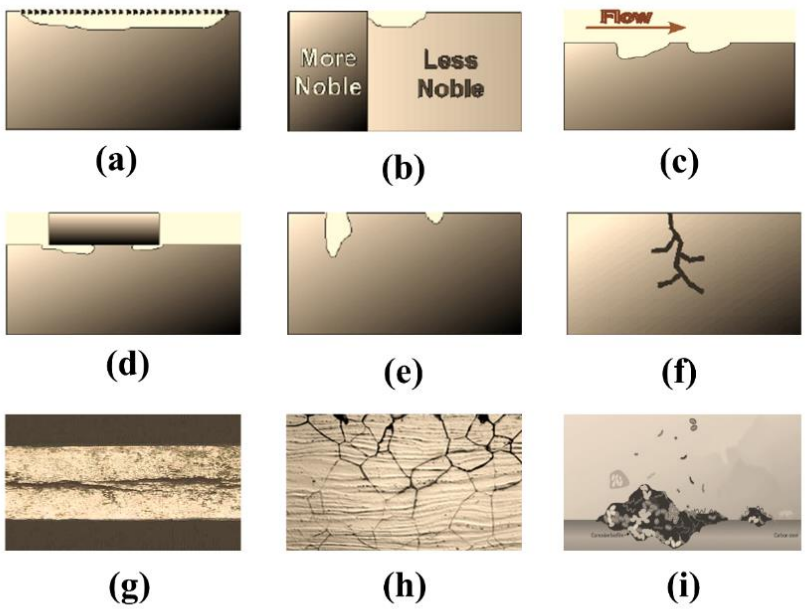

Fig. 1.3 Various types of corrosion: (a) Uniform Corrosion, (b) Galvanic Corrosion, (c) Erosion corrosion, (d) Crevice corrosion, (e) Pitting Corrosion, (f) Exfoliation Corrosion, (g) Intergranular Corrosion, (h) Stress cracking Corrosion, (i) Microbial induced corrosion.

1.1.3.3 Erosion corrosion

Corrosion by erosion occurs in moving media. This type of corrosion is related to the flow speed of the fluid. It leads to local thinning of the metal, which results in

TH-3102_146107038

scratches, gullies, and undulations, which are always oriented in the same direction, namely the flow direction, as shown in Fig. 1.3 (c).

1.1.3.4 Crevice corrosion

Crevice corrosion is localized corrosion. Overlapping zones for riveting, bolting or welding, zones under joints and under various deposits. These zones, also called crevices, are very tiny and difficult to access for the aqueous liquid that is covering the rest of the readily accessible surfaces. The schematic of the galvanic corrosion is shown in Fig. 1.3 (d).

1.1.3.5 Pitting corrosion

As seen in the schematic of the pitting corrosion is shown in Fig. 1.3 (e). This localized form of corrosion is characterized by the formation of irregularly shaped cavities on the surface of the metal. Their diameter and depth depend on several parameters related to the metal, the medium, and service conditions.

1.1.3.6 Exfoliation corrosion

Exfoliation corrosion is a type of selective corrosion that propagates along a large number of planes running parallel to the direction of rolling or extrusion. The schematic of the galvanic corrosion is shown in Fig. 1.3 (f)

1.1.3.7 Intergranular corrosion

It spreads in all directions, and corrosion indifferently affects all the metallurgical constituents; there is no selective corrosion because it propagates within the grains. A typical formation of intergranular corrosion is shown in Fig. 1.3 (g)

1.1.3.8 Stress cracking corrosion

This type of corrosion results from the combined action of mechanical stress (bending, tension) and a corrosive environment. The schematic of the stress cracking corrosion is shown in Fig. 1.3 (h).

TH-3102_146107038

1.1.3.9 Microbial induced corrosion

Acidic habitats may be created by bacteria by altering the pH and oxygen levels of the environment. Bacteria that reduce sulfate, such as *Desulfovibrio*, create H_2S, which dissolves to form sulfuric acid. Microbial corrosion is not induced by an easy chemical interaction between oil and water but rather by bacteria and fungi altering the environment Fig. 1.3 (i).

1.1.4 The adversity of corrosion

Corrosion has a significant impact on the economy, with estimates ranging from 3.4% GDP of a country (Koch et al., 2016). According to a report, India losses 5-7% of GDP every year. Corrosion of metallic materials is one of the most pressing issues in modern industry. Corrosion of metals costs the United States $450 billion annually. It has been predicted that 40% of corrosion-related expenditures might be reduced by using existing knowledge and technology. Environment and human health are also impacted by it. There are additional secondary expenses associated with plant downtime, poorer equipment efficiency, pollution, and overdesign in addition to these direct ones mentioned above. The cost of replacing corroded equipment is usually minimal when compared to the output losses that occur while the unit is not in operation. Consequently, pipeline and tank leakages result in the loss of expensive items and may also constitute a severe environmental hazard. Decontamination of a system contaminated with soluble corrosion products may be expensive. Increased corrosion on heat exchanger tubes and pipes affects heat transfer efficiency and pumping capacity. Decontamination of a system contaminated with soluble corrosion products may be costly. Corrosion rates (metal weight loss/unit area/ unit time) cannot be predicted accurately. Hence overdesign (such as a thicker tube wall) is necessary to

TH-3102_146107038

ensure appropriate service life. As a result, resources are wasted, and the power needs for moving components are increased (Javaherdashti, 2000).

The effect of corrosion is taken into account primarily for economic and ecological reasons. The three types of corrosion-related losses are as follows:

I. Waste of energy and material

II. Economic loss

III. Impact on environment and health

1.1.4.1 Waste of energy and material

One ton of steel rusts worldwide every 90 seconds. The energy required to produce one ton of steel fulfills the energy requirement for three months in a family. Another example is a 225-mile-long, 8-inch-diameter pipe with a 0.322-inch-thick wall thickness. A 0.250-inch wall thickness would have saved 3,700 tons of steel and boosted internal capacity by 5% if it had been adequately protected against corrosion. Approximately half of the world's steel production is utilized to replace rusted steel (Javaherdashti, 2000).

1.1.4.2 Economical loss

According to a study, corrosion costs 2% to 4% of a country's GDP (Koch et al., 2016). During the 1995 fiscal year, corrosion cost Shell $400 million. The expense for corrosion in pulp manufacture is $3 billion per year, with Canada contributing $400 million per year. These figures don't take into account lost production, equipment downtime, etc. The net asset value is reduced by 6% due to corrosion for British Petroleum (BP). The US electric power industry loses $10 billion annually due to corrosion. Corrosion is responsible for 55% of all unplanned outages, according to Electric Power Research Institute (EPRI), and accounts for 10% of the average monthly cost of household electricity. According to a study on inspection results of various

TH-3102_146107038

offshore production facilities, the corrosion factor was found in 35 % of the buildings, 33 % of the process systems, and 25 % of the pipelines during a 1993 examination. Well impediment is caused by microbiological corrosion almost every year, according to the Turkish Petroleum Corporation (TPAO). To remove defective pipelines, production has to be halted for at least five days, and the disposal of defective pipelines is done by an expensive machine called a "work-over tower" (1992 rates). Due to corrosion and water degradation, 30 percent of treated drinkable water is lost in Tehran each year (Esmailzadeh et al., 2018; Hansson, 2011; Javaherdashti, 2000; Kamaruzzaman et al., 2022).

1.1.4.3 Impact on environment and health

Pipelines are susceptible to corrosion on both the interior wall and the exterior surface, although the former is far more likely to be affected. The majority of the environment pollution that is caused by corrosion may be traced back to leaks that occur in perforated tanks, containers, and pipes. It is reasonable to anticipate that this kind of pollution will increase in frequency along with the quantity and length of pipelines that carry oil, gas, water, and sewage. Between the years 1994 and 2000, internal corrosion was the cause of 15% of all pipeline accidents in the United States. During the same time period, the number of pipeline incidents caused by internal corrosion in Alberta, Canada, averaged out to approximately one per day. In many instances, due to MIC (microbial-induced corrosion), by sulfate-reducing bacteria, the pit and perforation cause damage in a carbon steel heavy oil pipe. In addition to bacteria, ammonia, and sulfur compounds, sewage also includes substances that may escape from pipes, which can be detrimental to the environment. Corrosion also has the potential to endanger our lives. When corrosion products accumulate, they may harm the organs, such as the digestive, respiratory, ocular, and skin systems of the human body. As soon as corrosion

TH-3102_146107038

begins, structural collapse is nearly guaranteed, as is the potential of damage to employees or the general public. Corrosion on bridges, parking structures, buildings, electrical towers, roads, and other infrastructure may put public safety at risk and cause large maintenance expenses. A rusted part might lead to calamity if they fall (Esmailzadeh et al., 2018; Hansson, 2011; Javaherdashti, 2000; Kamaruzzaman et al., 2022).

1.1.5 Protection from corrosion

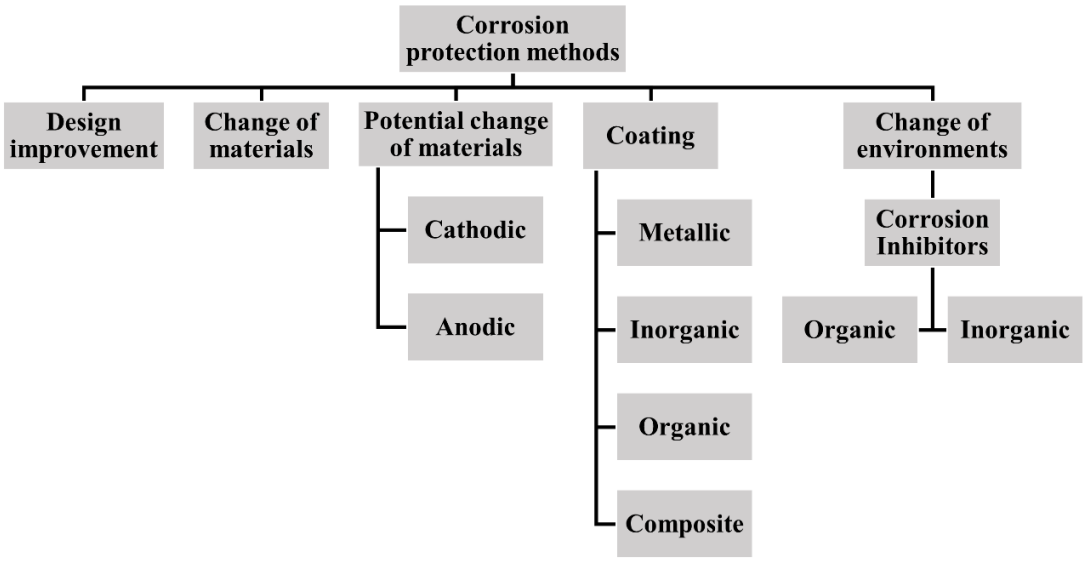

Fig. 1.4 Type of corrosion protection methods.

1.1.5.1 Design improvement

Preventing corrosion requires a multipronged approach, the first of which is ensuring that the structure was designed and constructed using appropriate practices and materials. As for example a well-designed building will have no sharp edges or crevices, will have no puddles or mud or other inaccessible regions, will have adequate drainage, and will be simple to navigate both inside and out. In most cases, the most cost-effective option selected by designers is to periodically replace the sections of

TH-3102_146107038

buildings that have corroded beyond acceptable limits. Due to its high cost and corrosion resistance, stainless steel is only utilized in exceptional circumstances in ship and offshore constructions, such as the exteriors of chemical tankers (RIZZO, 2008).

1.1.5.2 Change of materials

Choosing the right materials is crucial to ensuring a long service life and avoiding operational failure due to inadequate mechanical strength or an undesirable appearance caused by corrosion products. The material must have the appropriate mechanical strength, corrosion, and erosion-resistant properties under the defined service conditions. Corrosion-resistant metals are essentially required in the valve and pipe systems of refineries and chemical processing plants. Product functionality and performance should be taken into account while choosing materials. As an example, the density and corrosion resistance of fiberglass makes it an excellent choice for a saltwater storage tank over AISI 304. Water supply, wastewater disposal, and irrigation systems all benefit from the long life of PVC (polyvinyl chloride), lack of corrosion, low maintenance requirements, and reasonable cost. The electrical conductivity, coefficient of thermal expansion, and thermal conductivity of a material are all crucial characteristics. Heat exchanger tubes made of cupronickel (90-10 Cu-Ni) are suited for use in thermal desalination plants that process seawater. The ability of a product to withstand stresses in service is determined by its tensile strength, yield strength, fatigue strength, and creep strength, all of which are essential to design. Some mechanical properties are affected by their surroundings. As like, yield strength may gradually decrease when exposed to saline water. Quantitative analysis of all elements is required to determine the metal composition after exposure to seawater. Corrosion in a medium is also affected by physical factors, including pH, conductivity, temperature, and velocity. Since more than 40,000 metal alloys and non-metallic materials are already

TH-3102_146107038

available, material selection has grown complex and difficult due to the rapid development of innovative materials. All important factors need to be thought through when still in the planning stages. Aspects of size, shape, and weight are all examples of physical characteristics. The stress resistance of a material is affected by its mechanical properties. Mechanic features are used as failure criteria in the design process. Various mechanical properties are considered to choose a material, such as (1) Density (2) Modulus of elasticity (3) Strength (4) Ductility (5) Fracture toughness (6) Fatigue (7) Corrosion fatigue (8) Creep (9) Impact (10) Hardness. It is advised to use recyclable or biodegradable products. Of course, they have to be resistant to corrosion throughout the duration of their use (Ahmad, 2006).

1.1.5.3 Potential change of materials

Anodic and cathodic protection are two electrochemical processes to prevent surfaces from corrosion. In an electrochemical process, the anode and cathode are two electrodes. In this protection process, a surface (substrate) is used as either anode or cathode, which leads to the name of those processes as such.

The idea of cathodic protection is the use of metal in the role of a sacrificial anode. In this method, the sacrificial metal is allowed to corrode while the cathode remains unaffected. The major difference between anodic protection and cathodic protection is that the protected surface acts as the anode in anodic protection, and the cathode in cathodic protection. There are two modes of cathodic protection, such as sacrificial anode cathodic protection and impressed current cathodic protection (also known as ICCP). In a sacrificial anode cathodic protection system, a sacrificial anode is connected with a cathode using metal wire and buried in soil or any corrosive environment. The anode is less noble and has a higher oxidation potential compared to the cathode. Generally, Zn, Al, and Mg are used as sacrificial anodes as they are less

TH-3102_146107038

noble metals and easily oxidized in a corrosive environment. Due to the potential difference between these two electrodes, the electron liberates from the anode and flows to the cathode. The positively charged metal ions leave the anodic surface, too; thus, the sacrificial anode gets corroded with time. The reduction occurs on the cathode (protected metal). However, this process has limitations in that it can only be used in small sections of pipes. So if the structure is big, the required number of sacrificial anodes is higher. The use of a large number of anodes to provide adequate current is impractical and costly. So an external power source is used to flow the current and drive the electrochemical reactions. This technique is known as ICCP.

When the pH of the environment is extremely low or high, or in any state where the corrosion current is high, then anodic protection is required. Any vessels that stores concentrated acids and alkaline can be protected by this method. In this technique, the corrosion is controlled by making the metallic surface an anode connected to an inert cathode of the electrochemical cell. The electrode potential of the system is exploited to maintain the metal in a passive state. This method is only helpful on the condition that the supply of direct current is carefully monitored during the process. Metals are protected against corrosion by a passive layer that forms on their surfaces due to anodic polarization caused by a DC potential (Ahmad, 2006; Bahadori, 2014; Schofield, 2001).

TH-3102_146107038

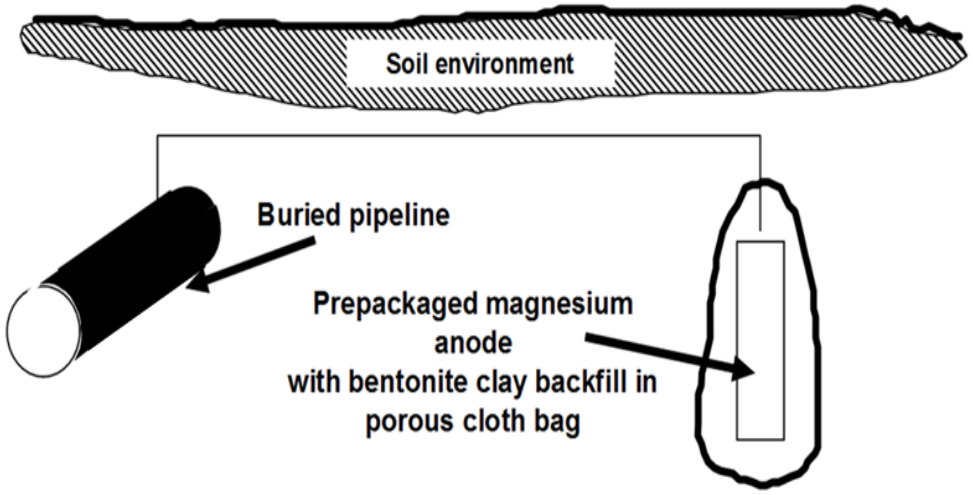

Fig. 1.5 Corrosion protection using anodic/cathodic protection method.

1.1.5.4 Coating

Using anti-corrosive coating is one of the widely used approaches across the globe. Corrosion-resistant coatings might be useful for reducing the degradation that occurs as a result of oxidation, moisture, chemical exposure, and other environmental causes. They act as a barrier, keeping corrosive materials and chemical compounds from coming into contact with metal parts and preventing additional wear and corrosion. Depending on the mode of action, they are broadly classified into three categories as (a) barrier, (b) inhibitive, and (c) sacrificial.

The barrier type is a non-porous protective layer. It requires an additional coating or film to protect the barrier, and once the barrier is damaged, the metal is exposed to a corrosive environment.

The second one, an inhibitive coating, is porous and forms a passive layer on the surface. In this type of coating, the humidity affect the metal surface as the coating is porous. The protection may be degraded over time which can be overcome by the use of a primer.

TH-3102_146107038

The third type, the sacrificial type, act as an additive on the surface that sacrificially corroded to protect the metal surface under it. The main advantage is if it is worn, then also it protects the surface. In this type, the additive type and content regulate the protection of the surface.

Depending on the type of materials used in the coating, the corrosion coatings are classified into three types, viz. (a) metallic, (b) inorganic, and (c) organic.

Metals like copper, zinc, nickel, and aluminum are mainly used for metal coatings. The factors those are considered for making metal coatings: (i) the resistance ability of the metal against the corrosive environment, (ii) thickness uniformity, (iii) porosity, (iv) adherence capability, (v) average thickness. The metal should also be hard. There are already various methods available for the metal coatings like galvanization, electroplating, thermal spray etc.

Chromate, phosphate, potassium silicate, and calcium aluminate compounds are generally used in the fabrication of inorganic coatings. These types of coating are formed using process like diffusion, spraying and chemical conversion. The inorganic coatings should also form a barrier with less porosity and brittleness.

The organic coatings are a thin layer of paint, varnish, or lacquer by organic compounds that gives protection to active metal surfaces. The majority of organic material coatings stick to the surface of the metal by two different mechanisms: first one is mechanical adhesion, and the second one is chemical adhesion. The procedures of properly preparing the surface, choosing an appropriate priming coat, and applying a top coat are the ones that need to be taken into consideration in order to have effective organic coatings. Painting has been around for a long time and is a tried and true means of preventing rust. The primary purpose of painting is to provide a barrier covering that will isolate the surrounding environment. It is necessary to have a good user method in

TH-3102_146107038

order to guarantee that paint will perform correctly; failing to do so may result in a loss of money. There may be a change in appearance as a result of oxidation and/or exposure to UV radiation. For example, there may be a loss of glass or a decrease in the thickness of the film. In most cases, an early failure may be identified by a lack of adhesion, either with the substrate or between the many paint layers that were applied in succession.

Table 1.1 Some examples of PANI composite coating as anticorrosive coating.

PANI composite coating	Method for composite preparation	Corrosive medium	Substrate	Reference
PANI with AuNPs	Insitu polymerization and dispersion mixing	1 M KCl	Zinc	(Vimalanandan et al., 2013)
ND–PANI	In situ polymerization	HCl	Steel and aluminum	(Gomez et al., 2010)
PANI–CN	Ultrasonic oxidative polymerization	3.5% NaCl	Carbon steel	(Akbarinezhad et al., 2011)
PANI	Emulsion polymerization	3.5% NaCl	Mild steel	(Mahmoudian et al., 2012)
ZnO–PANI	In situ polymerization	3.5% NaCl	Carbon steel	(Mostafaei and Nasirpouri, 2014)

A liquid coating made from organic substances is applied to a surface, allowed to dry, and then tested for its durability and longevity as a film on that surface. Drying might include chemical reactions and polymerization, or it can simply consist of the solvent evaporating, depending on the kind of solvent that is being employed. Polyaniline (PANI) conducting polymer is a popular choice for organic protective coatings due to its low cost, ease of preparation, and excellent tunability, in addition to its high thermal stability. Moreover, it is one of the most common materials. The fact that this may be used as a single layer is the fundamental strength, which allows it to

TH-3102_146107038

be applied in a variety of ways. Anticorrosive coatings made of composites of polyaniline nanostructures, which may take the form of granules, nanospheres, nanofibers or nanotubes, have shown early signs of promise (Table 1.1).

1.1.5.5 Change of environments

One of the effective approaches to mitigate corrosion is by altering the environment. Some chemical substances are used in the environment to make it less aggressive for the corrosion of the material. These substances are known as **corrosion inhibitors**. Corrosion inhibitors are used in small concentrations for localized protection, which may be caused by the accumulation of small amounts of aggressive constituents. As the inhibitor can be directly incorporated into the media, it is extremely effective to counter the local corrosion and to reach into the small pits of the surface. It is also very convenient to use since it can be applied by dip, spray, brush, etc. (G. and F., 2014; Palanisamy, 2019).

1.1.5.5.1 Mechanisms of actions of inhibitors

The inhibition mainly results from one or three of these general mechanisms:

- The inhibitor molecules are adsorbed on the surface by chemical interaction (chemisorption), forming a thin film layer on the surface by itself or in conjunction with metal ions.
- The inhibitor leads the metal to form its own protective layer of metal oxides for the protection and development of resistance.
- The inhibitor makes complex potential corrosive components present in the media.

TH-3102_146107038

1.1.5.5.2 Classification of the inhibitors

The corrosion inhibitors are classified depending on the chemical nature and the mechanism of the action. Depending on the mechanism of the action, they are classified as:

- Anodic inhibitor
- Cathodic inhibitor
- Mixed-type inhibitor.

Depending on their chemical nature, they are classified as:

- Inorganic inhibitor
- Organic inhibitor

Generally, the inorganic inhibitor has cathodic and anodic modes of action. The organic inhibitors have both anodic and cathodic and mixed-type modes of action and protective film by adsorption (G. and F., 2014; Palanisamy, 2019).

A. Based on the mechanism of the action

I. Anodic inhibitors

The anodic inhibitors or sometimes called passivation inhibitors, reduce the corrosion rate by suppressing the anodic reactions. It blocks the anodic reactive sites by promoting the passivation and forming a film on the metal surface. This can be validated by the potentiodynamic polarization curve (Fig. 1.1) in the presence of an anodic inhibitor, the corrosion potential (E^{i}_{corr}) curve shifts towards more positive (anodic) side compared to corrosion potential in the absence of an inhibitor (E_{corr}) (Fig. 1.2 (a)). The corrosion potential is the potential at which corrosion of the metal occurs. The corrosion current in the present of an inhibitor (I^{i}_{corr}) is lower than the corrosion current without inhibitor (I_{corr}). The anodic inhibitors react with the metallic ions (M^{n+})

TH-3102_146107038

which are formed on the anodic sites and make an impermeable, insoluble hydroxide layer. The OH^- is released from the hydrolysis reaction. It is important that the inhibitor concentration should be high enough, or else the surface will not cover properly. Concentration below critical value is not effective; rather, it enhances the rate of corrosion. Since the area of the cathodic zone is higher than the anodic area, a higher cathodic current accelerates the corrosion rate. This occurs due to the breakdown of passivity. There are two types of anodic inhibitors such as:

- **Oxidizing anions**: chromates, nitrites, and nitrates, which can passivate steel in the absence of oxygen.
- **Non-oxidizing anions**: phosphates, tungstates, and molybdates, which need oxygen to passivate (G. and F., 2014; Palanisamy, 2019).

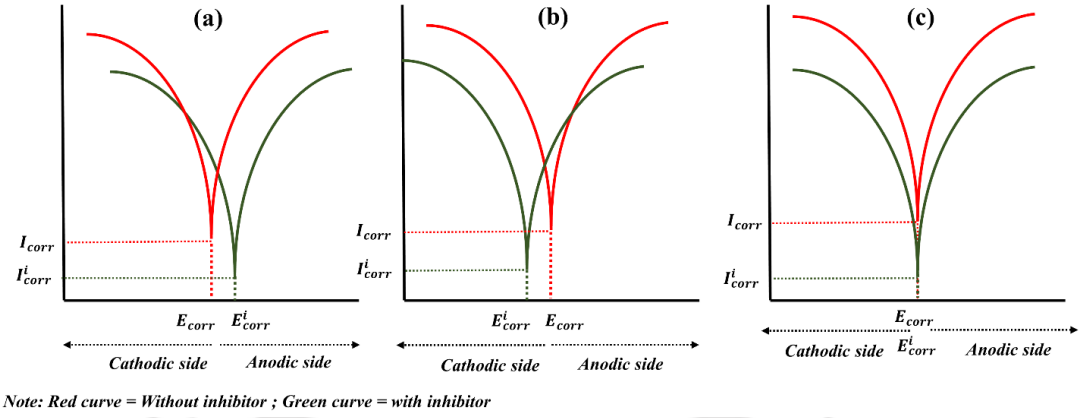

Fig. 1.6 Potentiostatic polarization diagram: electrochemical behavior of (a) anodic inhibitor, (b) cathodic inhibitor, and (c) mixed inhibitor.

II. Cathodic inhibitors

The cathodic inhibitor, on the other side retards the cathodic reactions by blocking the cathodic sites. The inhibitors initiate cathodic reactions due to the alkalinity and produce insoluble complexes which precipitate selectively on the cathodic sites. |Thus, the retardation in the hydrogen evolution or the cathodic reactions

TH-3102_146107038

reduces the overall corrosion rate. The deposition develops a compact adherent layer which increases the impedance of the surface and restricts the diffusion of reducible species like oxygen. In the presence of cathodic inhibitor, corrosion potential (E_{corr}^{i}) shift towards cathodic sites compared to the corrosion potential (E_{corr}) in the absence of inhibitor and corrosion current also (I_{corr}^{i}) decreases (Fig. 1.3. (b)). Various cathodic inhibitors are commercially used, such as:

- **Oxygen scavenger:** sodium sulphite, hydrazine, $As^{3+,}$ and Sb^{3+} etc. are used, which remove the oxygen from the solution.
- **Cathodic precipitates**: Calcium, Magnesium precipitate as oxides to form a barrier (G. and F., 2014; Palanisamy, 2019).

III. Mixed inhibitors

The mixed inhibitor is one that retard both cathodic and anodic reactions. They are basically film-forming compounds that block both anodic and cathodic sites of the reaction. The corrosion potential in the presence of the inhibitor (E_{corr}^{i}) does not change much than the potential in the absence of an inhibitor (E_{corr}) but the carrion current (I_{corr}^{i}) decreases in the presence of an inhibitor (Fig. 1.4 (c)). Various organic inhibitors are used as a mixed-type inhibitor (G. and F., 2014; Palanisamy, 2019).

B. Depending on the chemical nature

I. Inorganic inhibitors

The compounds such as As_2O_3, Sb_2O_3 have been reported as inhibitors in acid media. In this case, the protection is due to the reduction of electropositive ions, deposition on the metal surface, and lowering of the overvoltage of the main cathodic depolarization reaction. Recently it has been shown that the addition of heavy metal ions such as Pb^{2+}, Ti^{+}, Mn^{2+}, and Cd^{2+} is found to inhibit the corrosion of iron in acids.

TH-3102_146107038

As mentioned earlier, maximum anodic and cathodic inhibitors like sodium sulphite, hydrazine, chromates, nitrites, and nitrates are used as inorganic inhibitors (G. and F., 2014; Palanisamy, 2019).

II. Organic inhibitors

Organic inhibitors are compounds that act as cathodic, anodic, or, together, as cathodic and anodic inhibitors. They adsorb on the surface of the metal depending on the energy favourability. The inhibition efficiency of any organic inhibitors depends on various factors like

- Structure and the size of the molecule.
- The carbon chain length, as well as the aromaticity and/or conjugated bonding.
- Type of bonding in the molecule (either π or σ).
- Ability to form cross-linking
- Type of the electrolyte solution.

Many organic compounds like amines, aldehydes, alkaloids and nitro etc. have been used as organic inhibitors. The inhibition efficiency of organic corrosion inhibitors is mainly related to polar functional groups with S, O, or N heteroatoms and pi electrons of the heterocyclic compounds. These heteroatoms and π electrons are the important factors for the adsorption process. The main advantages of organic inhibitors are that they are biodegradable and eco-friendly (G. and F., 2014; Palanisamy, 2019). For this reason, these are called **green corrosion inhibitors.** This current research is about finding a novel green corrosion inhibitor.

1.1.6 Green corrosion inhibitors

As discussed earlier, the inhibitors are broadly classified into two categories, viz. organic and inorganic, which are found commercially and used in industrial areas.

TH-3102_146107038

But there is increased concern about the toxicity, biodegradability, and bioaccumulation of corrosion inhibitors discharged into the environment. Inorganic inhibitors are used widely, which cause environmental pollution later. Corrosion inhibitors in the aqueous phase are discharged into the water bodies; these become an environmental threat to aquatic life. These concerns urge corrosion inhibitors to be nontoxic and environment-friendly. Hence, the development of green corrosion inhibitors is bringing the attention of various industrialists and scientists. These inhibitors are biodegradable, do not contain heavy metals or other toxic compounds, and are economically viable. Researchers have reported the successful use of naturally occurring substances to inhibit the corrosion of metals in acidic and alkaline environments (Barouni et al., 2008; Barreto et al., 2017; Chakrabarty et al., 2017; da Rocha et al., 2010; M'hiri et al., 2016; Ostovari et al., 2009; Prabakaran et al., 2016a; Raja and Sethuraman, 2008; Sin et al., 2017; Singh and Quraishi, 2016). In some places where the coating is not feasible corrosion inhibitors are used for corrosion protection. These green corrosion inhibitors have no hazardous effects on nature. They have impressive corrosion inhibition efficiency also (Ji et al., 2015; M'hiri et al., 2016).

Green corrosion inhibitors mainly contain organic compounds like polysaccharides, amino acids, polyphenols, etc. These organic compounds mostly contain various heteroatoms like N, O, S, functional groups, and delocalized π electrons on their structure (Ji et al., 2015; Liao et al., 2018a; Salghi et al., 2017). The efficiency of these inhibitors mainly depends on their capability to replace water molecules from the metal surface and cover the surface. A number of studies have shown that the adsorption capability depends on the structure of the adsorbed molecule, the charge of the surface, and the type of electrolytes. An effective inhibitor must replace the water molecule from the surface to establish the electrostatic interaction

TH-3102_146107038

with the charged surface. For an ideal inhibitor, this interaction should be stronger than the interaction between the water molecule and the metal surface (Ali and Mahrous, 2017). This interaction primarily depends on the electronegativity and polarizability of the electron clouds, which are mostly found on the phenyl ring of any compound. The functional groups containing heteroatoms play the key role (N, O, S) in establishing such interactions as these can help to form a coordinate bond also. Conventionally, the tendency to create the coordinate bond is higher for S than N and O (Feng et al., 2018; Mourya et al., 2013; Srivastava et al., 2017, 2018). The green corrosion inhibitors have been found generally in two categories. Some are chemically synthesized, and some are extracted from biomass.

1.1.6.1 Chemically synthesized

Recently, it has been observed that the corrosion is inhibited by 200 ppm of a mixed-type inhibitor Poly(1-phenylethene) in 1 M HCl, which is even efficient at 329 K temperature (81% inhibition efficiency) (Khaoula Alaoui et al., 2016). N-((8-hydroxyquinolin-5-yl) methyl)-N- phenylacetamide (HQMP) is synthesized chemically and is applied to the XC38 steel corrosion in 1 M HCl. HQMP has revealed a maximum efficiency of about 93 % at 10^{-4} M at 298 K and 88% at 328 K. From the polarization study, HQMP is found as an anodic inhibitor that adsorbs on the surface spontaneously (El Faydy et al., 2016). Anti-corrosive properties of *Polyvinyl-Alcohol* for carbon steel in 1 M HCl media are tested, and maximum efficiency is found as 93 % (298 K) and 80% (328 K) with 200 ppm. Thermodynamic studies indicate that the studied inhibitors are adsorbed on carbon steel surfaces by an exothermic, spontaneous process. Interestingly, it has been noticed that beyond 200 ppm, the efficiency is found to decrease as the adsorbate (inhibitor) starts to dissolve back into the bulk solution. This leads to the weakening of metal–inhibitor interactions, resulting in the replacement

TH-3102_146107038

of inhibitors by water or chloride ions (Cl^-) (K. Alaoui et al., 2016). A study on α-brass and (α+β) brass alloys degradation processes in Azrou soil (19% moisture) reveals that EC5 (α-brass) and EC6 (α+β brass) are the most corrosion-resistant brass. It is clearly evident that the steady-state corrosion behavior of α+β brasses and α- brasses in Azrou soil is related to the presence of aggressive ions, chloride, and sulfate (Galai et al., 2017). Coriandrum Sativum seeds (CSE), an eco-friendly inhibitor, is found as an efficient inhibitor in HCl and H_2SO_4 in both acidic media (93.7% in 1.0 M HCl, 96.7% in 0.5 M H_2SO_4) with 1000 ppm. The study proves that the functional groups with O and other aromatic components help to increase the adsorption of the inhibitory molecule, but the inhibition efficiency decreases with increasing temperature (Kadiri et al., 2018). The quinazolinone derivatives, namely, 3-methyl-2-(p-tolyl) quinazolin-4(3H)-one (QZ-CH_3), 2- (4-hydroxyphenyl)-3-methylquinazolin-4(3H)-one (QZ-OH), 3-methyl-2-(4-nitrophenyl) quinazolin-4(3H)- one (QZ-NO_2) and 3-methyl-2-phenylquinazolin-4(3H)-one (QZ-H) are synthesized and is used as an organic inhibitor in 1.0 M HCl at different temperatures (298 K to 328 K) on mild steel. The study reveals that the inhibition efficiency depends on the nature substituent in quinazolinone, and they follow the order in terms of inhibition efficiency: QZ-CH_3 > QZ-OH > QZ- NO_2 > QZ-H (Errahmany et al., 2020). Chemically functionalized 8-hydroxyquinoline derivatives, namely BMQ and DEMQ, are studied as new eco-friendly inhibitors for mild steel in 1.0 M HCl solution. Both studied molecules provide high resistance and inhibition efficiency (94% at 10^{-3} M) and remain efficient even at high temperatures (86% at 328 K for the concentration 10^{-3} M). DFT calculations show that the heteroatoms, like oxygen (O), nitrogen (N), and methyl groups (–CH_3), favor the sharing of electrons between the studied molecules and the surface of the steel (Galai et al., 2020). Few heterocyclic organic compounds derived from imidazole, namely 2-

TH-3102_146107038

(1,4,5-triphenyl-1H-imidazol-2-yl) phenol (IM-OH), 1,4,5-triphenyl-2-(4-metyoxyphenyl)-1H-imidazole (IM-OCH_3), and 3-methoxy-4-(1,4,5-triphenyl-1H-imidazol-2-yl) phenol (IM-H) exhibit excellent inhibition efficiency in 0.5 M H_2SO_4 media for mild steel. The efficiencies are attained as 97.7%, 98.9%, and 88.9% at 10^{-3} M of IM-OH, IM-OCH_3, and IM-H, respectively. The thermodynamic studies indicate that the process is energy favorable, and the Monte Carlo simulations validate a great interaction between the compounds and the metal surface of iron (Ouakki et al., 2020). 2-mercaptobenzothiazole (MBT) encapsulated in hollow mesoporous organosilica nanoparticles (HMON) has been observed as an inhibitor (Chunling et al., 2021). A new gossypol derivative 6-aminopenicillanic acid sodium gossypol (APASG) is found as an efficient corrosion inhibitor for St2 steel in 1 M HCl + 1 M KCl media (Berdimurodov et al., 2021c). Some novel eco-friendly thioglycoluril derivatives (2–thioxo–5,5–di–p–tolylimidazolidin–4–one (TODTI) and 3a,6a−bistolylthioglycoluril (BSTGCU)) are also effective in reducing the corrosion rate of St2 steel in aggressive HCl media. Among them, BSTGCU even shows better inhibition in HCl media in the presence of sulfate ions (Berdimurodov et al., 2021a, 2021d). The self-assembling anchored films based on tetrazole derivatives like 5-Benzyl-1H-Tetrazole (BTA) and 5-(Benzylthio)-1H-tetrazole (BTTA), which are found to be very effective inhibitors on copper in 0.5 (M) H_2SO_4 with 96.3% (BTA) and 99.8% (BTTA) inhibition efficiencies (Qiang et al., 2020). More interestingly, a pH-responsive and self-healing coating has been developed by in-building 2-Mercaptobenzimidazole (M) successfully in zeolitic imidazolate framework-8 (ZIF-8) on GO nanosheets and then embedding into the epoxy coating to prepare the composite coating. The composite M-ZIF-8/GO/EP coating the long-term anti-corrosion ability and excellent self-healing performance (Li et al., 2021).

TH-3102_146107038

1.1.6.2 Extracted from bio-mass

Interestingly some natural bio-mass from plant origin can also be the source of green corrosion inhibitors due to their low cost, easy availability, and environmental friendliness. These bio-masses are nothing but the plant body parts which are generally accumulated from various sites like industries, kitchens, and agricultural lands. The performance of inhibition by these plant extracts primarily depends on the presence of complex organic species like amino acids, carbohydrates, proteins, polyphenolic compounds, etc. In recent years many studies have been performed on plant extract and some of them like *Zenthoxylum alatum* (Chauhan and Gunasekaran, 2007), *Phyllanthus amarus* (Shabani-Nooshabadi and Ghandchi, 2015), *Teucrium oliverianum* (Al-Otaibi et al., 2014), *Tragia plukenetii* (Prabakaran et al., 2016b), *Gingko biloba* (Singh et al., 2015), *Tripleurospermum auriculatum*, *Ligularia fischeri* (Al-Otaibi et al., 2014), *Cryptostegia grandiflora* (Prabakaran et al., 2016a), *Oxandra asbeckii* (Shabani-Nooshabadi and Ghandchi, 2015), have shown impressive inhibition efficiencies. It has been found that the extract of Epimedium (EPM) and its iodide composite are tested to inhibit the corrosion of X80 steel in 5% HCl solution as oilfield acid wash solution. Even a small concentration of EPM (1.0 gL^{-1}) has shown 96.7% inhibition efficiency in 60°C. The EPM molecules are adsorbed spontaneously on the surface involving the interaction between the O, N and C=C sites of the compounds and the X80 (Singh et al., 2019). An innovative inhibitor such as tobacco extracted from discarded cigarettes has exhibited inhibition efficiency of 96.8% (copper) and 98.2% (zinc), and the inhibitor molecules adsorbed on the surface by forming an inhibitor-metal complex. It is clearly observed from the scanning electrochemical microscopy (SECM) that without an inhibitor, the surface produces more current like a conductor but exhibits an inhibitive lower current in the presence of an inhibitor (Singh et al., 2020). *Ginkgo* leaf

TH-3102_146107038

extract has been used as a green corrosion inhibitor on X-70 steel in an HCl medium, and it was observed that only 200 mgL^{-1} of the extract was able to show 90% inhibition efficiency (Qiang et al., 2018). Some innovative and new approaches, like oxidation/polymerization reactions, have been used to enhance the efficiency of the Nettle bio extract. Nettle extract was modified by oxidation in alkaline conditions. Some of the components of the Nettle extract, like serotonin and histamine, are polymerized or dimerized and show better adsorption capability on steel (Keramatinia et al., 2019). It has been established that flowers, leaves, and peel contain a higher amount of polyphenols which shows higher antioxidant and corrosion inhibition. Extract of leaves, flowers, and stems of *Cistus monspeliensis L* has been tested to inhibit the corrosion of carbon steel in acidic media. It is observed that the plant mass, which contains a high amount of polyphenols (flowers and leaves), shows better antioxidant activity and better inhibition efficiency. (Mechbal et al., 2021). Raphanus sativus L. is also found as an effective inhibitor and antiscalant for mild steel, even in tap water. The anti-scaling efficiency is tested using chronoamperometry and thermal scaling techniques. The scaling inhibition efficiency is determined from the changes in hardness using the titration technique. From the experiments, it is observed that the hydroxyl and carboxyl functional groups of the extract compounds interact with cations like Ca^{2+}. The polyphenols also chelate the cations. It is discovered that the scaling inhibition efficiency is improved by five times in the presence of the extract (Vasyliev et al., 2020). The peach pomace extract has been investigated for corrosion inhibition on carbon steel in chloride-induced corrosion (NaCl medium). The volatile organic compounds of the extract were explored GC-MS and HPLC. The study showed that longer exposure to extract increases inhibition efficiency (Vorobyova and Skiba, 2021).

TH-3102_146107038

1.2 Inspiration of the research work

Concurrently, the increasing amount of agro and food waste from different sources has certainly become a concern at the current time. So the valorization of various biomaterials and agricultural by-products or wastes and food wastes is drawing attention to enhancing the economic viability of agricultural industries as these by-products and wastes contain different valuable bio-active compounds that have diverse applications (Chaubey et al., 2021; Ogungbenro et al., 2020). So these by-products could be a good source of organic bioactive compounds, which can be used as a source of green corrosion inhibitors. The use of these wastes as a source of corrosion inhibitor enhances the economic viability as well as minimizes environmental pressures (Bong et al., 2018; Skoronski et al., 2016). There are mainly three areas where wastes are generated abundantly, which also are sources of various valuable bioactive organic compounds having all the qualities of an ideal green corrosion inhibitor. These three categories of bio-waste are discussed below.

1.2.1 Food industrial waste

The solid wastes and the by-products of the food industries are getting used in numerous innovative applications, such as the protection of keratinocytes and fibroblasts against the oxidative environment with the help of grape pomace extract incorporated in phospholipid vesicles (Manca et al., 2016). The extract of red grapes pomaces was incorporated in polymer-associated liposomes to observe the protection capability against oxidative stress in Caco-2 cells and the gastrointestinal environment (Manconi et al., 2016). A combination of grape extract and propylene glycol-liposomes has also shown adequate protection against oxidative stress in human keratinocytes and 3T3 mouse fibroblasts (Castangia et al., 2017). Grape pomace, which is a by-product

TH-3102_146107038

of vinification, contains a high amount of bioactive compounds. Over 60 million tons of grapevine are produced per year, and Italy, France, and Spain are the leading countries in Europe. For that reason, grape pomace has an impactful application in the cosmetic and skin care industry due to its antioxidant, anti-hyperpigmentation, and antiaging activity. Grape seed also has skin depigmentation and antiaging activity (Hoss et al., 2021). According to recent estimates from FAOSTAT, the world's olive crop area was close to 10.5 Mha in 2018; in Spain, 2.5 Mha are devoted to this crop, which represents 23.8% of the total global output and places Spain as the world's top producer of olive trees. The primary solid by-product of olive oil extraction, making around 35–40% of the total weight of olives treated in the mill, is live oil pomace. Several authors have described using it as a raw material to create a variety of beneficial chemicals with health-improving qualities. The bioactivities of olive oil by-products have been characterized as containing antioxidant, antibacterial, antitumoral, anti-inflammatory, hypoglycaemic, anti-hypertensive, and anti-cholesterolemic properties, among others. The majority of these qualities are connected to the high concentration of biomolecules, with phenolic acids like hydroxytyrosol, tyrosol, verbascoside, oleuropein, oleacin, or oleocanthal and other substances being particularly significant (Gullón et al., 2020). Whey is a by-product of the dairy industry, which is a major water pollutant. Researchers found an eco-friendly method to combine the whey with four different water-dispersible biopolymers (xanthan gum, tragacanth, Arabic gum, and sodium alginate), phospholipid, and a natural antioxidant (gingerol) to produce biopolymer-whey liposomes loaded to heal intestinal wounds and neutralize oxidative stress (Rezvani et al., 2022). Interestingly, the grape extract was used to produce extract-SiO_2 nanocomposites by ball milling technique to develop a novel drug delivery system (Scano et al., 2018). Later on, the phyto complexes derived from grape seeds and stalk

TH-3102_146107038

embodied with different types of phospholipids transfersomes, hyalurosomes, and hyalo-transfersomes showed better efficacy in protecting against the oxidative stress on the skin (Manca et al., 2019). These solid by-products of the plant materials contain multiple organic compounds and are effective against oxidative damage. Hence, various agricultural solid wastes or by-products can be used as raw materials for corrosion inhibitors (Liao et al., 2018b; Salinas-Solano et al., 2018). In search of that, it has been noticed that tea is one such daily consumed beverage that has demand all over the world. As a result, there are enormous tea factories in almost every country, which produce a vast amount of solid waste. Studies have been done on the recycling of solid waste from tea factories, as these waste materials contain numerous phenolic compounds (Serdar et al., 2017). Since there are very few available studies on the usage of solid waste from the tea factory, the scope of research is high.

1.2.2 Agro by-product or waste

For the last few years, by-products from apple, pomegranate, olive, citrus material, and grapes have been used for the synthesis of phenolic and other bioactive compounds (El-Etre, 2007; Gu et al., 2018; Verma et al., 2018). In that context, purple rice, especially from Northeast India, has emerged as an attractive source of phenolic compounds. The purple rice bran is enriched with anthocyanin, which is a potent antioxidant (Das et al., 2018). Earlier studies have revealed that anthocyanin-containing bio-extract is an efficient natural corrosion inhibitor on metal surfaces as the structures of anthocyanin consist of heteroatoms and phenyl rings and are water-soluble (Thomas et al., 2020). The heteroatoms and phenyl rings were observed in imidazole-based 4,5-dihydroxy-4,5-di-p-tolylimidazolidine-2-thione (DHDTIT) and (3ar,6ar)-3a,6a-di-ptolyltetrahydroimidazo[4,5-d] imidazole-2,5(1 h,3h)-dithione (TTHIIDT), which

TH-3102_146107038

were found to be effective as green corrosion inhibitors on steel in both acidic and alkaline media. It was revealed that these compounds block the active corrosion sites due to the presence of various heteroatoms and benzene rings in their structures (Berdimurodov et al., 2021b, 2020).

1.2.3 Kitchen waste

One of the major waste resources is the domestic and industrial kitchen which is piling up day after day. In this regard, it has been discovered that banana (*Muss* spp.) is one of the critical crops which is widely consumed across the globe. As it is widely consumed, a large amount which is estimated to be around 125 million tons, is produced. Though Asian countries produce the highest quantity of bananas due to the high demand, they can not export (15–20%). 70-80% of the world's bananas are exported by Latin America and the Caribbean. So the waste of banana plants shows an immense possibility to be explored as a source of value-added products. Though people have been investigating the pulp, there are minimal pieces of literature available on the valorization of inflorescence. The inflorescence, or the banana flower, is a purple-red heart-shaped structure. It contains purple-colored bracts under which the male and female flowers are arranged (Lau et al., 2020). The bract is a potential source of polyphenolic compounds, especially anthocyanin (Alexandra Pazmio-Durán et al., 2001; Begum and Deka, 2017; Mathew and Negi, 2021). The ability of anthocyanin as an efficient corrosion inhibitor in acidic media has already been explored (Hadisaputra et al., 2019; Teng et al., 2021; Thomas et al., 2020).

Onion is also one of the most widely used ubiquitous crops, which has enormous applications in our daily life. But the concern is the increasing amount of generated waste each year across the globe. It has been reported that only developed countries

TH-3102_146107038

produce 100,000–500,000 tons of waste per year (Sharma et al., 2016). Interestingly, scientists have recently found that onion waste is a potential source of phenolic compounds and can be used in numerous applications like the synthesis of biosenols and nanoparticles, therapeutic purposes, etc. (Chia et al., 2018; Santhosh et al., 2020; Sharma et al., 2016). Onion waste is a potential source of various organic compounds like flavonoids, carbohydrates, fatty acids, vitamins, amino acids, etc. (Celano et al., 2021; Jang et al., 2013). Among these bio-organic compounds, quercetin is one of the most valuable compounds, which has a wide range of therapeutic novelties, high antioxidant activity, ability to form a complex with metal (Xu et al., 2019). Even recently, scholars have predicted the therapeutic potential of quercetin against COVID-19 disease, which is caused by a coronavirus (Derosa et al., 2021)

1.3 Knowledge gap

After the literature review, it was clear that solid waste from tea factories is an efficient source of phenolic compounds, like catechin, gallocatechin, epigallocatechin, and other bioactive compounds (Serdar et al., 2017). The purple rice bran as an agro by-product also was also abundant with anthocyanin (Das et al., 2018). Kitchen waste like banana flower bract and onion peel is the source of anthocyanin and quercetin (Alexandra Pazmio-Durán et al., 2001; Begum and Deka, 2017; Celano et al., 2021; Jang et al., 2013; Mathew and Negi, 2021). As all these bio-wastes contain a high amount of phenolic compounds, there was an enormous possibility to explore them as a source of green corrosion inhibitors. Among the various reasons, the usage of acid solution in industries for chemical cleaning, descaling, and pickling is very likely to cause corrosion on the metal parts of the industries. Generally, HCl and H_2SO_4 are two commonly used acids in industries for such uttered purposes, which are pernicious to

TH-3102_146107038

the metal parts as they induce metal oxidation by containing a high concentration of H^+. So depending on the existing literature, a few major lacunae were found, which are discussed below:

I. The usage of extract from bio-waste material as potential corrosion inhibitors and the characterization of the bio-extract from those waste materials is unexplored.

II. The corrosion inhibition efficiency of the extract from this biowaste is yet to be explored.

III. There is less information about the electro-kinetic study and the adsorption behavior of the bio-extract from these waste material

IV. The corrosion inhibition mechanism of the extracted compounds from waste material based on the experimental and theoretical studies has lots of scope to research.

1.4 Objectives

Considering the outlook of industrial application and the presence of phenolic compounds in solid waste from tea factories (food industrial waste), purple rice bran (agro-byproduct), banana flower bract, and onion peel (kitchen waste) were chosen to find their inhibition efficiency. However, as there are some lacunae in the literature, especially on boiler quality steel (BQ) steel in acidic media, the BQ steel samples were selected as the material of interest, and HCl and H_2SO_4 media were chosen as acidic electrolytes. To examine the inhibition efficiency of solid tea waste extract (STWE), purple rice bran extract (PRBE), banana flower bract extract (BBE), and onion peel extract (OPE), various experimental and theoretical investigations are required. So

TH-3102_146107038

based on the literature studied and the lacunae in the literature, the following objectives have been identified:

I. Extraction and characterization of green corrosion inhibitors from industrial waste, agricultural byproducts, and kitchen wastes using a sustainable, simple approach.

II. Electrochemical kinetic study of inhibitors on boiler quality steel study in acidic media to find out their corrosion rate and corrosion current.

III. Study on inhibition mechanism of the waste extracts on the boiler quality steel using electrochemical impedance spectroscopy.

IV. Adsorption kinetics of the inhibitors on the metal surface in different acidic media.

V. Theoretical studies of inhibitory molecules identified in the extract.

1.5 References:

Ahmad, Z., 2006. SELECTION OF MATERIALS FOR CORROSIVE ENVIRONMENT, in: Principles of Corrosion Engineering and Corrosion Control. Elsevier, pp. 479–549. https://doi.org/10.1016/B978-075065924-6/50010-6

Akbarinezhad, E., Ebrahimi, M., Sharif, F., Attar, M.M., Faridi, H.R., 2011. Synthesis and evaluating corrosion protection effects of emeraldine base PAni/clay nanocomposite as a barrier pigment in zinc-rich ethyl silicate primer. Prog. Org. Coatings 70, 39–44. https://doi.org/10.1016/j.porgcoat.2010.09.016

Al-Otaibi, M.S., Al-Mayouf, A.M., Khan, M., Mousa, A.A., Al-Mazroa, S.A., Alkhathlan, H.Z., 2014. Corrosion inhibitory action of some plant extracts on the corrosion of mild steel in acidic media. Arab. J. Chem. https://doi.org/10.1016/j.arabjc.2012.01.015

Alaoui, K., El Kacimi, Y., Galai, M., Touir, R., Dahmani, K., Harfi, A., Ebn Touhami, M., 2016. Anti-corrosive properties of polyvinyl-alcohol for carbon steel in hydrochloric acid media: Electrochemical and thermodynamic investigation. J. Mater. Environ. Sci. 7, 2389–2403.

Alaoui, Khaoula, Kacimi, Y. El, Galai, M., Dahmani, K., Touir, R., Harfi4, A. El, Touhami, M.E., 2016. Poly (1-phenylethene): As a Novel Corrosion Inhibitor for Carbon Steel / Hydrochloric Acid Interface. Anal. Bioanal. Electrochem. 8, 830–

TH-3102_146107038

847.

Alexandra Pazmio-Durán, E., Giusti, M.M., Wrolstad, R.E., Glória, M.B.A., 2001. Anthocyanins from banana bracts (Musa X paradisiaca) as potential food colorants. Food Chem. 73, 327–332. https://doi.org/10.1016/S0308-8146(00)00305-8

Ali, A.I., Mahrous, Y.S., 2017. Corrosion inhibition of C-steel in acidic media from fruiting bodies of: Melia azedarach L extract and a synergistic Ni2+ additive. RSC Adv. 7, 23687–23698. https://doi.org/10.1039/c7ra00111h

Bahadori, A., 2014. Design Considerations on Cathodic Protection for Buried Pipelines and Marine Structures, Cathodic Corrosion Protection Systems. https://doi.org/10.1016/b978-0-12-800274-2.00003-x

Barouni, K., Bazzi, L., Salghi, R., Mihit, M., Hammouti, B., Albourine, A., El Issami, S., 2008. Some amino acids as corrosion inhibitors for copper in nitric acid solution. Mater. Lett. 62, 3325–3327. https://doi.org/10.1016/j.matlet.2008.02.068

Barreto, L.S., Tokumoto, M.S., Guedes, I.C., De Melo, H.G., Amado, F.D.R., Capelossi, V.R., 2017. Evaluation of the anticorrosion performance of peel garlic extract as corrosion inhibitor for astm 1020 carbon steel in acidic solution. Rev. Mater. 22. https://doi.org/10.1590/S1517-707620170003.0186

Begum, Y.A., Deka, S.C., 2017. Stability of spray-dried microencapsulated anthocyanins extracted from culinary banana bract. Int. J. Food Prop. 20, 3135–3148. https://doi.org/10.1080/10942912.2016.1277739

Berdimurodov, E., Kholikov, A., Akbarov, K., Guo, L., 2021a. Experimental and theoretical assessment of new and eco–friendly thioglycoluril derivative as an effective corrosion inhibitor of St2 steel in the aggressive hydrochloric acid with sulfate ions. J. Mol. Liq. 335, 116168. https://doi.org/10.1016/j.molliq.2021.116168

Berdimurodov, E., Kholikov, A., Akbarov, K., Guo, L., 2021b. Inhibition properties of 4,5-dihydroxy-4,5-di-p-tolylimidazolidine-2-thione for use on carbon steel in an aggressive alkaline medium with chloride ions: Thermodynamic, electrochemical, surface and theoretical analyses. J. Mol. Liq. 327, 114813. https://doi.org/10.1016/j.molliq.2020.114813

Berdimurodov, E., Kholikov, A., Akbarov, K., Guo, L., Abdullah, A.M., Elik, M., 2021c. A gossypol derivative as an efficient corrosion inhibitor for St2 steel in 1 M HCl + 1 M KCl: An experimental and theoretical investigation. J. Mol. Liq. 328, 115475. https://doi.org/10.1016/j.molliq.2021.115475

Berdimurodov, E., Kholikov, A., Akbarov, K., Obot, I.B., Guo, L., 2021d. Thioglycoluril derivative as a new and effective corrosion inhibitor for low carbon steel in a 1 M HCl medium: Experimental and theoretical investigation. J. Mol. Struct. 1234, 130165. https://doi.org/10.1016/j.molstruc.2021.130165

Berdimurodov, E., Kholikov, A., Akbarov, K., Xu, G., Abdullah, A.M., Hosseini, M.,

TH-3102_146107038

2020. New anti-corrosion inhibitor (3ar,6ar)-3a,6a-di-p-tolyltetrahydroimidazo[4,5-d]imidazole-2,5(1 h,3h)-dithione for carbon steel in 1 M HCl medium: gravimetric, electrochemical, surface and quantum chemical analyses. Arab. J. Chem. 13, 7504–7523. https://doi.org/10.1016/j.arabjc.2020.08.025

Bong, C.P.C., Lim, L.Y., Lee, C.T., Klemeš, J.J., Ho, C.S., Ho, W.S., 2018. The characterisation and treatment of food waste for improvement of biogas production during anaerobic digestion – A review. J. Clean. Prod. 172, 1545–1558. https://doi.org/10.1016/j.jclepro.2017.10.199

Castangia, I., Marongiu, F., Manca, M.L., Pompei, R., Angius, F., Ardu, A., Fadda, A.M., Manconi, M., Ennas, G., 2017. Combination of grape extract-silver nanoparticles and liposomes: A totally green approach. Eur. J. Pharm. Sci. 97, 62–69. https://doi.org/10.1016/j.ejps.2016.11.006

Celano, R., Docimo, T., Piccinelli, A.L., Gazzerro, P., Tucci, M., Di Sanzo, R., Carabetta, S., Campone, L., Russo, M., Rastrelli, L., 2021. Onion peel: Turning a food waste into a resource. Antioxidants 10, 1–18. https://doi.org/10.3390/antiox10020304

Chakrabarty, T., Pérez-Manríquez, L., Neelakanda, P., Peinemann, K.V., 2017. Bioinspired tannic acid-copper complexes as selective coating for nanofiltration membranes. Sep. Purif. Technol. 184, 188–194. https://doi.org/10.1016/j.seppur.2017.04.043

Chaubey, N., Savita, Qurashi, A., Chauhan, D.S., Quraishi, M.A., 2021. Frontiers and advances in green and sustainable inhibitors for corrosion applications: A critical review. J. Mol. Liq. 321, 114385. https://doi.org/10.1016/j.molliq.2020.114385

Chauhan, L.R., Gunasekaran, G., 2007. Corrosion inhibition of mild steel by plant extract in dilute HCl medium. Corros. Sci. https://doi.org/10.1016/j.corsci.2006.08.012

Chia, P.W., Lim, B.S., Yong, F.S.J., Poh, S.C., Kan, S.Y., 2018. An efficient synthesis of bisenols in water extract of waste onion peel ash. Environ. Chem. Lett. 16, 1493–1499. https://doi.org/10.1007/s10311-018-0764-1

Chunling, L., Xiyu, Z., Meng, C., Tengfang, Z., Shuangqing, S., Songqing, H., 2021. Application of hollow mesoporous organosilica nanoparticles as pH and redox double stimuli-responsive nanocontainer in the controlled release of corrosion inhibitor molecules. Prog. Org. Coatings 159, 106437. https://doi.org/10.1016/j.porgcoat.2021.106437

da Rocha, J.C., da Cunha Ponciano Gomes, J.A., D'Elia, E., 2010. Corrosion inhibition of carbon steel in hydrochloric acid solution by fruit peel aqueous extracts. Corros. Sci. 52, 2341–2348. https://doi.org/10.1016/j.corsci.2010.03.033

Das, A.B., Goud, V. V., Das, C., 2018. Extraction and characterization of phenolic content from purple and black rice (Oryza sativa L) bran and its antioxidant activity. J. Food Meas. Charact. 12, 332–345. https://doi.org/10.1007/s11694-017-9645-8

TH-3102_146107038

Derosa, G., Maffioli, P., D'Angelo, A., Di Pierro, F., 2021. A role for quercetin in coronavirus disease 2019 (COVID-19). Phyther. Res. 35, 1230–1236. https://doi.org/10.1002/ptr.6887

Dhawan, S.K., S, A.K., Bhandari, H., Bisht, B.M.S., Khatoon, F., 2015. Development of Highly Hydrophobic and Anticorrosive Conducting Polymer Composite Coating for Corrosion Protection in Marine Environment. Am. J. Polym. Sci. 5, 7–17. https://doi.org/10.5923/s.ajps.201501.02

El-Etre, A.Y., 2007. Inhibition of acid corrosion of carbon steel using aqueous extract of olive leaves. J. Colloid Interface Sci. 314, 578–583. https://doi.org/10.1016/j.jcis.2007.05.077

El Faydy, M., Galai, M., Touir, R., El Assyry, A., Ebn Touhami, M., Benali, B., Lakhrissi, B., Zarrouk, A., 2016. Experimental and theoretical studies for steel XC38 corrosion inhibition in 1 M HCl by N-(8-hydroxyquinolin-5-yl)-methyl)-N-phenylacetamide. J. Mater. Environ. Sci. 7, 1406–1416.

Errahmany, N., Rbaa, M., Abousalem, A.S., Tazouti, A., Galai, M., Kafssaoui, E.H. El, Touhami, M.E., Lakhrissi, B., Touir, R., 2020. Experimental, DFT calculations and MC simulations concept of novel quinazolinone derivatives as corrosion inhibitor for mild steel in 1.0 M HCl medium. J. Mol. Liq. 312, 113413. https://doi.org/10.1016/j.molliq.2020.113413

Esmailzadeh, S., Aliofkhazraei, M., Sarlak, H., 2018. Interpretation of Cyclic Potentiodynamic Polarization Test Results for Study of Corrosion Behavior of Metals: A Review. Prot. Met. Phys. Chem. Surfaces 54, 976–989. https://doi.org/10.1134/S207020511805026X

Feng, L., Zhang, S., Qiang, Y., Xu, S., Tan, B., Chen, S., 2018. The synergistic corrosion inhibition study of different chain lengths ionic liquids as green inhibitors for X70 steel in acidic medium. Mater. Chem. Phys. 215, 229–241. https://doi.org/10.1016/j.matchemphys.2018.04.054

G., C., F., A., 2014. Corrosion Inhibitors – Principles, Mechanisms and Applications, in: Developments in Corrosion Protection. InTech, pp. 1–161. https://doi.org/10.5772/57255

Galai, M., Ouassir, J., Ebn Touhami, M., Nassali, H., Benqlilou, H., Belhaj, T., Berrami, K., Mansouri, I., Oauki, B., 2017. α-Brass and (α + β) Brass Degradation Processes in Azrou Soil Medium Used in Plumbing Devices. J. Bio- Tribo-Corrosion 3, 1–15. https://doi.org/10.1007/s40735-017-0087-y

Galai, M., Rbaa, M., Ouakki, M., Abousalem, A.S., Ech-chihbi, E., Dahmani, K., Dkhireche, N., Lakhrissi, B., EbnTouhami, M., 2020. Chemically functionalized of 8-hydroxyquinoline derivatives as efficient corrosion inhibition for steel in 1.0 M HCl solution: Experimental and theoretical studies. Surfaces and Interfaces 21, 100695. https://doi.org/10.1016/j.surfin.2020.100695

Gomez, H., Ram, M.K., Alvi, F., Stefanakos, E., Kumar, A., 2010. Novel synthesis, characterization, and corrosion inhibition properties of nanodiamond-polyaniline films. J. Phys. Chem. C 114, 18797–18804. https://doi.org/10.1021/jp106379e

TH-3102_146107038

Gu, X.F., Chang, X.F., Cheng, C., Zhang, L., Zhang, Y.M., Zhang, J., Chen, G., 2018. Anti-corrosion and Anti-bacteria Property of Modified Pomegranate Peel Extract. IOP Conf. Ser. Mater. Sci. Eng. 322. https://doi.org/10.1088/1757-899X/322/2/022004

Gullón, P., Gullón, B., Astray, G., Carpena, M., Fraga-Corral, M., Prieto, M.A., Simal-Gandara, J., 2020. Valorization of by-products from olive oil industry and added-value applications for innovative functional foods. Food Res. Int. 137, 109683. https://doi.org/10.1016/j.foodres.2020.109683

Hadisaputra, S., Abhi Purwoko, A., Hamdiani, S., Nuryono, N., 2019. Which anthocyanin is the best corrosion inhibitor? IOP Conf. Ser. Mater. Sci. Eng. 509, 012129. https://doi.org/10.1088/1757-899X/509/1/012129

Hansson, C.M., 2011. The Impact of Corrosion on Society. Metall. Mater. Trans. A 42, 2952–2962. https://doi.org/10.1007/s11661-011-0703-2

Hoss, I., Rajha, H.N., El Khoury, R., Youssef, S., Manca, M.L., Manconi, M., Louka, N., Maroun, R.G., 2021. Valorization of Wine-Making By-Products' Extracts in Cosmetics. Cosmetics 8, 109. https://doi.org/10.3390/cosmetics8040109

Jang, M., Asnin, L., Nile, S.H., Keum, Y.S., Kim, H.Y., Park, S.W., 2013. Ultrasound-assisted extraction of quercetin from onion solid wastes. Int. J. Food Sci. Technol. https://doi.org/10.1111/j.1365-2621.2012.03180.x

Javaherdashti, R., 2000. How corrosion affects industry and life. Anti-Corrosion Methods Mater. 47, 30–34. https://doi.org/10.1108/00035590010310003

Ji, G., Anjum, S., Sundaram, S., Prakash, R., 2015. Musa paradisica peel extract as green corrosion inhibitor for mild steel in HCl solution. Corros. Sci. 90, 107–117. https://doi.org/10.1016/j.corsci.2014.10.002

Kadiri, L., Galai, M., Ouakki, M., Essaadaoui, Y., Ouass, A., Cherkaoui, M., Rifi, E.-H., Lebkiri, A., 2018. Coriandrum Sativum.L Seeds Extract as a Novel Green Corrosion Inhibitor for Mild Steel in 1.0 M Hydrochloric and 0.5 M Sulfuric Solutions. Anal. Bioanal. Electrochem. 10, 249–268.

Kamaruzzaman, W.M.I.W.M., Nasir, N.A.M., Hamidi, N.A.S.M., Yusof, N., Shaifudin, M.S., Suhaimi, A.M.A.A.M., Badruddin, M.A., Adnan, A., Nik, W.M.N.W., Ghazali, M.S.M., 2022. 25 years of progress on plants as corrosion inhibitors through a bibliometric analysis using the Scopus database (1995–2020). Arab. J. Chem. 15, 103655. https://doi.org/10.1016/j.arabjc.2021.103655

Keramatinia, M., Ramezanzadeh, B., Mahdavian, M., 2019. Green production of bioactive components from herbal origins through one-pot oxidation/polymerization reactions and application as a corrosion inhibitor for mild steel in HCl solution. J. Taiwan Inst. Chem. Eng. 105, 134–149. https://doi.org/10.1016/j.jtice.2019.10.005

Koch, G., Varney, J., Thompson, N., Moghissi, O., Gould, M., Payer, J., 2016. International Measures of Prevention, Application, and Economics of Corrosion Technologies Study.

TH-3102_146107038

Lau, B.F., Kong, K.W., Leong, K.H., Sun, J., He, X., Wang, Z., Mustafa, M.R., Ling, T.C., Ismail, A., 2020. Banana inflorescence: Its bio-prospects as an ingredient for functional foods. Trends Food Sci. Technol. 97, 14–28. https://doi.org/10.1016/j.tifs.2019.12.023

Li, H., Qiang, Y., Zhao, W., Zhang, S., 2021. 2-Mercaptobenzimidazole-inbuilt metal-organic-frameworks modified graphene oxide towards intelligent and excellent anti-corrosion coating. Corros. Sci. 191, 109715. https://doi.org/10.1016/j.corsci.2021.109715

Liao, L.L., Mo, S., Luo, H.Q., Li, N.B., 2018a. Corrosion protection for mild steel by extract from the waste of lychee fruit in HCl solution: Experimental and theoretical studies. J. Colloid Interface Sci. 520, 41–49. https://doi.org/10.1016/j.jcis.2018.02.071

Liao, L.L., Mo, S., Luo, H.Q., Li, N.B., 2018b. Corrosion protection for mild steel by extract from the waste of lychee fruit in HCl solution: Experimental and theoretical studies. J. Colloid Interface Sci. 520, 41–49. https://doi.org/10.1016/j.jcis.2018.02.071

M'hiri, N., Veys-Renaux, D., Rocca, E., Ioannou, I., Boudhrioua, N.M., Ghoul, M., 2016. Corrosion inhibition of carbon steel in acidic medium by orange peel extract and its main antioxidant compounds. Corros. Sci. 102, 55–62. https://doi.org/10.1016/j.corsci.2015.09.017

Mahmoudian, M.R., Alias, Y., Basirun, W.J., 2012. Effect of narrow diameter polyaniline nanotubes and nanofibers in polyvinyl butyral coating on corrosion protective performance of mild steel. Prog. Org. Coatings 75, 301–308. https://doi.org/10.1016/j.porgcoat.2012.08.004

Manca, M.L., Firoznezhad, M., Caddeo, C., Marongiu, F., Escribano-Ferrer, E., Sarais, G., Peris, J.E., Usach, I., Zaru, M., Manconi, M., Fadda, A.M., 2019. Phytocomplexes extracted from grape seeds and stalks delivered in phospholipid vesicles tailored for the treatment of skin damages. Ind. Crops Prod. 128, 471–478. https://doi.org/10.1016/j.indcrop.2018.11.052

Manca, M.L., Marongiu, F., Castangia, I., Catalán-Latorre, A., Caddeo, C., Bacchetta, G., Ennas, G., Zaru, M., Fadda, A.M., Manconi, M., 2016. Protective effect of grape extract phospholipid vesicles against oxidative stress skin damages. Ind. Crops Prod. 83, 561–567. https://doi.org/10.1016/j.indcrop.2015.12.069

Manconi, M., Marongiu, F., Castangia, I., Manca, M.L., Caddeo, C., Tuberoso, C.I.G., D'hallewin, G., Bacchetta, G., Fadda, A.M., 2016. Polymer-associated liposomes for the oral delivery of grape pomace extract. Colloids Surfaces B Biointerfaces 146, 910–917. https://doi.org/10.1016/j.colsurfb.2016.07.043

Mathew, N.S., Negi, P.S., 2021. Phenolic content and anti-oxidative attributes of various parts of wild banana (Ensete superbum Roxb. Cheesman) plant. J. Food Biochem. 45, 1–13. https://doi.org/10.1111/jfbc.13657

Mechbal, N., Bouhrim, M., Bnouham, M., Hammouti, B., Karzazi, Y., Kaya, S., Serdaroğlu, G., 2021. Anticorrosive and antioxidant effect of the aqueous extract

TH-3102_146107038

of the leaves, flowers, and stems of Cistus monspeliensis L: Experimental and computational study. J. Mol. Liq. 331. https://doi.org/10.1016/j.molliq.2021.115771

Mostafaei, A., Nasirpouri, F., 2014. Epoxy/polyaniline-ZnO nanorods hybrid nanocomposite coatings: Synthesis, characterization and corrosion protection performance of conducting paints. Prog. Org. Coatings 77, 146–159. https://doi.org/10.1016/j.porgcoat.2013.08.015

Mourya, P., Banerjee, S., Rastogi, R.B., Singh, M.M., 2013. Inhibition of mild steel corrosion in hydrochloric and sulfuric acid media using a thiosemicarbazone derivative. Ind. Eng. Chem. Res. 52, 12733–12747. https://doi.org/10.1021/ie4012497

Ogungbenro, A.E., Quang, D. V., Al-Ali, K.A., Vega, L.F., Abu-Zahra, M.R.M., 2020. Synthesis and characterization of activated carbon from biomass date seeds for carbon dioxide adsorption. J. Environ. Chem. Eng. 8, 104257. https://doi.org/10.1016/j.jece.2020.104257

Ostovari, A., Hoseinieh, S.M., Peikari, M., Shadizadeh, S.R., Hashemi, S.J., 2009. Corrosion inhibition of mild steel in 1 M HCl solution by henna extract: A comparative study of the inhibition by henna and its constituents (Lawsone, Gallic acid, α-d-Glucose and Tannic acid). Corros. Sci. 51, 1935–1949. https://doi.org/10.1016/j.corsci.2009.05.024

Ouakki, M., Galai, M., Rbaa, M., Abousalem, A.S., Lakhrissi, B., Rifi, E.H., Cherkaoui, M., 2020. Investigation of imidazole derivatives as corrosion inhibitors for mild steel in sulfuric acidic environment: experimental and theoretical studies. Ionics (Kiel). 26, 5251–5272. https://doi.org/10.1007/s11581-020-03643-0

Palanisamy, G., 2019. Corrosion Inhibitors, in: Corrosion Inhibitors. IntechOpen, pp. 1–24. https://doi.org/10.5772/intechopen.80542

Prabakaran, M., Kim, S.H., Hemapriya, V., Chung, I.M., 2016a. Evaluation of polyphenol composition and anti-corrosion properties of Cryptostegia grandiflora plant extract on mild steel in acidic medium. J. Ind. Eng. Chem. 37, 47–56. https://doi.org/10.1016/j.jiec.2016.03.006

Prabakaran, M., Kim, S.H., Hemapriya, V., Chung, I.M., 2016b. Tragia plukenetii extract as an eco-friendly inhibitor for mild steel corrosion in HCl 1 M acidic medium. Res. Chem. Intermed. 42, 3703–3719. https://doi.org/10.1007/s11164-015-2240-x

Qiang, Y., Li, H., Lan, X., 2020. Self-assembling anchored film basing on two tetrazole derivatives for application to protect copper in sulfuric acid environment. J. Mater. Sci. Technol. 52, 63–71. https://doi.org/10.1016/j.jmst.2020.04.005

Qiang, Y., Zhang, S., Tan, B., Chen, S., 2018. Evaluation of Ginkgo leaf extract as an eco-friendly corrosion inhibitor of X70 steel in HCl solution. Corros. Sci. 133, 6–16. https://doi.org/10.1016/j.corsci.2018.01.008

Raja, P.B., Sethuraman, M.G., 2008. Natural products as corrosion inhibitor for metals

TH-3102_146107038

in corrosive media - A review. Mater. Lett. 62, 113–116. https://doi.org/10.1016/j.matlet.2007.04.079

RIZZO, C.M., 2008. Maintenance of aged ships and offshore structures, in: Condition Assessment of Aged Structures. Elsevier, pp. 430–458. https://doi.org/10.1533/9781845695217.5.430

Rezvani, M., Manca, M.L., Muntoni, A., De Gioannis, G., Pedraz, J.L., Gutierrez, G., Matos, M., Fadda, A.M., Manconi, M., 2022. From process effluents to intestinal health promotion: Developing biopolymer-whey liposomes loaded with gingerol to heal intestinal wounds and neutralize oxidative stress. Int. J. Pharm. 613, 121389. https://doi.org/10.1016/j.ijpharm.2021.121389

Salghi, R., Jodeh, S., Ebenso, E.E., Lgaz, H., Ben Hmamou, D., Belkhaouda, M., Ali, I.H., Messali, M., Hammouti, B., Fattouch, S., 2017. Inhibition of C-steel corrosion by green tea extract in hydrochloric solution. Int. J. Electrochem. Sci. 12, 3283–3295. https://doi.org/10.20964/2017.04.46

Salinas-Solano, G., Porcayo-Calderon, J., Martinez de la Escalera, L.M., Canto, J., Casales-Diaz, M., Sotelo-Mazon, O., Henao, J., Martinez-Gomez, L., 2018. Development and evaluation of a green corrosion inhibitor based on rice bran oil obtained from agro-industrial waste. Ind. Crops Prod. 119, 111–124. https://doi.org/10.1016/j.indcrop.2018.04.009

Santhosh, A., Theertha, V., Prakash, P., Smitha Chandran, S., 2020. From waste to a value added product: Green synthesis of silver nanoparticles from onion peels together with its diverse applications. Mater. Today Proc. 0–3. https://doi.org/10.1016/j.matpr.2020.09.680

Scano, A., Ebau, F., Manca, M.L., Cabras, V., Cesare Marincola, F., Manconi, M., Pilloni, M., Fadda, A.M., Ennas, G., 2018. Novel drug delivery systems for natural extracts: The case study of Vitis Vinifera extract-SiO2 nanocomposites. Int. J. Pharm. 551, 84–96. https://doi.org/10.1016/j.ijpharm.2018.08.057

Schofield, M.J., 2001. Corrosion, in: Plant Engineer's Handbook. Elsevier, pp. 961–985. https://doi.org/10.1016/B978-075067328-0/50055-0

Serdar, G., Demir, E., Sökmen, M., 2017. Recycling of Tea Waste: Simple and Effective Separation of Caffeine and Catechins by Microwave Assisted Extraction (MAE). Int. J. Second. Metab. 4, 78–78. https://doi.org/10.21448/ijsm.288226

Shabani-Nooshabadi, M., Ghandchi, M.S., 2015. Santolina chamaecyparissus extract as a natural source inhibitor for 304 stainless steel corrosion in 3.5% NaCl. J. Ind. Eng. Chem. 31, 231–237. https://doi.org/10.1016/j.jiec.2015.06.028

Sharma, K., Mahato, N., Nile, S.H., Lee, E.T., Lee, Y.R., 2016. Economical and environmentally-friendly approaches for usage of onion (: Allium cepa L.) waste. Food Funct. https://doi.org/10.1039/c6fo00251j

Sin, H.L.Y., Umeda, M., Shironita, S., Rahim, A.A., Saad, B., 2017. Adenosine as corrosion inhibitor for mild steel in hydrochloric acid solution. Res. Chem. Intermed. 43, 1919–1934. https://doi.org/10.1007/s11164-016-2739-9

TH-3102_146107038

Singh, A., Dayu, X., Ituen, E., Ansari, K., Quraishi, M.A., Kaya, S., Lin, Y., 2020. Tobacco extracted from the discarded cigarettes as an inhibitor of copper and zinc corrosion in an ASTM standard D1141-98(2013) artificial seawater solution. J. Mater. Res. Technol. 9, 5161–5173. https://doi.org/10.1016/j.jmrt.2020.03.033

Singh, A., Ituen, E.B., Ansari, K.R., Chauhan, D.S., Quraishi, M.A., 2019. Surface protection of X80 steel using Epimedium extract and its iodide-modified composites in simulated acid wash solution: a greener approach towards corrosion inhibition. New J. Chem. 43, 8527–8538. https://doi.org/10.1039/C9NJ01691K

Singh, A., Lin, Y., Ebenso, E.E., Liu, W., Pan, J., Huang, B., 2015. Gingko biloba fruit extract as an eco-friendly corrosion inhibitor for J55 steel in CO<inf>2</inf> saturated 3.5% NaCl solution. J. Ind. Eng. Chem. https://doi.org/10.1016/j.jiec.2014.09.034

Singh, P., Quraishi, M.A., 2016. Corrosion inhibition of mild steel using Novel Bis Schiff's Bases as corrosion inhibitors: Electrochemical and Surface measurement. Measurement 86, 114–124. https://doi.org/10.1016/j.measurement.2016.02.052

Skoronski, E., De Oliveira, D.C., Fernandes, M., Da Silva, G.F., Magalhães, M.D.L.B., João, J.J., 2016. Valorization of agro-industrial by-products: Analysis of biodiesel production from porcine fat waste. J. Clean. Prod. 112, 2553–2559. https://doi.org/10.1016/j.jclepro.2015.10.026

Srivastava, M., Tiwari, P., Srivastava, S.K., Prakash, R., Ji, G., 2017. Electrochemical investigation of Irbesartan drug molecules as an inhibitor of mild steel corrosion in 1 M HCl and 0.5 M H2SO4 solutions. J. Mol. Liq. 236, 184–197. https://doi.org/10.1016/j.molliq.2017.04.017

Srivastava, V., Chauhan, D.S., Joshi, P.G., Maruthapandian, V., Sorour, A.A., Quraishi, M.A., 2018. PEG-Functionalized Chitosan: A Biological Macromolecule as a Novel Corrosion Inhibitor. ChemistrySelect 3, 1990–1998. https://doi.org/10.1002/slct.201701949

Teng, Y., Zhang, W., Wang, M., Yu, C., Ma, Y., Bian, J., Yang, X., Zhang, D., 2021. Anthocyanin as sustainable and non-toxic corrosion inhibitor for mild steel in HCl media: Electrochemical, surface morphology and theoretical investigations. J. Mol. Liq. 344, 117721. https://doi.org/10.1016/j.molliq.2021.117721

Thomas, A., Prajila, M., Shainy, K.M., Joseph, A., 2020. A green approach to corrosion inhibition of mild steel in hydrochloric acid using fruit rind extract of Garcinia indica (Binda). J. Mol. Liq. 312, 113369. https://doi.org/10.1016/j.molliq.2020.113369

Vasyliev, G., Vorobyova, V., Zhuk, T., 2020. Raphanus sativus L. Extract as a Scale and Corrosion Inhibitor for Mild Steel in Tap Water. J. Chem. 2020. https://doi.org/10.1155/2020/5089758

Verma, C., Ebenso, E.E., Bahadur, I., Quraishi, M.A., 2018. An overview on plant extracts as environmental sustainable and green corrosion inhibitors for metals and alloys in aggressive corrosive media. J. Mol. Liq. 266, 577–590. https://doi.org/10.1016/j.molliq.2018.06.110

TH-3102_146107038

Vimalanandan, A., Lv, L.-P., Tran, T.H., Landfester, K., Crespy, D., Rohwerder, M., 2013. Redox-Responsive Self-Healing for Corrosion Protection. Adv. Mater. 25, 6980–6984. https://doi.org/10.1002/adma.201302989

Vorobyova, V., Skiba, M., 2021. Peach Pomace Extract as Efficient Sustainable Inhibitor for Carbon Steel Against Chloride-Induced Corrosion. J. Bio- Tribo-Corrosion 7, 1–11. https://doi.org/10.1007/s40735-020-00450-y

Xu, D., Hu, M.J., Wang, Y.Q., Cui, Y.L., 2019. Antioxidant activities of quercetin and its complexes for medicinal application. Molecules 24. https://doi.org/10.3390/molecules24061123

TH-3102_146107038

TH-3102_146107038

2

Materials and methods

TH-3102_146107038

TH-3102_146107038

Materials and methods

This chapter describes the reagents used, equipment employed, and experimental methods to synthesize, characterize and find out the inhibition efficiency of bio-mass extract as green corrosion inhibition. To accomplish the mentioned objectives of this research, the experimentation was designed systematically, following major steps: (i) preparation and characterization of the inhibitory extract, (ii) Preparation of test specimen and electrochemical set-up, (iii) performing gravimetric and electrochemical tests to find the inhibition efficiency, and (iv) theoretical experimentation to explore the optimized molecular structures of the inhibitory molecules and their structural compatibility with inhibition efficiency. The theories of the electrochemical tests are also discussed in brief.

TH-3102_146107038

2.1 Materials

1. Boiler quality (BQ) steel (ASTM A-537 grade B) was provided by (North Eastern Electric Power Corporation Limited (NEEPCO).

2. Ag/AgCl reference and platinum wire counter electrodes were purchased from M/s. Metrohm, India.

3. Emery papers of grade 320, 600, 1000, 1200, and 1500 grade were purchased from CUMI, Parry House, 3rd Floor, 43, Moore Street, Chennai - 600 001

2.1.1 Chemicals used

Name of chemical	Supplier	CAS No	Purity
Acetone	Merck, India, Ltd.	67-64-1	99.99%
Ethanol	Merck, India, Ltd.	64-17-5	99.99%
Sulfuric acid	Merck, India, Ltd.	7664-93-9	AR 98
Hydrochloric acid	Merck, India, Ltd.	1.93001.2521	AR 98

2.1.2 Instruments and equipment used

Name of Instrument	Make and model	Description
AFM	**Make:** Bruker, United States of America **Model:** Dimension Icon SPM	Atomic force microscopy (AFM) or scanning force microscopy (SFM) is a very-high-resolution type of scanning probe microscopy (SPM) with a resolution of fractions of Angstrom, which has more than 1000 times higher resolution when compared to the classical optical microscope. It has the abilities like force measurement, topographic imaging, and manipulation.
Analytical weighing balance	**Make:** Sartorius, Germany **Model:** BSA224S-CW	The complete range of weighing equipment: laboratory balances that excel in speed and

TH-3102_146107038

		accuracy, mass comparators for determination of mass at the highest level of accuracy
Centrifuge	**Make:** REMI, India **Model:** R24	A centrifuge is a piece of equipment that puts an object in rotation around a fixed axis (spins it in a circle), applying a potentially strong force perpendicular to the axis of spin (outward). The centrifuge works using the sedimentation principle, where the centripetal acceleration causes denser substances and particles to move outward in the radial direction. At the same time, objects that are less dense are displaced and move to the center. In a laboratory centrifuge that uses sample tubes, the radial acceleration causes denser particles to settle to the bottom of the tube, while low-density substances rise to the top.
Corrosion Cell	Indigenous	Useful For performing the electrochemical experiments
FESEM-EDX	**Make:** ZEISS, Germany **Model:** Sigma	Energy-dispersive X-ray spectroscopy (EDS, EDX, EDXS or XEDS), sometimes called energy dispersive X-ray analysis (EDXA) or energy dispersive X-ray microanalysis (EDXMA), is an analytical technique used for the elemental analysis or chemical characterization of a sample. It relies on interaction of some source of X-ray excitation and a sample.
Freeze-dryer	**Make:** Christ, Germany **Model:** Alpha 2-4 LDplus	This equipment removes water from the sample using lyophilization or cryodesiccation, which is a low-temperature dehydration process under vacuum condition. The process includes three steps as Freezing, primary

TH-3102_146107038

		drying (Sublimation), and secondary drying (Adsorption).
Micropipette	**Make:** Eppendorf, Germany **Model:** 3120000.941	Micropipettes are utilized in the laboratory to transfer small quantities of liquid, usually down to 0.1 uL. They are most commonly used in chemistry, biology, forensic, pharmaceutical, and drug discovery labs, among others.
Potentiostat	**Make:** M/s. Metrohm Autolab B.V., Netherlands **Model:** Autolab PGSTAT302N	A potentiostat is an electronic hardware required to control a three-electrode cell and run most electroanalytical experiments. A Bipotentiostat and polypotentiostat are potentiostats capable of controlling two working electrodes and more than two working electrodes, respectively. This equipment is fundamental to modern electrochemical studies using three electrode systems for investigations of reaction mechanisms related to redox chemistry and other chemical phenomena.
Rotary-evaporator	**Make:** Buchi, Switzerland **Model:** Rotavapor® R-300	The Rotary-evaporator is an equipment which is used to remove the solvent from the solution through evaporation under reduced pressure. The solvent vapor travels into the cooler water condenser, where it condenses and drips into a separate receiving flask.

TH-3102_146107038

2.2 Methodology

To accomplish the mentioned objectives of this research, the experimentation was designed systematically. The structure of the experimentation includes the following major steps:

I. Preparation and characterization of the inhibitory extract.

II. Preparation of test specimen.

III. Performing Weight-loss experiments to measure inhibition efficiency.

IV. Design of electrochemical set-up.

V. Performing electrochemical experiments to measure the inhibition efficiencies and study the corrosion kinetics and mechanism.

VI. Theoretical studies to explore the optimized molecular structures of the inhibitory molecules and their structural compatibility with inhibition efficiency.

This uttered experimentation procedure was followed for each inhibitor, viz. solid tea waste extract (STWE), purple rice bran extract (PRBE), banana flower bract extract (BBE), and onion peel extract (OPE). The detailed experimental procedures are discussed below:

2.2.1 Preparation of green corrosion inhibitor (extract)

2.2.1.1 Solid tea waste extract (STWE)

Solid tea waste was collected from M/s. Sindhu Tea Pvt. Ltd, Golaghat (26.2078° N and 92.406° E) in the state of Assam, India. The waste materials were ground and stored at - 4°C. The STWE was prepared from solid tea waste (10 g) in 100 mL of deionized water (resistivity: 18.2 MΩ.cm) by the conventional extraction process using magnetic stirring at 40°C (313 K) for 24 h. After that, solid materials were filtered

TH-3102_146107038

out, and the filtrate was collected and centrifuged at 1556 RCF for 5 mins to remove the residual solids. The supernatant liquid, which is the extract of the solid tea waste, was collected and evaporated using the freeze-drying process to obtain the crude phenolic compounds containing solid. This crude solid (named as STWE) was used as a corrosion inhibitor at different concentrations in 1 (M) HCl solution.

2.2.1.2 Purple rice bran extract (PRBE)

Chakhao Poireiton, one of the commonly found purple rice cultivars in Imphal (24.8074°N and 93.9384°E), Manipur, North-East India, was collected from the local market. Rice bran was obtained by polishing the rice in a dehusking machine, and it was immediately packaged in zip-lock bags and kept at room temperature (28±2 °C) until needed. The extract was prepared by a conventional extraction process using a magnetic stirrer from purple rice bran in an ethanol-water solution. The optimal condition for extraction were 8.75 (mL g^{-1}) solvent to solid (purple rice bran) ratio, 43.74% (v/v) ethanol concentration, 37.5 °C temperature, and 22.5 min of extraction time. The extract solution was then filtered using filter paper (Whatman No.2), and the filtrate was kept in a freeze dryer for 24 h to evaporate the solvent. After 24 h, the solid residue was collected and preserved, which was used as an inhibitor (PRBE) in acidic media for various studies (Das et al., 2018).

2.2.1.3 Banana flower bract extract (BBE)

The fresh banana inflorescence was purchased from the local market of Amingaon (26.1847° N, and 91.6672° E), Guwahati, Assam, India. The outer bracts were separated from the inflorescence and washed properly to remove the dust. Then the bracts were dried for 8 hours at a constant temperature of 55°C to keep their phenolic content intact. As the binary ethanol-water solvent has more polarity than pure water or absolute ethanol (Lohvina et al., 2021; Sun et al., 2015), the dried powder was

TH-3102_146107038

extracted in 80% ethanol (1: 10) and placed in an ultrasonic bath (35 kHz) for 15 mins. The extract was collected after filtering out the slurry through Whatman filter paper (Whatman No. 2; Whatman, Kent, UK). The ethanol from the solvent of the extract was evaporated using a rotary evaporator, and the water was evaporated through a freeze-drying or lyophilization process. Before freeze-drying, the extract was stored at -20°C (Begum and Deka, 2019; Mathew and Negi, 2021). Once the freeze-drying was accomplished, dried solid residues were collected and used as an inhibitor (BBE).

2.2.1.4 Onion peel extract (OPE)

The onion peels were obtained from the kitchen wastes of Brahmaputra Hostel, Indian Institute of Technology, Guwahati, India (26.1445° N, 91.7362° E). The peels were then dried in a hot air oven at 60 °C for 10 h until the moisture contents were 4%-5% (w/w) and powdered using a mixer grinder. To obtain the ethanolic extract, 20 g of dried onion peels were mixed with 200 mL of 70% (v/v) ethanol and heated for 3 h at 60 °C in a water bath. After carrying out two extractions of the same slurry, the filtrate was collected using a Whatman No. 2 filter paper (Whatman, UK). Later, the filtrate was evaporated using a rotary evaporator and lyophilized using a freeze-dryer for 24 h, and the remaining solid residue was preserved at -20 °C, which was later used as a natural inhibitor (OPE) (Lee et al., 2014).

2.2.2 Characterization of inhibitor

2.2.2.1 Solid tea waste extract (STWE)

The STWE was analyzed using LC-MS to identify the main compounds present in the crude STWE extract. The powdered STWE was dissolved in deionized (resistivity: 18.2 mΩ.cm) water and was analyzed using an auto-sampler (3000 rapid separation LC, Dionex Inc., Sunnyvale, CA, USA) connected to an MS (Q Exactive™

TH-3102_146107038

Plus Hybrid Planet-Orbitrap™, Thermo Fisher Scientific) which is associated with an electrospray ionization (ESI) interface to ionize the sample. A hyper sail gold C-18 column with the dimensions of 2.1 mm × 100 mm × 1.9 µm was employed at 25°C for chromatographic separation. The solvents used as a mobile phase were 0.1% formic acid (solvent A) and 100% acetonitrile (solvent B). The gradient profile was applied as B 5% (2 min), B 90% (20 min), B 90% (25 min), B 5% (30 min) at a flow rate of 0.3 $mLmin^{-1}$. The fractions after elution were scanned from 150 to 2000 amu (m/z) in both positive and negative. Different compounds were identified by finding the specific peaks of mass-to-charge ratio (m/z) with the help of Xcalibur 3.1 software. Every peak with a specific m/z indicates a particular compound (Mata-Bilbao et al., 2007).

2.2.2.2 Purple rice bran extract (PRBE)

All the nonpolar compounds and the carotenoids were filtered out from the extracted sample using Whatman No.2 filter paper. Then the sample volume was adjusted to a total volume of 50 mL by adding Millipore water, and also pH of that solution was adjusted to 7.0. Thereafter to perform the HPLC analysis, 10 mL was taken from the solution. The characterization of PRBE to identify phenolic compounds which are present in the extract is accomplished by HPLC (Make: Ms. Thermo Fisher Scientific, USA; Model: Ultimate 3000 LC), equipped with a UV detector at 280 nm and 360 nm. To obtain the HPLC profile 20 µL of the sample was carried at a flow rate of 1.5 mL min^{-1} through a C18 column (5 µm, 120 Å, 4.6 × 250 mm) at 25 °C. In the mobile phase, the acidified water of pH 2.64 was used as eluent A, and acidified water: acetonitrile (20:80) was used as eluent B. The compounds were identified by respective peaks and compared those peaks with the peaks of pure compounds with the help of the software chameleon of version 6.80 (Das et al., 2018).

TH-3102_146107038

2.2.2.3 Banana flower bract extract (BBE)

The characterization of BBE was accomplished by liquid chromatography-mass spectrometry (LC-MS) to identify the phenolic compounds in the extract. 1g of dried extract was dissolved into 10 mL HPLC grade methanol and filtered through a nylon filter (0.45 µm). Then the sample was injected into an LC-MS system (LC/MS, 1260 Infinity LC, and 6410 Triple Quadrupole MS, Agilent Technologies, USA) to obtain the chromatogram. An electrospray ionization (ESI) was assembled with a mass spectrometer to ionize the sample. The filtered sample was passed through a ZORBAX C18 column (2.1 × 50 mm^2, 3.5 µm) at a 30 °C constant temperature. The sample was injected into the column through a mobile phase, combining solvent A (formic acid 0.1%, in Milli- Q water) and solvent B (acetonitrile) at a flow rate of 0.20 mL min^{-1}. The elution gradient was as follows: initially, it was 98% A and 2% B and increased to 100% B in 8 mins. The sample volume was 2 µmL. The elute was passed through the Mass spectrometer and scanned in negative ionization mood in the m/z range of 50-1000 to obtain the mass spectra. The collision energy for the MS (nass spectra) accusation was 4.0 eV (Mathew and Negi, 2021).

2.2.2.4 Onion peel extract (OPE)

The OPE was characterized using liquid chromatography-mass spectrometry (LC/MS, 1260 Infinity LC, and 6410 Triple Quadrupole MS, Agilent Technologies, USA) to detect the phenolic compounds in the onion peel. 1g of dried extract powder was dissolved in 10 mL of Milli-Q water (resistivity: 18.2 MΩ cm) and kept in the ultrasonic bath for 15 min. Then the solution was filtered using a nylon filter (0.2 µm) and diluted. The sample was passed through the ZORBAX C18 column (2.1 × 50 mm^2, 3.5 µm) column (maintained at 35 °C) using mobile phase A (water + 0.1% formic acid) and mobile phase B (100% water) at a flow rate of 200 µL min^{-1}. The elution

TH-3102_146107038

gradient profile was used as follows: 2% B (0–3 min), 2–13% B (3–5 min), 13% B (5–9 min), 13–18% B (9–12 min), 18% B (12–13 min), 18–30% B (13–17 min), 30–50% B, (17–21 min), 50–98% B (21–22 min), 98% B (22–27 min). After elution, the mass spectra of the analytes were obtained by scanning the m/z ratio from 50 to 950 in negative ionization mode at 300°C of capillary temperature (Bedrníček et al., 2020; Celano et al., 2021).

2.2.3 Preparation of test specimen

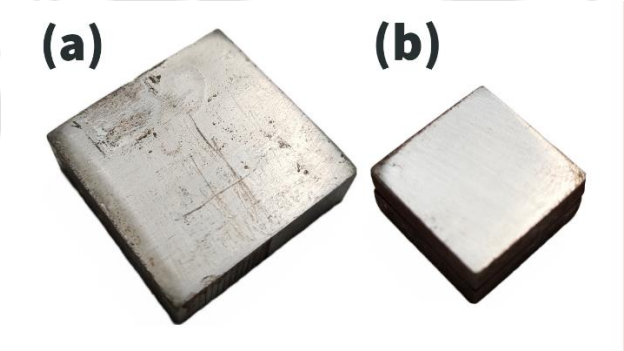

Fig. 2.1 Test specimens for weight loss and electrochemical experiments.

All of the tests were conducted using boiler quality steel of ASTM A-537, Grade B, which has the following composition: C: 0.24%; S: 0.025%; Cu: 0.38%; Si: 0.55%; Mn: 1.72%; P: 0.025%. The BQ steel was cut into pieces of 3 × 3 × 1 cm^3 dimensions (Fig. 2.1(a)) for the weight loss method whereas pieces of 2 × 2× 1 cm^3 dimensions (Fig. 2.1(b)) were used for electrochemical experiments as the working electrode. Before performing each experiment, the exposed areas of the metal coupons were abraded by sandpapers of different grit sizes (320, 600, 1000, 1200, and 1500) and then polished on a disc polisher (Make: Ms. Chennai Metco Pvt Ltd., India; Model: Bainpol-VT) with the help of alumina paste. The coupons were washed with acetone and double distilled water to degrease and remove the dust particles before experiments (Pal and Das, 2020). The samples were dried and stored in a desiccator before performing the

TH-3102_146107038

tests (ASTM G1) (Ali Asaad et al., 2018; Singh and Quraishi, 2016b; Varvara et al., 2017).

2.2.4 Gravimetric analysis (weight loss method)

The corrosion rate was measured crudely by the weight loss method in a specific environment. The corrosion rate of BQ samples were measured using the weight loss method by immersing them in 1 (M) HCl and 0.5 (M) of H_2SO_4 separately at room temperature (28 ± 2 °C) for 72 h, both in the absence and presence of different inhibitor concentrations (100, 200, 300, 400, and 500 mg L^{-1} of STWE in 1 M HCl and 50, 100, 150, and 200 mg L^{-1} of PRBE, BBE and OPE in both 1 M HCl and 0.5 M H_2SO_4). The BQ samples were washed with deionized water and acetone each time before and after the immersion to remove all the debris from the surface as per the ASTM G1. The weight before and after immersion was measured by weighing balance (Make: Sartorius; Model: BSA4S-cW) (ASTM G1). These initial and final weights were used to calculate the corrosion rate using the following expression:

$$\boldsymbol{CR = \frac{87600W}{At\rho}} \qquad \textbf{2.1}$$

Where CR represents the corrosion rate (millimeter per year or mmpy), W represents weight loss (g), A represents effective area (cm^2), t represents exposure time (h), and ρ represents the density (g cm^{-3}), which was assumed 7.86 g cm^{-3} In order to calculate the corrosion rate the density of the BQ was assumed as (Zhao et al., 2017).

The inhibition efficiency ($\mu_{CR}\%$) values of PRBE was calculated using the following equation:

$$\boldsymbol{\mu_{CR}\% = \frac{w_o - w_i}{w_o} \times 100} \qquad \textbf{2.2}$$

Where, w_o (g) and w_i (g) represents the weight loss values of the BQ specimen in the acidic solution without and with inhibitor, respectively (Pal and Das, 2020).

TH-3102_146107038

2.2.5 Fabrication of electrochemical cell and set-up

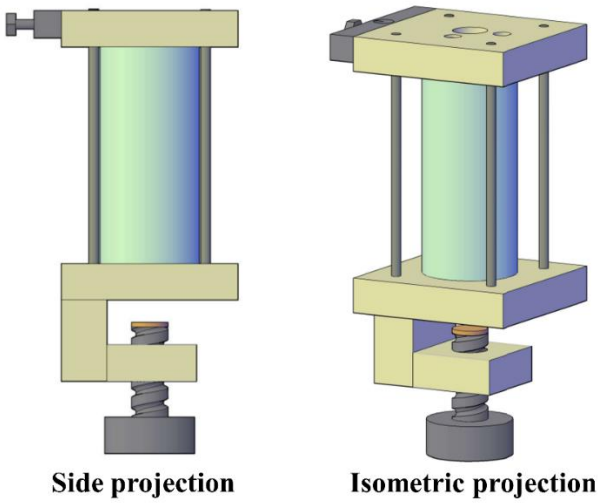

Fig. 2.2 Graphical representation of the electrochemical cell (reactor)

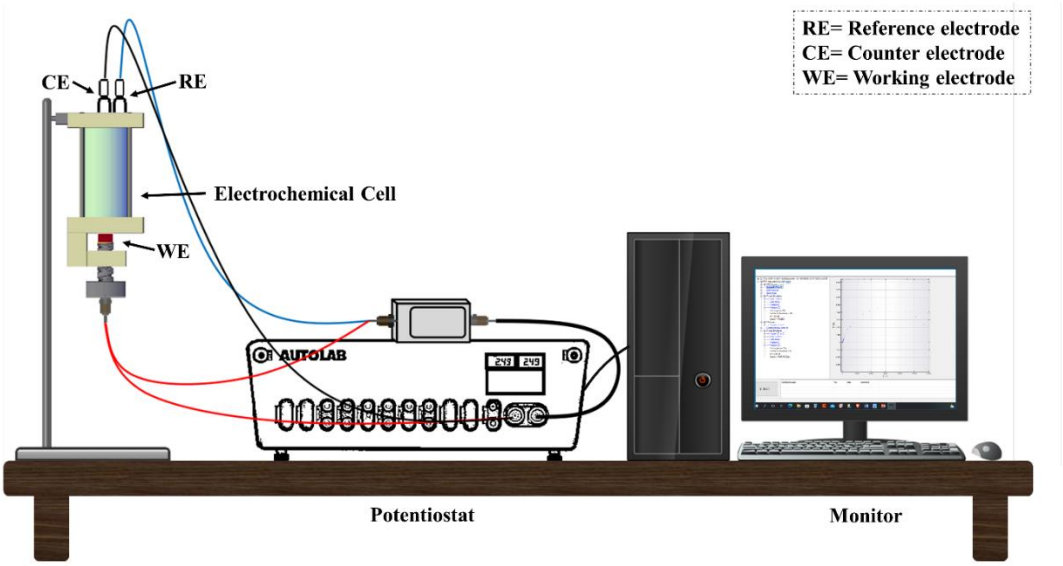

Fig. 2.3 Graphical representation of electrochemical setup

All the electrochemical measurements were performed in a three-electrode cell configuration. The corrosion cell or electrochemical cell (200 mL) was a flat bottom flask built with Flexi glass. The design of this cell was indigenous (Fig. 2.2). Mainly, the cell was designed in such a way that there was a provision to insert three electrodes. The three electrodes were the reference electrode of Ag/AgCl (saturated with 3 M KCl),

TH-3102_146107038

the counter electrode of platinum wire, and a working electrode (test specimen of BQ steel) having a working area of 1 cm^2. The reference and counter electrodes used to be inserted from the top, and the working electrode used to be fitted at the bottom of the cell. The total volume of the cell is 500ml. All these electrodes were connected to a workstation (Autolab Potentiostat/Galvanostat (PGSTAT302N) to perform various electrochemical experiments. There is an opening on the top of the cell, which is used to pour the electrolyte solution (Fig. 2.3).

2.2.6 Electrochemical measurements

All the electrodes were fitted into the electrochemical cell so that the surfaces of the electrodes were exposed to the acidic solution. Before every experiment, the electrodes were washed and polished with sandpaper, as mentioned in section 2.4.3. This cell used to be filled up with electrolyte solutions. The series of electrochemical experiments were performed in the absence and presence of 100, 200, 300, 400, and 500 mg L^{-1} of STWE in 1 M HCl media and 50, 100, 150, and 200 mg L^{-1} of PRBE, BBE, and OPE in both 1 M HCl and 0.5 M H_2SO_4 without. This electrochemical setup was connected to a workstation (Autolab Potentiostat/Galvanostat (PGSTAT302N) to accomplish the following electrochemical experiments.

2.2.6.1 Open circuit potential measurements

Before performing each experiment of Tafel polarization and EIS, the working electrode surface was exposed to an acidic electrolyte solution and left unperturbed for 60 minutes without applying any external current to attain a steady-state condition and stable open circuit potential (OCP). The average OCP values were measured in the presence and the absence of PRBE in both HCl and H_2SO_4 and used as a fixed potential for the measurement of impedance as a function of time. (Salinas-Solano et al., 2018).

TH-3102_146107038

2.2.6.2 Potentiodynamic polarization measurements

Potentiodynamic polarization measurements were accomplished at a scan rate of 1 mVs^{-1} ranging from -250 mV vs. Ag/AgCl to +250 mV vs. Ag/AgCl with respect to OCP. Different electrochemical kinetics parameters, such as corrosion current density(i_{corr}), corrosion potential (E_{corr}), cathodic Tafel slope (b_c) and anodic Tafel slope (b_a) were obtained by the extrapolation of the Tafel curves. (Naghi Tehrani et al., 2021a).

2.2.6.2.1 Theoretical consideration

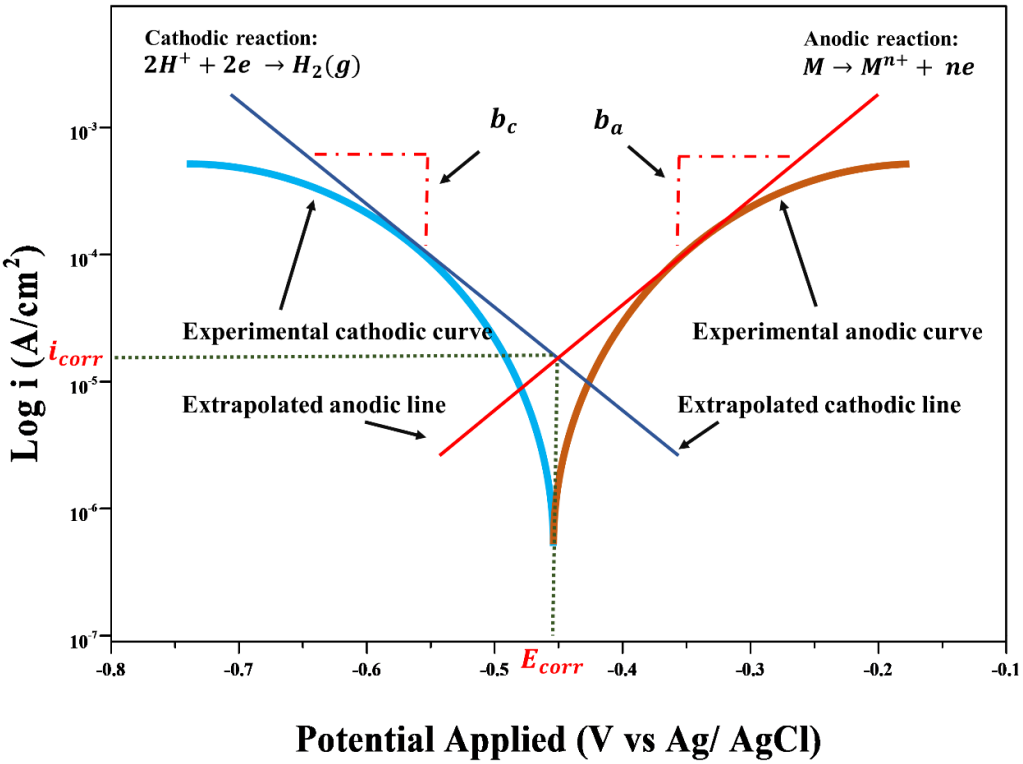

Note: I_{corr} = *Corrosion current,* E_{corr} = *corrosion potential,* b_a = *anodic slope,* b_c = *cathodic slope*

Fig. 2.4 Pictorial representation of Potentiodynamic Polarization curve (Tafel plot)

The corrosion rate is dependent on anodic (oxidation) and cathodic (reduction) reactions. According to that Faraday's law the linear relationship between corrosion current (i_{corr}) and corrosion rate (CR) is as follows

TH-3102_146107038

$$\boldsymbol{CR = \frac{M}{nF\rho} i_{corr}} \quad \textbf{2.3}$$

Where M is the atomic weight of the metal, n represents the charge number which actually means the number of electrons exchanged in reaction, F is the Faraday constant (96.485 C mol^{-1}), ρ is the density of the metal, M/n ration sometimes also known as equivalent weight. When there is no external potential is applied to the system, the equilibrium potential is assumed as the Open Circuit Potential (OCP). In most electrochemical corrosion experiments, the first step is the measurement of Open Circuit Potential. It is very important to measure the OCP and allows sufficient time for the potential to stabilize before beginning the electrochemical experiment. A stable OCP is taken to indicate that the system being studied has reached a steady state. Sometimes the OCP and corrosion potential are interchangeable. Polarizing is basically forcing the potential to move away from OCP. Then the response (sample) of the polarized sample is measured. The potential is applied to both anodic and cathodic directions to have the anodic current and cathodic current. As corrosion is an anodic and cathodic reaction process, the rate of corrosion is controlled by kinetics electron transfer (Kakaei et al., 2019; Mansfeld, 2005). A reaction controlled by electron transfer kinetics follows the Tafel equation, which is as follows:

$$\boldsymbol{i = i_0 e^{2.303 \frac{E - E_{corr}}{b}}} \quad \textbf{2.4}$$

Where $\boldsymbol{i}$ is measured current density, $\boldsymbol{i_0}$ is a reaction-dependent constant called the exchange current density, b is Tafel constant (*V/decade*), applied potential and the corrosion potential are denoted by E and E_{corr} respectively. The Tafel equation describes the isolated reaction, whereas corrosion is a combination of anodic and cathodic reactions. So Tafel equations for both anodic and cathodic processes are combined to get the Butler-Volmer equation. Under a charge transfer condition, the

TH-3102_146107038

potential of anodic and cathodic reactions on the working electrode is related to the current density (Zhang et al., 2009). This relationship is given by the Butler-Volmer equation (Eq. 2.5), from which the other electrochemical parameters can be measured.

$$\boldsymbol{i = i_a + i_c = i_{corr}\left(e^{2.203\frac{\eta}{b_a}} - e^{-2.303\frac{\eta}{b_c}}\right)} \quad \textbf{2.5}$$

$$\boldsymbol{\eta = E - E_{corr}} \quad \textbf{2.6}$$

The above equations express that the overpotential η is related to the measured current density (i), which helps to calculate the corrosion rate. i_a and i_c are anodic and cathodic current density, respectively. The overpotential is nothing but the difference between the applied potential (E) and the corrosion potential (E_{corr}). The corrosion potential, E_{corr} is assumed as OCP of corroding metal and i_{corr}, can be measured directly from the experimental data by finding out the Tafel anodic (b_a) and cathodic slopes (b_c) of the experimental curves.

When the anodic potential is large ($\eta/b_a >> 1$) the simplified Butler-Volmer equation for the anodic reaction is as follows:

$$\boldsymbol{\eta = \log(i_{corr}) + b_a.log(i)} \quad \textbf{2.7}$$

Analogously, when the cathodic potential is found to be large ($\eta/b_c << -1$), then the equation for the cathodic reaction is simplified as follows:

$$\boldsymbol{\eta = log(i_{corr}) + b_c.log(i)} \quad \textbf{2.8}$$

Conventionally, the Tafel plots are portrayed as semi-logarithmic plots (Fig. 2.4). The logarithm of absolute current is plotted against potential though theoretically, the anodic and cathodic currents are predicted as a straight line for the variation with potential. A curved line used to appear as the current is the total current, which is nothing but the sum of anodic and cathodic current.

TH-3102_146107038

The inhibition efficiency (μ_p) at different concentrations of PRBE, and $\mu_{R_{ct}}$ was computed from corrosion current density by the following equation:

$$\mu_P\% = \frac{I^o_{corr} - I^i_{corr}}{I^o_{corr}} \times 100 \qquad \textbf{2.9}$$

Where, I^i_{corr} and I^o_{corr} represent corrosion current density in the presence and absence of the PRBE, respectively (Eq. 2.9).

2.2.6.3 Electrochemical impedance spectroscopy (EIS) measurement

The EIS measurement was carried out under steady-state conditions at OCP in the frequency range of 0.01 -10000 Hz with a peak amplitude of 10 mV, peak to peak (AC signal). The responses of frequencies in the absence and presence of inhibitors in acidic solutions of HCl and H_2SO_4 are demonstrated by the Nyquist plot and Bode plots. An effective electrochemical circuit was fitted to the Nyquist plots to measure various impedance parameters (Amin et al., 2007; Hong et al., 2002).

2.2.6.3.1 Theoretical Consideration

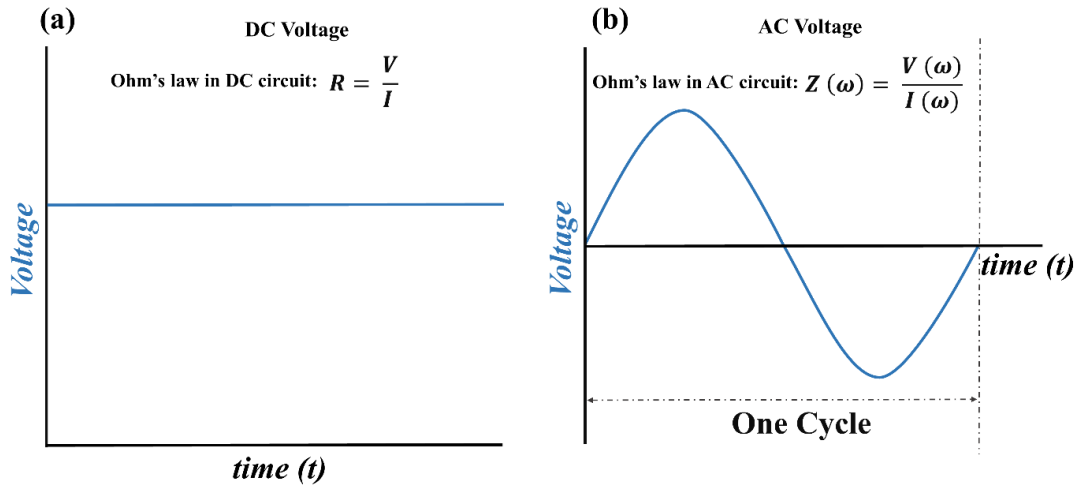

Fig. 2.5 Schematic diagram and equation showing Ohm's law for (a) DC circuit when DC voltage is applied and (b) AC circuit when AC voltage is applied.

TH-3102_146107038

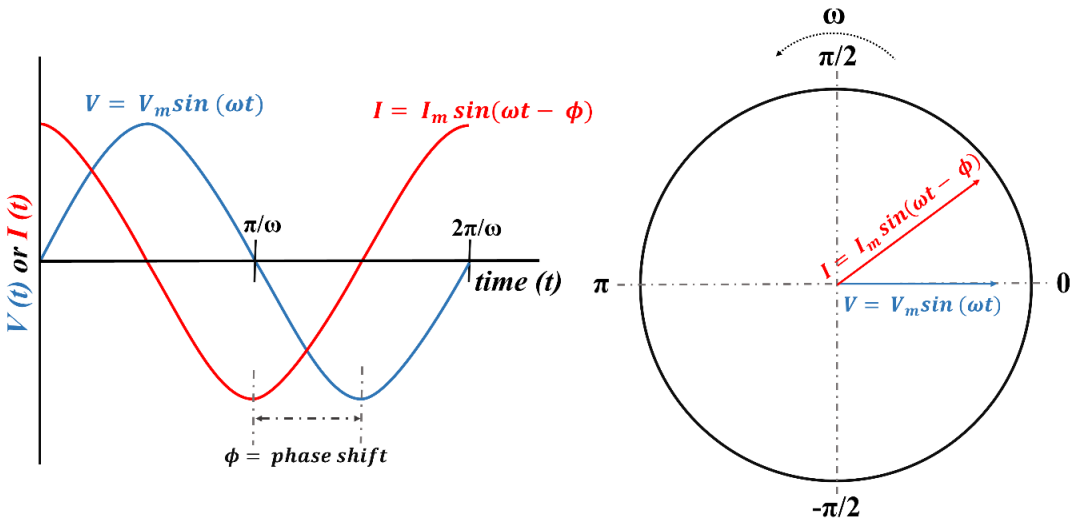

Fig. 2.6 The illustration and equations about the relationship between the voltage and current when AC voltage is applied with the angular frequency ω.

In EIS technique various circuit elements like capacitance (C) resistance (R) inductance (L) are measured by applying AC voltage in an electrochemical cell. When a DC voltage is applied, in any system, the voltage (V), resistance (R), and current (I) satisfy Ohm's law, as shown in Fig. 2.5(a). Similarly, when an AC voltage is applied to an electrochemical cell, the impedance interrupts the current flow. This impedance ($\omega = 2\pi f$ is the angular frequency of the applied AC voltage) can be expressed as $Z(\omega) = V(\omega)/I(\omega)$, which is the equation for Ohm's law in an AC circuit (Fig. 2.5(b)). These interruptions are represented by various circuit elements, such as resistors, inductors, and conductors, which constitute the overall impedance in a circuit. In an actual system, the electrochemical cell contains various circuit elements with diverse combinations. Thus, it is more accurate to use the concept of impedance than a circuit model consisting solely of a resistor to represent an electrochemical system. When potential is applied with angular frequency (ω), the response of voltage (V) and current (I) shows a phase difference (ϕ) (Fig. 2.6) (Choi et al., 2020; Laschuk et al.,

TH-3102_146107038

2021; Mei et al., 2018). The values of V and I be expressed as by the following equations where V_m and I_m are the maximum values of voltage and current:

$$\boldsymbol{V = V_m sin\,(\omega t)} \quad \textbf{2.10}$$

$$\boldsymbol{I = I_m\, sin(\omega t - \phi)} \quad \textbf{2.11}$$

The above equation can be expressed using a complex function $j = \sqrt{-1} = \exp\left(\frac{j\pi}{2}\right)$. So the above equation can be expressed as:

$$\boldsymbol{V = V_m exp\,(j\omega t)} \quad \textbf{2.12}$$

$$\boldsymbol{I = I_m \exp\,[j\,(\omega t - \phi)]} \quad \textbf{2.13}$$

As V and I obey ohm's law in AC circuit model, the impedance $Z(\omega)$ can be expressed as:

$$\boldsymbol{Z(\omega) = \frac{V(\omega)}{I(\omega)} = \frac{V_m exp\,(j\omega t)}{I_m \exp\,[j\,(\omega t - \phi)]} = \frac{V_m}{I_m}\, exp(j\phi)} \quad \textbf{2.14}$$

The above equation can be simplified using Euler's equation, $exp(j\phi) = \cos(\phi) + j\sin(\phi)$. So the equation becomes as follows:

$$\boldsymbol{Z(\omega) = \frac{V_m}{I_m}\, exp(j\phi) = \frac{V_m}{I_m}\,[\cos(\phi) + j\sin(\phi)] = Z_0\,[\cos(\phi) + j\sin(\phi)]} \quad \textbf{2.15}$$

This equation can be represented as an equation having a real and imaginary part which is given below:

$$\boldsymbol{Z(\omega) = Z_0 \cos\phi + Z_0 j \sin(\phi)} \quad \textbf{2.16}$$

On the basis of Eq. 2.16, the EIS data can be represented in two ways:

(i) **Nyquist plot** (Fig. 2.7 (a)) that represents the real and imaginary parts of $Z(\omega)$ using cartesian coordinates. In Eq. 2.16,

$Z_{real} = Z_0 \cos\phi$, that signifies R (resistance)

$Z_{img} = Z_0 j \sin(\phi)$, which signifies C(capacitance) + L (inductance)

TH-3102_146107038

(ii) **Bode plot** (Fig. 2.7(b)) that shows changes in the phase shift and magnitude changes in the applied frequency ranges. In Nyquist plot

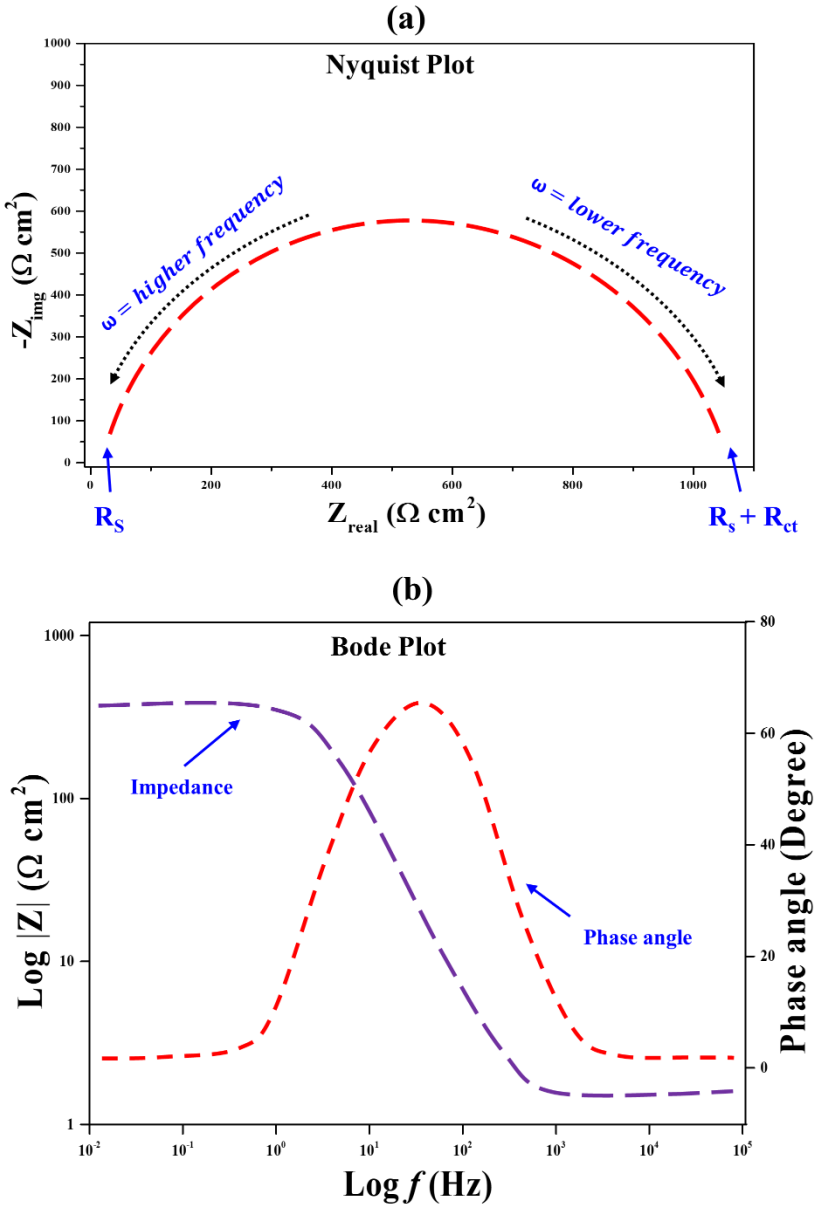

***Note**: R_s: solution resistance, R_{ct}: charge transfer resistance, f = frequency, ω = angular frequency. Z = impedance*

Fig. 2.7 Pictorial representation of Nyquist and Bode plot from EIS study.

Nyquist plots (Fig. 2.7(a)) and bode plots (Fig. 2.7(b)) are two important plots of the EIS study which express the responses of impedance on each frequency. The EIS data were fitted to a simple equivalent circuit to obtain various EIS parameters. The

TH-3102_146107038

circuit contains various electrical elements, such as capacitors, resistors, and inductors which are significant in explaining the physical electrochemistry of the system. The capacitor in the circuit does not behave ideally, especially when the system is not homogenous. The lack of homogeneity on the surface under investigation is modeled with an element called constant phase element (CPE) replacing a capacitor. The CPE in the modeled electrochemical circuit is expressed in terms of various elements of the circuit based on the following formula:

$$\boldsymbol{Z_{CPE} = \frac{1}{Y_o(j\omega)^n}} \qquad \textbf{2.17}$$

Where the impedance of the CPE is denoted as Z_{CPE}, Y_0 represents constant of CPE and admittance (ideal capacitor), n is CPEexponent (or the phase shift) which provides the information regarding surface heterogeneity and has a value from 0 to 1. ω is the angular frequency ($\omega = 2\pi f$) in rad s^{-1}, and j represents the imaginary number. Based on the value of n, the CPE will reflect in such a way that when $n = 0$, $Y_o = R$ (resistance); $n = +1$, $Y_o = C$ (capacitance); $n = -1$, $Y_o = L$ (inductance) and $n = 0.5$, $Y_o = W$ (Warburg impedance). The double-layer capacitance (C_{dl}) of CPE belonging to the modeled circuit on the BQ steel/electrolyte can be evaluated from Y_o, ω_{max} and C_{dl} (Eq. 2.18).

$$\boldsymbol{C_{dl} = \frac{Y_o}{(\omega_{max})^{n-1}}} \qquad \textbf{2.18}$$

ω_{max} (rad s^{-1}) is considered as the angular frequency at which the imaginary part of the impedance is maximum in the Nyquist plot (Galai et al., 2020; M'hiri et al., 2016; Srivastava et al., 2018a; Verma et al., 2018b).

The inhibition efficiency ($\mu_{R_{ct}}$) was also computed from charge transfer resistance using the following equation:

TH-3102_146107038

$$\mu_{R_{ct}}\% = \frac{R_{ct}^{i} - R_{ct}^{0}}{R_{ct}^{i}} \times 100 \quad \textbf{2.19}$$

R_{ct}^{i} and R_{ct}^{0} represent charge transfer resistance on the surface of BQ in inhibited and uninhibited conditions, respectively. R_{ct}^{i} and R_{ct}^{0} were derived from the impedance data of EIS studies.

2.2.7 Adsorption studies

The adsorption isotherms and thermodynamic adsorption parameters are necessary to understand the basic principle of the adsorption process and the type of adsorption. To obtain the fundamental interaction between the adsorbate (inhibitor) and the adsorbent (metallic surface), a few commonly employed adsorption isotherms (Langmuir, Temkin, and Frumkin) of corrosion studies were tested.

The thermodynamic parameter such as adsorption equilibrium constant (K_{ads}) and the adsorption-free energy (ΔG°_{ads}) were calculated using the following equations of the isotherms (Shabani-Nooshabadi and Ghandchi, 2015) :

Langmuir isotherm: $\boldsymbol{\theta/(1-\theta) = K_{ads}C}$ **2.20**

Temkin isotherm: $\boldsymbol{log\frac{\theta}{C} = LogK_{ads} - g\theta}$ **2.21**

Frumkin isotherm: $\boldsymbol{log\frac{\theta}{(1-\theta)C} = logK_{ads} + g\theta}$ **2.22**

where the concentration of inhibitor (C), and surface coverage (θ) were plotted in a straight-line equation to find out K_{ads} (De Souza et al., 2012; Shabani-Nooshabadi and Ghandchi, 2015).

Surface coverage (θ) was calculated from $\mu_{R_{ct}}\%$ by the following relationship:

$$\boldsymbol{\theta = \frac{\mu_{R_{ct}}\%}{100}} \quad \textbf{2.23}$$

TH-3102_146107038

K_{ads} is the adsorption equilibrium constant from which the adsorption free energy, also known as standard Gibbs free energy (ΔG°_{ads}) can be calculated using the following expression:

$$\Delta G^{\circ}_{ads} = -RTln(C_{water}K_{ads}) \quad \textbf{2.24}$$

Where R denotes the universal gas constant (8.314 $Jmol^{-1}K^{-1}$), the concentration of water (C_{water}) was considered 1000 gL^{-1} rather than 55.5 mol L^{-1} as the K_{ads} is expressed in Lg^{-1}, T is the absolute temperature (298.15 K) (Ali Asaad et al., 2018; Mourya et al., 2014a; Zhou and Zhou, 2014).

2.2.8 Surface characterization

Before each experiment, the surface test specimen used to be polished and washed with water and acetone as described in section 2.4.3.

2.2.8.1 Field emission scanning electron microscopy - Energy dispersive X-Ray analysis (FESEM-EDX)

The BQ steel samples were dipped in 1 (M) HCl and 0.5 (M) H_2SO_4 solution in the absence and presence of effective inhibitor concentration (500 mg L^{-1} of STWE and 200 mg L^{-1} of PRBE, BBE, OPE) for 24 h. Then to observe the changes on the surface under the field emission scanning electron microscope, microscopic images were collected (FESEM, Sigma, Zeiss). In order to observe the effect of inhibitors on the elementary composition of the BQ surface in the presence and absence of inhibitors, the same conditions were used for the energy dispersive X-Ray analysis (EDX) (Saxena et al., 2018a; Solmaz, 2014; Umoren, 2016).

2.2.8.2 Atomic force microscopy (AFM)

The topology of the BQ surface was examined by AFM Bruker Dimension Icon SPM to observe the effect of the inhibitors on the surface morphology. Before

TH-3102_146107038

experiments, the BQ coupons were immersed in 1(M) HCl and 0.5 (M) H_2SO_4 solution in the absence and presence of effective inhibitor concentration (500 mg L^{-1} of STWE and 200 mg L^{-1} of PRBE, BBE, OPE) for 3 h. Then the samples were tested at a frequency of 302 kHz in the air with tapping mode to obtain images of 50 μm × 50 μm area, and the average surface roughness was measured (Ali Asaad et al., 2018; Singh et al., 2016).

2.2.9 Theoretical studies by quantum chemical calculations

The quantum chemical calculations for the identified molecules of PRBE were accomplished using Gaussian 09W tools to attain their optimized structures and electron clouds which correlate with their efficiency of corrosion inhibition and interaction with the BQ surface. Density functional theory was applied for frequency optimization as well as the structures utilizing B3LYP functional along with 6-311G basis set. In the present analysis, the energy of the Frontier Molecular Orbital (FMO) was calculated and visualized in the images. Few selected quantum chemical parameters along with the lowest unoccupied molecular orbital (LUMO) and the highest occupied molecular orbital (HOMO), and the energy gap between HOMO and LUMO were also calculated (Eq. 2.25) (Ganash, 2018; Verma et al., 2018b, 2018c). The energy of HOMO energy (E_{HOMO}) and LUMO (E_{LUMO}) mean electron donation and acceptance power, respectively whereas the energy difference between LUMO and HOMO intimates the equilibrium of the interaction. (Feng et al., 2018).

$$\boldsymbol{E_{LUMO} - E_{HOMO} = \Delta E} \qquad \textbf{2.25}$$

Various other quantum chemical parameters which were computed are given by the following reactions.

$$\boldsymbol{-E_{HOMO} = I} \qquad \textbf{2.26}$$

TH-3102_146107038

$$-E_{LUMO} = A \quad \textbf{2.27}$$

$$\chi = -\frac{1}{2}(E_{LUMO} + E_{HOMO}) = \frac{I+A}{2} \quad \textbf{2.28}$$

$$\eta = \frac{1}{2}(E_{LUMO} - E_{HOMO}) = \frac{I-A}{2} \quad \textbf{2.29}$$

$$\sigma = \frac{1}{\eta} \quad \textbf{2.30}$$

$$\Delta N = \frac{\chi_{Fe}-\chi_{inh}}{2(\eta_{Fe}+\eta_{inh})} \quad \textbf{2.31}$$

Where ionization potential (I) and electron affinity (A) are directly related to E_{HOMO} and E_{LUMO} (Eq. 2.26 and Eq. 2.27) based on Koopman's theory. Various other quantum chemical descriptors, such as electronegativity (χ) (Eq. 2.28), global hardness (η) (Eq. 2.29), softness (σ) (Eq. 2.30) and the fraction of transferable electrons from inhibitor molecules to iron (ΔN) (Eq. 2.31) were computed using electronegativity and hardness. In this study, the theoretical values of χ_{Fe} and η_{Fe} were considered 7 eV and 0 eV, respectively (Belghiti et al., 2019a; Ganash, 2018; Liao et al., 2018a; Mechbal et al., 2021; Naghi Tehrani et al., 2021a; Srivastava et al., 2018a; Thomas et al., 2020; Verma et al., 2018c, 2018b).

The promising local reactive sites on the identified molecules in inhibitor molecules have been investigated by computing the Fukui indices, f_k^+ and f_k^- as indicators of the expected position of electrophilic and nucleophilic reactivity, respectively (Berdimurodov et al., 2021d; Galai et al., 2020; Oubaaqa et al., 2022; Verma et al., 2021). The finite difference (FD) approximation was applied to calculate the Fukui function as follows:

$$f_k^+ = q_k(N+1) - q_k(N) \quad \textbf{2.32}$$

$$f_k^- = q_k(N) - q_k(N-1) \quad \textbf{2.33}$$

TH-3102_146107038

In the above equations the $q_k(N+1)$, $q_k(N)$ and $q_k(N-1)$ represent the electron densities of any k atom in $N+1$, N, and $N-1$ electron system, respectively. Mulliken's gross charge was in place of electron densities. A second Fukui function (f_k^2) which is also known as a dual descriptor also provides information regarding chemical reactivity (Hsissou et al., 2021; Naghi Tehrani et al., 2021a). This can be calculated by the following equation:

$$f_k^2 = f_k^+ - f_k^- \qquad \textbf{2.34}$$

2.3 References:

Abdallah, M., Altass, H.M., Al-Gorair, A.S., Al-Fahemi, J.H., Jahdaly, B.A.A.L., Soliman, K.A., 2021. Natural nutmeg oil as a green corrosion inhibitor for carbon steel in 1.0 M HCl solution: Chemical, electrochemical, and computational methods. J. Mol. Liq. 323, 115036. https://doi.org/10.1016/j.molliq.2020.115036

Ahmad, Z., 2006. SELECTION OF MATERIALS FOR CORROSIVE ENVIRONMENT, in: Principles of Corrosion Engineering and Corrosion Control. Elsevier, pp. 479–549. https://doi.org/10.1016/B978-075065924-6/50010-6

Akbarinezhad, E., Ebrahimi, M., Sharif, F., Attar, M.M., Faridi, H.R., 2011. Synthesis and evaluating corrosion protection effects of emeraldine base PAni/clay nanocomposite as a barrier pigment in zinc-rich ethyl silicate primer. Prog. Org. Coatings 70, 39–44. https://doi.org/10.1016/j.porgcoat.2010.09.016

Al-Moubaraki, A.H., 2015. Corrosion Protection of Mild Steel in Acid Solutions Using Red Cabbage Dye. Chem. Eng. Commun. 202, 1069–1080. https://doi.org/10.1080/00986445.2014.907565

Al-Otaibi, M.S., Al-Mayouf, A.M., Khan, M., Mousa, A.A., Al-Mazroa, S.A., Alkhathlan, H.Z., 2014. Corrosion inhibitory action of some plant extracts on the corrosion of mild steel in acidic media. Arab. J. Chem. https://doi.org/10.1016/j.arabjc.2012.01.015

Alaoui, K., El Kacimi, Y., Galai, M., Touir, R., Dahmani, K., Harfi, A., Ebn Touhami, M., 2016. Anti-corrosive properties of polyvinyl-alcohol for carbon steel in hydrochloric acid media: Electrochemical and thermodynamic investigation. J. Mater. Environ. Sci. 7, 2389–2403.

Alaoui, Khaoula, Kacimi, Y. El, Galai, M., Dahmani, K., Touir, R., Harfi4, A. El, Touhami, M.E., 2016. Poly (1-phenylethene): As a Novel Corrosion Inhibitor for Carbon Steel / Hydrochloric Acid Interface. Anal. Bioanal. Electrochem. 8, 830–847.

Alexandra Pazmio-Durán, E., Giusti, M.M., Wrolstad, R.E., Glória, M.B.A., 2001.

TH-3102_146107038

Anthocyanins from banana bracts (Musa X paradisiaca) as potential food colorants. Food Chem. 73, 327–332. https://doi.org/10.1016/S0308-8146(00)00305-8

Ali, A.I., Mahrous, Y.S., 2017. Corrosion inhibition of C-steel in acidic media from fruiting bodies of: Melia azedarach L extract and a synergistic Ni2+ additive. RSC Adv. 7, 23687–23698. https://doi.org/10.1039/c7ra00111h

Ali Asaad, M., Sarbini, N.N., Sulaiman, A., Ismail, M., Huseien, G.F., Abdul Majid, Z., Bothi Raja, P., 2018. Improved corrosion resistance of mild steel against acid activation: Impact of novel Elaeis guineensis and silver nanoparticles. J. Ind. Eng. Chem. 63, 139–148. https://doi.org/10.1016/j.jiec.2018.02.010

Amin, M.A., Abd El-Rehim, S.S., El-Sherbini, E.E.F., Bayoumi, R.S., 2007. The inhibition of low carbon steel corrosion in hydrochloric acid solutions by succinic acid. Part I. Weight loss, polarization, EIS, PZC, EDX and SEM studies. Electrochim. Acta 52, 3588–3600. https://doi.org/10.1016/j.electacta.2006.10.019

Azmi, M.F., Soedarsono, J.W., 2018. Study of corrosion resistrance of pipeline API 5L X42 using green inhibitor bawang dayak (Eleutherine americanna Merr.) in 1M HCl. IOP Conf. Ser. Earth Environ. Sci. 105. https://doi.org/10.1088/1755-1315/105/1/012061

Bahadori, A., 2014. Design Considerations on Cathodic Protection for Buried Pipelines and Marine Structures, Cathodic Corrosion Protection Systems. https://doi.org/10.1016/b978-0-12-800274-2.00003-x

Barouni, K., Bazzi, L., Salghi, R., Mihit, M., Hammouti, B., Albourine, A., El Issami, S., 2008. Some amino acids as corrosion inhibitors for copper in nitric acid solution. Mater. Lett. 62, 3325–3327. https://doi.org/10.1016/j.matlet.2008.02.068

Barreto, L.S., Tokumoto, M.S., Guedes, I.C., De Melo, H.G., Amado, F.D.R., Capelossi, V.R., 2017. Evaluation of the anticorrosion performance of peel garlic extract as corrosion inhibitor for astm 1020 carbon steel in acidic solution. Rev. Mater. 22. https://doi.org/10.1590/S1517-707620170003.0186

Bedrníček, J., Jirotková, D., Kadlec, J., Laknerová, I., Vrchotová, N., Tříska, J., Samková, E., Smetana, P., 2020. Thermal stability and bioavailability of bioactive compounds after baking of bread enriched with different onion by-products. Food Chem. 319. https://doi.org/10.1016/j.foodchem.2020.126562

Begum, Y.A., Deka, S.C., 2019. Chemical profiling and functional properties of dietary fibre rich inner and outer bracts of culinary banana flower. J. Food Sci. Technol. 56, 5298–5308. https://doi.org/10.1007/s13197-019-04000-4

Begum, Y.A., Deka, S.C., 2017. Stability of spray-dried microencapsulated anthocyanins extracted from culinary banana bract. Int. J. Food Prop. 20, 3135–3148. https://doi.org/10.1080/10942912.2016.1277739

Belghiti, M.E., Echihi, S., Dafali, A., Karzazi, Y., Bakasse, M., Elalaoui-Elabdallaoui, H., Olasunkanmi, L.O., Ebenso, E.E., Tabyaoui, M., 2019a. Computational

TH-3102_146107038

simulation and statistical analysis on the relationship between corrosion inhibition efficiency and molecular structure of some hydrazine derivatives in phosphoric acid on mild steel surface. Appl. Surf. Sci. 491, 707–722. https://doi.org/10.1016/j.apsusc.2019.04.125

Belghiti, M.E., Echihi, S., Dafali, A., Karzazi, Y., Bakasse, M., Elalaoui-Elabdallaoui, H., Olasunkanmi, L.O., Ebenso, E.E., Tabyaoui, M., 2019b. Computational simulation and statistical analysis on the relationship between corrosion inhibition efficiency and molecular structure of some hydrazine derivatives in phosphoric acid on mild steel surface. Appl. Surf. Sci. https://doi.org/10.1016/j.apsusc.2019.04.125

Berdimurodov, E., Kholikov, A., Akbarov, K., Guo, L., 2021a. Experimental and theoretical assessment of new and eco–friendly thioglycoluril derivative as an effective corrosion inhibitor of St2 steel in the aggressive hydrochloric acid with sulfate ions. J. Mol. Liq. 335, 116168. https://doi.org/10.1016/j.molliq.2021.116168

Berdimurodov, E., Kholikov, A., Akbarov, K., Guo, L., 2021b. Inhibition properties of 4,5-dihydroxy-4,5-di-p-tolylimidazolidine-2-thione for use on carbon steel in an aggressive alkaline medium with chloride ions: Thermodynamic, electrochemical, surface and theoretical analyses. J. Mol. Liq. 327, 114813. https://doi.org/10.1016/j.molliq.2020.114813

Berdimurodov, E., Kholikov, A., Akbarov, K., Guo, L., Abdullah, A.M., Elik, M., 2021c. A gossypol derivative as an efficient corrosion inhibitor for St2 steel in 1 M HCl + 1 M KCl: An experimental and theoretical investigation. J. Mol. Liq. 328, 115475. https://doi.org/10.1016/j.molliq.2021.115475

Berdimurodov, E., Kholikov, A., Akbarov, K., Obot, I.B., Guo, L., 2021d. Thioglycoluril derivative as a new and effective corrosion inhibitor for low carbon steel in a 1 M HCl medium: Experimental and theoretical investigation. J. Mol. Struct. 1234, 130165. https://doi.org/10.1016/j.molstruc.2021.130165

Berdimurodov, E., Kholikov, A., Akbarov, K., Xu, G., Abdullah, A.M., Hosseini, M., 2020. New anti-corrosion inhibitor (3ar,6ar)-3a,6a-di-p-tolyltetrahydroimidazo[4,5-d]imidazole-2,5(1 h,3h)-dithione for carbon steel in 1 M HCl medium: gravimetric, electrochemical, surface and quantum chemical analyses. Arab. J. Chem. 13, 7504–7523. https://doi.org/10.1016/j.arabjc.2020.08.025

Biezma, M. V., San Cristóbal, J.R., 2005. Methodology to study cost of corrosion. Corros. Eng. Sci. Technol. 40, 344–352. https://doi.org/10.1179/174327805X75821

Bong, C.P.C., Lim, L.Y., Lee, C.T., Klemeš, J.J., Ho, C.S., Ho, W.S., 2018. The characterisation and treatment of food waste for improvement of biogas production during anaerobic digestion – A review. J. Clean. Prod. 172, 1545–1558. https://doi.org/10.1016/j.jclepro.2017.10.199

Cang, H., Fei, Z., Xiao, H., Huang, J., Xu, Q., 2012. Inhibition effect of reed leaves

TH-3102_146107038

extract on steel in hydrochloric acid and sulphuric acid solutions. Int. J. Electrochem. Sci. 7, 8869–8882.

Castangia, I., Marongiu, F., Manca, M.L., Pompei, R., Angius, F., Ardu, A., Fadda, A.M., Manconi, M., Ennas, G., 2017. Combination of grape extract-silver nanoparticles and liposomes: A totally green approach. Eur. J. Pharm. Sci. 97, 62–69. https://doi.org/10.1016/j.ejps.2016.11.006

Celano, R., Docimo, T., Piccinelli, A.L., Gazzerro, P., Tucci, M., Di Sanzo, R., Carabetta, S., Campone, L., Russo, M., Rastrelli, L., 2021. Onion peel: Turning a food waste into a resource. Antioxidants 10, 1–18. https://doi.org/10.3390/antiox10020304

Chakrabarty, T., Pérez-Manríquez, L., Neelakanda, P., Peinemann, K.V., 2017. Bioinspired tannic acid-copper complexes as selective coating for nanofiltration membranes. Sep. Purif. Technol. 184, 188–194. https://doi.org/10.1016/j.seppur.2017.04.043

Chaubey, N., Savita, Qurashi, A., Chauhan, D.S., Quraishi, M.A., 2021. Frontiers and advances in green and sustainable inhibitors for corrosion applications: A critical review. J. Mol. Liq. 321, 114385. https://doi.org/10.1016/j.molliq.2020.114385

Chauhan, L.R., Gunasekaran, G., 2007. Corrosion inhibition of mild steel by plant extract in dilute HCl medium. Corros. Sci. https://doi.org/10.1016/j.corsci.2006.08.012

Chia, P.W., Lim, B.S., Yong, F.S.J., Poh, S.C., Kan, S.Y., 2018. An efficient synthesis of bisenols in water extract of waste onion peel ash. Environ. Chem. Lett. 16, 1493–1499. https://doi.org/10.1007/s10311-018-0764-1

Choi, W., Shin, H.C., Kim, J.M., Choi, J.Y., Yoon, W.S., 2020. Modeling and applications of electrochemical impedance spectroscopy (Eis) for lithium-ion batteries. J. Electrochem. Sci. Technol. 11, 1–13. https://doi.org/10.33961/jecst.2019.00528

Chunling, L., Xiyu, Z., Meng, C., Tengfang, Z., Shuangqing, S., Songqing, H., 2021. Application of hollow mesoporous organosilica nanoparticles as pH and redox double stimuli-responsive nanocontainer in the controlled release of corrosion inhibitor molecules. Prog. Org. Coatings 159, 106437. https://doi.org/10.1016/j.porgcoat.2021.106437

da Rocha, J.C., da Cunha Ponciano Gomes, J.A., D'Elia, E., 2010. Corrosion inhibition of carbon steel in hydrochloric acid solution by fruit peel aqueous extracts. Corros. Sci. 52, 2341–2348. https://doi.org/10.1016/j.corsci.2010.03.033

Das, A.B., Goud, V. V., Das, C., 2018. Extraction and characterization of phenolic content from purple and black rice (Oryza sativa L) bran and its antioxidant activity. J. Food Meas. Charact. 12, 332–345. https://doi.org/10.1007/s11694-017-9645-8

De Souza, F.S., Giacomelli, C., Gonçalves, R.S., Spinelli, A., 2012. Adsorption behavior of caffeine as a green corrosion inhibitor for copper. Mater. Sci. Eng. C

TH-3102_146107038

32, 2436–2444. https://doi.org/10.1016/j.msec.2012.07.019

Derosa, G., Maffioli, P., D'Angelo, A., Di Pierro, F., 2021. A role for quercetin in coronavirus disease 2019 (COVID-19). Phyther. Res. 35, 1230–1236. https://doi.org/10.1002/ptr.6887

Dhawan, S.K., S, A.K., Bhandari, H., Bisht, B.M.S., Khatoon, F., 2015. Development of Highly Hydrophobic and Anticorrosive Conducting Polymer Composite Coating for Corrosion Protection in Marine Environment. Am. J. Polym. Sci. 5, 7–17. https://doi.org/10.5923/s.ajps.201501.02

El-Etre, A.Y., 2007. Inhibition of acid corrosion of carbon steel using aqueous extract of olive leaves. J. Colloid Interface Sci. 314, 578–583. https://doi.org/10.1016/j.jcis.2007.05.077

El Faydy, M., Galai, M., Touir, R., El Assyry, A., Ebn Touhami, M., Benali, B., Lakhrissi, B., Zarrouk, A., 2016. Experimental and theoretical studies for steel XC38 corrosion inhibition in 1 M HCl by N-(8-hydroxyquinolin-5-yl)-methyl)-N-phenylacetamide. J. Mater. Environ. Sci. 7, 1406–1416.

Errahmany, N., Rbaa, M., Abousalem, A.S., Tazouti, A., Galai, M., Kafssaoui, E.H. El, Touhami, M.E., Lakhrissi, B., Touir, R., 2020. Experimental, DFT calculations and MC simulations concept of novel quinazolinone derivatives as corrosion inhibitor for mild steel in 1.0 M HCl medium. J. Mol. Liq. 312, 113413. https://doi.org/10.1016/j.molliq.2020.113413

Esmailzadeh, S., Aliofkhazraei, M., Sarlak, H., 2018. Interpretation of Cyclic Potentiodynamic Polarization Test Results for Study of Corrosion Behavior of Metals: A Review. Prot. Met. Phys. Chem. Surfaces 54, 976–989. https://doi.org/10.1134/S207020511805026X

Feng, L., Zhang, S., Qiang, Y., Xu, S., Tan, B., Chen, S., 2018. The synergistic corrosion inhibition study of different chain lengths ionic liquids as green inhibitors for X70 steel in acidic medium. Mater. Chem. Phys. 215, 229–241. https://doi.org/10.1016/j.matchemphys.2018.04.054

G., C., F., A., 2014. Corrosion Inhibitors – Principles, Mechanisms and Applications, in: Developments in Corrosion Protection. InTech, pp. 1–161. https://doi.org/10.5772/57255

Galai, M., Ouassir, J., Ebn Touhami, M., Nassali, H., Benqlilou, H., Belhaj, T., Berrami, K., Mansouri, I., Oauki, B., 2017. α-Brass and (α + β) Brass Degradation Processes in Azrou Soil Medium Used in Plumbing Devices. J. Bio- Tribo-Corrosion 3, 1–15. https://doi.org/10.1007/s40735-017-0087-y

Galai, M., Rbaa, M., Ouakki, M., Abousalem, A.S., Ech-chihbi, E., Dahmani, K., Dkhireche, N., Lakhrissi, B., EbnTouhami, M., 2020. Chemically functionalized of 8-hydroxyquinoline derivatives as efficient corrosion inhibition for steel in 1.0 M HCl solution: Experimental and theoretical studies. Surfaces and Interfaces 21, 100695. https://doi.org/10.1016/j.surfin.2020.100695

Ganash, A.A., 2018. Theoretical and experimental studies of dried marjoram leaves

TH-3102_146107038

extract as green inhibitor for corrosion protection of steel substrate in acidic solution. Chem. Eng. Commun. 205, 350–362. https://doi.org/10.1080/00986445.2017.1391096

Gomez, H., Ram, M.K., Alvi, F., Stefanakos, E., Kumar, A., 2010. Novel synthesis, characterization, and corrosion inhibition properties of nanodiamond-polyaniline films. J. Phys. Chem. C 114, 18797–18804. https://doi.org/10.1021/jp106379e

Gu, X.F., Chang, X.F., Cheng, C., Zhang, L., Zhang, Y.M., Zhang, J., Chen, G., 2018. Anti-corrosion and Anti-bacteria Property of Modified Pomegranate Peel Extract. IOP Conf. Ser. Mater. Sci. Eng. 322. https://doi.org/10.1088/1757-899X/322/2/022004

Hadisaputra, S., Abhi Purwoko, A., Hamdiani, S., Nuryono, N., 2019. Which anthocyanin is the best corrosion inhibitor? IOP Conf. Ser. Mater. Sci. Eng. 509, 012129. https://doi.org/10.1088/1757-899X/509/1/012129

Hansson, C.M., 2011. The Impact of Corrosion on Society. Metall. Mater. Trans. A 42, 2952–2962. https://doi.org/10.1007/s11661-011-0703-2

Haruna, K., Saleh, T.A., 2021. N,N′-Bis-(2-aminoethyl)piperazine functionalized graphene oxide (NAEP-GO) as an effective green corrosion inhibitor for simulated acidizing environment. J. Environ. Chem. Eng. https://doi.org/10.1016/j.jece.2020.104967

Heydari, M., Javidi, M., 2012. Corrosion inhibition and adsorption behaviour of an amido-imidazoline derivative on API 5L X52 steel in CO 2-saturated solution and synergistic effect of iodide ions. Corros. Sci. 61, 148–155. https://doi.org/10.1016/j.corsci.2012.04.034

Hong, T., Sun, Y.H., Jepson, W.P., 2002. Study on corrosion inhibitor in large pipelines under multiphase flow using EIS. Corros. Sci. 44, 101–112. https://doi.org/10.1016/S0010-938X(01)00052-X

Hsissou, R., Abbout, S., Safi, Z., Benhiba, F., Wazzan, N., Guo, L., Nouneh, K., Briche, S., Erramli, H., Ebn Touhami, M., Assouag, M., Elharfi, A., 2021. Synthesis and anticorrosive properties of epoxy polymer for CS in [1 M] HCl solution: Electrochemical, AFM, DFT and MD simulations. Constr. Build. Mater. 270, 121454. https://doi.org/10.1016/j.conbuildmat.2020.121454

Jang, M., Asnin, L., Nile, S.H., Keum, Y.S., Kim, H.Y., Park, S.W., 2013. Ultrasound-assisted extraction of quercetin from onion solid wastes. Int. J. Food Sci. Technol. https://doi.org/10.1111/j.1365-2621.2012.03180.x

Javaherdashti, R., 2000. How corrosion affects industry and life. Anti-Corrosion Methods Mater. 47, 30–34. https://doi.org/10.1108/00035590010310003

Ji, G., Anjum, S., Sundaram, S., Prakash, R., 2015. Musa paradisica peel extract as green corrosion inhibitor for mild steel in HCl solution. Corros. Sci. 90, 107–117. https://doi.org/10.1016/j.corsci.2014.10.002

Ji, G., Dwivedi, P., Sundaram, S., Prakash, R., 2013. Inhibitive effect of Chlorophytum

TH-3102_146107038

borivilianum root extract on mild steel corrosion in HCl and H2SO4 solutions. Ind. Eng. Chem. Res. 52, 10673–10681. https://doi.org/10.1021/ie4008387

Ji, G., Shukla, S.K., Dwivedi, P., Sundaram, S., Prakash, R., 2011. Inhibitive effect of argemone mexicana plant extract on acid corrosion of mild steel. Ind. Eng. Chem. Res. 50, 11954–11959. https://doi.org/10.1021/ie201450d

Kadiri, L., Galai, M., Ouakki, M., Essaadaoui, Y., Ouass, A., Cherkaoui, M., Rifi, E.-H., Lebkiri, A., 2018. Coriandrum Sativum.L Seeds Extract as a Novel Green Corrosion Inhibitor for Mild Steel in 1.0 M Hydrochloric and 0.5 M Sulfuric Solutions. Anal. Bioanal. Electrochem. 10, 249–268.

Kakaei, K., Esrafili, M.D., Ehsani, A., 2019. Graphene and Anticorrosive Properties. pp. 303–337. https://doi.org/10.1016/B978-0-12-814523-4.00008-3

Kamaruzzaman, W.M.I.W.M., Nasir, N.A.M., Hamidi, N.A.S.M., Yusof, N., Shaifudin, M.S., Suhaimi, A.M.A.A.M., Badruddin, M.A., Adnan, A., Nik, W.M.N.W., Ghazali, M.S.M., 2022. 25 years of progress on plants as corrosion inhibitors through a bibliometric analysis using the Scopus database (1995–2020). Arab. J. Chem. 15, 103655. https://doi.org/10.1016/j.arabjc.2021.103655

Keramatinia, M., Ramezanzadeh, B., Mahdavian, M., 2019. Green production of bioactive components from herbal origins through one-pot oxidation/polymerization reactions and application as a corrosion inhibitor for mild steel in HCl solution. J. Taiwan Inst. Chem. Eng. 105, 134–149. https://doi.org/10.1016/j.jtice.2019.10.005

Khanra, A., Srivastava, M., Rai, M.P., Prakash, R., 2018. Application of Unsaturated Fatty Acid Molecules Derived from Microalgae toward Mild Steel Corrosion Inhibition in HCl Solution: A Novel Approach for Metal-Inhibitor Association. ACS Omega 3, 12369–12382. https://doi.org/10.1021/acsomega.8b01089

Laschuk, N.O., Easton, E.B., Zenkina, O. V., 2021. Reducing the resistance for the use of electrochemical impedance spectroscopy analysis in materials chemistry. RSC Adv. 11, 27925–27936. https://doi.org/10.1039/D1RA03785D

Lau, B.F., Kong, K.W., Leong, K.H., Sun, J., He, X., Wang, Z., Mustafa, M.R., Ling, T.C., Ismail, A., 2020. Banana inflorescence: Its bio-prospects as an ingredient for functional foods. Trends Food Sci. Technol. 97, 14–28. https://doi.org/10.1016/j.tifs.2019.12.023

Lee, K.A., Kim, K.T., Kim, H.J., Chung, M.S., Chang, P.S., Park, H., Pai, H.D., 2014. Antioxidant activities of onion (Allium cepa L.) peel extracts produced by ethanol, hot water, and subcritical water extraction. Food Sci. Biotechnol. 23, 615–621. https://doi.org/10.1007/s10068-014-0084-6

Li, H., Qiang, Y., Zhao, W., Zhang, S., 2021. 2-Mercaptobenzimidazole-inbuilt metal-organic-frameworks modified graphene oxide towards intelligent and excellent anti-corrosion coating. Corros. Sci. 191, 109715. https://doi.org/10.1016/j.corsci.2021.109715

Li, X., Deng, S., Fu, H., 2012. Inhibition of the corrosion of steel in HCl, H2SO4

TH-3102_146107038

solutions by bamboo leaf extract. Corros. Sci. 62, 163–175. https://doi.org/10.1016/j.corsci.2012.05.008

Liao, L.L., Mo, S., Luo, H.Q., Li, N.B., 2018a. Corrosion protection for mild steel by extract from the waste of lychee fruit in HCl solution: Experimental and theoretical studies. J. Colloid Interface Sci. 520, 41–49. https://doi.org/10.1016/j.jcis.2018.02.071

Liao, L.L., Mo, S., Luo, H.Q., Li, N.B., 2018b. Corrosion protection for mild steel by extract from the waste of lychee fruit in HCl solution: Experimental and theoretical studies. J. Colloid Interface Sci. 520, 41–49. https://doi.org/10.1016/j.jcis.2018.02.071

Lohvina, H., Sándor, M., Wink, M., 2021. Effect of Ethanol Solvents on Total Phenolic Content and Antioxidant Properties of Seed Extracts of Fenugreek (Trigonella foenum-graecum L.) Varieties and Determination of Phenolic Composition by HPLC-ESI-MS. Diversity 14, 7. https://doi.org/10.3390/d14010007

M'hiri, N., Veys-Renaux, D., Rocca, E., Ioannou, I., Boudhrioua, N.M., Ghoul, M., 2016. Corrosion inhibition of carbon steel in acidic medium by orange peel extract and its main antioxidant compounds. Corros. Sci. 102, 55–62. https://doi.org/10.1016/j.corsci.2015.09.017

Mahmoudian, M.R., Alias, Y., Basirun, W.J., 2012. Effect of narrow diameter polyaniline nanotubes and nanofibers in polyvinyl butyral coating on corrosion protective performance of mild steel. Prog. Org. Coatings 75, 301–308. https://doi.org/10.1016/j.porgcoat.2012.08.004

Manca, M.L., Firoznezhad, M., Caddeo, C., Marongiu, F., Escribano-Ferrer, E., Sarais, G., Peris, J.E., Usach, I., Zaru, M., Manconi, M., Fadda, A.M., 2019. Phytocomplexes extracted from grape seeds and stalks delivered in phospholipid vesicles tailored for the treatment of skin damages. Ind. Crops Prod. 128, 471–478. https://doi.org/10.1016/j.indcrop.2018.11.052

Manca, M.L., Marongiu, F., Castangia, I., Catalán-Latorre, A., Caddeo, C., Bacchetta, G., Ennas, G., Zaru, M., Fadda, A.M., Manconi, M., 2016. Protective effect of grape extract phospholipid vesicles against oxidative stress skin damages. Ind. Crops Prod. 83, 561–567. https://doi.org/10.1016/j.indcrop.2015.12.069

Manconi, M., Marongiu, F., Castangia, I., Manca, M.L., Caddeo, C., Tuberoso, C.I.G., D'hallewin, G., Bacchetta, G., Fadda, A.M., 2016. Polymer-associated liposomes for the oral delivery of grape pomace extract. Colloids Surfaces B Biointerfaces 146, 910–917. https://doi.org/10.1016/j.colsurfb.2016.07.043

Mansfeld, F., 2005. Tafel slopes and corrosion rates obtained in the pre-Tafel region of polarization curves. Corros. Sci. 47, 3178–3186. https://doi.org/10.1016/j.corsci.2005.04.012

Mata-Bilbao, M.D.L., Andrés-Lacueva, C., Roura, E., Jáuregui, O., Torre, C., Lamuela-Raventós, R.M., 2007. A new LC/MS/MS rapid and sensitive method for the determination of green tea catechins and their metabolites in biological samples. J. Agric. Food Chem. 55, 8857–8863. https://doi.org/10.1021/jf0713962

TH-3102_146107038

Mathew, N.S., Negi, P.S., 2021. Phenolic content and anti-oxidative attributes of various parts of wild banana (Ensete superbum Roxb. Cheesman) plant. J. Food Biochem. 45, 1–13. https://doi.org/10.1111/jfbc.13657

Mechbal, N., Bouhrim, M., Bnouham, M., Hammouti, B., Karzazi, Y., Kaya, S., Serdaroğlu, G., 2021. Anticorrosive and antioxidant effect of the aqueous extract of the leaves, flowers, and stems of Cistus monspeliensis L: Experimental and computational study. J. Mol. Liq. 331. https://doi.org/10.1016/j.molliq.2021.115771

Mei, B.-A., Munteshari, O., Lau, J., Dunn, B., Pilon, L., 2018. Physical Interpretations of Nyquist Plots for EDLC Electrodes and Devices. J. Phys. Chem. C 122, 194–206. https://doi.org/10.1021/acs.jpcc.7b10582

Melitas, N., Chuffe-Moscoso, O., Farrell, J., 2001. Kinetics of soluble chromium removal from contaminated water by zerovalent iron media: Corrosion inhibition and passive oxide effects. Environ. Sci. Technol. 35, 3948–3953. https://doi.org/10.1021/es001923x

Mobin, M., Rizvi, M., Olasunkanmi, L.O., Ebenso, E.E., 2017. Biopolymer from Tragacanth Gum as a Green Corrosion Inhibitor for Carbon Steel in 1 M HCl Solution. ACS Omega 2, 3997–4008. https://doi.org/10.1021/acsomega.7b00436

Mostafaei, A., Nasirpouri, F., 2014. Epoxy/polyaniline-ZnO nanorods hybrid nanocomposite coatings: Synthesis, characterization and corrosion protection performance of conducting paints. Prog. Org. Coatings 77, 146–159. https://doi.org/10.1016/j.porgcoat.2013.08.015

Mourya, P., Banerjee, S., Rastogi, R.B., Singh, M.M., 2013. Inhibition of mild steel corrosion in hydrochloric and sulfuric acid media using a thiosemicarbazone derivative. Ind. Eng. Chem. Res. 52, 12733–12747. https://doi.org/10.1021/ie4012497

Mourya, P., Banerjee, S., Singh, M.M., 2014a. Corrosion inhibition of mild steel in acidic solution by Tagetes erecta (Marigold flower) extract as a green inhibitor. Corros. Sci. 85, 352–363. https://doi.org/10.1016/j.corsci.2014.04.036

Mourya, P., Banerjee, S., Singh, M.M., 2014b. Corrosion inhibition of mild steel in acidic solution by Tagetes erecta (Marigold flower) extract as a green inhibitor. Corros. Sci. 85, 352–363. https://doi.org/10.1016/j.corsci.2014.04.036

Naghi Tehrani, M.E.H., Ghahremani, P., Ramezanzadeh, M., Bahlakeh, G., Ramezanzadeh, B., 2021a. Theoretical and experimental assessment of a green corrosion inhibitor extracted from Malva sylvestris. J. Environ. Chem. Eng. 9, 105256. https://doi.org/10.1016/j.jece.2021.105256

Naghi Tehrani, M.E.H., Ghahremani, P., Ramezanzadeh, M., Bahlakeh, G., Ramezanzadeh, B., 2021b. Theoretical and experimental assessment of a green corrosion inhibitor extracted from Malva sylvestris. J. Environ. Chem. Eng. https://doi.org/10.1016/j.jece.2021.105256

Ogungbenro, A.E., Quang, D. V., Al-Ali, K.A., Vega, L.F., Abu-Zahra, M.R.M., 2020.

TH-3102_146107038

Synthesis and characterization of activated carbon from biomass date seeds for carbon dioxide adsorption. J. Environ. Chem. Eng. 8, 104257. https://doi.org/10.1016/j.jece.2020.104257

Okafor, P.C., Ebenso, E.E., Ekpe, U.J., 2010. Azadirachta Indica Extracts as Corrosion Inhibitor for Mild Steel in Acid Medium. Int. J. Electrochem. Sci 5, 978–993.

Okafor, P.C., Liu, X., Zheng, Y.G., 2009. Corrosion inhibition of mild steel by ethylamino imidazoline derivative in CO2-saturated solution. Corros. Sci. 51, 761–768. https://doi.org/10.1016/j.corsci.2009.01.017

Ostovari, A., Hoseinieh, S.M., Peikari, M., Shadizadeh, S.R., Hashemi, S.J., 2009. Corrosion inhibition of mild steel in 1 M HCl solution by henna extract: A comparative study of the inhibition by henna and its constituents (Lawsone, Gallic acid, α-d-Glucose and Tannic acid). Corros. Sci. 51, 1935–1949. https://doi.org/10.1016/j.corsci.2009.05.024

Ouakki, M., Galai, M., Rbaa, M., Abousalem, A.S., Lakhrissi, B., Rifi, E.H., Cherkaoui, M., 2020. Investigation of imidazole derivatives as corrosion inhibitors for mild steel in sulfuric acidic environment: experimental and theoretical studies. Ionics (Kiel). 26, 5251–5272. https://doi.org/10.1007/s11581-020-03643-0

Oubaaqa, M., Ouakki, M., Rbaa, M., Benhiba, F., Galai, M., Idouhli, R., Maatallah, M., Jarid, A., Warad, I., Lakhrissi, B., Zarrouk, A., Ebn Touhami, M., 2022. Experimental and theoretical investigation of corrosion inhibition effect of two 8-hydroxyquinoline carbonitrile derivatives on mild steel in 1 M HCl solution. J. Phys. Chem. Solids 169, 110866. https://doi.org/10.1016/j.jpcs.2022.110866

Pal, A., Das, C., 2020. A novel use of solid waste extract from tea factory as corrosion inhibitor in acidic media on boiler quality steel. Ind. Crops Prod. https://doi.org/10.1016/j.indcrop.2020.112468

Palanisamy, G., 2019. Corrosion Inhibitors, in: Corrosion Inhibitors. IntechOpen, pp. 1–24. https://doi.org/10.5772/intechopen.80542

Parthipan, P., Elumalai, P., Narenkumar, J., Machuca, L.L., Murugan, K., Karthikeyan, O.P., Rajasekar, A., 2018. Allium sativum (garlic extract) as a green corrosion inhibitor with biocidal properties for the control of MIC in carbon steel and stainless steel in oilfield environments. Int. Biodeterior. Biodegrad. 132, 66–73. https://doi.org/10.1016/j.ibiod.2018.05.005

Prabakaran, M., Kim, S.H., Hemapriya, V., Chung, I.M., 2016a. Evaluation of polyphenol composition and anti-corrosion properties of Cryptostegia grandiflora plant extract on mild steel in acidic medium. J. Ind. Eng. Chem. 37, 47–56. https://doi.org/10.1016/j.jiec.2016.03.006

Prabakaran, M., Kim, S.H., Hemapriya, V., Chung, I.M., 2016b. Tragia plukenetii extract as an eco-friendly inhibitor for mild steel corrosion in HCl 1 M acidic medium. Res. Chem. Intermed. 42, 3703–3719. https://doi.org/10.1007/s11164-015-2240-x

Qiang, Y., Guo, L., Li, H., Lan, X., 2021. Fabrication of environmentally friendly

TH-3102_146107038

Losartan potassium film for corrosion inhibition of mild steel in HCl medium. Chem. Eng. J. 406, 126863. https://doi.org/10.1016/j.cej.2020.126863

Qiang, Y., Li, H., Lan, X., 2020. Self-assembling anchored film basing on two tetrazole derivatives for application to protect copper in sulfuric acid environment. J. Mater. Sci. Technol. 52, 63–71. https://doi.org/10.1016/j.jmst.2020.04.005

Qiang, Y., Zhang, S., Guo, L., Zheng, X., Xiang, B., Chen, S., 2017a. Experimental and theoretical studies of four allyl imidazolium-based ionic liquids as green inhibitors for copper corrosion in sulfuric acid. Corros. Sci. 119, 68–78. https://doi.org/10.1016/j.corsci.2017.02.021

Qiang, Y., Zhang, S., Tan, B., Chen, S., 2018. Evaluation of Ginkgo leaf extract as an eco-friendly corrosion inhibitor of X70 steel in HCl solution. Corros. Sci. 133, 6–16. https://doi.org/10.1016/j.corsci.2018.01.008

Qiang, Y., Zhang, S., Yan, S., Zou, X., Chen, S., 2017b. Three indazole derivatives as corrosion inhibitors of copper in a neutral chloride solution. Corros. Sci. 126, 295–304. https://doi.org/10.1016/j.corsci.2017.07.012

Raja, P.B., Sethuraman, M.G., 2008. Natural products as corrosion inhibitor for metals in corrosive media - A review. Mater. Lett. 62, 113–116. https://doi.org/10.1016/j.matlet.2007.04.079

RIZZO, C.M., 2008. Maintenance of aged ships and offshore structures, in: Condition Assessment of Aged Structures. Elsevier, pp. 430–458. https://doi.org/10.1533/9781845695217.5.430

Salghi, R., Jodeh, S., Ebenso, E.E., Lgaz, H., Ben Hmamou, D., Belkhaouda, M., Ali, I.H., Messali, M., Hammouti, B., Fattouch, S., 2017. Inhibition of C-steel corrosion by green tea extract in hydrochloric solution. Int. J. Electrochem. Sci. 12, 3283–3295. https://doi.org/10.20964/2017.04.46

Salinas-Solano, G., Porcayo-Calderon, J., Martinez de la Escalera, L.M., Canto, J., Casales-Diaz, M., Sotelo-Mazon, O., Henao, J., Martinez-Gomez, L., 2018. Development and evaluation of a green corrosion inhibitor based on rice bran oil obtained from agro-industrial waste. Ind. Crops Prod. 119, 111–124. https://doi.org/10.1016/j.indcrop.2018.04.009

Santhosh, A., Theertha, V., Prakash, P., Smitha Chandran, S., 2020. From waste to a value added product: Green synthesis of silver nanoparticles from onion peels together with its diverse applications. Mater. Today Proc. 0–3. https://doi.org/10.1016/j.matpr.2020.09.680

Saxena, A., Prasad, D., Haldhar, R., 2018a. Investigation of corrosion inhibition effect and adsorption activities of Cuscuta reflexa extract for mild steel in 0.5 M H2SO4. Bioelectrochemistry 124, 156–164. https://doi.org/10.1016/j.bioelechem.2018.07.006

Saxena, A., Prasad, D., Haldhar, R., 2018b. Investigation of Corrosion Inhibition Effect and Adsorption Activities of Achyranthes aspera Extract for Mild Steel in 0.5 M H2SO4. J. Fail. Anal. Prev. 18, 957–968. https://doi.org/10.1007/s11668-018-

TH-3102_146107038

0491-8

Saxena, A., Prasad, D., Haldhar, R., 2018c. Investigation of Corrosion Inhibition Effect and Adsorption Activities of Achyranthes aspera Extract for Mild Steel in 0.5 M H2SO4. J. Fail. Anal. Prev. 18, 957–968. https://doi.org/10.1007/s11668-018-0491-8

Scano, A., Ebau, F., Manca, M.L., Cabras, V., Cesare Marincola, F., Manconi, M., Pilloni, M., Fadda, A.M., Ennas, G., 2018. Novel drug delivery systems for natural extracts: The case study of Vitis Vinifera extract-SiO2 nanocomposites. Int. J. Pharm. 551, 84–96. https://doi.org/10.1016/j.ijpharm.2018.08.057

Schofield, M.J., 2001. Corrosion, in: Plant Engineer's Handbook. Elsevier, pp. 961–985. https://doi.org/10.1016/B978-075067328-0/50055-0

Serdar, G., Demir, E., Sökmen, M., 2017. Recycling of Tea Waste: Simple and Effective Separation of Caffeine and Catechins by Microwave Assisted Extraction (MAE). Int. J. Second. Metab. 4, 78–78. https://doi.org/10.21448/ijsm.288226

Shabani-Nooshabadi, M., Ghandchi, M.S., 2015. Santolina chamaecyparissus extract as a natural source inhibitor for 304 stainless steel corrosion in 3.5% NaCl. J. Ind. Eng. Chem. 31, 231–237. https://doi.org/10.1016/j.jiec.2015.06.028

Shahmoradi, A.R., Ranjbarghanei, M., Javidparvar, A.A., Guo, L., Berdimurodov, E., Ramezanzadeh, B., 2021. Theoretical and surface/electrochemical investigations of walnut fruit green husk extract as effective inhibitor for mild-steel corrosion in 1M HCl electrolyte. J. Mol. Liq. 338, 116550. https://doi.org/10.1016/j.molliq.2021.116550

Sharma, K., Mahato, N., Nile, S.H., Lee, E.T., Lee, Y.R., 2016. Economical and environmentally-friendly approaches for usage of onion (: Allium cepa L.) waste. Food Funct. https://doi.org/10.1039/c6fo00251j

Sin, H.L.Y., Umeda, M., Shironita, S., Rahim, A.A., Saad, B., 2017. Adenosine as corrosion inhibitor for mild steel in hydrochloric acid solution. Res. Chem. Intermed. 43, 1919–1934. https://doi.org/10.1007/s11164-016-2739-9

Singh, A., Dayu, X., Ituen, E., Ansari, K., Quraishi, M.A., Kaya, S., Lin, Y., 2020. Tobacco extracted from the discarded cigarettes as an inhibitor of copper and zinc corrosion in an ASTM standard D1141-98(2013) artificial seawater solution. J. Mater. Res. Technol. 9, 5161–5173. https://doi.org/10.1016/j.jmrt.2020.03.033

Singh, A., Ituen, E.B., Ansari, K.R., Chauhan, D.S., Quraishi, M.A., 2019. Surface protection of X80 steel using Epimedium extract and its iodide-modified composites in simulated acid wash solution: a greener approach towards corrosion inhibition. New J. Chem. 43, 8527–8538. https://doi.org/10.1039/C9NJ01691K

Singh, A., Lin, Y., Ebenso, E.E., Liu, W., Pan, J., Huang, B., 2015. Gingko biloba fruit extract as an eco-friendly corrosion inhibitor for J55 steel in CO<inf>2</inf> saturated 3.5% NaCl solution. J. Ind. Eng. Chem. https://doi.org/10.1016/j.jiec.2014.09.034

TH-3102_146107038

Singh, A.K., Mohapatra, S., Pani, B., 2016. Corrosion inhibition effect of Aloe Vera gel: Gravimetric and electrochemical study. J. Ind. Eng. Chem. 33, 288–297. https://doi.org/10.1016/j.jiec.2015.10.014

Singh, P., Quraishi, M.A., 2016a. Corrosion inhibition of mild steel using Novel Bis Schiff's Bases as corrosion inhibitors: Electrochemical and Surface measurement. Measurement 86, 114–124. https://doi.org/10.1016/j.measurement.2016.02.052

Singh, P., Quraishi, M.A., 2016b. Corrosion inhibition of mild steel using Novel Bis Schiff's Bases as corrosion inhibitor: Electrochemical and Surface measurement. Meas. J. Int. Meas. Confed. 86, 114–124. https://doi.org/10.1016/j.measurement.2016.02.052

Skoronski, E., De Oliveira, D.C., Fernandes, M., Da Silva, G.F., Magalhães, M.D.L.B., João, J.J., 2016. Valorization of agro-industrial by-products: Analysis of biodiesel production from porcine fat waste. J. Clean. Prod. 112, 2553–2559. https://doi.org/10.1016/j.jclepro.2015.10.026

Solmaz, R., 2014. Investigation of corrosion inhibition mechanism and stability of Vitamin B1 on mild steel in 0.5M HCl solution. Corros. Sci. 81, 75–84. https://doi.org/10.1016/j.corsci.2013.12.006

Srivastava, M., Tiwari, P., Srivastava, S.K., Prakash, R., Ji, G., 2017a. Electrochemical investigation of Irbesartan drug molecules as an inhibitor of mild steel corrosion in 1 M HCl and 0.5 M H2SO4 solutions. J. Mol. Liq. 236, 184–197. https://doi.org/10.1016/j.molliq.2017.04.017

Srivastava, M., Tiwari, P., Srivastava, S.K., Prakash, R., Ji, G., 2017b. Electrochemical investigation of Irbesartan drug molecules as an inhibitor of mild steel corrosion in 1 M HCl and 0.5 M H2SO4 solutions. J. Mol. Liq. 236, 184–197. https://doi.org/10.1016/j.molliq.2017.04.017

Srivastava, V., Chauhan, D.S., Joshi, P.G., Maruthapandian, V., Sorour, A.A., Quraishi, M.A., 2018a. PEG-Functionalized Chitosan: A Biological Macromolecule as a Novel Corrosion Inhibitor. ChemistrySelect 3, 1990–1998. https://doi.org/10.1002/slct.201701949

Srivastava, V., Chauhan, D.S., Joshi, P.G., Maruthapandian, V., Sorour, A.A., Quraishi, M.A., 2018b. PEG-Functionalized Chitosan: A Biological Macromolecule as a Novel Corrosion Inhibitor. ChemistrySelect 3, 1990–1998. https://doi.org/10.1002/slct.201701949

Sun, C., Wu, Z., Wang, Z., Zhang, H., 2015. Effect of Ethanol/Water Solvents on Phenolic Profiles and Antioxidant Properties of Beijing Propolis Extracts. Evidence-Based Complement. Altern. Med. 2015, 1–9. https://doi.org/10.1155/2015/595393

Teng, Y., Zhang, W., Wang, M., Yu, C., Ma, Y., Bian, J., Yang, X., Zhang, D., 2021. Anthocyanin as sustainable and non-toxic corrosion inhibitor for mild steel in HCl media: Electrochemical, surface morphology and theoretical investigations. J. Mol. Liq. 344, 117721. https://doi.org/10.1016/j.molliq.2021.117721

TH-3102_146107038

Thomas, A., AT, J.R., Joseph, A., 2021. Extended protection of mild steel in molar HCl using the Garcinia Indica fruit rind extract (GIW) and iodide ions; electrochemical, thermodynamic and kinetic studies. J. Indian Chem. Soc. 98, 100167. https://doi.org/10.1016/j.jics.2021.100167

Thomas, A., Prajila, M., Shainy, K.M., Joseph, A., 2020. A green approach to corrosion inhibition of mild steel in hydrochloric acid using fruit rind extract of Garcinia indica (Binda). J. Mol. Liq. 312, 113369. https://doi.org/10.1016/j.molliq.2020.113369

Umoren, S.A., 2016. Biomaterials for corrosion protection: Evaluation of mustard seed extract as eco-friendly corrosion inhibitor for X60 steel in acid media. J. Adhes. Sci. Technol. 30, 1858–1879. https://doi.org/10.1080/01694243.2016.1168339

Varvara, S., Bostan, R., Bobis, O., Găină, L., Popa, F., Mena, V., Souto, R.M., 2017. Propolis as a green corrosion inhibitor for bronze in weakly acidic solution. Appl. Surf. Sci. 426, 1100–1112. https://doi.org/10.1016/j.apsusc.2017.07.230

Vasyliev, G., Vorobyova, V., Zhuk, T., 2020. Raphanus sativus L. Extract as a Scale and Corrosion Inhibitor for Mild Steel in Tap Water. J. Chem. 2020. https://doi.org/10.1155/2020/5089758

Verma, C., Ebenso, E.E., Bahadur, I., Quraishi, M.A., 2018a. An overview on plant extracts as environmental sustainable and green corrosion inhibitors for metals and alloys in aggressive corrosive media. J. Mol. Liq. 266, 577–590. https://doi.org/10.1016/j.molliq.2018.06.110

Verma, C., Olasunkanmi, L.O., Ebenso, E.E., Quraishi, M.A., 2018b. Adsorption characteristics of green 5-arylaminomethylene pyrimidine-2,4,6-triones on mild steel surface in acidic medium: Experimental and computational approach. Results Phys. 8, 657–670. https://doi.org/10.1016/j.rinp.2018.01.008

Verma, C., Quraishi, M.A., Ebenso, E.E., Bahadur, I., 2018c. A Green and Sustainable Approach for Mild Steel Acidic Corrosion Inhibition Using Leaves Extract: Experimental and DFT Studies. J. Bio- Tribo-Corrosion 4. https://doi.org/10.1007/s40735-018-0150-3

Verma, D.K., Kazi, M., Alqahtani, M.S., Syed, R., Berdimurodov, E., Kaya, S., Salim, R., Asatkar, A., Haldhar, R., 2021. N–hydroxybenzothioamide derivatives as green and efficient corrosion inhibitors for mild steel: Experimental, DFT and MC simulation approach. J. Mol. Struct. 1241. https://doi.org/10.1016/j.molstruc.2021.130648

Vimalanandan, A., Lv, L.-P., Tran, T.H., Landfester, K., Crespy, D., Rohwerder, M., 2013. Redox-Responsive Self-Healing for Corrosion Protection. Adv. Mater. 25, 6980–6984. https://doi.org/10.1002/adma.201302989

Vorobyova, V., Skiba, M., 2021. Peach Pomace Extract as Efficient Sustainable Inhibitor for Carbon Steel Against Chloride-Induced Corrosion. J. Bio- Tribo-Corrosion 7, 1–11. https://doi.org/10.1007/s40735-020-00450-y

Wang, Cai, Chen, J., Hu, B., Liu, Z., Wang, Chongbin, Han, J., Su, M., Li, Y., Li, C.,

TH-3102_146107038

2019. Modified chitosan-oligosaccharide and sodium silicate as efficient sustainable inhibitor for carbon steel against chloride-induced corrosion. J. Clean. Prod. 238, 117823. https://doi.org/10.1016/j.jclepro.2019.117823

Xu, D., Hu, M.J., Wang, Y.Q., Cui, Y.L., 2019. Antioxidant activities of quercetin and its complexes for medicinal application. Molecules 24. https://doi.org/10.3390/molecules24061123

Zhang, X.L., Jiang, Z.H., Yao, Z.P., Song, Y., Wu, Z.D., 2009. Effects of scan rate on the potentiodynamic polarization curve obtained to determine the Tafel slopes and corrosion current density. Corros. Sci. 51, 581–587. https://doi.org/10.1016/j.corsci.2008.12.005

Zhao, Y., Zhou, E., Liu, Y., Liao, S., Li, Z., Xu, D., Zhang, T., Gu, T., 2017. Comparison of different electrochemical techniques for continuous monitoring of the microbiologically influenced corrosion of 2205 duplex stainless steel by marine Pseudomonas aeruginosa biofilm. Corros. Sci. 126, 142–151. https://doi.org/10.1016/j.corsci.2017.06.024

Zhou, Xueyong, Zhou, Xin, 2014. the Unit Problem in the Thermodynamic Calculation of Adsorption Using the Langmuir Equation. Chem. Eng. Commun. 201, 1459–1467. https://doi.org/10.1080/00986445.2013.818541

TH-3102_146107038

3

Corrosion inhibition by extract of solid waste from tea factory (industrial waste)

TH-3102_146107038

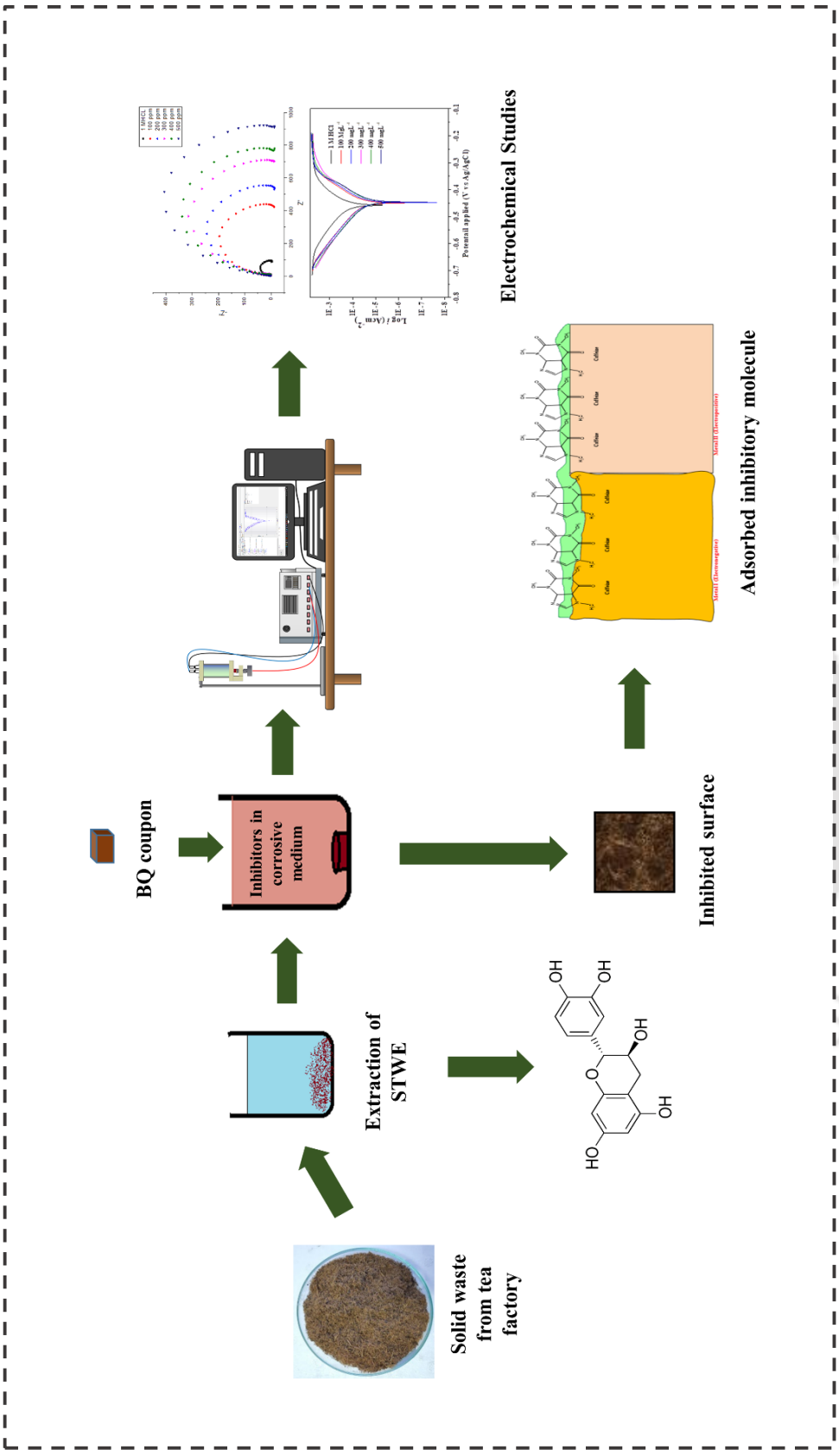

TH-3102_146107038

Corrosion inhibition by extract of solid waste from tea factory (industrial waste)

This chapter represents the results and discussion associated with the use of solid waste from a tea factory as an environment-friendly, inexpensive "green corrosion inhibitor". The solid tea waste extract (STWE) was prepared from the solid waste by the conventional extraction method and characterized by liquid chromatography-mass spectroscopy (LC-MS). The inhibition performance of this synthesized STWE was evaluated in 1 (M) HCl on boiler quality (BQ) steel. Their efficiency of inhibition was assessed by electrochemical techniques, namely the potentiodynamic polarization test (PDP), and electrochemical impedance spectroscopy (EIS). The results depict that the increase in the concentration of STWE increases the inhibition efficiency of the extract. Various models were fitted to explore the type of adsorption, and among them, Langmuir was found to fit the best. The free energy ΔG°_{ads} *was calculated as -24.92 kJmol*$^{-1}$ *from adsorption isotherm and revealed mixed-type adsorption of STWE on the BQ surface. The inhibitive strength or effectiveness of inhibitor molecules was assessed based on donor-acceptor capabilities between the molecules and the metallic surface. This capability was evaluated with the help of quantum chemical calculations based on density functional theory.*

Published Artcle: Pal, A., Das, C., 2020. A novel use of solid waste extract from tea factory as corrosion inhibitor in acidic media on boiler quality steel. **Ind. Crops Prod.** https://doi.org/10.1016/j.indcrop.2020.112468.

TH-3102_146107038

3.1 Identification of the compounds in STWE

Fig. 3.1 shows the mass spectra of crude STWE after chromatographic separation. From the mass spectra, mainly three compounds were identified. The compounds in STWE were identified by comparing the m/z values with the standards from the literature. A positive ionization mode was used to identify the compounds. Three dominant compounds were identified, which are caffeine, catechin (C), and gallocatechin (GC). The peak of protonated ion $[M+H]^+$ occurs at m/z of 195.09 (Fig. 3.1(a)), identified as caffeine. According to the mass fragment, ions protonated $[M+H]^+$ ion at m/z 291 (Fig. 3.1(b) and 307 (Fig. 3.1(c) and were identified as catechin and gallocatechin, respectively (Mata-Bilbao et al., 2007).

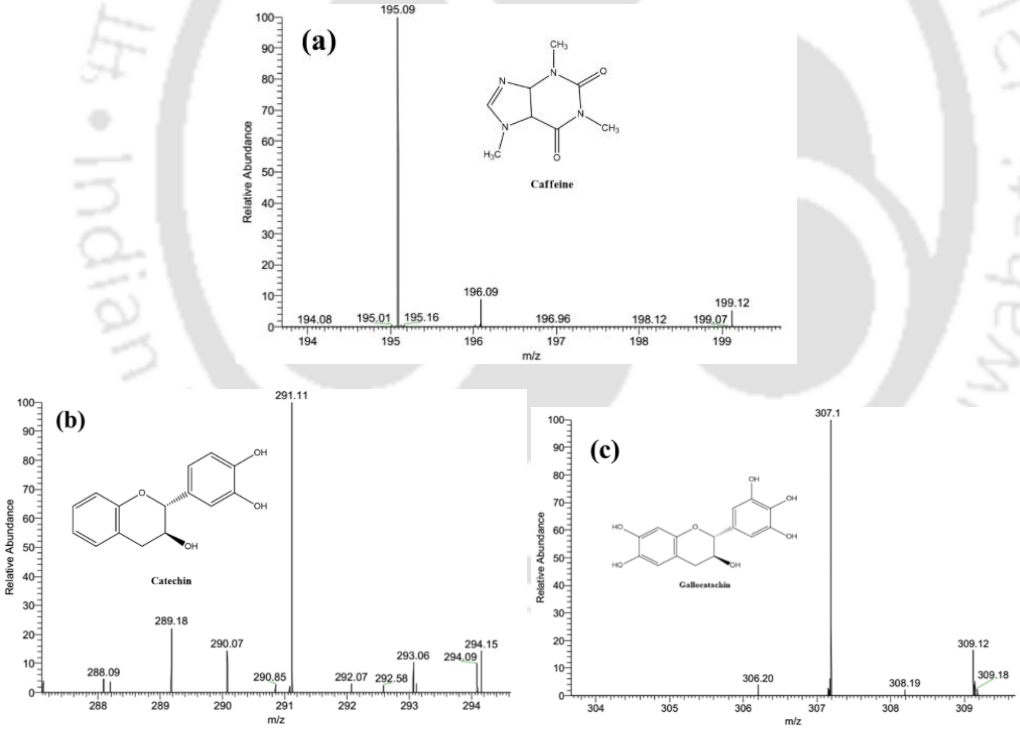

Fig. 3.1 Mass spectra of Caffeine 195 (m/z) (a), Catechin 291.11 (m/z) (b), Gallocatechin 307 (m/z) (c).

TH-3102_146107038

All of these are polyphenolic compounds having atoms such as N, S, O, P, and aromatic functional groups with π electrons inside their structure, which helps them to build different kinds of interactions like chemisorption and physisorption.

3.2 Weight loss method

The values of CR and $\mu_{CR}\%$ were calculated using Eq. 2.1 and Eq. 2.2 in the presence and absence of different STWE concentrations. It was observed from Table 3.1 that at a higher concentration of STWE, the corrosion rate becomes lower. The amount of weight loss also got decreased at a higher concentration of STWE. Hence, The inhibition efficiency was increased at higher concentrations.

Table 3.1 Weight loss and corrosion rate of BQ plate in 1 (M) HCl with and without STWE.

Conc (mg L^{-1})	$CR \times 10^2$ (mm $year^{-1}$)	$\mu_{CR}\%$
0 (Blank) 1(M)HCl	190.38 ± 8.67	0 ± 0.00
100	44.47 ± 1.29	76.6 ± 0.83
200	41.59 ± 0.23	78.2 ± 0.30
300	38.64 ± 0.09	79.7 ± 0.16
400	33.07 ± 0.10	82.6 ± 0.40
500	31.24 ± 0.12	83.6 ± 0.65

From Table 3.1, it is observed that even a lower concentration of STWE shows a significant efficiency. The main reason behind this inhibition efficiency is the depletion of oxidation and reduction reaction rate, which occurs conventionally in a corrosion process. The corrosion process in acid solution includes two basic chemical reactions, namely anodic and cathodic reactions. In anodic reaction the iron becomes

TH-3102_146107038

oxidized into Fe^{2+} ($Fe \rightarrow Fe^{2+} + 2e^-$) and cathodic reaction H^+ becomes H_2 gas ($2H^+ + 2e^- \rightarrow 2(H)_{ads} + H_2$). The presence of STWE reduces the reaction rate of iron oxidation and proton reduction. As a consequence less amount of iron is oxidized on the surface of the BQ plate (Ali Asaad et al., 2018; Ji et al., 2013; Mourya et al., 2014).

3.3 Electrochemical studies

The electrochemical studies were performed to determine the rate of corrosion and predict the electrochemical behavior of BQ steel in different conditions. These studies mainly help to find out the corrosion current density i_{corr} also, charge transfer resistance R_{ct} from which inhibition efficiency of inhibitor species on BQ plate was inferred.

3.3.1 Open circuit potential

In Fig. 3.2, it is seen that the open circuit potential for different concentrations of corrosion inhibitors on BQ steel varies with changes in concentrations. The variations of the open circuit potential are towards a positive direction in the presence of STWE as compared to the absence. These changes in OCP are mainly due to the formation of a protective layer on the material, and the stable potential indicates the stability of the layer on the surface. From Fig. 3.2, it is observed that the potential moves toward a positive direction after the addition of the corrosion inhibitor. As the concentration of the inhibitors increase, the potential shifts towards the positive side. At zero concentration of and low concentration of inhibitors (100 mg L^{-1}), there is fluctuation in the potential for the first 25 min due to the stability of the protective film, which became stable after 30 min. Interestingly at high concentrations (500 mg L^{-1}), this fluctuation was reduced, and a steady state was attained readily since, at higher

TH-3102_146107038

concentrations, the formation of the film is easily accomplished and stable (Khanra et al., 2018; M'hiri et al., 2016; Melitas et al., 2001).

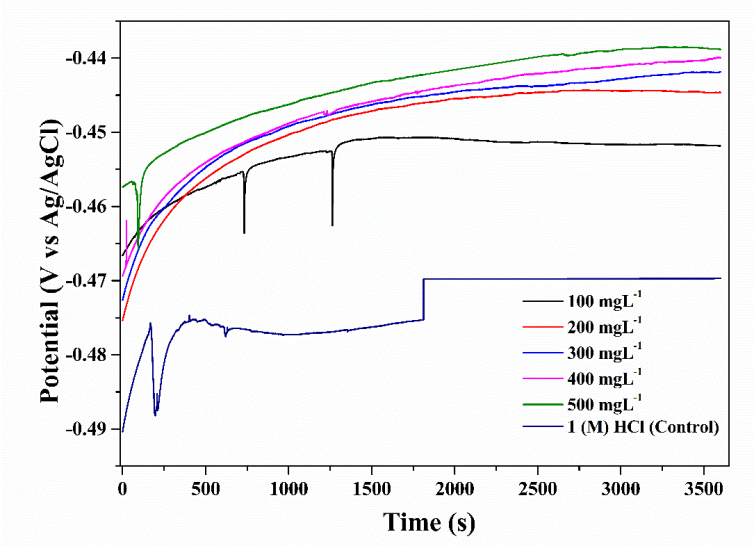

Fig. 3.2 OCP measurements in different concentrations of STWE [Control represents the absence of STWE].

3.3.2 Potentiodynamic polarization study

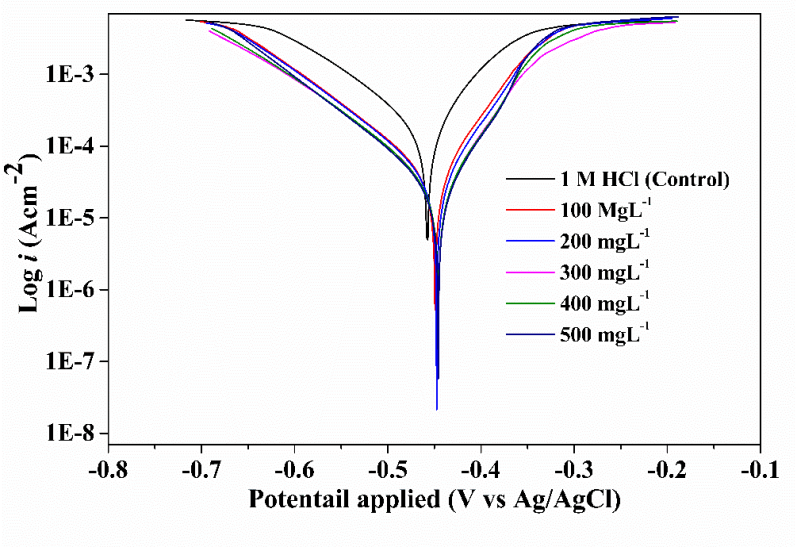

Fig. 3.3 Tafel polarization of BQ metal in the presence of the different amounts of STWE [Control represents the absence of STWE].

TH-3102_146107038

The measurement of potentiodynamic polarization test provides a clear platform for monitoring the mechanistic phenomenon of electrochemical behavior using corrosion inhibitors on the BQ surface. Fig. 3.3 shows that without inhibitors, both the anodic and cathodic current is aggressive. The reason for this aggressive current is the rapid dissolution of the metal due to the oxidation reaction at the anodic zone and the hydrogen evolution reaction at the cathodic zone. It is observed that after the addition of corrosion inhibitors, the corrosion potential E_{corr} has shifted toward the positive side compared to the uninhibited system, but this shift is not more than 85mV. Few present studies have illustrated that if the shift of E_{corr} after the addition of inhibitors is less than 85 mV, then the inhibitor is considered as a mixed-type inhibitor. Various corrosion parameters, viz., cathodic slope (b_c), anodic slope (b_a), corrosion potential E_{corr}, corrosion current density i_{corr}, polarization resistance (R_P), and which are related to corrosion kinetics, were calculated by fitting Tafel polarization curve using NOVA software and listed in Table 3.2. A close view in Table 3.2 revealed that the anodic slopes are much higher than the cathodic slope for every case, which suggests that the inhibitors are more effective for retarding the cathodic reaction than the anodic. Fig. 3.3 also depicts that both anodic and cathodic current has decreased in the presence of inhibitors as metal dissolution and hydrogen evolution both the reaction have retarded. Moreover, the corrosion current density (i_{corr}) has also decreased with the increase in the concentration of STWE. Unlike i_{corr}, the decrease in R_P with an increased concentration of inhibitors observed. These two phenomena of a decrease in i_{corr} and an increase in R_P indicates that the STWE forms a strong barrier on the surface of the metal and protects the metal from corrosion. Besides, inhibition efficiency (μ_p) was calculated (Eq. 2.9), and it was found that μ_p increases with increasing

TH-3102_146107038

concentration of inhibitors, but at the higher concentrations, the change in inhibition efficiency was not so much. Because, after a certain concentration, the concentration can not make any extensive change in inhibition efficiency (Ali Asaad et al., 2018; Ji et al., 2011; Liao et al., 2018; Saxena et al., 2018). However, the maximum inhibition efficiency (μ_p) was found 84.53 % at maximum concentration of 500 mg L^{-1}.

Table 3.2 Parameters of Tafel polarization of BQ metal in the presence of the different amount of STWE.

Conc (mg L^{-1})	b_a (mVdec^{-1})	$-b_c$ (mVdec^{-1})	E_{corr} (mV vs AgCl)	i_{corr} (µAcm^{-2})	R_P (Ωcm^{-2})	($\mu_{P\%}$)
0 (Blank)	103.22	61.74	-457.67	163.51	102.62	0.00
1(M)HCl	± 1.81	± 0.73	± -3.34	± 6.72	± 1.54	± 0.00
100	88.57	51.98	-449.27	35.70	398.46	78.17
	± 1.54	± 0.41	± -1.55	± 0.37	± 4.85	± 0.92
200	92.06	56.43	-447.55	33.21	457.57	79.69
	± 0.75	± 0.27	± -3.85	± 0.12	± 7.21	± 0.52
300	94.01	60.58	-445.78	26.92	594.40	83.54
	± 0.56	± 0.29	± -5.09	± 0.07	± 9.82	± 0.37
400	113.40	68.79	-445.84	25.88	584.87	84.17
	± 2.71	± 0.32	± -4.52	± 0.12	± 9.19	± 0.39
500	92.12	62.53	-445.82	25.29	639.61	84.53
	± 1.29	± 0.52	± -1.73	± 0.10	± 10.45	± 0.00

3.3.3 Electrochemical impedance spectroscopy

The representation of EIS is displayed as Nyquist and Bode plots in Fig. 3.4 and Fig. 3.5, respectively, the presence and absence of inhibitors. The Nyquist plots obtained from the experiments were a slightly depressed semicircle, which is expected according to the theory of the corroding substance. The Bode plot shows the single-time constant equivalent circuit. A slight deviation in the semicircle shapes is mainly

TH-3102_146107038

attributed to the frequency dispersion and the heterogeneity on the surface. However, the semicircle plots of the Nyquist plots reveal that the reaction on the BQ surface is mostly charge-transfer resistance (R_{ct}) controlled. The R_{ct} is an element of the equivalent circuit model, which describes the resistance mechanism of the surface (Fig. 3.6). To get an in-depth idea about the mechanism of resistance, all the parameters, like, collective solution resistance (R_s), charge-transfer resistance (R_{ct}) and the constant phase element (CPE) and related Nyquist plot were calculated and given in Table 3.4. All of these parameters were determined by fitting the proposed equivalent circuit model (Randles circuit) on the Nyquist plots. The circuit which was used for fitting the Nyquist plot consists mainly of three elements of R_s, $R_{ct}$and CPE (Fig. 3.6). The R_s is in a series with $R_{ct}$and CPE, whereas R_{ct} is in parallel with CPE. The constant phase element (CPE) is the substitution of the classical double-layer capacitor.

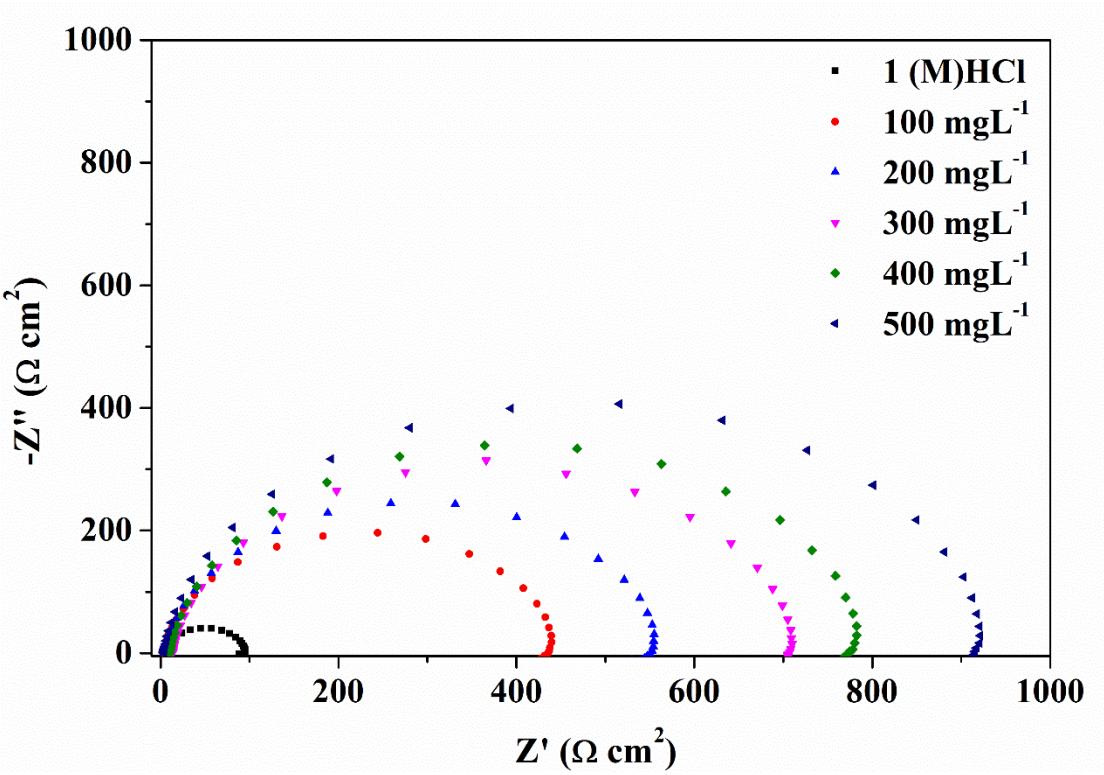

Fig. 3.4 Nyquist plots for BQ steel in 1 (M) HCl with and without different concentrations of STWE [Control represents the absence of STWE].

TH-3102_146107038

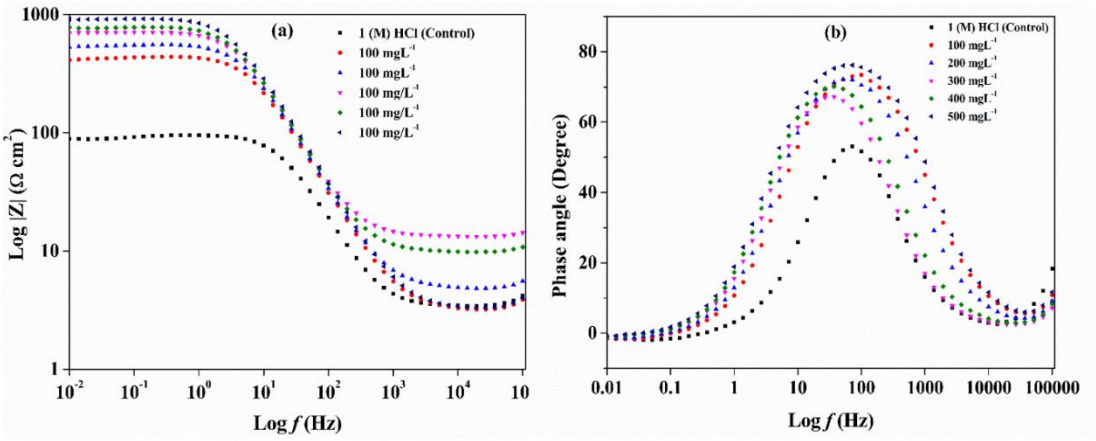

Fig. 3.5 Bode Plots for BQ steel in 1 (M) HCl in the presence and absence of STWE [Control represents the absence of STWE].

Table 3.3 Impedance parameter of tea extract on BQ steel.

Conc (mg L^{-1})	R_S (Ω cm^2)	R_{ct} (Ω cm^2)	CPE parameters		C_{dl} (μF cm^{-2})	$\mu_{R_{ct}}$%
			n	Y_o (μMho cm^{-2})		
0 (Blank) 1(M)HCl	3.49 ± 0.00	89.72 ± 1.67	0.928 ± 0.00	137.01 ± 4.94	96.93 ± 0.94	0.00 ± 0.00
100	3.28 ± 0.00	438.91 ± 11.94	0.914 ± 0.00	85.65 ± 0.50	63.59 ± 0.17	79.56 ± 0.32
200	4.93 ± 0.00	549.33 ± 8.93	0.917 ± 0.00	81.61 ± 0.29	61.06 ± 0.09	83.67 ± 0.42
300	13.39 ± 0.00	699.27 ± 14.95	0.915 ± 0.00	78.65 ± 0.16	60.14 ± 0.06	87.17 ± 0.18
400	9.94 ± 0.00	774.82 ± 25.80	0.916 ± 0.00	78.53 ± 0.11	60.01 ± 0.06	88.42 ± 0.13
500	3.35 ± 0.00	923.40 ± 27.71	0.917 ± 0.00	71.72 ± 0.17	56.71 ± 0.09	90.28 ± 0.20

It is so apparent from the Nyquist plots that resistance on the surface is increased with increased concentration of STWE, which is observed at lower frequencies. Impedance becomes higher at a higher concentration of inhibitors, indicated by the radius of semicircles in the Nyquist plot. Careful observation from Table 3.4 reveals

TH-3102_146107038

the continuous augmentation of R_{ct} values with the enhanced concentration of inhibitor. The reason behind this was probably the accumulation of inhibitor compounds and the formation of a thin layer at the metal-acid interface. This layer reduced the charge transfer from the bulk electrolyte to the metal surface. Thus the corroding substances were blocked from reaching the metal surface, and the double layer becomes inactive. It was also noticed that the capacitance of the double layer was found to diminish at a higher amount of STWE. The reason was that, at higher concentrations, the protective layer becomes thick, so the available area for corrosion was lesser. The change in the impedance modulus (Fig. 3.5(a) and phase angle (Fig. 3.5(b) with respect to frequency in the presence and absence of STWE is portrayed by bode plots. In the presence of inhibitors, both impedance modulus and phase angle show a positive difference, indicating retardant in corrosion (Al-Moubaraki, 2015; Al-Otaibi et al., 2014; Liao et al., 2018; Singh and Quraishi, 2016). The extent of adsorption can be implied by the double-layer capacitance C_{dl} of the metal solution interface. It is observed from Table 3.3 that the C_{dl} is decreased at higher concentrations of STWE. The decrease in C_{dl} could be attributed to the increase in the thickness of the double layer due to the adsorption of STWE on the BQ steel surface. The introduction of an inhibitor into the media changes the composition and structure of the electric double layer. The inhibitor molecules on the metal surface affect the electric double layer by causing a change in the local dielectric properties of the electric double layer. In this case, these molecules may change the orientation of the dipoles of the water molecules, which causes a lowering of the dielectric constant and then decreases the double-layer capacitance. The decrease in double-layer capacitance may also be due to the decrease in the area where the electrolyte is present due to the formation of the inhibitor film (Wang et al., 2001).

TH-3102_146107038

Hence, the extent of adsorption on the metal solution interface increased with a higher concentration of STWE (Heydari and Javidi, 2012; Okafor et al., 2009).

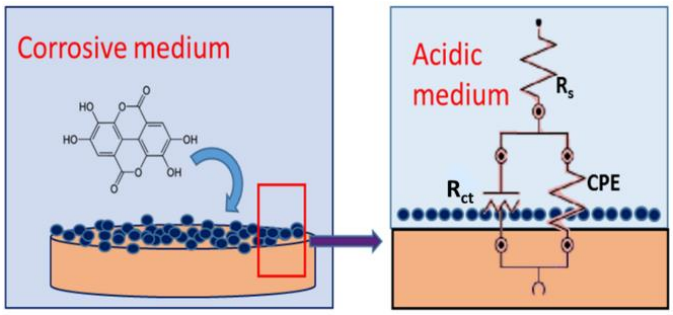

Fig. 3.6 Equivalent circuit for BQ plates in the presence of inhibitors.

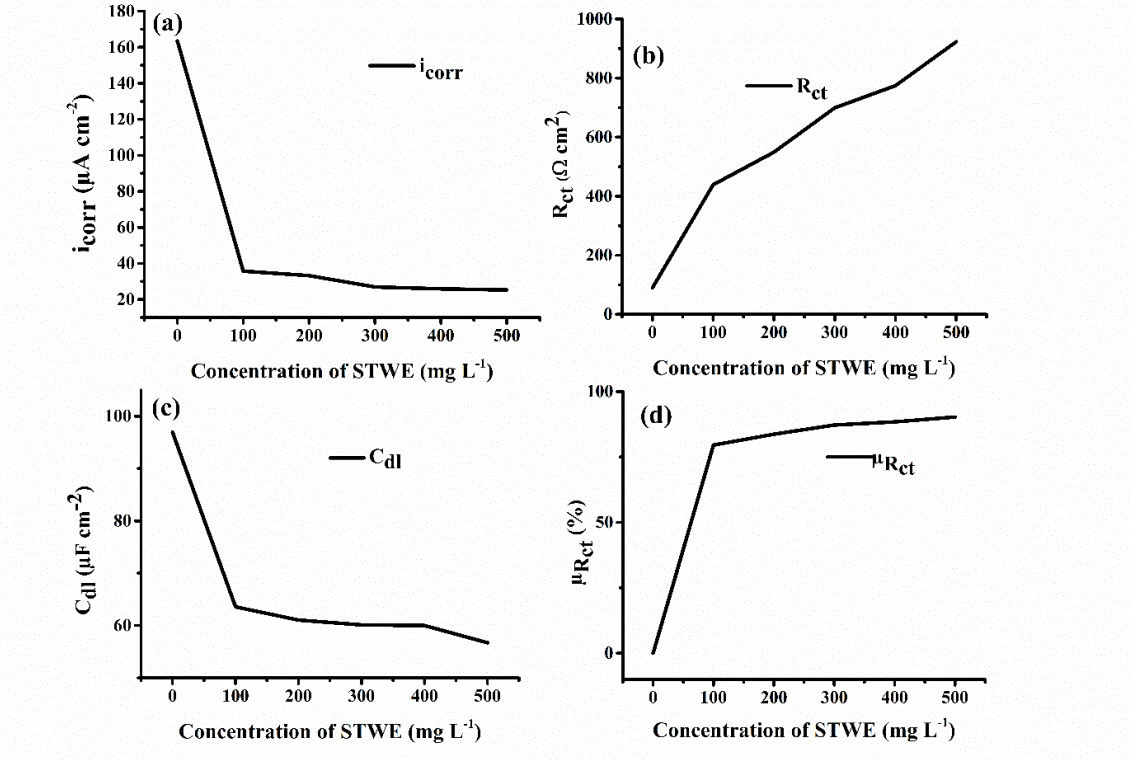

Fig. 3.7 Effect of concentration on the i_{corr} (a), R_{ct} (b), C_{dl} (c), $\mu_{R_{ct}}$ (d).

The changes in electrochemical parameters with respect to different concentrations of STWE are depicted in Fig. 3.7. The i_{corr} was decreased (Fig. 3.7(a)), R_{ct} was increased (Fig. 3.7(b)) and C_{dl} was decreased at a higher concentration of STWE (Fig. 3.7(c)). The $\mu_{R_{ct}}$ was increased with the increased amount of STWE (Fig. 3.7(d)), and it was observed that the maximum $\mu_{R_{ct}}$ is 90.28 % at the highest

TH-3102_146107038

concentration of STWE (500 mg L^{-1}). It has been noticed that at higher concentrations when i_{corr} is low C_{dl} is also low due to the presence of high charge transfer resistance. This phenomenon confirms that at high concentrations, the resistance on the surface obstructed the polarization and reduced the corrosion current, and thus, the conductivity on the surface was reduced. The reduction in conductivity and corrosion current lead to protecting the BQ metal in an acidic solution.

3.4 Determination of thermodynamic parameters

Langmuir (Fig. 3.8(a) and (b)), Temkin (Fig. 3.8(c)), and Frumkin (Fig. 3.8(d)) adsorption isotherm were plotted to observe the relation between concentration (*C*) of STWE and surface coverage (θ). These isotherms also help to understand the type of adsorption of the inhibitors on the BQ steel surface in 1 (M) HCl medium. All of the models were fitted well with a regression coefficient value of 0.99. Among them, Langmuir isotherm (Eq. 3.1) fitted best with a regression coefficient of 0.99 and formed a straight line shown in Fig. 3.8 (a). The straight-line form of Langmuir isotherm is given as follows:

$$\frac{C}{\theta} = \frac{1}{K_{ads}} + C \qquad \textbf{3.1}$$

Where C is the concentration of inhibitor, θ is the surface coverage determined by $\mu_{R_{ct}} 100^{-1}$, $\mu_{R_{ct}}$ is the inhibition efficiency, K_{ads} is the adsorption equilibrium constant.

K_{ads}, the equilibrium constant of the adsorption process and is related to the adsorption-free energy, ΔG°_{ads}, (standard Gibbs free energy) by the following equation:

$$\Delta G^{\circ}_{ads} = -RTln(C_{water} K_{ads}) \qquad \textbf{3.2}$$

TH-3102_146107038

Where R, is the universal gas constant (8.314 $Jmol^{-1}K^{-1}$), T is the ambient temperature (298.15 K) at which the experiment was accomplished, C_{water} is the concentration of water in 1000 gL^{-1}. The linear regression coefficient (R^2), ΔG°_{ads}, K_{ads} , derived from the Langmuir plot, are depicted in Table 3.4.

Table 3.4 Adsorption isotherm parameters for STWE in HCl

	R^2	$1/K_{ads}$(g L^{-1})	K_{ads}(Lg^{-1})	ΔG°_{ads}($kJmol^{-1}$)
Polarisation	0.99	0.061	16.41	-24.06
EIS	0.99	0.043	23.25	-24.92

The negative values of $\Delta G°_{ads}$ indicates that the adsorption process is spontaneous. Generally, if the value of $\Delta G°_{ads}$ is -20 $kJmol^{-1}$ or lower negative than that, then the interaction is considered electrostatic, known as physisorption. When values of $\Delta G°_{ads}$ are found more negative than -40 $kJmol^{-1}$ the interaction between the inhibitor molecules and the metal surface is based on electron sharing and coordinate bonding (chemisorption). In this case, the value of $\Delta G°_{ads}$ indicates that the adsorption processis mixed-type .

TH-3102_146107038

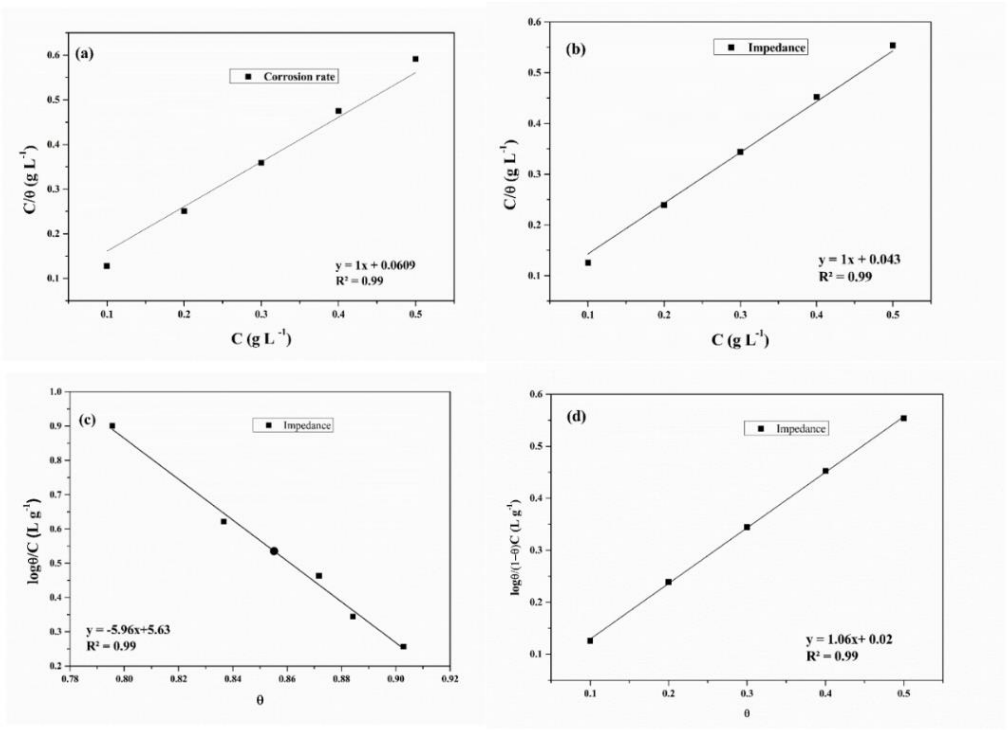

Fig. 3.8 Langmuir adsorption isotherm plots for polarization (a), impedance method(b), Temkin (c) and Frumkin adsorption isotherm plots (d) for impedance methods.

3.5 Surface morphology

3.5.1 FESEM- EDX study

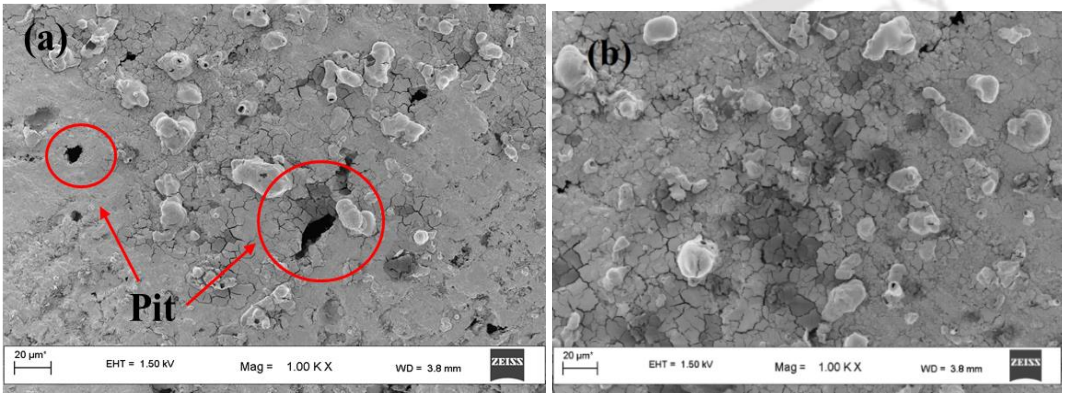

Fig. 3.9 FESEM images of uninhibited (a), and inhibited (presence of STWE) (b) BQ steel.

Fig. 3.9 (a) illustrates the FESEM images of the BQ plate in the absence of inhibitors. The cracks and the pit are prominent in the absence of the inhibitors in 1 (M) HCl. Fig. 3.9 (b) shows the images of BQ steel in the presence of STWE at the same medium. There is a noticeable difference in both cases at the microstructure level. In the absence of STWE, the microcracks and pits are visible due to acid attacks, which are absent in the presence of STWE. This type of damaged surface is missing in the presence of STWE in the acidic medium. The phenolic compounds present in STWE made a thin layer on the surface of the BQ plate. Subsequently, the pits and cracks were not formed as the corrosion on the surface was reduced.

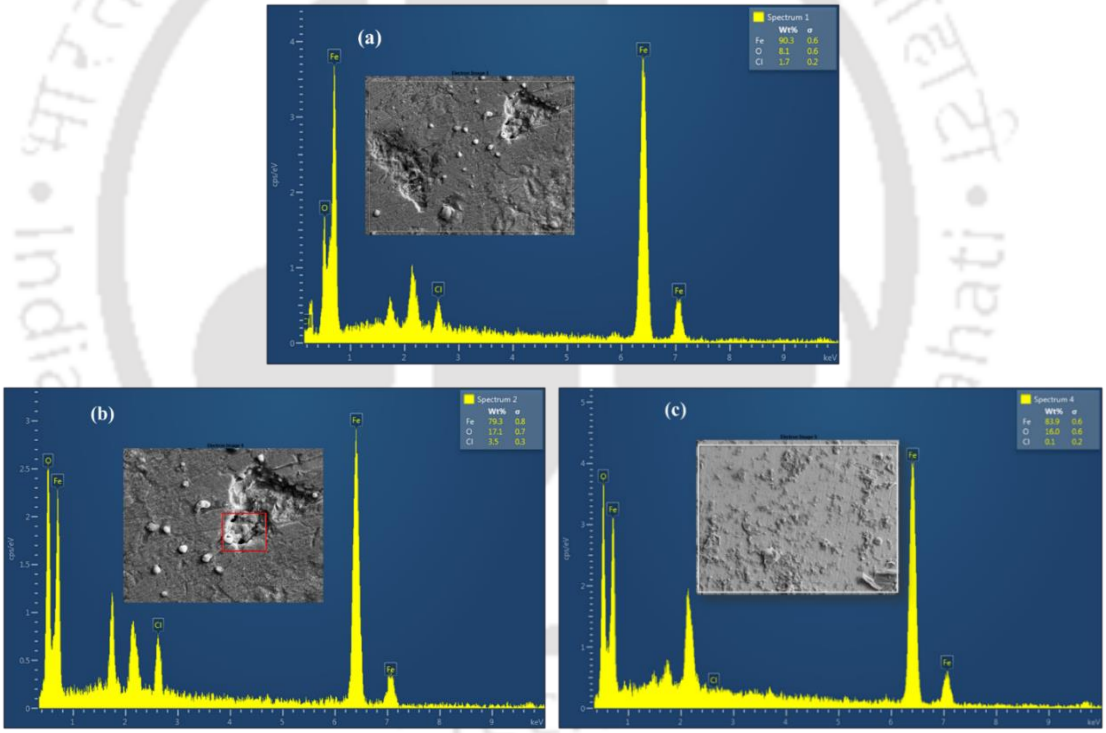

Fig. 3.10 EDX of uninhibited (a and b), and inhibited (c) (presence of STWE) BQ steel.

From the EDX spectra (Fig. 3.10), it is observed that exposure of 1 (M) HCl for 24 h in the absence and presence of STWE made the differences in the elementary composition of the surface. The iron weight percentage in BQ is changed. Fig. 3.10 (a) and (b) show the EDX spectra of Fe and Cl in the absence of STWE, and Fig. 3.10 (c)

TH-3102_146107038

shows the same in the presence of STWE. The presence of Fe and Cl^- in EDX spectra proves that the Cl^- was adsorbed on the surface due to redox reaction on the surface of the BQ plate in the presence of HCl. The weight percentage of Fe and Cl^- in the absence of the inhibitor was 90.3% and 1.7%, respectively. The Cl^- made the electrostatic bond with positive ions on a metal surface (Fe^{2+}). In Fig. 3.10, it is noticed that on the BQ surface, mainly where few pits are formed, the weight percentage of Fe (79.3%) is lower, and Cl^- (3.5%) is higher than the overall surface due to the aggressive corrosion in the pits. On the other hand, the weight percentage of Cl^- and Fe ions were drastically changed in the presence of STWE. The weight percentage of Fe changed from 90.3% to 83.9%, and Cl^- changed from 1.7% to 0.1%. The weight percentage of these ions was reduced as a result of less oxidation and reduction reaction. The phenolic compounds of the STWE gradually deposited on the BQ surface and formed a protective layer, which diminished the oxidation of iron. This protective film resisted the ingression of the Cl^- into the pit of the BQ surface. Thus the metal got protected from the corrosive media (Ali Asaad et al., 2018).

3.5.2 AFM study

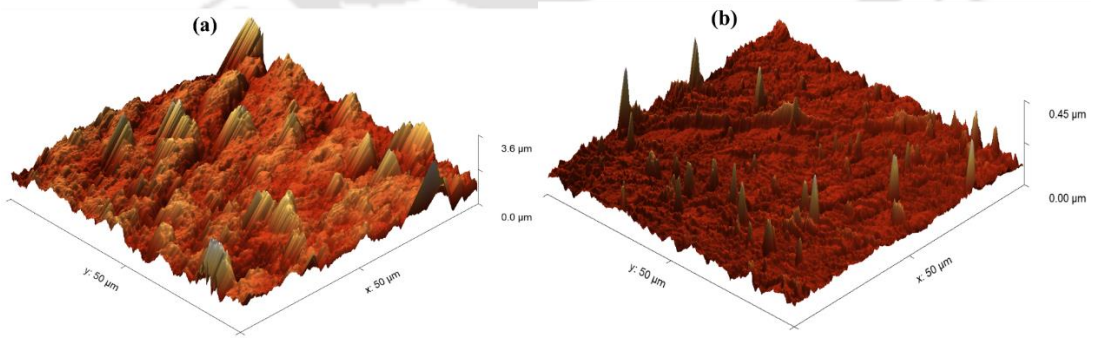

Fig. 3.11 AFM images of uninhibited (a), and inhibited (presence of STWE) (b) BQ steel.

TH-3102_146107038

The changes in the surface pattern in the presence and absence of STWE were also noticeable in the AFM study (Fig. 3.11). The effect of the STWE was visible as the roughness in the presence of STWE was reduced marginally due to the less oxidation reaction on the surface of the BQ plate. The presence of 500 ppm of STWE on the BQ surface created a protective film, which worked as a barrier to corrosive constituents. Whereas in the absence of STWE, the damages on the surface were visible, and the roughness was found to be high enough. The average surface roughness in the presence and absence of STWE was 18 nm and 240 nm, respectively (Prabakaran et al., 2016; Singh and Quraishi, 2016; Srivastava et al., 2018).

3.6 Quantum chemical calculation studies

The electrochemical techniques enlighted the kinetics of corrosion and the underlying corrosion mechanism of BQ steel in the presence and absence of inhibitors in an acidic medium. Characterization of the interaction between inhibitor molecules and the BQ surface was needed to understand the mechanism and the type of interaction. To characterize this interaction between the BQ surface and inhibitor molecules, theoretical approaches like quantum-level calculations provided useful insights. The efficiency of corrosion inhibitors can be explained with the help of quantum-level calculations, which are based on the frontier molecular orbital (FMO) theorem (Srivastava et al., 2018).

The frontier molecular orbital (FMO) theory helps to accomplish quantum chemical calculations. The FMOs, highest occupied molecular orbital (HOMO), and lowest unoccupied molecular orbitals (LUMO) play a pivotal role in determining the efficacy of corrosion inhibition. According to Fukui's theory, the HOMO regions tend to donate an electron and are considered as the site for adsorption. Generally, phenyl

TH-3102_146107038

rings, π bonds, and charged heteroatoms are associated with HOMO regions. The LUMO region illustrates the tendency of electron acceptance (Ganash, 2018).

The energy of HOMO (E_{HOMO}) and (E_{LUMO}) signify electron donation and acceptance ability, respectively, as discussed earlier. Besides that, the energy gap (ΔE) between LUMO and HOMO (Eq. 2.25) intimate the stability of any interaction between two molecules in the reaction process (Feng et al., 2018). The optimized structure and and HOMO and LUMO are portrayed in Fig. 3.12.

3.6.1 Frontier molecular orbitals and their energies

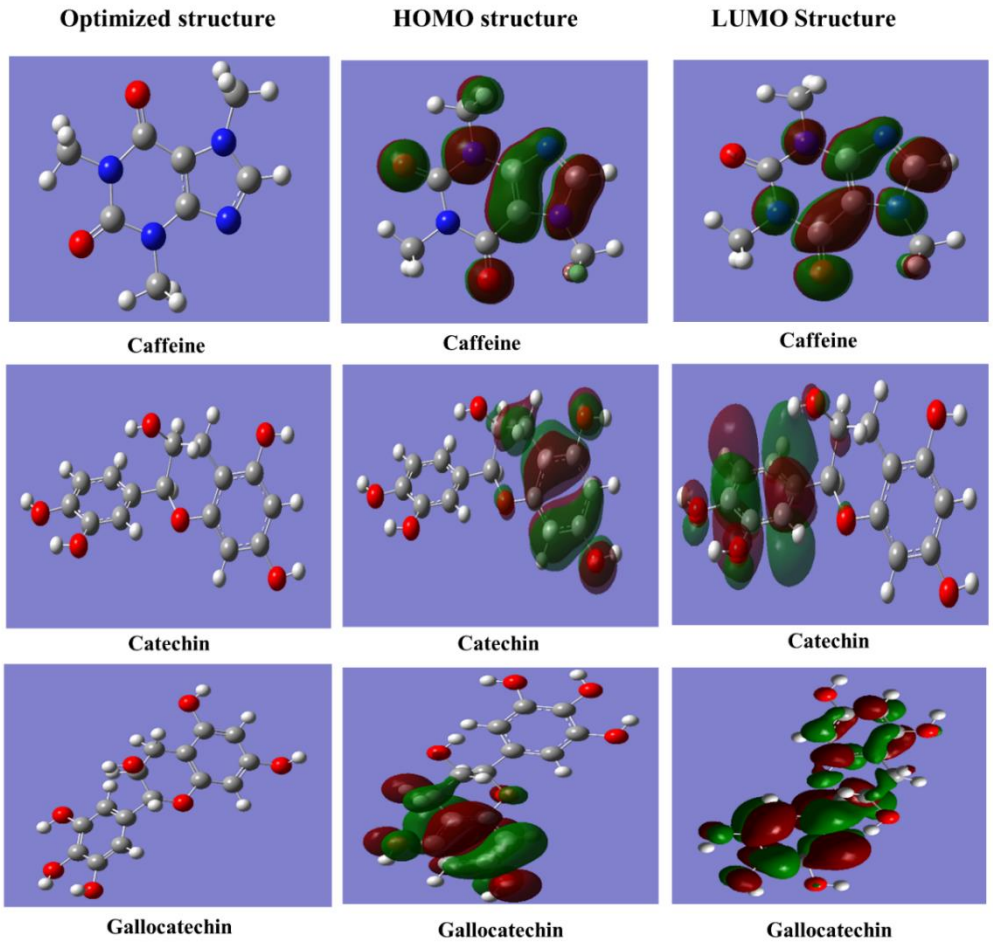

Fig. 3.12 The Electron Density Distribution of caffeine, catechin, and gallocatechin monomers.

TH-3102_146107038

According to Koopman's theory, ionization potential (I) and electron affinity (A) is related to the energy of FMOs. (Eq. 2.26 and 2.27) Other parameters like electronegativity (χ), global hardness (η), softness (σ) and fraction of electron (ΔN) transferable from inhibitor to iron were also calculated using ionization potential and electron affinity. In this study, ΔN was calculated using the theoretical values of χ_{Fe} (7 ev) and η_{Fe} (0 ev). The energy levels HOMO-LUMO for the caffeine, catechin, and gallocatechin were calculated, and the relevant chemical quantum parameters are listed in Table 3.5.

Table 3.5 Quantum parameters of inhibitors

Inhibitors name	E_{HOMO} (eV)	E_{LUMO} (eV)	ΔE (eV)	I (eV)	A (eV)	χ (eV)	η (eV)	σ ($1eV^{-1}$)	ΔN (eV)
Caffeine	-6.363	-1.387	4.976	6.363	1.387	3.875	2.488	0.402	0.628
Catechin	-5.887	-0.119	5.767	5.887	0.119	3.003	2.884	0.347	0.693
Gallocatechin	-6.081	-0.298	5.783	6.081	0.298	3.189	2.891	0.346	0.659

The molecule having higher E_{HOMO} value has a higher tendency to donate electrons to the empty molecular orbital of lower energy. Increase in E_{HOMO} facilitates adsorption by transferring electrons to an acceptor surface; thus, the electron transport process through the adsorbed layer is influenced. The molecules having lower E_{LUMO} Values have a higher electron acceptance ability from an orbital of higher energy. The higher E_{HOMO} value of catechin indicates the higher electron-donating ability of catechin and lower E_{LUMO} value of caffeine indicates higher electron acceptability (Table 3.5). It is observed that the ΔE values obtained for caffeine, catechin, and gallocatechin are 4.976, 5.767, and 5.783 eV, respectively, and ΔE value obtained for caffeine is lower than catechin and gallocatechin. A higher energy gap (ΔE) value confines the interaction between electrons and interrupts to electron donation and

TH-3102_146107038

acceptance process. Because to transfer a single electron from a higher energy level to a lower energy, more ionization energy is required. As caffeine has the lowest energy gap among them, it has a higher efficacy for corrosion inhibition. Though electronegativity (χ) did not show any trend, but the lowest global hardness (η) and highest softness (σ) was found for caffeine. Both η and σ support the chemical reactivity of any molecule. The higher value of σ and lower value of η stimulate consistent reactivity and better inhibition capacity. The difference in the number of electrons transferable from the inhibitor to Fe (ΔN) among the inhibitors is not much. However, catechin has a higher value of 0.693, and caffeine has a lower value of 0.628. This higher value of ΔN suggests that the catechin has a higher electron-donating ability than caffeine. In contrast, caffeine has higher electron acceptability than catechin, which is also supported by the E_{LUMO} and E_{HOMO} value (Ali Asaad et al., 2018; Biezma and San Cristóbal, 2005; Khanra et al., 2018; Parthipan et al., 2018; Saxena et al., 2018; Verma et al., 2018).

3.7 Mechanism of inhibition

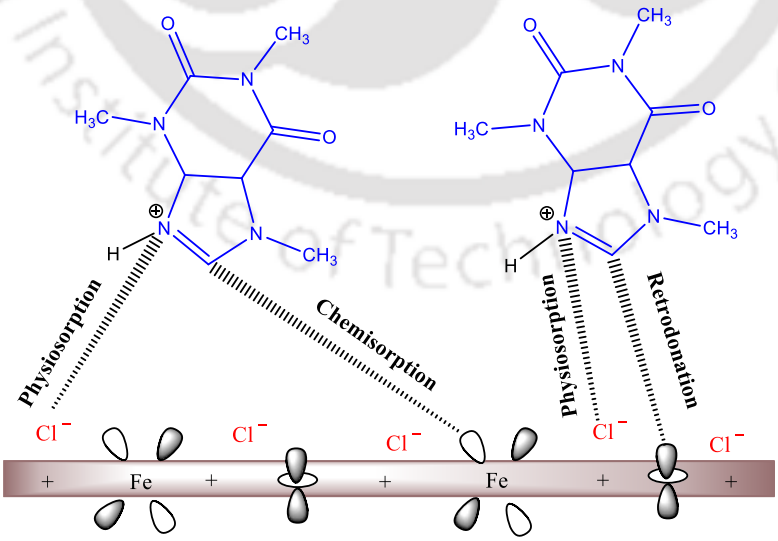

Fig. 3.13 Representation of the mechanism of corrosion inhibition in acidic medium

TH-3102_146107038

The mechanism of corrosion for iron in chloride medium can be explained by the following anodic and cathodic reaction:

Anodic Reaction:

$$Fe + Cl^- \leftrightharpoons (FeCl^-)_{ads} \quad \textbf{3.3}$$

$$(FeCl^{--})_{ads} \leftrightharpoons (FeCl)_{ads} + e^- \quad \textbf{3.4}$$

$$(FeCl)_{ads} \rightarrow (FeCl^+) + e^- \quad \textbf{3.5}$$

$$(FeCl^+) \leftrightharpoons Fe^{2+} + Cl^- \quad \textbf{3.6}$$

Cathodic reaction:

$$Fe + H+ \rightleftharpoons (FeH^+)ads \quad \textbf{3.7}$$

$$(FeH^+)_{ads} + e^- \rightarrow (FeH)_{ads} \quad \textbf{3.8}$$

$$(FeH)_{ads} + H^+ + e^- \rightarrow Fe + H_2 \quad \textbf{3.9}$$

In an anodic reaction, oxidation of iron leads to evolution and $Fe^{2+,}$ whereas in a cathodic reaction, the proton gets reduced to generate hydrogen gas. When inhibitor molecules are incorporated in an acidic medium, they start to become protonated, and these protonated molecules get adsorbed on the surface via electrostatic interaction with Cl^-, which is physical adsorption (Fig. 3.13). The H^+ and the protonated inhibitors also start to compete with each other to make interaction with a nucleophilic zone of the surface. When these negatively charged nucleophilic areas donate the electron to protonated inhibitors, then these inhibitor molecules become neutralized. As a result of neutralization, the lone pair electron present in heteroatoms initiates chemical adsorption. Once the surface is saturated with the electron, the surface becomes more negatively charged. Then to release the excess electron from the surface, the electron present in the "d" orbital of iron gets transferred to the vacant π antibonding orbital of the inhibitor molecules (retrodonation) (Srivastava et al., 2018).

TH-3102_146107038

3.8 Summary

Our current study has described an experimental and theoretical investigation of corrosion inhibition by STWE as corrosion inhibitors in 1 (M) HCl on the BQ surface. The extraction from solid waste was a conventional extraction process using water as the solvent. After all the investigations, the following conclusions are obtained:

1. Mainly three compounds were identified as corrosion inhibitors in solid tea waste extract (STWE, which are caffeine, catechin, and gallocatechin from the LC-MS data.
2. The corrosion current (i_{corr}) and polarization resistance R_P were 163.51 µA cm^{-2} and 102.62 Ω $cm^{2,}$ respectively, in the absence of STWE. The corrosion current (i_{corr}) was found the minimum, 25.29 µA cm^{-2} at 500 mg L^{-1} of STWE.
3. The charge-transfer resistance (R_{ct}) was found at 89.72 Ωcm^{-2} and 923.40 Ωcm^{-2} in the absence and presence of 500 mg L^{-1} STWE, respectively. So the maximum inhibition efficiency in terms of charge transfer resistance was found to be 90% after the incorporation of 500 mg L^{-1} of tea waste extract.
4. The type of adsorption was physisorption, which was validated by the value of K_{ads} (23.25 L g^{-1}) and $\Delta G°_{ads}$ (- 24.92 kJ mol^{-1}), which is obtained from Langmuir isotherm and the adsorption was thermodynamically favorable.
5. The inhibition was mainly caused by the formation of a protective barrier on the metal electrolyte interface. This barrier was formed by the adsorption of the phenolic compounds present in the STWE, which was confirmed by FESEM, EDX, and AFM studies.
6. Among the identified compounds, caffeine had a lower energy gap (ΔE) of 4.976 eV; hence, it may have higher efficiency than others in getting adsorbed on the surface.

TH-3102_146107038

3.9 Reference

Al-Moubaraki, A.H., 2015. Corrosion Protection of Mild Steel in Acid Solutions Using Red Cabbage Dye. Chem. Eng. Commun. 202, 1069–1080. https://doi.org/10.1080/00986445.2014.907565

Al-Otaibi, M.S., Al-Mayouf, A.M., Khan, M., Mousa, A.A., Al-Mazroa, S.A., Alkhathlan, H.Z., 2014. Corrosion inhibitory action of some plant extracts on the corrosion of mild steel in acidic media. Arab. J. Chem. https://doi.org/10.1016/j.arabjc.2012.01.015

Ali Asaad, M., Sarbini, N.N., Sulaiman, A., Ismail, M., Huseien, G.F., Abdul Majid, Z., Bothi Raja, P., 2018. Improved corrosion resistance of mild steel against acid activation: Impact of novel Elaeis guineensis and silver nanoparticles. J. Ind. Eng. Chem. 63, 139–148. https://doi.org/10.1016/j.jiec.2018.02.010

Biezma, M. V., San Cristóbal, J.R., 2005. Methodology to study cost of corrosion. Corros. Eng. Sci. Technol. 40, 344–352. https://doi.org/10.1179/174327805X75821

Feng, L., Zhang, S., Qiang, Y., Xu, S., Tan, B., Chen, S., 2018. The synergistic corrosion inhibition study of different chain lengths ionic liquids as green inhibitors for X70 steel in acidic medium. Mater. Chem. Phys. 215, 229–241. https://doi.org/10.1016/j.matchemphys.2018.04.054

Ganash, A.A., 2018. Theoretical and experimental studies of dried marjoram leaves extract as green inhibitor for corrosion protection of steel substrate in acidic solution. Chem. Eng. Commun. 205, 350–362. https://doi.org/10.1080/00986445.2017.1391096

Heydari, M., Javidi, M., 2012. Corrosion inhibition and adsorption behaviour of an amido-imidazoline derivative on API 5L X52 steel in CO 2-saturated solution and synergistic effect of iodide ions. Corros. Sci. 61, 148–155. https://doi.org/10.1016/j.corsci.2012.04.034

Ji, G., Dwivedi, P., Sundaram, S., Prakash, R., 2013. Inhibitive effect of Chlorophytum borivilianum root extract on mild steel corrosion in HCl and H2SO4 solutions. Ind. Eng. Chem. Res. 52, 10673–10681. https://doi.org/10.1021/ie4008387

Ji, G., Shukla, S.K., Dwivedi, P., Sundaram, S., Prakash, R., 2011. Inhibitive effect of argemone mexicana plant extract on acid corrosion of mild steel. Ind. Eng. Chem.

TH-3102_146107038

Res. 50, 11954–11959. https://doi.org/10.1021/ie201450d

Khanra, A., Srivastava, M., Rai, M.P., Prakash, R., 2018. Application of Unsaturated Fatty Acid Molecules Derived from Microalgae toward Mild Steel Corrosion Inhibition in HCl Solution: A Novel Approach for Metal-Inhibitor Association. ACS Omega 3, 12369–12382. https://doi.org/10.1021/acsomega.8b01089

Liao, L.L., Mo, S., Luo, H.Q., Li, N.B., 2018. Corrosion protection for mild steel by extract from the waste of lychee fruit in HCl solution: Experimental and theoretical studies. J. Colloid Interface Sci. 520, 41–49. https://doi.org/10.1016/j.jcis.2018.02.071

M'hiri, N., Veys-Renaux, D., Rocca, E., Ioannou, I., Boudhrioua, N.M., Ghoul, M., 2016. Corrosion inhibition of carbon steel in acidic medium by orange peel extract and its main antioxidant compounds. Corros. Sci. 102, 55–62. https://doi.org/10.1016/j.corsci.2015.09.017

Mata-Bilbao, M.D.L., Andrés-Lacueva, C., Roura, E., Jáuregui, O., Torre, C., Lamuela-Raventós, R.M., 2007. A new LC/MS/MS rapid and sensitive method for the determination of green tea catechins and their metabolites in biological samples. J. Agric. Food Chem. 55, 8857–8863. https://doi.org/10.1021/jf0713962

Melitas, N., Chuffe-Moscoso, O., Farrell, J., 2001. Kinetics of soluble chromium removal from contaminated water by zerovalent iron media: Corrosion inhibition and passive oxide effects. Environ. Sci. Technol. 35, 3948–3953. https://doi.org/10.1021/es001923x

Mourya, P., Banerjee, S., Singh, M.M., 2014. Corrosion inhibition of mild steel in acidic solution by Tagetes erecta (Marigold flower) extract as a green inhibitor. Corros. Sci. 85, 352–363. https://doi.org/10.1016/j.corsci.2014.04.036

Okafor, P.C., Liu, X., Zheng, Y.G., 2009. Corrosion inhibition of mild steel by ethylamino imidazoline derivative in CO2-saturated solution. Corros. Sci. 51, 761–768. https://doi.org/10.1016/j.corsci.2009.01.017

Parthipan, P., Elumalai, P., Narenkumar, J., Machuca, L.L., Murugan, K., Karthikeyan, O.P., Rajasekar, A., 2018. Allium sativum (garlic extract) as a green corrosion inhibitor with biocidal properties for the control of MIC in carbon steel and stainless steel in oilfield environments. Int. Biodeterior. Biodegrad. 132, 66–73. https://doi.org/10.1016/j.ibiod.2018.05.005

Prabakaran, M., Kim, S.H., Hemapriya, V., Chung, I.M., 2016. Evaluation of

TH-3102_146107038

polyphenol composition and anti-corrosion properties of Cryptostegia grandiflora plant extract on mild steel in acidic medium. J. Ind. Eng. Chem. 37, 47–56. https://doi.org/10.1016/j.jiec.2016.03.006

Saxena, A., Prasad, D., Haldhar, R., 2018. Investigation of Corrosion Inhibition Effect and Adsorption Activities of Achyranthes aspera Extract for Mild Steel in 0.5 M H2SO4. J. Fail. Anal. Prev. 18, 957–968. https://doi.org/10.1007/s11668-018-0491-8

Singh, P., Quraishi, M.A., 2016. Corrosion inhibition of mild steel using Novel Bis Schiff's Bases as corrosion inhibitor: Electrochemical and Surface measurement. Meas. J. Int. Meas. Confed. 86, 114–124. https://doi.org/10.1016/j.measurement.2016.02.052

Srivastava, V., Chauhan, D.S., Joshi, P.G., Maruthapandian, V., Sorour, A.A., Quraishi, M.A., 2018. PEG-Functionalized Chitosan: A Biological Macromolecule as a Novel Corrosion Inhibitor. ChemistrySelect 3, 1990–1998. https://doi.org/10.1002/slct.201701949

Verma, C., Olasunkanmi, L.O., Ebenso, E.E., Quraishi, M.A., 2018. Adsorption characteristics of green 5-arylaminomethylene pyrimidine-2,4,6-triones on mild steel surface in acidic medium: Experimental and computational approach. Results Phys. 8, 657–670. https://doi.org/10.1016/j.rinp.2018.01.008

Wang, H.B., Shi, H., Hong, T., Kang, C., Jepson, W.P., 2001. Characterization of inhibitor and corrosion product film using electrochemical impedance spectroscopy (EIS). NACE - Int. Corros. Conf. Ser. 2001-March.

TH-3102_146107038

TH-3102_146107038

4

Corrosion inhibition by extract of purple rice bran (agro by-product)

TH-3102_146107038

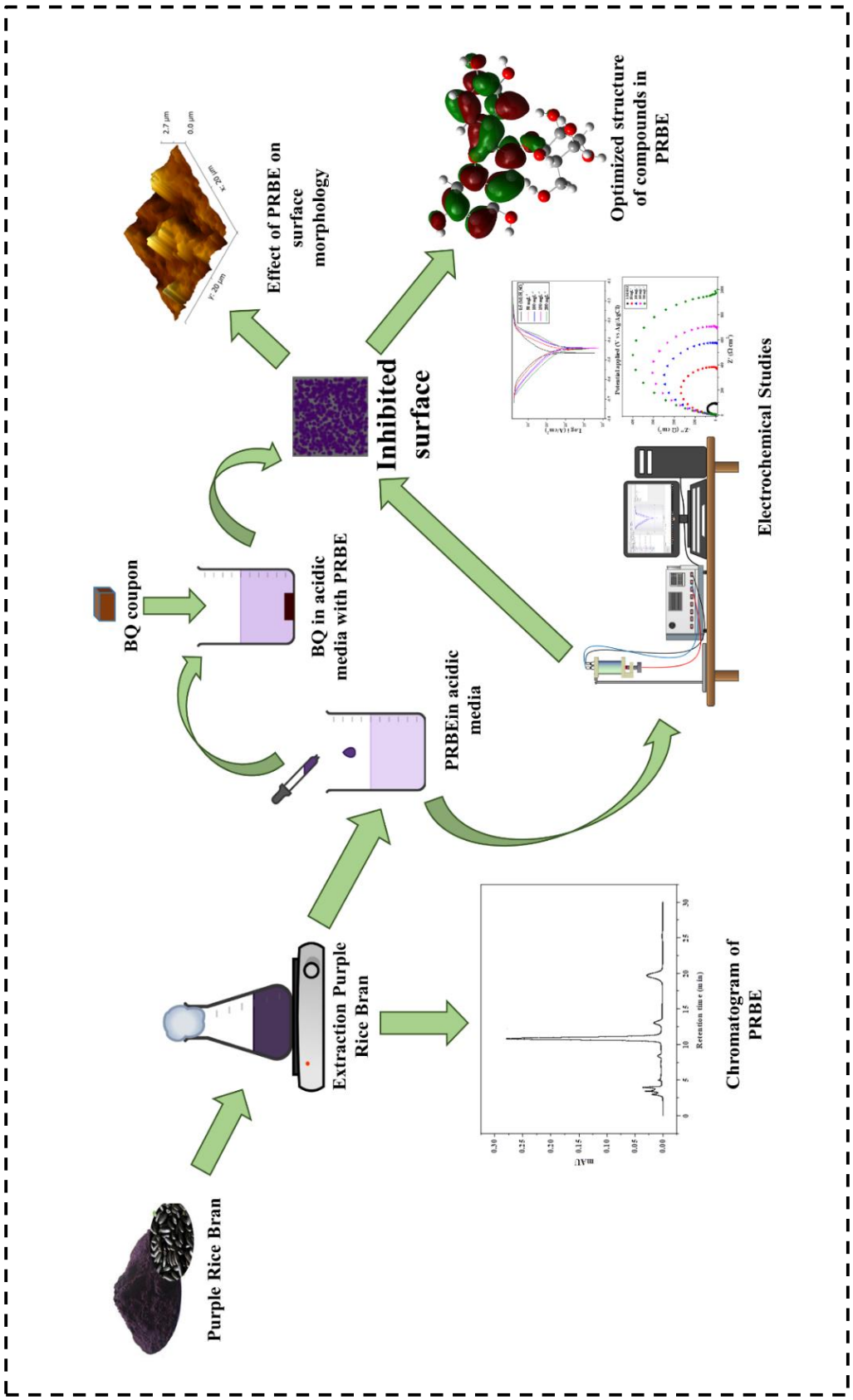

TH-3102_146107038

Corrosion inhibition by extract of purple rice bran (agro by-product)

In this chapter, corrosion inhibition efficiency and other related findings of purple rice bran extract, which is an agricultural by-product enriched with antioxidants, are discussed. The inhibitor was extracted from purple rice bran using conventional extraction methods and characterized by HPLC, which revealed the presence of two prime compounds named cyaniding-3-glucoside (C3G) and peonidin-3-glucoside (P3G). This purple rice bran extract (PRBE) was used to inhibit as a green corrosion inhibitor on boiler quality (BQ) steel to assess its inhibition performance in 1 (M) HCl and 0.5 (M) H_2SO_4. The inhibition performance was investigated by some electrochemical techniques such as open circuit potential (OCP), potentiodynamic polarization test (PDP), and electrochemical impedance spectroscopy (EIS). The investigation revealed that the maximum efficiency was 91.13% and 87.43% in the presence of 200 mg L^{-1} of PRBE in HCl and H_2SO_4 media, respectively. After applying various adsorption isotherm models, Langmuir isotherm was found as the best-fitted model that indicated both physical and chemical spontaneous adsorption of PRBE on the BQ surface. Both electrochemical and adsorption studies indicated the PRBE as a mixed-type inhibitor. Various quantum chemical parameters were calculated to find out the active sites and the donor-acceptor interaction capability of the inhibitor molecules. The quantum chemical calculation was achieved with the help of density functional theory (DFT). The theoretical studies disclosed that P3G has a lower energy gap than C3G but a higher dipole moment than C3G.

Published Artcle: Pal, A., Das, C., 2022. New eco-friendly anti-corrosion inhibitor of purple rice bran extract for boiler quality steel: Experimental and theoretical investigations. **J. Mol. Struct.** 1251, 131988. https://doi.org/10.1016/j.molstruc.2021.131988

TH-3102_146107038

4.1 Characterization of PRBE

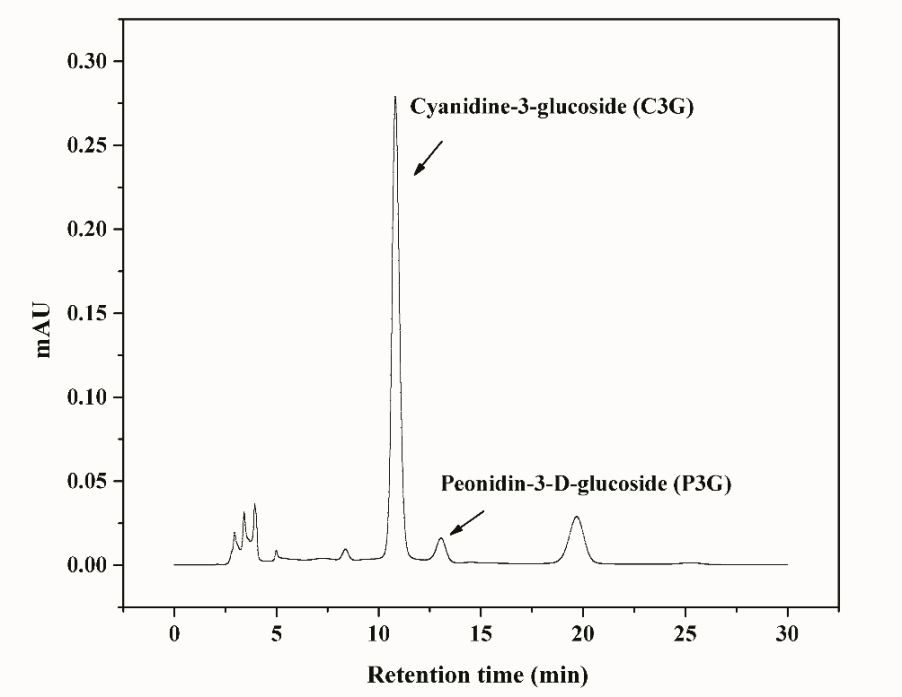

Fig. 4.1 The chromatogram of cyanidin-3-glucoside and Peonidin-3-d-glucoside identified in PRBE with retention time 11 and 13 min, respectively.

The distribution of compounds in crude PRBE after chromatographic separation is portrayed as a chromatogram in Fig. 4.1. From the ion chromatograms and each signal peak that corresponds to a particular compound, two main compounds were identified as the constituents of the crude purple rice bran extract Cyanidin-3-glucoside (C3G), and Peonidin-3-D-glucoside (P3G) are the two compounds that were detected by HPLC at 530 nm. The C3G, and P3G, were pointed out at the retention time of 11 and 13 min, respectively, which are visible on their respective peak. It was observed from Fig. 4.1 that C3G was the main anthocyanin over P3G in purple rice bran extract (Das et al., 2018).

These compounds contain various functional groups, aromatic rings consisting of heteroatoms such as N, S, O, P, and the π electrons, which assist them in interacting with various polar surfaces by various kinds of adsorption processes.

TH-3102_146107038

4.2 Weight loss method

To observe the outcome of PRBE on the BQ steel, the corrosion rate (CR) was calculated using the weight loss method in the absence and the presence of different PRBE concentrations (50 mg L^{-1} to 200 mg L^{-1}) in both HCl and H_2SO_4 media. The inhibition efficiency $\mu_{CR}\%$ was also calculated and mentioned along with the corrosion rate (CR) in Table 4.1. It is observed from Table 4.1 that PRBE is an effective inhibitor in reducing the corrosion rate. It is also noticed that the *CR* decreases and the inhibition efficiency rises with the increase in the concentration of PRBE.

Table 4.1 Corrosion rate and inhibition efficiency for BQ plate in 1 (M) HCl and 0.5 (M) H_2SO_4 with and without PRBE.

	Conc. (mg L^{-1})	$CR \times 10^2$ (mm $year^{-1}$)	$\mu_{CR}\%$
HCl media	**0 (Blank) 1(M)HCl**	212.07 ± 8.54	0.00 ± 0.00
	50	55.57 ± 2.28	73.80 ± 1.09
	100	40.15 ± 1.56	81.07 ± 1.79
	150	32.79 ± 1.49	84.54 ± 2.01
	200	25.10 ± 0.95	88.17 ± 1.40
H_2SO_4 media	**0 (Blank) 0.5 (M) H_2SO_4**	214.69 ± 10.38	0.00 ± 0.00
	50	69.63 ± 2.57	67.57 ± 0.83
	100	44.22 ± 1.24	79.40 ± 1.30
	150	34.11 ± 1.36	84.11 ± 1.86
	200	26.35 ± 1.02	87.73 ± 1.35

TH-3102_146107038

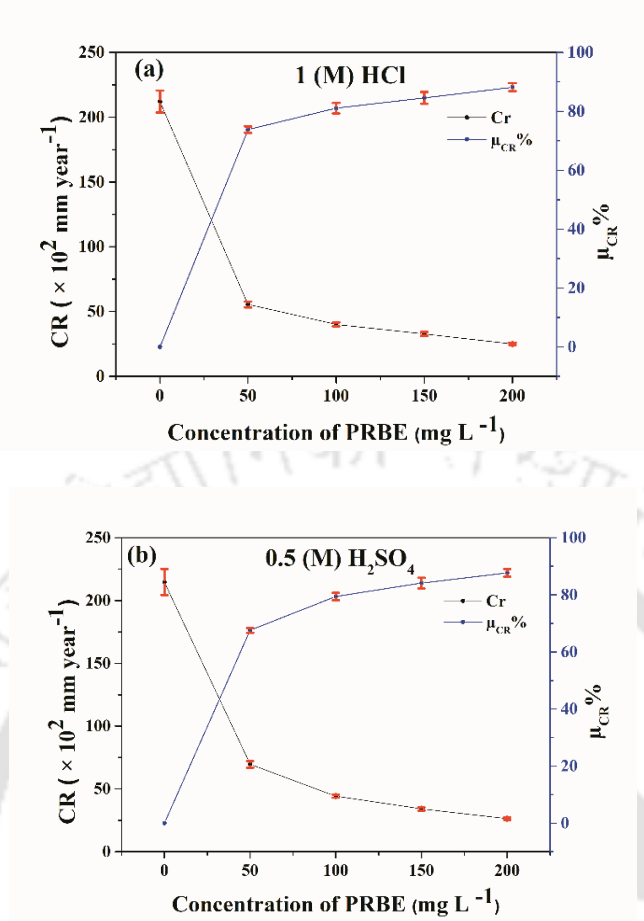

Fig. 4.2 Weight loss and corrosion rate of BQ plate in (a) 1 (M) HCl and (b) 0.5 M H_2SO_4 with and without PRBE.

From Fig. 4.2 (a) and (b), also it is clearly noticed that the presence of PRBE exhibits a significant inhibition efficiency even at the lowest concentration. This increment of inhibition efficiency in the presence of PRBE is mainly due to the depletion of the reaction rate of the redox reactions, which take place during corrosion. There are two types of reactions that occur in the corrosion process, which play a key role in the intensity of the corrosion process. One of them is an anodic reaction that leads iron to become oxidized into Fe^{2+} by the oxidation process ($Fe \rightarrow Fe^{2+} + 2e^-$). The other one is a cathodic reaction where H_2 gas is generated from H^+ ($2H^+ + 2e^- \rightarrow 2(H)_{ads} + H_2$). When the PRBE was introduced to the acidic media, both anodic reaction and cathodic reduction were hindered, leading to less iron oxidation from the BQ steel

TH-3102_146107038

surface. (Ali Asaad et al., 2018; Mourya et al., 2014b). A careful look into Table 4.1 reveals that the efficiency in HCl is much higher compared to H_2SO_4 at the lowest concentration (50 mg L^{-1}) of PRBE. However, at the highest concentrations, the efficiency is almost identical in both the acidic media. It is already established that the adsorbability of Cl^- is much higher than the SO_4^{2-}, which leads to the lesser negatively charged surface in the H_2SO_4 solution. A less negatively charged surface is less favorable for the adsorption of the protonated organic compounds of the inhibitor if the interaction between the two surfaces and the species is based on physical adsorption. So the Cl^- media is much more aggressive for adsorption of the positively charged organic compounds compared to SO_4^{2-} media in lower concentrations. The interaction between these anions and the protonated organic compounds could be based on physical or chemical adsorption, which was examined in the following studies (Cang et al., 2012; Mourya et al., 2013; Srivastava et al., 2017b).

4.3 Electrochemical measurements

To evaluate the electrochemical kinetics of the corrosion for BQ steel in a defined electrolyte and to assess the efficiency of the inhibition, different electrochemical studies are needed to be studied. These studies primarily focus on the revelation of i_{corr} and R_{ct} from which inhibition efficiencies of PRBE can be inferred.

TH-3102_146107038

4.3.1 Open circuit potential measurements

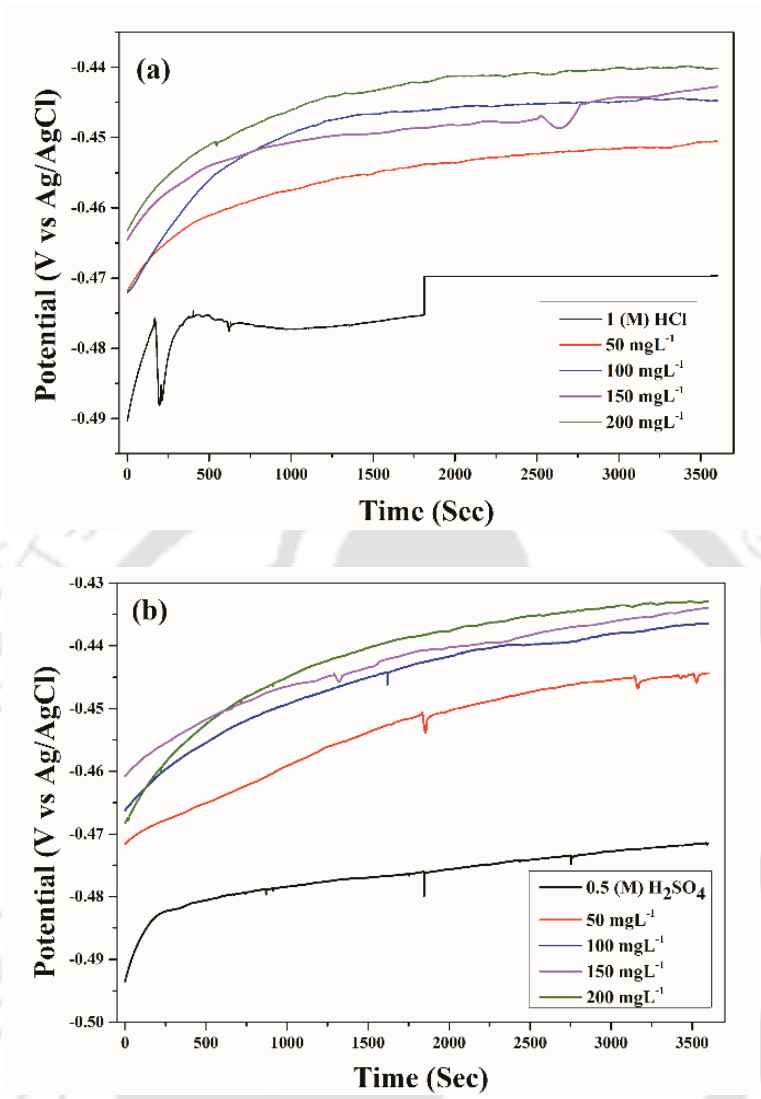

Fig. 4.3 OCP of BQ metal in the presence of the different amounts of PRBE in (a) HCl and (b) H_2SO_4.

The average OCP values were recorded for one hour for each experiment, and the changes in OCP with respect to time are displayed in Fig. 4.3 (a) and (b). The figures show clearly that in the presence of PRBE, OCP moves towards positive values compared to the absence of inhibitors. Moreover, at higher concentrations, the plots move towards more positive directions. These changes of the OCP, towards a favorable direction, in the presence of PRBE, are considered an improvement in the OCP that

TH-3102_146107038

might be caused by the formation of the protective layer on BQ. The unchanged potential over time also indicates the stability of the system. At zero concentration of PRBE, the surface did not become stabilized readily, as there was no chance of protective layer formation by PRBE. From the figures, it can be observed that the OCP is shifted maximum toward the positive side at the higher concentration, and there is less fluctuation in the OCP plots due to easy attainment of steady-state because of the stable film of PRBE (Li et al., 2021; Naghi Tehrani et al., 2021a; Qiang et al., 2021, 2017a; Singh and Quraishi, 2016b).

4.3.2 Potentiodynamic Polarization Measurements

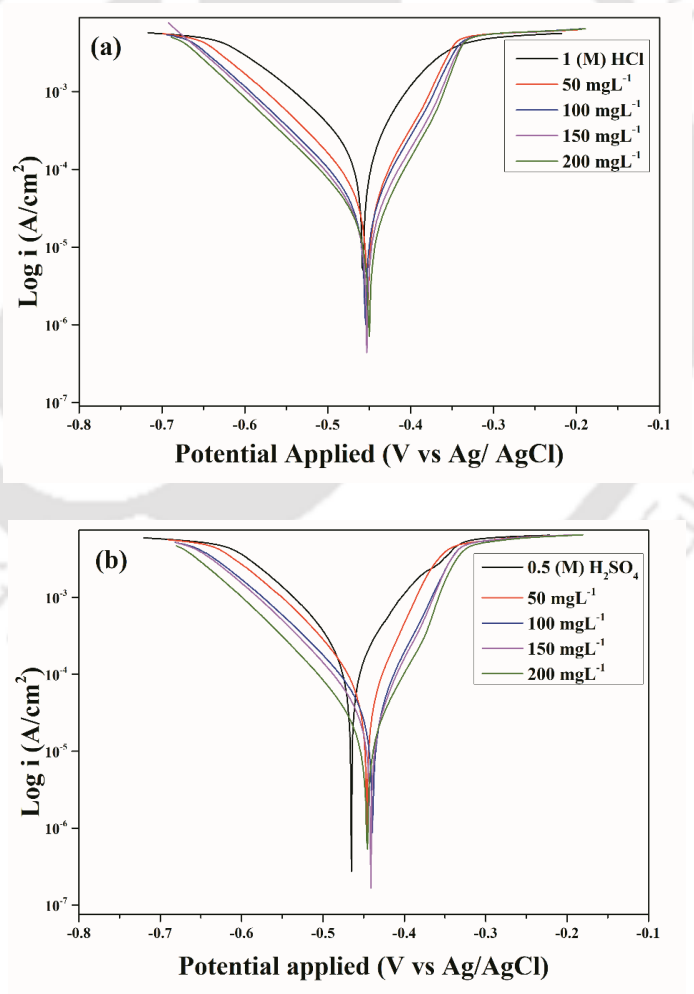

Fig. 4.4 Tafel polarization of BQ metal in the absence and presence of different amounts of PRBE in (a) HCl and (b) H_2SO_4.

TH-3102_146107038

The study of Tafel polarization is required to understand the electrochemical kinetics of the corrosion reaction occurring on the surface of the material. The effects of polarization are represented in Fig. 4.4 (a) and (b) as Tafel plots for PRBE in HCl and H_2SO_4 media. Numerous corrosion parameters which were computed by extrapolating the Tafel curves are displayed in Table 4.2. The inhibition efficiencies (IE) at different concentrations in terms of corrosion current were also mentioned in Table 4.2.

From the potentiodynamic experimental findings, it is clearly observed that in the presence of the extracts, both the anodic and cathodic currents are found to decrease, which is an indicator of the decrease in the rate of corrosion. The higher current in both anodic and cathodic sides is higher in the absence of PRBE, mainly due to the higher metal dissolution in the anodic site and higher hydrogen evolution on the cathodic site. Besides the reduction in the anodic and cathodic current, Fig. 4.4 (a) and (b) depicts that PRBE changed the corrosion potential (E_{corr}) towards the positive or anodic side compared to the uninhibited Tafel curves in both acidic media. Certainly, the addition of the inhibitors prevented the anodic reaction of metal dissolution and regulated the process of corrosion. But as the shift was not more than 85 mV, this PRBE inhibitor can not be considered an anodic inhibitor; instead, it can be regarded as a mixed-type inhibitor. However, the addition of inhibitors also showed changes in corrosion current and Tafel constant values b_c and b_a which, suggests that the PRBE inhibitors monitored corrosion on the BQ surface by regulating both the reactions of metal dissolution at the anodic site and hydrogen evolution reaction at the cathodic site (Verma et al., 2018b).

TH-3102_146107038

Table 4.2 Tafel polarization parameters obtained in the presence of different amounts PRBE in HCl and H_2SO_4.

	Conc. (mg L^{-1})	b_a ($mVdec^{-1}$)	$-b_c$ ($mVdec^{-1}$)	E_{corr} (mV vs AgCl)	i_{corr} (μAcm^{-2})	R_P (Ωcm^{-2})	(μ_P%)
HCl media	0 (Blank) 1(M)HCl	110.98 ± 2.05	66.84 ± 0.80	-457.12 ± 3.32	179.06 ± 7.08	101.17 ± 0.49	0.00 ± 0.00
	50	85.27 ± 1.52	58.76 ± 0.45	-449.61 ± -1.54	46.29 ± 0.46	326.42 ± 5.62	74.15 ± 0.85
	100	86.31 ± 0.65	59.07 ± 0.28	-453.43 ± -5.93	33.23 ± 0.12	458.39 ± 8.23	81.44 ± 0.51
	150	85.32 ± 0.48	61.20 ± 0.28	-451.43 ± -5.15	26.12 ± 0.07	592.47 ± 11.78	85.41 ± 0.37
	200	79.49 ± 1.97	57.81 ± 0.27	-450.21 ± -2.55	19.48 ± 0.07	746.04 ± 11.73	89.12 ± 0.40
H_2SO_4 media	0 (Blank) 0.5 (M) H_2SO_4	93.13 ± 2.26	81.36 ± 1.40	-464.44 ± -3.17	180.25 ± 7.01	104.62 ± 1.25	0.00 ± 0.00
	50	74.70 ± 2.30	52.57 ± 1.07	-444.71 ± -1.77	58.26 ± 1.75	230.01 ± 6.60	67.68 ± 1.02
	100	84.87 ± 1.81	50.68 ± 0.48	-440.46 ± -4.77	35.42 ± 0.35	389.10 ± 11.08	80.35 ± 0.74
	150	80.85 ± 0.82	52.05 ± 0.19	-441.27 ±-3.33	27.34 ± 0.11	502.97 ± 13.69	84.83 ± 0.42
	200	85.77 ± 1.30	63.23 ± 0.58	-445.14 ± -1.77	20.07 ± 0.08	787.51 ± 19.02	88.86 ± 0.36

From Table 4.2, it is noticed that in every experiment, the b_a is higher than the b_c , which may allude that the anodic current is more than the cathodic (Khanra et al., 2018). The effect of the PRBE on the reduction of corrosion reaction was further convinced by corrosion current density (i_{corr}). The i_{corr} was drastically changed in the

TH-3102_146107038

presence of PRBE in both the acidic media and at higher concentration of PRBE the i_{corr} was decreased more. As the corrosion rate is directly proportional to $i_{corr}$the lower i_{corr} values at higher concentrations of PRBE indicate the reduction of corrosion rate. The increase in R_P values at higher concentrations of PRBE was also observed. The increase in R_P values indicate that the presence of PRBE caused polarization resistance, which leads to corrosion inhibition. In another way, it can be stated that the inhibitory compounds of the PRBE were adsorbed at the active anodic and cathodic sites on the surface of BQ steel which results in corrosion resistance (Srivastava et al., 2017a). The decrease in corrosion rates, as well as i_{corr} and increase in the R_P values after addition of PRBE indicates that inhibitory molecules covered wide surface areas by flat orientation. When the amount of PRBE was high, more inhibitory molecules were adsorbed on the surface perpendicularly. Because the inhibitory molecules were water soluble, highly polarized and also the higher amount of inhibitor molecules increased the electrostatic and repulsion forces between the inhibitory molecules (Berdimurodov et al., 2020; Shahmoradi et al., 2021). In addition, values of inhibition efficiency (μ_P%) also signifies that the presence of PRBE inhibitors in both the media drastically increased the μ_P%, but at the elevated concentrations, the change in μ_P% was not so much. (Okafor et al., 2010; Prabakaran et al., 2016a; Qiang et al., 2020, 2018, 2017b).

TH-3102_146107038

4.3.3 EIS measurement

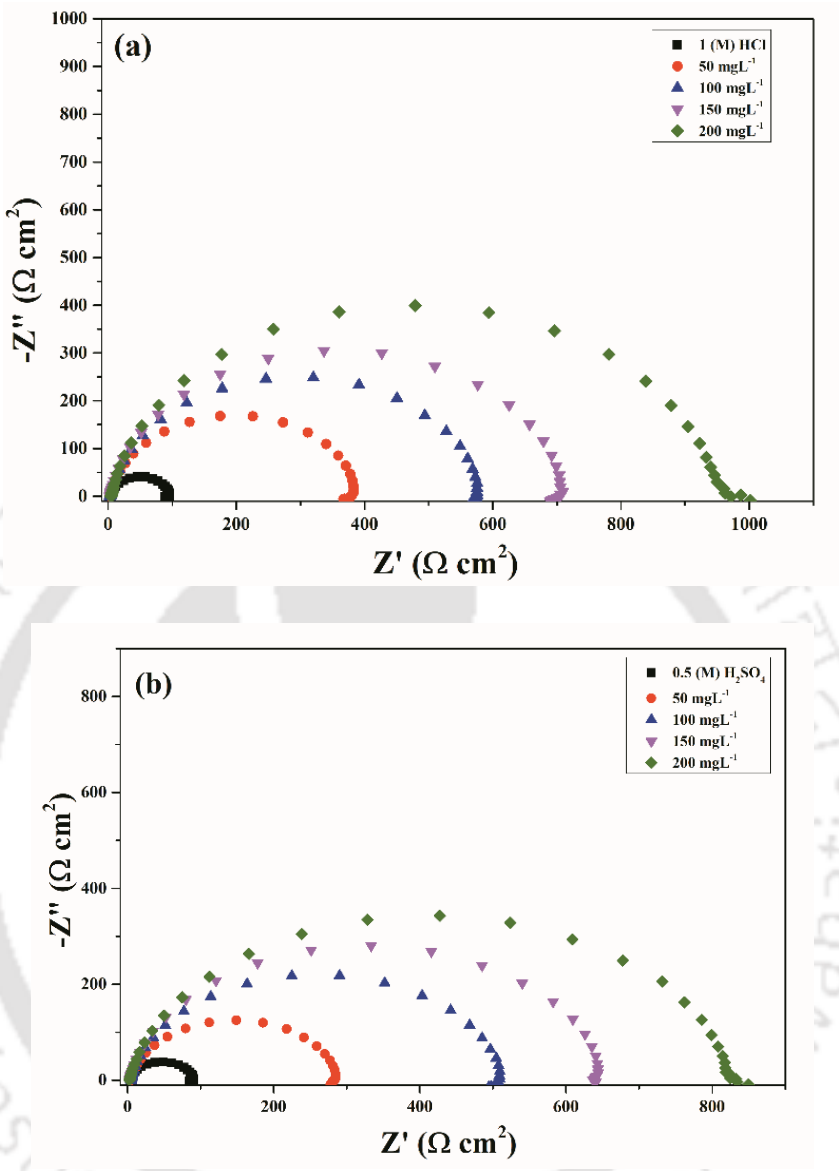

Fig. 4.5 Nyquist plots of PRBE on BQ steel at different concentrations in (a) HCl and (b) H_2SO_4 media.

TH-3102_146107038

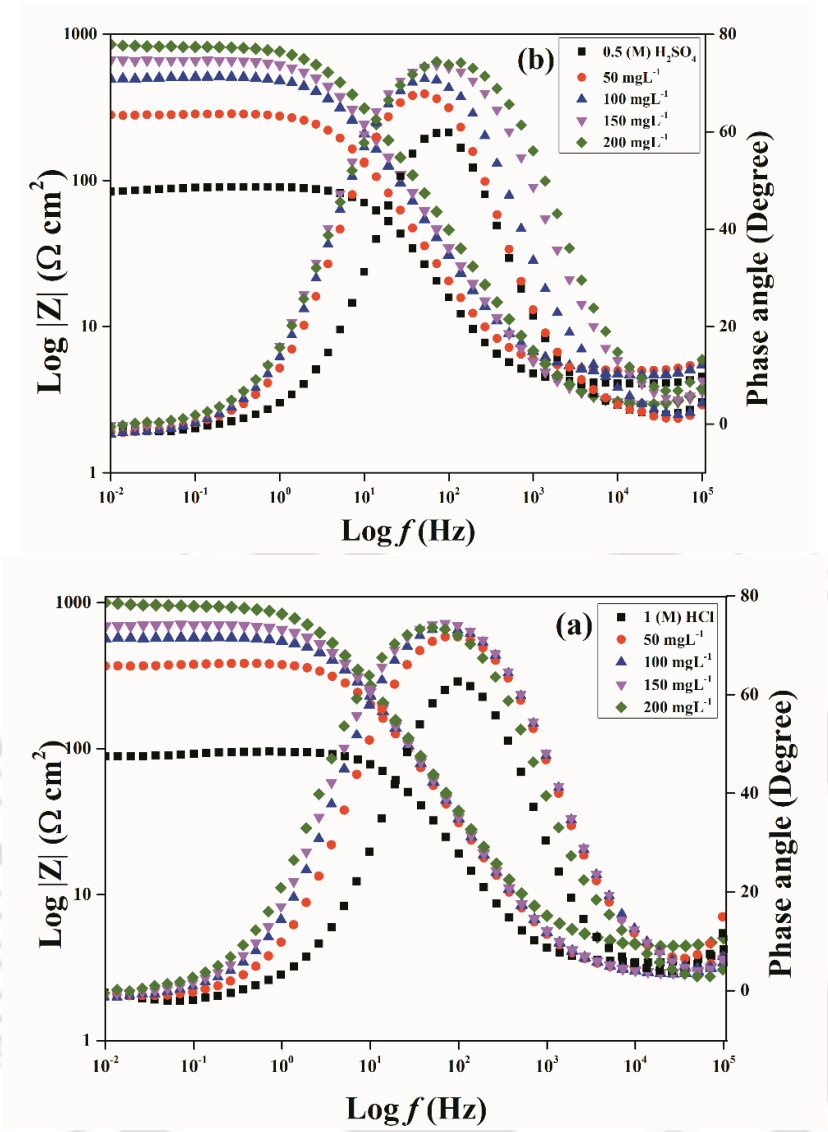

Fig. 4.6 Bode plots of PRBE on BQ steel at different concentrations in (a) HCl and (b) H_2SO_4 media.

Fig. 4.5 and Fig. 4.6 represent the EIS as Nyquist and Bode plots, respectively, at the presence and absence of PRBE inhibitors in both HCl and H_2SO_4 media. The obtained semicircle Nyquist plots from the experiments are slightly depressed for all the experiments. The depressed semicircles indicate the heterogeneity on the metallic surface of the steel. The pattern and shapes of the Nyquist plots are similar for inhibited and uninhibited conditions in both acidic media. The matching shapes and patterns suggest that the PRBE inhibitors did not change the mechanism of corrosion. In all the

TH-3102_146107038

semicircles, large capacitive loops at higher frequencies are observed. The existence of a capacitive loop suggests a capacitive layer on the surface. This indicates that the reactions in the metal-surface interface were mostly charge transfer controlled, so the developed resistance on the surface also primarily charges transfer resistance (R_{ct}). The diameter of the capacitive loops or the semicircles reveals the charge transfer resistance of the metal-electrolyte interface (Ji et al., 2015). In Fig. 4.5 (a) and (b), the Nyquist plots exhibit that the diameters of the semicircles are increased at the higher concentration of the PRBE, which apprises the superior charge transfer resistance (R_{ct}). The Bode plots of (Fig. 4.6 (a) and (b)) clearly indicate the single time constant equivalent circuit model for the corrosion process on the metal solution interface in every experiment, which is supported by the apparent single narrow peak in each frequency-phase angle plot. The phase angles of 90° or 0° indicate the capacitive or resistive electrochemical nature of the metal electrolyte interface of the system, respectively. Though none of the plots is indicating pure capacitor behavior, none of them have a phase angle of 90° or above 90°. Still, at a higher concentration of inhibitors, the increased peak heights indicate a more capacitive response of the metal solution interface. Moreover, the enhanced values of $log|z|$ at higher concentrations of PRBE are higher at lower frequencies, supporting the protective behavior of the adsorbed PRBE inhibitors on the surface in the acidic media (Liao et al., 2018a). To understand the resistance mechanism of the inhibitors on the surface of BQ, various parameters of the impedance like R_s, R_{ct}, CPE were calculated by fitting the EIS spectra to an equivalent circuit model (Fig. 4.7). A simple Randles circuit was used for fitting, which is constructed with R_s in series with R_{ct} and CPE, a substitution of ideal double-layer capacitance of distributed frequency whereas R_{ct} and CPE are in parallel with each other (M'hiri et al., 2016; Srivastava et al., 2018a; Verma et al., 2018b). The

TH-3102_146107038

inductor was not considered in the circuit for fitting because the inductive loop was not observed in all cases except in the absence of PRBE.

Table 4.3 Parameters of impedance in the absence and presence of different concentrations of PRBE in HCl and H_2SO_4.

	Conc (mg L^{-1})	R_S (Ω cm^2)	R_{ct} (Ω cm^2)	CPE parameters		$\mu_{R_{ct}}$ %
				n	Y_o (μMho cm^{-2})	
HCl media	**0 (Blank) 1 (M) HCl**	3.49 ± 0.001	89.72 ± 1.670	0.93 ± 0.001	137.01 ± 4.940	0.00 ± 0.00
	50	3.00 ± 0.001	379.33 ± 5.554	0.91 ± 0.001	92.86 ± 0.238	76.35 ± 0.32
	100	2.93 ± 0.001	576.84 ± 11.309	0.90 ± 0.001	90.90 ± 0.180	84.45 ± 0.23
	150	2.98 ± 0.002	707.28 ± 13.980	0.90 ± 0.001	88.15 ± 0.996	87.31 ± 0.20
	200	4.54 ± 0.006	958.08 ± 15.290	0.89 ± 0.001	85.31 ± 1.107	90.64 ± 0.19
H_2SO_4 media	**0 (Blank) 0.5 (M) H_2SO_4**	4.13 ± 0.001	85.08 ± 1.38	0.92 ± 0.001	178.23 ± 8.43	0.00 ± 0.00
	50	5.11 ± 0.001	280.34 ± 6.04	0.92 ± 0.000	142.45 ±1.38	69.65 ± 0.24
	100	4.80 ± 0.001	504.89 ± 12.03	0.90 ±0.001	99.82 ±0.35	83.15 ± 0.33
	150	2.95 ± 0.001	646.33 ± 15.34	0.90 ±0.001	88.09 ± 0.17	86.84 ± 0.18
	200	2.94 ± 0.001	822.84 ± 17.64	0.90 ± 0.001	68.52 ± 0.08	89.66 ± 0.15

TH-3102_146107038

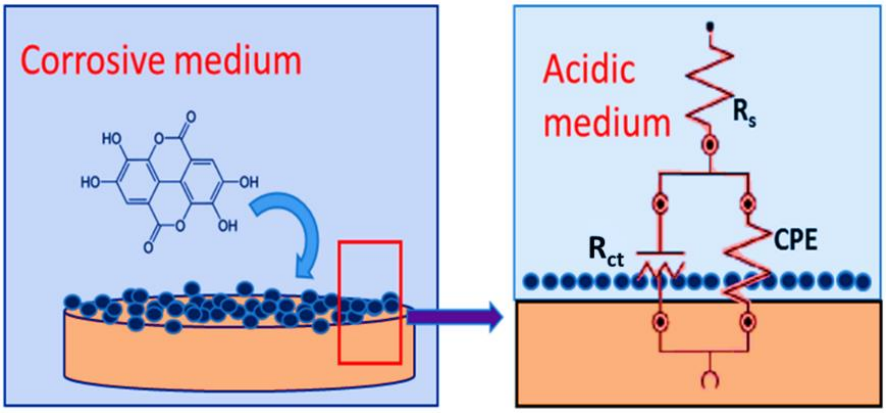

Fig. 4.7 Equivalent circuit for BQ plates in the presence of inhibitors.

Obviously, the lower frequencies of Nyquist plots and Bode plots reveal that the higher concentration of the PRBE contributed more resistance on the surface in both acidic media. Table 4.3 brings attention by revealing the changes in EIS parameters at different concentrations of PRBE, which helps to understand more about the electrochemical behavior of the steel-solution interface. It is observed from Table 4.3, the values of n (0.89-0.92) are not equal to 1. So CPE in the circuit does not behave like an ideal capacitor but closely like a capacitor (Wang et al., 2019). The values of CPE (Y_o) were found to be decreased at higher concentrations (Table 4.3). Furthermore, Table 4.3 also reveals that the values of R_{ct} was increased with the higher concentration of PRBE in both the HCl and H_2SO_4 media. These phenomena could be caused by the adsorption of the inhibitory compounds on the BQ surface, leading to forming a protective layer on the surface. This layer minimized the flow of charge between the electrolyte or acid solution and the surface of BQ, which eventually led to the blocking of active local sites of corrosion from the corroding substances. Moreover, when the concentration of PRBE was higher, the film became thicker, and more surface area of the BQ steel was covered. Hence there was a lesser chance for the corroding components to be exposed with the active sites of steel surface in both HCl and H_2SO_4

TH-3102_146107038

media. Thus the rate of corrosion was also beme reduced (Chaubey et al., 2021; Haruna and Saleh, 2021; Hsissou et al., 2021; Oubaaqa et al., 2022; Srivastava et al., 2017a).

4.4 Adsorption studies

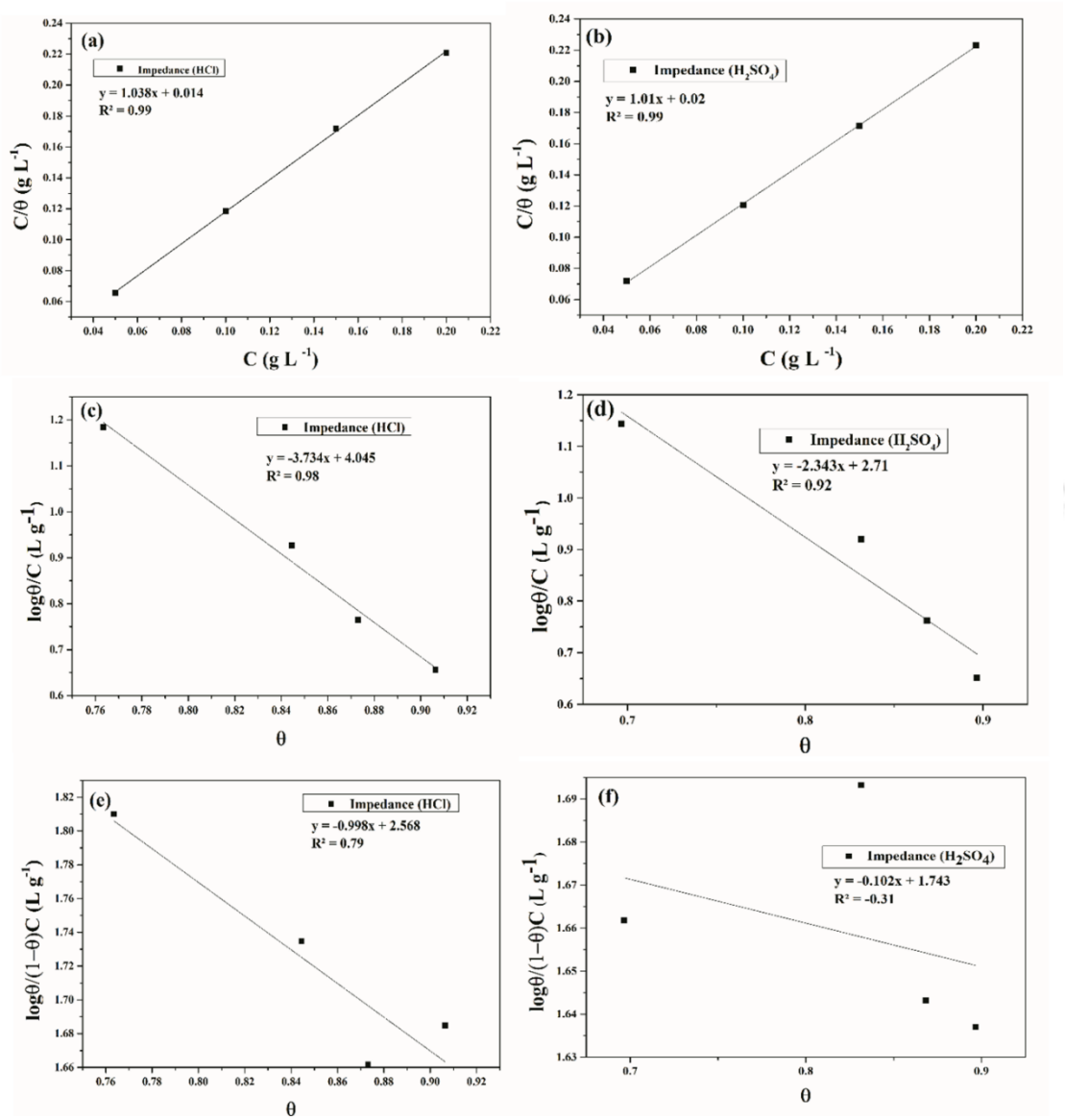

Fig. 4.8 (a, b) Langmuir, (c, d) Temkin, (e, f) Frumkin adsorption isotherm plots PRBE in HCl and H_2SO_4.

The results of PDP and EIS tests already supported the adsorption of PRBE compounds on the steel surface and enlightened about the electrochemical interaction mechanism between the BQ surface (adsorbent) and inhibitor components (adsorbate).

TH-3102_146107038

The compounds of PRBE might be adsorbed on the surface of BQ steel by the interaction of physical (physisorption) or chemical (chemisorption), or both. So to investigate the mode of adsorption of the PRBE components in 1 (M) HCl and 0.5 (M) H_2SO_4 media, some commonly used adsorption isotherms such as Langmuir (Fig. 4.8 (a) and (b)), Temkin (Fig. 4.8 (c) and (d), and Frumkin (Fig. 4.8 (e) and (f)) were tested, which established relations between the concentration of inhibitor (C), surface coverage ($\theta = \mu_{R_{ct}} 100^{-1}$) and adsorption equilibrium constant (K_{ads}). After calculating the slopes, intercept, and regression coefficient for all the isotherms, Langmuir (Fig. 4.8(a) and (b)) was found to be the best-fitted model for having a regression coefficient of 0.99 (R^2) in HCl and H_2SO_4 media (Haruna and Saleh, 2021). According to Langmuir isotherm, it can be assumed that the adsorption is monolayer, and there is less chance for interaction between the molecule (Shahmoradi et al., 2021).

The Langmuir isotherm can be expressed as follows:

$$\frac{C}{\theta} = \frac{1}{K_{ads}} + C \qquad \textbf{4.1}$$

Where $\frac{C}{\theta}$ is plotted against C, to find out the K_{ads} (adsorption equilibrium constant), standard Gibbs free energy (ΔG°_{ads}) can be computed from K_{ads} with the help of the following equation:

$$\Delta G^{\circ}_{ads} = -RTln(C_{water} K_{ads}) \qquad \textbf{4.2}$$

Where universal gas constant (8.314 $Jmol^{-1}K^{-1}$) is expressed by R, the concentration of water (C_{water}) was considered 1000 gL^{-1} rather than 55.5 mol L^{-1} as the K_{ads} is expressed in Lg^{-1}, T is the absolute temperature (298.15 K) (Ali Asaad et al., 2018; Mourya et al., 2014a; Zhou and Zhou, 2014). The derived ΔG°_{ads}, K_{ads} are presented in Table 4.4 along with linear regression coefficient (R^2).

TH-3102_146107038

Table 4.4 Adsorption isotherm parameters for PRBE in HCl and H_2SO_4

Media	R^2	$1/K_{ads}$ (g L^{-1})	K_{ads} (Lg^{-1})	$\Delta G°_{ads}$ ($kJmol^{-1}$)
1 M HCl	0.99	0.01	69.59	-27.64
0.5 M H_2SO_4	0.99	0.02	48.83	-26.76

The obtained negative values of $\Delta G°_{ads}$ at ambient temperature indicates the inhibitor components in PRBE are adsorbed spontaneously on the BQ plate. Besides, from the literature survey, it was found that the value of $\Delta G°_{ads}$ describes the nature of adsorption in such a way that when the value of $\Delta G°_{ads}$ is up to -20 $kJmol^{-1}$, then the interaction between inhibitors and the surface is considered electrostatic, and the adsorption process is known as physisorption. If the value of $\Delta G°_{ads}$ are found to be more negative than -40 $kJmol^{-1}$, then the electrons are shared or transferred between inhibitor molecules and the metal surface to form a coordinate bond which is also known as chemisorption (Azmi and Soedarsono, 2018). The values of $\Delta G°_{ads}$ for PRBE in HCl and H_2SO_4 were found -27.64 and -26.76 $kJmol^{-1}$. The values of $\Delta G°_{ads}$ are between the range of -20 $kJmol^{-1}$ to -40 $kJmol^{-1}$ which indicate the mixed-type of adsorption following the both physisorption and chemisorption (Srivastava et al., 2018b). Also, the temperature can influence the adsorption as well as the corrosion. An increase in temperature increases the corrosion rate in both the absence and the presence of an inhibitor, and it impacts more in the case of physisorption. Moreover, the activation energy is usually higher in the presence of an inhibitor than in the absence (Berdimurodov et al., 2021d). This means the corrosion process requires high activation energy barrier for the corrosion on the metal surface in the presence of an inhibitor, and it goes higher as the inhibitor concentration increases. The required activation energy

TH-3102_146107038

is also increased if the double-layer thickness is enhanced (Al-Moubaraki, 2015; Berdimurodov et al., 2020).

4.5 Surface characterization

4.5.1 FESEM- EDX study

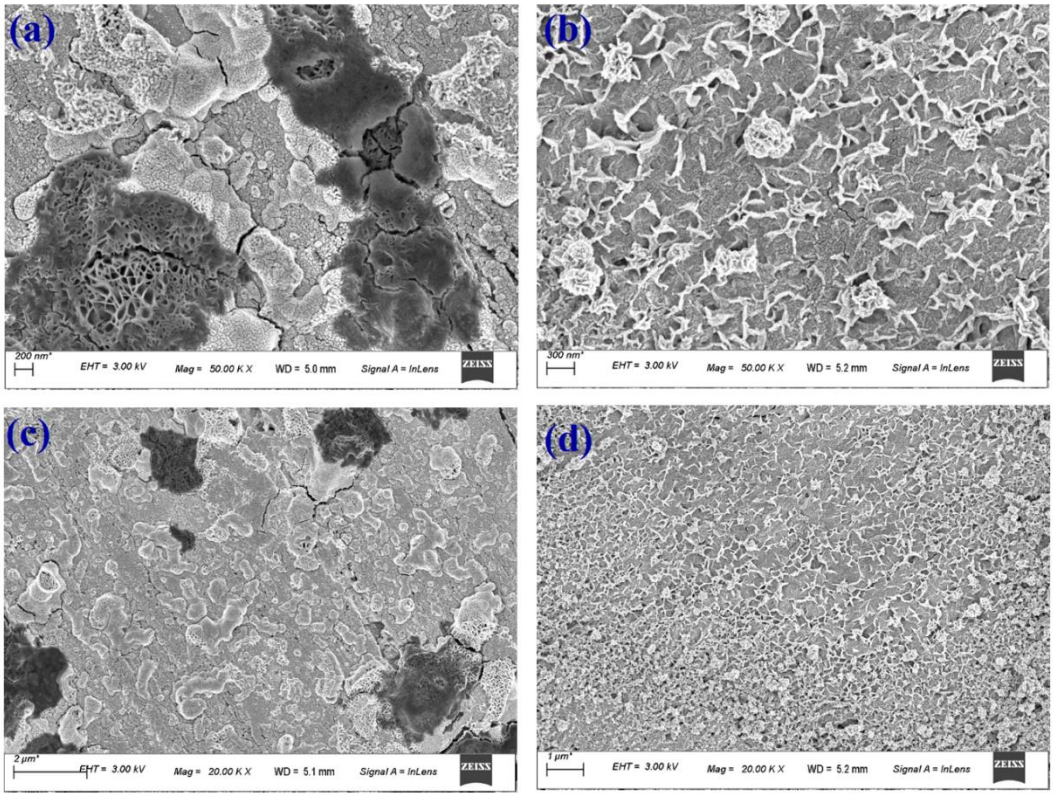

Fig. 4.9 FESEM images of BQ steel sample after corrosion (a) without PRBE in 1 M HCl, (b) in the presence of PRBE (200 mg L^{-1}) in 1 M HCl, (c) without PRBE in 0.5 M H_2SO_4, and in the presence of PRBE (200 mg L^{-1}) in 0.5 M H_2SO_4.

The FESEM study was carried out in both HCl and H_2SO_4 media in the presence and absence of optimum concentrations of PRBE to analyze the surface morphology and support the interpretations obtained from weight loss and electrochemical studies. The difference between the absence and presence of PRBE inhibitors in 1 (M) HCl solution is represented by FESEM images in Fig. 4.9 (a) and (b), respectively. In the

TH-3102_146107038

same way, Fig. 4.9 (c) and (d) illustrate the exposed surface of BQ in 0.5 (M) H_2SO_4 without and with the treatment of PRBE, respectively. The presence of PRBE made a noticeable difference in the microstructures of the BQ in both acidic media. In the absence of PRBE, the acid attacked the surface fiercely and corroded the surface by inducing anodic and cathodic reactions on the surface, which was proved by the presence of cracks and pits in the absence of PRBE. Whereas when the surface was exposed to PRBE, such kinds of intensely damaged structures were not prominent in both acidic media. Actually, in the presence of PRBE, the surface of the steel was protected by phenolic compounds of PRBE, which were adsorbed on the steel surface and blocked the active reaction sites of corrosion. Hence, lesser cracks and pits are visualized on the BQ steel surface as the PRBE was incorporated in both HCl and H_2SO_4 media.

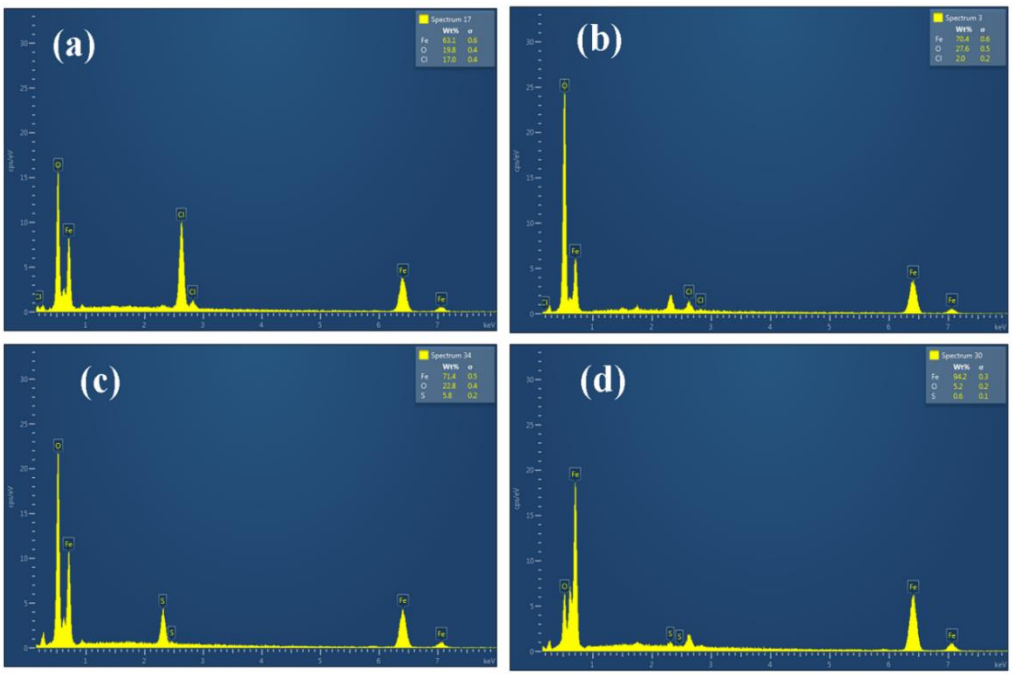

Fig. 4.10 EDX spectra of BQ steel sample after corrosion (a) without PRBE in 1 M HCl, (b) in the presence of PRBE (200 mg L^{-1}) in 1 M HCl, (c) without PRBE in 0.5 M H_2SO_4, and in the presence of PRBE (200 mg L^{-1}) in 0.5 M H_2SO_4.

TH-3102_146107038

As the EDX spectra of the surface give the elementary composition of the surface, EDX spectra were acquired for the BQ steel without and with adding the PRBE in both the acidic media to investigate the elementary changes of the BQ surface by the inhibitor components**.** Fig. 4.10 displays the EDX spectra of the BQ surface in both the acidic media in the absence and the presence of the PRBE. In Fig. 4.10 (a), the EDX spectra show that in the absence of PRBE, the weight percentage of iron is much lower, and chloride is higher than in the presence of PRBE (Fig. 4.10 (b)). No exception is observed in the case of H_2SO_4 media, as the amount of iron is much lower and sulfur is higher in the absence of PRBE (Fig. 4.10 (c)) than in the presence (Fig. 4.10 (d)) of PRBE. In HCl media, the Fe^{2+} of the surface attracted the Cl^- electrostatically, which caused the adsorption of Cl^- onto the metallic surface. On the other hand, in H_2SO_4 media, the chance of sulfur to be adsorbed on the surface was lesser than Cl^- as SO_4^{2-} was less electronegative than Cl^-. This increase in weight percentages of iron in the presence of PRBE signifies the protective surface of the BQ was formed by the inhibitor compounds of PRBE, which prevented the surface from the aggressive attack of corrosive components (Wang et al., 2019)

4.5.2 AFM study

Adsorption of the PRBE in both HCl and H_2SO_4 is furthermore proved by the AFM study of 20 × 20 µm steel surface area in the absence and presence of PRBE. The three-dimensional AFM micrographs of the BQ surface show a noticeable difference in the average surface roughness in the absence and presence of PRBE in both the acidic media (Fig. 4.11). The presence of an optimum concentration of PRBE in both acidic media changed the average surface roughness much lower in comparison to the absence of PRBE. The average surface roughness in HCl media in the absence of PRBE is 275 nm (Fig. 4.11 (a**)**), whereas, in the presence of PRBE, the roughness is 18.8 nm (Fig.

TH-3102_146107038

4.11 (b)). Similarly, the average roughness in H_2SO_4 in the absence of PRBE is 19 nm (Fig. 4.11 (c)) and 277 nm in the presence of PRBE (Fig. 4.11 (d)). This reduction in average roughness or increase in smoothness was mainly due to the adsorption of the organic compounds of PRBE (Naghi Tehrani et al., 2021b; Wang et al., 2019).

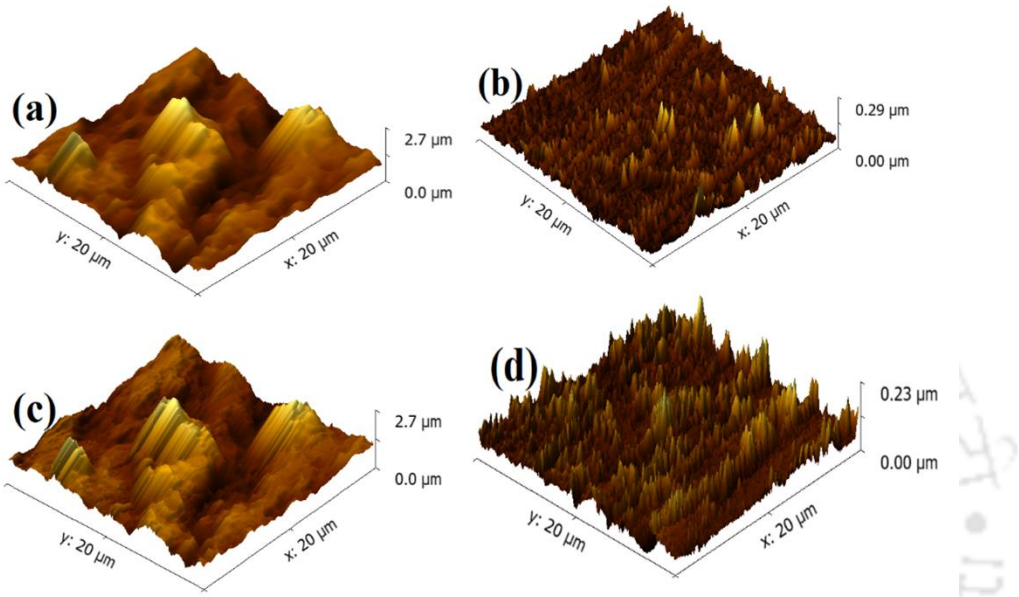

Fig. 4.11 3D AFM images obtained for the surface morphology of BQ steel sample after corrosion (a) without PRBE in 1 M HCl, (b) with PRBE (200 mg L^{-1}) in 1 M HCl, (c) without PRBE in 0.5 M H_2SO_4, and (d) with PRBE (200 mg L^{-1}) in 0.5 M H_2SO_4.

4.6 Theoretical studies by quantum chemical calculations

The changes on the surface of BQ steel in the presence of PRBE in acidic media were examined by electrochemical techniques, which illuminate the corrosion kinetics and fundamental corrosion inhibition process of BQ steel by PRBE. The correlation between corrosion protection and molecular structures of inhibitor molecules is required to understand the protection mechanism at the molecular level. Theoretical

TH-3102_146107038

methods, such as quantum level simulations, give valuable observations to describe this relationship between structures of inhibitor molecules and the inhibition efficiencies (Liao et al., 2018a).

4.6.1 Frontier molecular orbitals (FMO) and their energies

The theory of FMO is one of the common approaches for obtaining quantum chemical calculations. The prime indicators to find out the efficacy of a corrosion inhibitor are the two FMOs, i.e., HOMO and LUMO. Because during the chelation of the adsorption process, the transition state is formed by the HOMO and LUMO of the reactant species (Mourya et al., 2014a). The HOMO regions are electron donors and sites for adsorption. They are abundant with π bonds, phenyl rings, and various charged heteroatoms. The LUMO area shows the tendency towards acceptance of electrons. (Ganash, 2018).

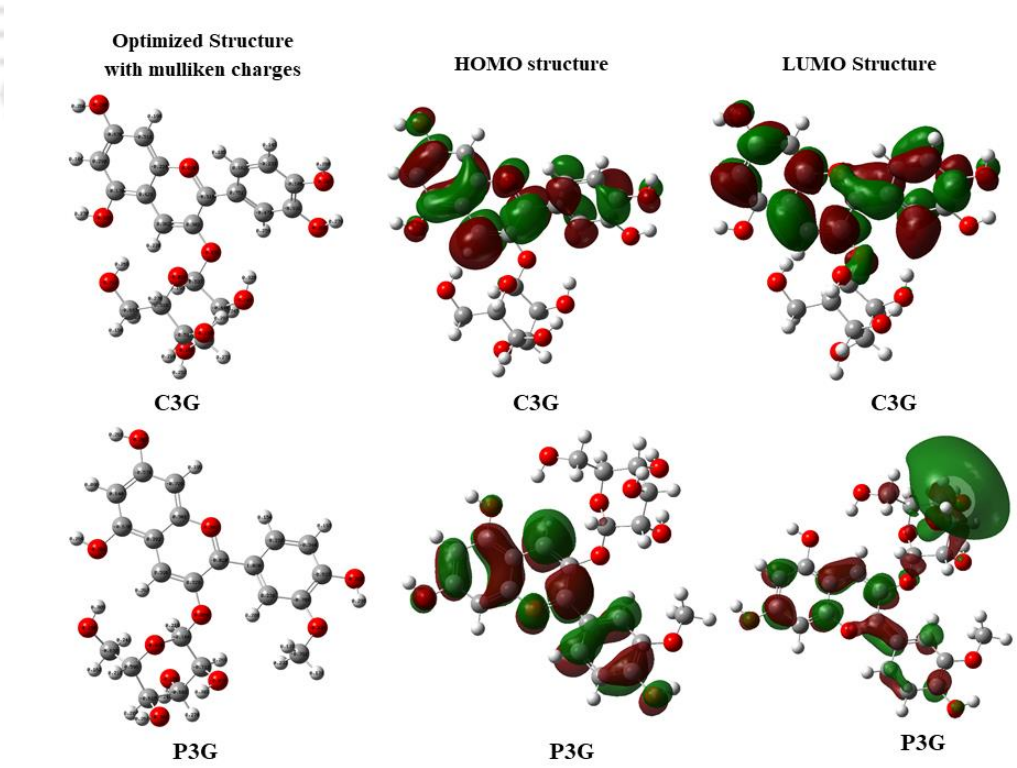

Fig. 4.12 The electron density distribution of C3G and P3G Monomers.

TH-3102_146107038

Two significant compounds have been identified from HPLC results, C3G and P3G. However, there is a possibility of the existence of different compounds in the extract as it is a natural extract. Earlier studies indicated the abundance of C3G and P3G as vital anthocyanin in PRBE (Das et al., 2018). So these two compounds were considered as possible inhibitory compounds in the PRBE. The images of the optimized structure and the sites of FMO on the identified inhibitors found in PRBE are displayed in Fig. 4.12. Green and red-colored lobes indicate the electronegativity properties of the compounds. Red lobes usually represent the more electronegative regions, and the green lobes represent less negative regions (Mobin et al., 2017). The colored lobes of the images signify the existence of π electron clouds in the HOMO-LUMO (Fig. 4.12) regions. Fig. 4.12 shows that all of the HOMOs and LUMOs of C3G and P3G compounds are localized evenly over the whole molecule, which indicates that a flat-adsorption mode can be obtained by the compounds to gain the largest protective area from the inhibitors, which are absorbed on BQ steel surface (Qiang et al., 2017b). The electrons in these regions are susceptible to being delocalized to participate in several interactions. The significant atoms from those HOMO-LUMO regions also interact with the surface of the BQ plate to obtain stability (Ostovari et al., 2009). These interactions are mainly based on electron-donating and accepting capability or electrostatic force by various functional groups, phenyl rings, and a single atom of those HOMO-LUMO regions (Ganash, 2018).

The energy of energy levels (HOMO-LUMO) and the relevant quantum chemical parameters for the C3G and P3G are reported in Table 4.5. It is an established theory that higher E_{HOMO} indicates the higher electron-donating capability of an orbital. The molecule with a lower E_{LUMO} value is prone to accept an electron from orbitals with a higher level of energy. Thus the higher value of E_{HOMO} and lower value of

TH-3102_146107038

E_{LUMO} enhance the chance of stronger and more stable interaction between the inhibitory molecule and BQ surface, which results in better absorption of the inhibitory molecules.

Table 4.5 Quantum parameters of inhibitors.

Inhibitors name	E_{LUMO} (eV)	E_{HOMO} (eV)	ΔE (eV)	I (eV)	A (eV)	χ (eV)	η (eV)	σ ($1eV^{-1}$)	ΔN (eV)	μ (D)
C3G	-0.977	-4.187	3.210	4.187	0.977	2.582	1.605	0.623	1.376	2.66
P3G	-0.824	-3.958	3.134	3.958	0.824	2.391	1.567	0.638	1.471	7.58

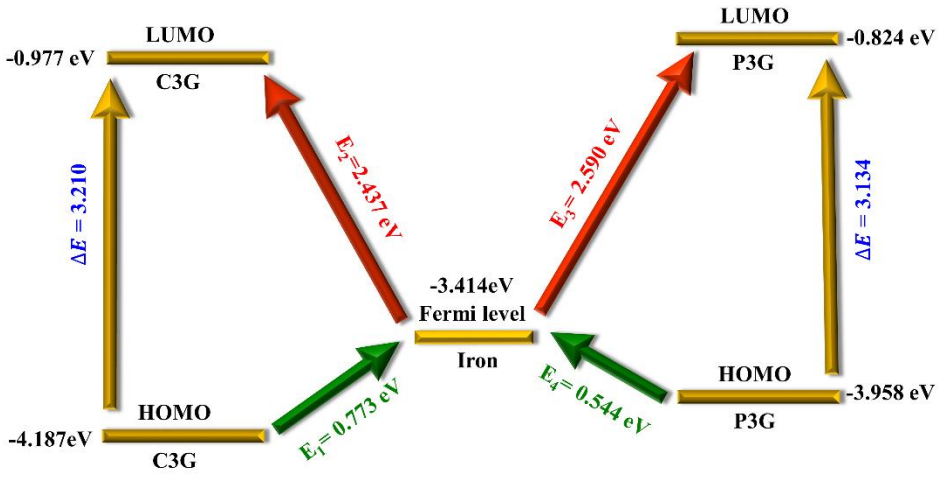

Fig. 4.13 Interaction between molecular orbitals and iron Fermi level

It is noticed from Table 4.5 that P3G has a higher LUMO value (-0.824 eV) than C3G (-0.977 eV) as well as a higher HOMO value (-3.958 eV) than C3G (-4.187 eV). The literature shows that higher energy gaps (ΔE) make the molecule more confined to interact with other substances as more energy is required to transfer the electrons from orbitals. In contrast, a lower energy gap gives more chemical stability to the inhibitor, which helps to better inhibition efficiency. The energy gap (ΔE) of P3G is lower (3.134 eV) than C3G (3.210 eV), which makes it more flexible, chemically reactive, and polarizable to interact with the surface of the BQ steel (Qiang et al., 2021,

TH-3102_146107038

2017a). As P3G has a lower energy gap, it faced lesser interruption in electron donation and acceptance processes and required lesser ionization energy. The adsorption of the inhibitory molecules depends on the energy levels of the molecules and the Fermi level ($E_f = E_{HOMO} + 0.5\Delta E$) of iron. The orbital energies of the molecules and the Fermi level of iron are depicted in Fig. 4.13. The Fermi level is the energy at which the probability of occupying an electronic state is 0.5. At energies ≤ HOMO, the probability is close to 1. At energies ≥ LUMO, the probability is close to 0. Therefore, by definition, the Fermi level falls between the HOMO and LUMO, i.e., HOMO < Fermi level < LUMO. Fig. 4.13 indicates that the energy transfer from HOMO of C3G and P3G to iron is more feasible than the electron transfer from iron to molecule as the energy gap between Fermi level of iron and HOMO of C3G and P3G is less (0.773 eV and 0.544 eV) (Bashiri et al., 2017; Singh et al., 2019). Moreover, the lower electronegativity (χ), higher softness (σ) and lower global hardness (η) make it an even better inhibitor than C3G. Besides this, the higher value of ΔN (transferable electrons from inhibitor) of P3G (1.471) than C3G (1.376) makes it more reactive and better inhibitor as higher ΔN indicates the better electron-donating capability (Feng et al., 2018; Naghi Tehrani et al., 2021a; Thomas et al., 2020). The dipole moments (μ) of C3G and P3G are 2.66 and 7.58 D, respectively. The dipole moment generally estimates the polarity of bonds in any molecules which are associated with electron distribution on the molecular structure. The higher μ of P3G indicates that it is highly polarized which means that the positive and negative charges of P3G are non-uniformly distributed. The higher μ also indicates that the dipole-dipole interaction between the inhibitor molecule and the metal surface could enhance the adsorption strength on the surface which helps in better inhibition efficiencies. This also indicates that the molecules were more soluble in

TH-3102_146107038

polarized environment and caused the perpendicular adsorption. In contrast, the lower μ value of C3G may caused the accumulation of C3G molecules on the surface of BQ (Berdimurodov et al., 2020; Qiang et al., 2017b, 2017a; Shahmoradi et al., 2021). Hence, both C3G and P3G contributed to the corrosion inhibition efficiency of PRBE.

Table 4.6 Fukui function with highest f_k^+ and f_k^- values of some atoms from C3G and P3G.

Detected compound in PRBE	Atom	f_k^+	f_k^-
C3G	(18) C	0.605	-0.131
	(5) C	0.365	-0.836
	(9) C	0.308	-0.046
	(19) C	0.255	-0.189
	(7) C	-0.351	0.748
	(8) C	0.056	0.352
	(2) C	-0.214	0.343
	(33) C	-0.056	0.337
P3G	(36) C	0.270	0.174
	(32) C	0.262	0.335
	(8) C	0.193	0.073
	(34) C	0.180	-0.055
	(2) C	-0.253	0.376
	(1) C	-0.274	0.305
	(7) C	0.133	0.265
	(3) C	0.099	0.168

To observe the local sites of reactivity, Fukui indices of atoms in C3G and P3G were calculated, and some of the highest f_k^+ (electrophilic sites) and f_k^- (nucleophilic sites) values are mentioned in Table 4.6. The surface of the BQ was very certain to be positively charged in acidic media, but sometimes, the surface might be negatively charged as the anions formed a layer on the positively charged surface. (Verma et al., 2018b) . The atomic sites with a higher f_k^+ value is more intended for the nucleophilic attack, whereas the atomic sites with lower negative values are more prone to electrophilic attack (Abdallah et al., 2021; Belghiti et al., 2019b; Ganash, 2018; Liao et

TH-3102_146107038

al., 2018a; Verma et al., 2018c). Table 4.6 shows that the C atoms in the phenyl ring had more local reactivity towards the BQ steel surface as the phenyl rings were abundant with electron density.

4.7 Corrosion and inhibition mechanism

From the Tafel polarisation studies, it has been observed that the magnitude of the shift in anodic direction is not the same in both mediums. This can be explained by the mechanism of the anodic dissolution in the presence and absence of PRBE. The reaction mechanisms of the anodic reactions in H_2SO_4 and HCl media are different and are discussed below (Cang et al., 2012; Li et al., 2012; Mourya et al., 2013; Srivastava et al., 2017b).

4.7.1 Corrosion mechanism reactions without inhibitor

4.7.1.1 Anodic reactions

In the anodic zone, iron can be oxidized into Fe^{2+} or Fe^{3+}, and the reactions are as follows:

$$Fe \rightarrow Fe^{2+} + 2e^{-} \quad \textbf{4.3}$$

$$Fe^{2+} \rightarrow Fe^{3+} + e^{-} \quad \textbf{4.4}$$

$$2Fe^{2+} + 2H_2O + O_2 + 2e^{-} \rightarrow 2FeOOH + 2H^{+} \quad \textbf{4.5}$$

The electrodissolution of iron in acidic sulfate solution depends primarily on the adsorbed intermediated $FeOH_{ads}$. The reaction mechanisms are as follows:

$$Fe + H_2O \leftrightharpoons Fe.H_2O_{ads} \quad \textbf{4.6}$$

$$FeH_2O_{ads} \leftrightharpoons FeOH_{ads} + H + e^{-} \quad \textbf{4.7}$$

$$FeOH_{ads} \rightarrow FeOH^{+} + e^{-} \quad \textbf{4.8}$$

$$FeOH^{+} + H^{+} \leftrightharpoons Fe^{2+} + 2e^{-} \quad \textbf{4.9}$$

TH-3102_146107038

The dissolution of iron in an HCl medium is different than H_2SO_4 and follows a different pathway:

$$Fe + Cl^{-} \leftrightharpoons (FeCl^{-})_{ads} \quad \textbf{4.10}$$

$$(FeCl^{-})_{ads} \leftrightharpoons (FeCl)_{ads} + e^{-} \quad \textbf{4.11}$$

$$(FeCl)_{ads} \rightarrow (FeCl^{+}) + e^{-} \quad \textbf{4.12}$$

$$(FeCl^{+}) \leftrightharpoons Fe^{2+} + Cl^{-} \quad \textbf{4.13}$$

The anodic dissolution in the HCl depends on the $(FeCl)_{ads,}$ while in the case of H_2SO_4 solution, it has been observed that the anodic dissolution depends on the $(FeOH)_{ads}$.

4.7.1.2 Cathodic reaction

In the cathodic zone, the reduction of oxygen occurred, which can be explained by the following reaction:

$$2H_2O + O_2 + 4e^{-} \rightarrow 4OH^{-} \quad \textbf{4.14}$$

The proton reduction also occurred in the cathodic, which follows different pathway and is given by the following equation:

$$Fe + H^{+} \rightleftharpoons (FeH^{+})_{ads} \quad \textbf{4.15}$$

$$(FeH^{+})_{ads} + e^{-} \rightarrow (FeH)_{ads} \quad \textbf{4.16}$$

$$(FeH)_{ads} + H^{+} + e^{-} \rightarrow Fe + H_2 \quad \textbf{4.17}$$

4.7.2 Corrosion mechanism reactions with inhibitor

4.7.2.1 Anodic reactions

The addition of the inhibitor to the acidic media may lead to different reaction steps depending on the nature of the electrolyte and the mechanism of the anodic dissolution of iron. So the difference in the mechanism of anodic dissolution is attributed to the difference in the anodic curve of the Tafel slope (Mourya et al., 2013).

TH-3102_146107038

The anodic oxidation of iron in the sulphuric acid media can be explained by the following reactions:

$Fe.H_2O_{ads} + Inh \leftrightharpoons FeOH^-_{ads} + H^+ + Inh$ **4.18**

$Fe.H_2O_{ads} + Inh \leftrightharpoons Fe.Inh_{ads} + H_2O$ **4.19**

$FeOH^-_{ads} \rightarrow FeOH_{ads} + e^-$ **4.20**

$Fe.Inh_{ads} \leftrightharpoons Fe.Inh_{ads}^+ + e^-$ **4.21**

$FeOH_{ads} + Fe.Inh_{ads}^+ \leftrightharpoons FeOH^+ + Fe.Inh_{ads}$ **4.22**

$FeOH^+ + H^+ \leftrightharpoons Fe^{2+} + H_2O$ **4.23**

In the HCl solution, the inhibitors lead to some additional chemical reactions in the presence of inhibitor:

$(FeCl^-)_{ads} + InhH^+ \leftrightharpoons (FeCl^-InH^+)_{ads}$ **4.24**

$(FeCl^-)_{ads} + InhH^+ \leftrightharpoons (Fe.InhH^+)_{ads} + Cl^-$ **4.25**

4.7.2.2 Cathodic reaction

The cathodic slope of the Tafel curve has suggested that the hydrogen evolution or the cathodic reactions may be affected by inhibitors. The possible pathways may explain the cathodic reaction:

$Fe + H^+ + e^- \leftrightharpoons (FeH)_{ads}$ **4.26**

$Fe + (InhH^+) + e^- \leftrightharpoons (Fe.InhH)_{ads}$ **4.27**

$(FeH)_{ads} + (FeH)_{ads} \rightarrow Fe + H_2$ **4.28**

The first two reactions indicated that protonated inhibitors ($InhH^+$) and H^+ compete with each other to be adsorbed on the common active site of the BQ surface. The above cathodic reactions are very much likely to be activation controlled. Among the reaction steps, the first step may be the rate-controlling step.

TH-3102_146107038

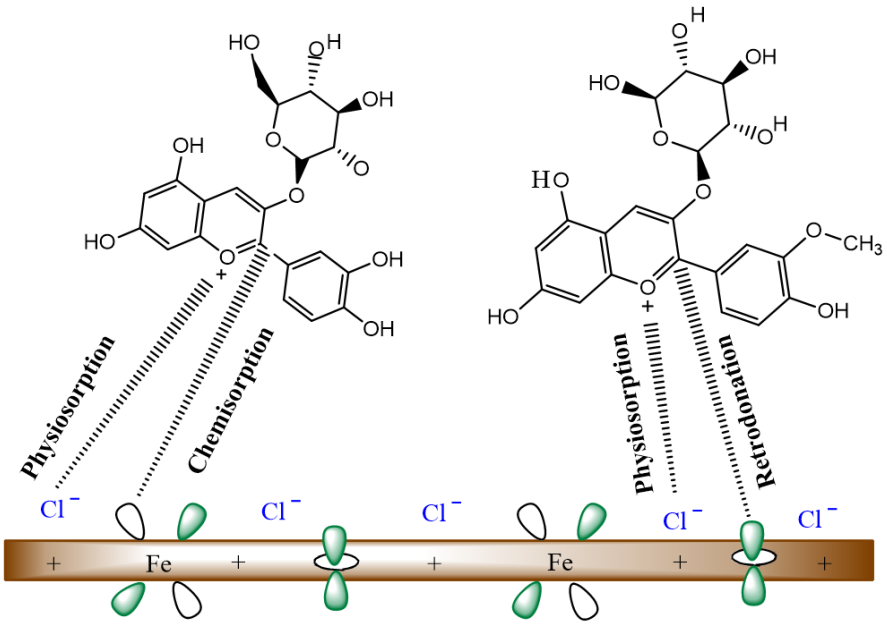

Fig. 4.14 Schematic representation of corrosion inhibition mechanism in HCl medium.

As mentioned earlier, the anodic reaction dissolution liberates $Fe^{2+,}$ and the cathodic reaction generates hydrogen gas. So when inhibitors are incorporated with the acidic media, the protonated inhibitors start to be adsorbed on the charged surface. The protonated inhibitors make electrostatic interactions with the adsorbed Cl^- of the surface. This type of interaction is known as physical adsorption (Fig. 4.14). Then the protons and the protonated inhibitors initiate competition among each other to interact with the nucleophilic sites of the BQ surface. Once the protonated inhibitors neutralize the surface, then the neutralized surface becomes rich with lone pair electrons of heteroatoms and initiates chemical adsorption. Eventually, the surface becomes negatively charged as it is totally saturated with electrons. To deliver the excess electrons from the surface, the vacant π (antibonding) orbitals of the inhibitory molecules accept the electrons from the "d" orbital of iron by the process of retrodonation (Naghi Tehrani et al., 2021a; Saxena et al., 2018c; Srivastava et al.,

TH-3102_146107038

2018a). Though the adsorption studies indicate a more probability of electrostatic interaction as the values of $\Delta G°_{ads}$ are close to -20 kJ mol^{-1} . But the chances of chemical interaction can not be ignored as the values are between -20 kJ mol^{-1} to -40 kJ mol^{-1}. When the Cl^- ions come in close proximity to the iron surface, they induce iron oxidation; as a result, tiny pits are formed on the surface of the metal. Having said that, these Cl^- ions also help attract the protonated molecules onto the surface, eventually forming a protected film. Moreover, the samples were immersed in the respective solution for an ample amount of time to attain a steady state when there was no change in the potential, signifying no such changes on the surface. This also indicates an existance of a stable film on the surface.

In the identified anthocyanin molecules (C3G and P3G), oxygen heteroatoms and hydroxyl functional groups are mainly responsible for the inhibition properties (Teng et al., 2021; Thomas et al., 2021, 2020).

4.8 Summary

Based on the present experimental and computational investigations, it can be concluded that the PRBE, which was extracted from an agricultural by-product (purple rice bran), is a potential environment-friendly natural corrosion inhibitor. The efficiency of PRBE as green corrosion inhibitors was explored by accomplishing some experimental investigations in 1 (M) HCl and 0.5 (M) H_2SO_4 on the BQ surface and the theoretical investigations on the compounds of PRBE. After all experiments, the following conclusions are obtained:

1. Cyanidin-3-glucoside (C3G) and Peonidin-3- D-glucoside (P3G) were identified as two corrosion inhibitors detected by HPLC.

TH-3102_146107038

2. The electrochemical results indicated that PRBE effectively reduced the corrosion of the BQ steel in both the HCl and H_2SO_4 media. Its inhibition efficiencies were increased with the incremental concentration of PRBE due to the formation of a protective film by the adsorbed inhibitor molecules on the surface. This was also supported by the charge transfer resistance of the metal-solution interface. The maximum inhibition efficiencies were found at 91.13% and 87.43% in HCl and H_2SO_4 media, respectively. At a lower concentration, the efficiency is higher in HCl media than in H_2SO_4 media.
3. The inhibiting effect of PRBE on BQ steel was caused by spontaneous adsorption phenomena, which was also supported by the value of K_{ads} and $\Delta G°_{ads}$ (-27.64 kJ mol^{-1} in HCl and -26.76 kJ mol^{-1} in H_2SO_4). The adsorption of PRBE components on the BQ steel surface was found to follow the Langmuir isotherm. The obtained values of $\Delta G°_{ads}$ indicated that the inhibitor reacts like a mixed-type inhibitor.
4. The outcomes of FESEM, EDX, and AFM studies also confirmed the retardation of the corrosion on the surface of BQ steel due to the formation of a protective layer of PRBE components.
5. Between the two compounds, P3G had a more inhibitive strength than C3G, as quantum chemical calculations disclosed the lower energy gap of P3G (ΔE = 3.134 eV) compared to C3G (ΔE = 3.210eV). This high dipole moment of P3G (high interaction strength) and low dipole moment of C3G (high accumulation of inhibitor molecules) make PRBE an efficient inhibitor.

TH-3102_146107038

4.9 References

Abdallah, M., Altass, H.M., Al-Gorair, A.S., Al-Fahemi, J.H., Jahdaly, B.A.A.L., Soliman, K.A., 2021. Natural nutmeg oil as a green corrosion inhibitor for carbon steel in 1.0 M HCl solution: Chemical, electrochemical, and computational methods. J. Mol. Liq. 323, 115036. https://doi.org/10.1016/j.molliq.2020.115036

Al-Moubaraki, A.H., 2015. Corrosion Protection of Mild Steel in Acid Solutions Using Red Cabbage Dye. Chem. Eng. Commun. 202, 1069–1080. https://doi.org/10.1080/00986445.2014.907565

Ali Asaad, M., Sarbini, N.N., Sulaiman, A., Ismail, M., Huseien, G.F., Abdul Majid, Z., Bothi Raja, P., 2018. Improved corrosion resistance of mild steel against acid activation: Impact of novel Elaeis guineensis and silver nanoparticles. J. Ind. Eng. Chem. 63, 139–148. https://doi.org/10.1016/j.jiec.2018.02.010

Azmi, M.F., Soedarsono, J.W., 2018. Study of corrosion resistrance of pipeline API 5L X42 using green inhibitor bawang dayak (Eleutherine americanna Merr.) in 1M HCl. IOP Conf. Ser. Earth Environ. Sci. 105. https://doi.org/10.1088/1755-1315/105/1/012061

Bashiri, S., Vessally, E., Bekhradnia, A., Hosseinian, A., Edjlali, L., 2017. Utility of extrinsic [60] fullerenes as work function type sensors for amphetamine drug detection: DFT studies. Vacuum 136, 156–162. https://doi.org/10.1016/j.vacuum.2016.12.003

Belghiti, M.E., Echihi, S., Dafali, A., Karzazi, Y., Bakasse, M., Elalaoui-Elabdallaoui, H., Olasunkanmi, L.O., Ebenso, E.E., Tabyaoui, M., 2019. Computational simulation and statistical analysis on the relationship between corrosion inhibition efficiency and molecular structure of some hydrazine derivatives in phosphoric acid on mild steel surface. Appl. Surf. Sci. https://doi.org/10.1016/j.apsusc.2019.04.125

Berdimurodov, E., Kholikov, A., Akbarov, K., Obot, I.B., Guo, L., 2021. Thioglycoluril derivative as a new and effective corrosion inhibitor for low carbon steel in a 1 M HCl medium: Experimental and theoretical investigation. J. Mol. Struct. 1234, 130165. https://doi.org/10.1016/j.molstruc.2021.130165

Berdimurodov, E., Kholikov, A., Akbarov, K., Xu, G., Abdullah, A.M., Hosseini, M., 2020. New anti-corrosion inhibitor (3ar,6ar)-3a,6a-di-p-

TH-3102_146107038

tolyltetrahydroimidazo[4,5-d]imidazole-2,5(1 h,3h)-dithione for carbon steel in 1 M HCl medium: gravimetric, electrochemical, surface and quantum chemical analyses. Arab. J. Chem. 13, 7504–7523. https://doi.org/10.1016/j.arabjc.2020.08.025

Cang, H., Fei, Z., Xiao, H., Huang, J., Xu, Q., 2012. Inhibition effect of reed leaves extract on steel in hydrochloric acid and sulphuric acid solutions. Int. J. Electrochem. Sci. 7, 8869–8882.

Chaubey, N., Savita, Qurashi, A., Chauhan, D.S., Quraishi, M.A., 2021. Frontiers and advances in green and sustainable inhibitors for corrosion applications: A critical review. J. Mol. Liq. 321, 114385. https://doi.org/10.1016/j.molliq.2020.114385

Das, A.B., Goud, V. V., Das, C., 2018. Extraction and characterization of phenolic content from purple and black rice (Oryza sativa L) bran and its antioxidant activity. J. Food Meas. Charact. 12, 332–345. https://doi.org/10.1007/s11694-017-9645-8

Feng, L., Zhang, S., Qiang, Y., Xu, S., Tan, B., Chen, S., 2018. The synergistic corrosion inhibition study of different chain lengths ionic liquids as green inhibitors for X70 steel in acidic medium. Mater. Chem. Phys. 215, 229–241. https://doi.org/10.1016/j.matchemphys.2018.04.054

Ganash, A.A., 2018. Theoretical and experimental studies of dried marjoram leaves extract as green inhibitor for corrosion protection of steel substrate in acidic solution. Chem. Eng. Commun. 205, 350–362. https://doi.org/10.1080/00986445.2017.1391096

Haruna, K., Saleh, T.A., 2021. N,N′-Bis-(2-aminoethyl)piperazine functionalized graphene oxide (NAEP-GO) as an effective green corrosion inhibitor for simulated acidizing environment. J. Environ. Chem. Eng. https://doi.org/10.1016/j.jece.2020.104967

Hsissou, R., Abbout, S., Safi, Z., Benhiba, F., Wazzan, N., Guo, L., Nouneh, K., Briche, S., Erramli, H., Ebn Touhami, M., Assouag, M., Elharfi, A., 2021. Synthesis and anticorrosive properties of epoxy polymer for CS in [1 M] HCl solution: Electrochemical, AFM, DFT and MD simulations. Constr. Build. Mater. 270, 121454. https://doi.org/10.1016/j.conbuildmat.2020.121454

Ji, G., Anjum, S., Sundaram, S., Prakash, R., 2015. Musa paradisica peel extract as green corrosion inhibitor for mild steel in HCl solution. Corros. Sci. 90, 107–117.

TH-3102_146107038

https://doi.org/10.1016/j.corsci.2014.10.002

Khanra, A., Srivastava, M., Rai, M.P., Prakash, R., 2018. Application of Unsaturated Fatty Acid Molecules Derived from Microalgae toward Mild Steel Corrosion Inhibition in HCl Solution: A Novel Approach for Metal-Inhibitor Association. ACS Omega 3, 12369–12382. https://doi.org/10.1021/acsomega.8b01089

Li, H., Qiang, Y., Zhao, W., Zhang, S., 2021. 2-Mercaptobenzimidazole-inbuilt metal-organic-frameworks modified graphene oxide towards intelligent and excellent anti-corrosion coating. Corros. Sci. 191, 109715. https://doi.org/10.1016/j.corsci.2021.109715

Li, X., Deng, S., Fu, H., 2012. Inhibition of the corrosion of steel in HCl, H2SO4 solutions by bamboo leaf extract. Corros. Sci. 62, 163–175. https://doi.org/10.1016/j.corsci.2012.05.008

Liao, L.L., Mo, S., Luo, H.Q., Li, N.B., 2018. Corrosion protection for mild steel by extract from the waste of lychee fruit in HCl solution: Experimental and theoretical studies. J. Colloid Interface Sci. 520, 41–49. https://doi.org/10.1016/j.jcis.2018.02.071

M'hiri, N., Veys-Renaux, D., Rocca, E., Ioannou, I., Boudhrioua, N.M., Ghoul, M., 2016. Corrosion inhibition of carbon steel in acidic medium by orange peel extract and its main antioxidant compounds. Corros. Sci. 102, 55–62. https://doi.org/10.1016/j.corsci.2015.09.017

Mobin, M., Rizvi, M., Olasunkanmi, L.O., Ebenso, E.E., 2017. Biopolymer from Tragacanth Gum as a Green Corrosion Inhibitor for Carbon Steel in 1 M HCl Solution. ACS Omega 2, 3997–4008. https://doi.org/10.1021/acsomega.7b00436

Mourya, P., Banerjee, S., Rastogi, R.B., Singh, M.M., 2013. Inhibition of mild steel corrosion in hydrochloric and sulfuric acid media using a thiosemicarbazone derivative. Ind. Eng. Chem. Res. 52, 12733–12747. https://doi.org/10.1021/ie4012497

Mourya, P., Banerjee, S., Singh, M.M., 2014a. Corrosion inhibition of mild steel in acidic solution by Tagetes erecta (Marigold flower) extract as a green inhibitor. Corros. Sci. 85, 352–363. https://doi.org/10.1016/j.corsci.2014.04.036

Mourya, P., Banerjee, S., Singh, M.M., 2014b. Corrosion inhibition of mild steel in acidic solution by Tagetes erecta (Marigold flower) extract as a green inhibitor. Corros. Sci. 85, 352–363. https://doi.org/10.1016/j.corsci.2014.04.036

TH-3102_146107038

Naghi Tehrani, M.E.H., Ghahremani, P., Ramezanzadeh, M., Bahlakeh, G., Ramezanzadeh, B., 2021a. Theoretical and experimental assessment of a green corrosion inhibitor extracted from Malva sylvestris. J. Environ. Chem. Eng. 9, 105256. https://doi.org/10.1016/j.jece.2021.105256

Naghi Tehrani, M.E.H., Ghahremani, P., Ramezanzadeh, M., Bahlakeh, G., Ramezanzadeh, B., 2021b. Theoretical and experimental assessment of a green corrosion inhibitor extracted from Malva sylvestris. J. Environ. Chem. Eng. https://doi.org/10.1016/j.jece.2021.105256

Okafor, P.C., Ebenso, E.E., Ekpe, U.J., 2010. Azadirachta Indica Extracts as Corrosion Inhibitor for Mild Steel in Acid Medium. Int. J. Electrochem. Sci 5, 978–993.

Ostovari, A., Hoseinieh, S.M., Peikari, M., Shadizadeh, S.R., Hashemi, S.J., 2009. Corrosion inhibition of mild steel in 1 M HCl solution by henna extract: A comparative study of the inhibition by henna and its constituents (Lawsone, Gallic acid, α-d-Glucose and Tannic acid). Corros. Sci. 51, 1935–1949. https://doi.org/10.1016/j.corsci.2009.05.024

Oubaaqa, M., Ouakki, M., Rbaa, M., Benhiba, F., Galai, M., Idouhli, R., Maatallah, M., Jarid, A., Warad, I., Lakhrissi, B., Zarrouk, A., Ebn Touhami, M., 2022. Experimental and theoretical investigation of corrosion inhibition effect of two 8-hydroxyquinoline carbonitrile derivatives on mild steel in 1 M HCl solution. J. Phys. Chem. Solids 169, 110866. https://doi.org/10.1016/j.jpcs.2022.110866

Prabakaran, M., Kim, S.H., Hemapriya, V., Chung, I.M., 2016. Evaluation of polyphenol composition and anti-corrosion properties of Cryptostegia grandiflora plant extract on mild steel in acidic medium. J. Ind. Eng. Chem. 37, 47–56. https://doi.org/10.1016/j.jiec.2016.03.006

Qiang, Y., Guo, L., Li, H., Lan, X., 2021. Fabrication of environmentally friendly Losartan potassium film for corrosion inhibition of mild steel in HCl medium. Chem. Eng. J. 406, 126863. https://doi.org/10.1016/j.cej.2020.126863

Qiang, Y., Li, H., Lan, X., 2020. Self-assembling anchored film basing on two tetrazole derivatives for application to protect copper in sulfuric acid environment. J. Mater. Sci. Technol. 52, 63–71. https://doi.org/10.1016/j.jmst.2020.04.005

Qiang, Y., Zhang, S., Guo, L., Zheng, X., Xiang, B., Chen, S., 2017a. Experimental and theoretical studies of four allyl imidazolium-based ionic liquids as green inhibitors for copper corrosion in sulfuric acid. Corros. Sci. 119, 68–78.

TH-3102_146107038

https://doi.org/10.1016/j.corsci.2017.02.021

Qiang, Y., Zhang, S., Tan, B., Chen, S., 2018. Evaluation of Ginkgo leaf extract as an eco-friendly corrosion inhibitor of X70 steel in HCl solution. Corros. Sci. 133, 6–16. https://doi.org/10.1016/j.corsci.2018.01.008

Qiang, Y., Zhang, S., Yan, S., Zou, X., Chen, S., 2017b. Three indazole derivatives as corrosion inhibitors of copper in a neutral chloride solution. Corros. Sci. 126, 295–304. https://doi.org/10.1016/j.corsci.2017.07.012

Salinas-Solano, G., Porcayo-Calderon, J., Martinez de la Escalera, L.M., Canto, J., Casales-Diaz, M., Sotelo-Mazon, O., Henao, J., Martinez-Gomez, L., 2018. Development and evaluation of a green corrosion inhibitor based on rice bran oil obtained from agro-industrial waste. Ind. Crops Prod. 119, 111–124. https://doi.org/10.1016/j.indcrop.2018.04.009

Saxena, A., Prasad, D., Haldhar, R., 2018. Investigation of Corrosion Inhibition Effect and Adsorption Activities of Achyranthes aspera Extract for Mild Steel in 0.5 M H2SO4. J. Fail. Anal. Prev. 18, 957–968. https://doi.org/10.1007/s11668-018-0491-8

Shahmoradi, A.R., Ranjbarghanei, M., Javidparvar, A.A., Guo, L., Berdimurodov, E., Ramezanzadeh, B., 2021. Theoretical and surface/electrochemical investigations of walnut fruit green husk extract as effective inhibitor for mild-steel corrosion in 1M HCl electrolyte. J. Mol. Liq. 338, 116550. https://doi.org/10.1016/j.molliq.2021.116550

Singh, A., Ansari, K.R., Quraishi, M.A., Kaya, S., Banerjee, P., 2019. The effect of an N-heterocyclic compound on corrosion inhibition of J55 steel in sweet corrosive medium. New J. Chem. 43, 6303–6313. https://doi.org/10.1039/C9NJ00356H

Singh, P., Quraishi, M.A., 2016. Corrosion inhibition of mild steel using Novel Bis Schiff's Bases as corrosion inhibitor: Electrochemical and Surface measurement. Meas. J. Int. Meas. Confed. 86, 114–124. https://doi.org/10.1016/j.measurement.2016.02.052

Srivastava, M., Tiwari, P., Srivastava, S.K., Prakash, R., Ji, G., 2017a. Electrochemical investigation of Irbesartan drug molecules as an inhibitor of mild steel corrosion in 1 M HCl and 0.5 M H2SO4 solutions. J. Mol. Liq. 236, 184–197. https://doi.org/10.1016/j.molliq.2017.04.017

Srivastava, M., Tiwari, P., Srivastava, S.K., Prakash, R., Ji, G., 2017b. Electrochemical

TH-3102_146107038

investigation of Irbesartan drug molecules as an inhibitor of mild steel corrosion in 1 M HCl and 0.5 M H2SO4 solutions. J. Mol. Liq. 236, 184–197. https://doi.org/10.1016/j.molliq.2017.04.017

Srivastava, V., Chauhan, D.S., Joshi, P.G., Maruthapandian, V., Sorour, A.A., Quraishi, M.A., 2018a. PEG-Functionalized Chitosan: A Biological Macromolecule as a Novel Corrosion Inhibitor. ChemistrySelect 3, 1990–1998. https://doi.org/10.1002/slct.201701949

Srivastava, V., Chauhan, D.S., Joshi, P.G., Maruthapandian, V., Sorour, A.A., Quraishi, M.A., 2018b. PEG-Functionalized Chitosan: A Biological Macromolecule as a Novel Corrosion Inhibitor. ChemistrySelect 3, 1990–1998. https://doi.org/10.1002/slct.201701949

Teng, Y., Zhang, W., Wang, M., Yu, C., Ma, Y., Bian, J., Yang, X., Zhang, D., 2021. Anthocyanin as sustainable and non-toxic corrosion inhibitor for mild steel in HCl media: Electrochemical, surface morphology and theoretical investigations. J. Mol. Liq. 344, 117721. https://doi.org/10.1016/j.molliq.2021.117721

Thomas, A., AT, J.R., Joseph, A., 2021. Extended protection of mild steel in molar HCl using the Garcinia Indica fruit rind extract (GIW) and iodide ions; electrochemical, thermodynamic and kinetic studies. J. Indian Chem. Soc. 98, 100167. https://doi.org/10.1016/j.jics.2021.100167

Thomas, A., Prajila, M., Shainy, K.M., Joseph, A., 2020. A green approach to corrosion inhibition of mild steel in hydrochloric acid using fruit rind extract of Garcinia indica (Binda). J. Mol. Liq. 312, 113369. https://doi.org/10.1016/j.molliq.2020.113369

Verma, C., Olasunkanmi, L.O., Ebenso, E.E., Quraishi, M.A., 2018a. Adsorption characteristics of green 5-arylaminomethylene pyrimidine-2,4,6-triones on mild steel surface in acidic medium: Experimental and computational approach. Results Phys. 8, 657–670. https://doi.org/10.1016/j.rinp.2018.01.008

Verma, C., Quraishi, M.A., Ebenso, E.E., Bahadur, I., 2018b. A Green and Sustainable Approach for Mild Steel Acidic Corrosion Inhibition Using Leaves Extract: Experimental and DFT Studies. J. Bio- Tribo-Corrosion 4. https://doi.org/10.1007/s40735-018-0150-3

Wang, Cai, Chen, J., Hu, B., Liu, Z., Wang, Chongbin, Han, J., Su, M., Li, Y., Li, C., 2019. Modified chitosan-oligosaccharide and sodium silicate as efficient

TH-3102_146107038

sustainable inhibitor for carbon steel against chloride-induced corrosion. J. Clean. Prod. 238, 117823. https://doi.org/10.1016/j.jclepro.2019.117823

Zhou, Xueyong, Zhou, Xin, 2014. the Unit Problem in the Thermodynamic Calculation of Adsorption Using the Langmuir Equation. Chem. Eng. Commun. 201, 1459–1467. https://doi.org/10.1080/00986445.2013.818541

भारतीय प्रौद्योगिकी संस्थान गुवाहाटी • Indian Institute of Technology Guwahati •

TH-3102_146107038

5

Corrosion inhibition by extract of banana flower bract (kitchen waste)

TH-3102_146107038

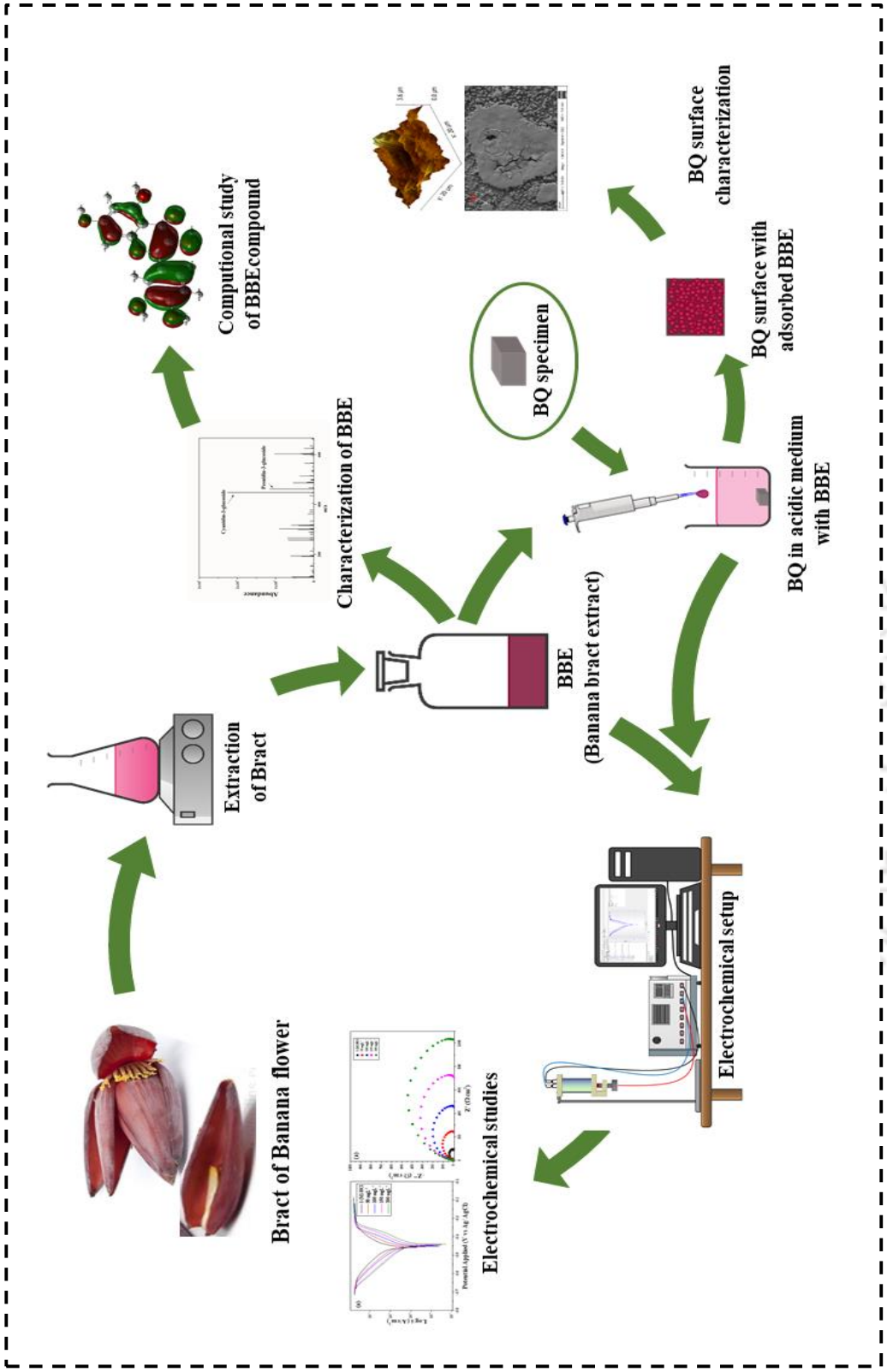

Corrosion inhibition by extract of banana flower bract (kitchen waste)

TH-3102_146107038

Corrosion inhibition by extract of banana flower bract (kitchen waste)

This chapter depicts the results and discussion about corrosion inhibition efficacy of a extract from kitchen waste, banana flower bract, which was used to mitigate the corrosion of boiler quality (BQ) industrially used steel in acidic media. The extract of the banana bract was obtained by the conventional extraction method, characterized by LC-MS was tested to find its corrosion inhibition efficiency in both HCl (1 M) and H_2SO_4 (0.5 M) media. The anti-corrosive performances were assessed by the gravimetric method, potentiodynamic polarization method, and electrochemical impedance spectroscopy method at ambient temperature (25 ± 2° C). The investigations revealed the maximum inhibition efficiencies of banana bract extract (BBE) was 90.84 % (1 M HCl) and 90.61% (0.5 M H_2SO_4) media after incorporating a maximum concentration of 200 mg L^{-1}. The adsorption studies exhibited that BBE acted as a mixed-type inhibitor, and it followed the Langmuir adsorption isotherm to be adsorbed on the BQ surface. Based on the density functional theory (DFT), a few quantum chemical descriptors and local reactive sites were discovered to find the donor-acceptor interaction capability between the identified molecules of BBE and BQ surface.

Published Artcle: Pal, A., Das, C., 2022. Investigations on corrosion inhibition in acidic media for BQ steel using banana flower bract, an eco-friendly novel agro-waste: Experimental and theoretical considerations. **Inorg. Chem. Commun.** 145, 110024. https://doi.org/10.1016/j.inoche.2022.110024

TH-3102_146107038

5.1 Characterization of the compound in BBE

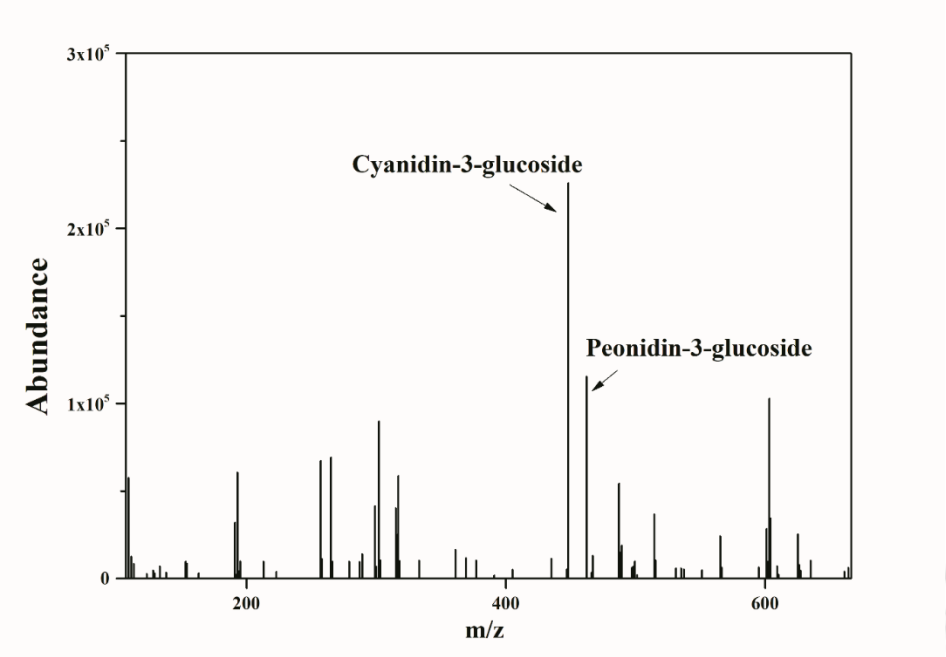

Fig. 5.1 Mass spectra of BBE indicating the presence of cyanidin-3-glucoside and peonidin-3-d-glucoside detected.

A viable and commonly acknowledged technique for qualitative and quantitative measurement of polyphenols in biomass is liquid chromatography-mass spectrometry (LC-MS). The LC-MS method was used to determine the qualitative profile of BBE, and the chromatogram of the extract is shown in Fig. 5.1 as an example. The mass spectrum was acquired using negative ionization to produce its mass spectrum. From the spectrum, it was noticed that maximum intensity was observed for the m/z values of 448.1 and 462.1. From the literature, it was found that in negative ionization mode, the m/z 448.1 and 462.1 indicate the presence of cyanidin-3-glucoside (C3G) and peonidin-3-glucoside (P3G). Some early works have also supported the adequacy of C3G and P3G in banana bract (Begum and Deka, 2017; Mathew and Negi, 2021). The presence of C3G and P3G makes the BBE an efficient inhibitor because of

TH-3102_146107038

its antioxidant property and ability to make a complex with iron (Alexandra Pazmio-Durán et al., 2001; Begum and Deka, 2017; Ove et al., 2019).

5.2 Gravimetric analysis

In order to evaluate the inhibitory efficiency of various compounds, the weight-loss method or gravimetric method is a simple and widely used method. The inhibitory efficiency was assessed using this method, and the results revealed that specimens lost a significant amount of weight after being immersed in acid solutions for an extended period of time. In acidic conditions, the presence of BBE, on the other hand, slowed the dissolution of BQ steel. By applying Eq. 2.1 and 2.2, CR and $\mu_{CR}\%$ of different BBE concentrations in both HCl and H_2SO_4 media were estimated. In accordance with Table 5.1 and Fig. 5.2, it can be stated that BBE is a potent corrosion inhibitor with a high ability to reduce corrosion. Because it has been noticed that as the concentration of BBE increases, CR decreases and the $\mu_{CR}\%$ increases.

Table 5.1 Parameters of gravimetric analysis for BQ steel in 1 (M) HCl and 0.5 (M) H_2SO_4 with and without BBE.

	Conc. (mg L^{-1})	$CR \times 10^2$ (mm $year^{-1}$)	$\mu_{CR}\%$
HCl media	**0 (Blank) 1(M)HCl**	210.13 ± 6.71	0.00 ± 0.00
	50	85.31 ± 1.23	59.40 ± 0.76
	100	54.72 ± 0.96	73.96 ± 0.49
	150	37.05 ± 0.35	82.37 ± 0.67
	200	24.23 ± 0.31	88.47 ± 0.85
H_2SO_4 media	**0 (Blank) 0.5 (M) H_2SO_4**	213.51 ± 7.12	0.00 ± 0.00
	50	98.85 ± 2.21	53.70 ± 1.17
	100	56.10 ± 0.83	73.72 ± 0.86
	150	42.38 ± 0.72	80.15 ± 0.51
	200	28.51 ± 0.32	86.65 ± 0.69

TH-3102_146107038

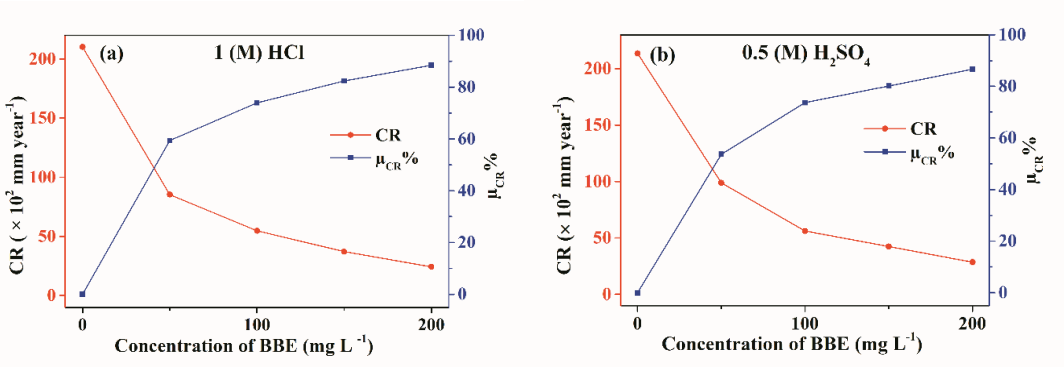

Fig. 5.2 Corrosion rate and inhibition efficiency of BQ steel from gravimetric analysis in (a) 1 (M) HCl and (b) 0.5 M H_2SO_4 without and with different concentration of BBE at 25° C after immersing 72 h.

According to Fig. 5.2 (a) and (b), even at the lowest concentrations of BBE, there was a significant increase in the efficiency of the process. The increase in the inhibition efficiency is related to the reduction in the redox reaction rate throughout the corrosion process. During the corrosion process, two types of reactions occur that have a substantial impact on the intensity of the corrosion process are as follows:

Anodic reaction (Oxidation): $Fe \rightarrow Fe^{2+} + 2e^-$ **5.1**

Cathodic reaction (Reduction): $2H^+ + 2e^- \rightarrow 2(H)_{ads} + H_2$ **5.2**

The addition of BBE into the media decreased anodic and cathodic reduction rates, reducing iron oxidation from BQ steel surfaces. Table 5.1 shows that when the lowest concentration of BBE (50 mg L^{-1}) is compared, the efficiency in HCl is much greater than H_2SO_4. However, at the maximum dosage (200 mg L^{-1}), the effectiveness is comparable in both acidic environments. Because it is generally known that SO_4^{2-} has a lower adsorbability than Cl-, the negatively charged surface of the H_2SO_4 solution will be lower than the positively charged surface. However, at the maximum dosage (200 mg L^{-1}), both acidic environments have a lesser difference in their efficiency. Because SO_4^{2-} was less adsorbable than Cl^-, the H_2SO_4 solution developed a lesser

TH-3102_146107038

negatively charged surface (Mourya et al., 2013). In acidic media, the protonated phenolic compounds are prone to be adsorbed on a negatively charged surface rather than a neutral surface in the case of physical adsorption. As the interaction of physisorption depends on the negative charge of the surface, Cl^- ions are more aggressive than SO_4^{2-} to attract the cations even at a lower concentration. (Haruna and Saleh, 2021; Shahmoradi et al., 2021; Thomas et al., 2020). In reality, the interaction between the protonated compounds and the anions of the surface may be physical or chemical, or mixed, which is discussed in the following studies.

5.3 Electrochemical measurements

Several electrochemical tests were required to understand the electrochemical kinetics and the kinetic parameters of BQ steel in an electrolyte and the effectiveness of inhibition. Particularly the revelation of the i_{corr}, R_{ct}, and other relevant parameters are necessary to elucidate the inhibitory effect of the inhibitor.

5.3.1 OCP measurements

The open-circuit potential or OCP (E_{oc}) is the potential of the working electrode when all the electrodes are introduced into electrolytes without applying any external load. OCP is often called zero-current potential since no external current is applied. Sometimes OCP is also regarded as having corrosion potential. OCP is a crucial metric in electrochemistry because it reflects system stability, which is vital in perturbation-based research. Before doing any further electrochemical research, the system under study should reach a stable state via stabilizing OCP. Once the OCP has stabilized, perturbation-based experiments can be performed. Depending on the various factors of the system, developing a stable OCP might take minutes to hours. An automated system records all OCP values over time until the average OCP is stabilized. After confirming

TH-3102_146107038

the stability of the system, it is ready for any perturbation-based experiment (Shabani-Nooshabadi and Ghandchi, 2015).

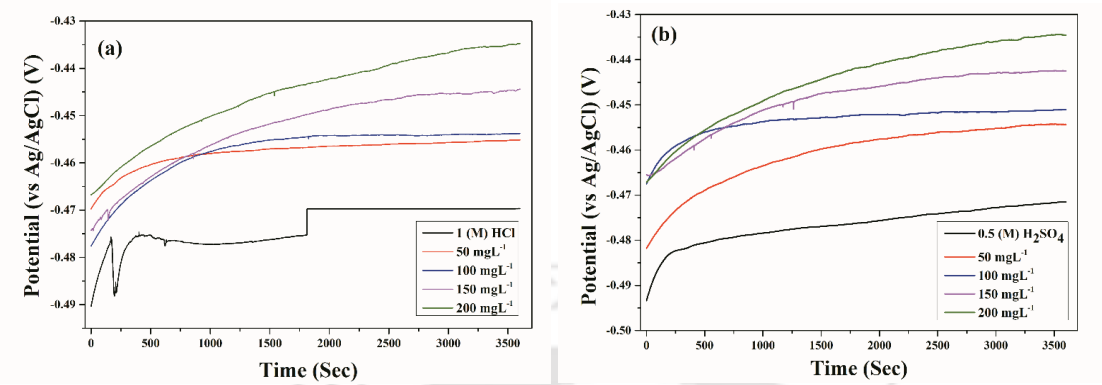

Fig. 5.3 OCP curves for BQ steel in (a) HCl and (b) H_2SO_4 without and with different concentrations of BBE at 25° C.

To ensure system stability, OCP values were recorded for 60 minutes. The studies were performed with and without BBE inhibitors. Fig 5.3 (a) and (b) demonstrate the fluctuations in OCP throughout time. According to the findings, when inhibitors are present, the OCP tends to shift towards more positive values than in their absence. More crucially, when the concentrations were increased from 50 mgL^{-1} to 200 mgL^{-1}, the curves changed in a more positive direction. The beneficial changes in the OCP values are interpreted as an improvement in the system, which may be occurred due to the establishment of the protective layer on BQ. The layer on BQ by adsorbed inhibitory compounds might enhance corrosion inhibition (Naghi Tehrani et al., 2021; Salinas-Solano et al., 2018; Singh and Quraishi, 2016).

5.3.2 Potentiodynamic polarization tests

Tafel polarization analysis is essential to comprehend the electrochemical kinetics of the surface corrosion process. Fig. 5.4 (a) and (b) exhibit polarisation effects on BBE in HCl and H_2SO_4 electrolytes, respectively. Different corrosion parameters, such as corrosion potential (E_{corr}), current density (i_{corr}) and $cathodic$ (b_c) and

TH-3102_146107038

anodic (b_a) Tafel slopes were computed by extrapolating the Tafel curves and are exhibited in Table 5.2, along with the efficiency (IE) of the corrosion process.

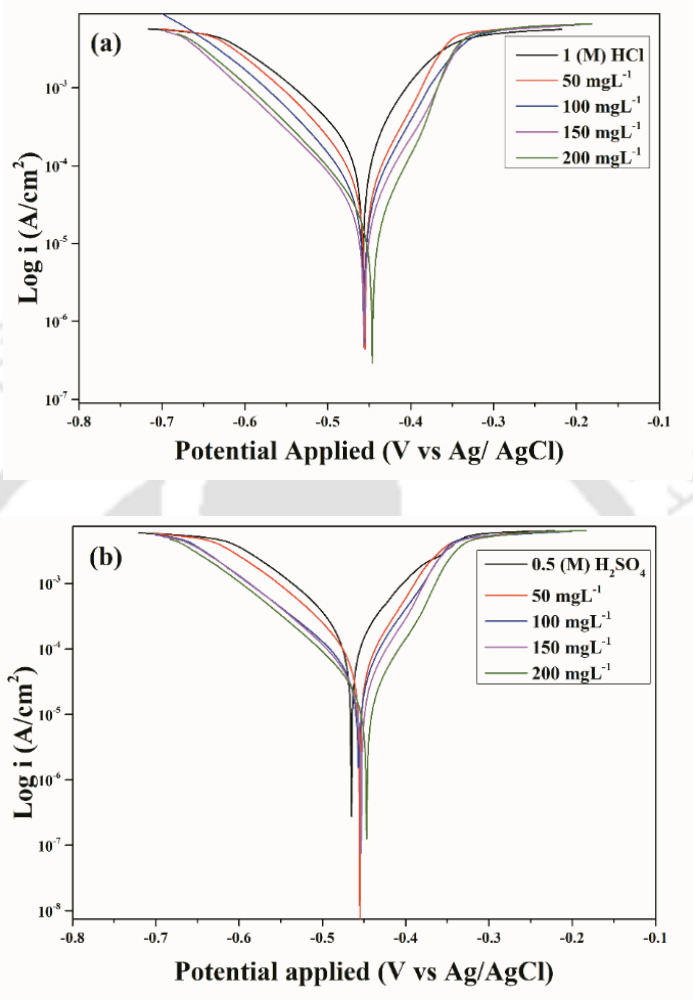

Fig. 5.4 Tafel polarization curves for BQ steel without and with different BBE concentrations in (a) HCl and (b) H_2SO_4 media at 25° C.

The potentiodynamic polarization studies show that in the absence of BBE, the anodic and cathodic currents were higher compared to the presence of BBE (Fig. 5.4 (a) and (b)). The reason behind this was the higher anodic metal dissolution and cathodic hydrogen evolution in both acidic media in the absence of the inhibitor. But the presence of an inhibitor reduced the anodic and cathodic currents, indicating a decrease in corrosion rate. This might be caused by the adsorption of inhibitors on the steel surface, thereby blocking the active sites on the steel surface (Galai et al., 2020).It

TH-3102_146107038

is also observed in Fig. 5.4 that in both acidic and basic media, the Tafel curves shift towards a positive direction in the presence of BBE. But as the shift is less than 85 mV, this BBE inhibitor can not be considered an anodic type inhibitor but rather can be considered a mixed-type inhibitor. So it can be inferred that BBE controlled the corrosion process by altering the anodic and cathodic reactions (Verma et al., 2018). Adding the BBE inhibitor brought a noticeable change in the metal dissolution or anodic reactions, which can be seen in anodic slopes. At the same time, the reduction of H^+ ions to H_2 or the cathodic reaction seems unaffected by inhibitors. So it can be inferred that BBE had merely any effect on the mechanism of hydrogen evolution. Moreover, the hydrogen evolution reaction took place by a charge transfer mechanism (Galai et al., 2020; Ouakki et al., 2020).

On the basis of Table 5.2, it can be expressed that the values of i_{corr} and b_c, b_a are seen to be changed in the presence of BBE. The values of b_a are consistently larger than b_c in all tests, showing that the inhibitors are more successful at lowering the anodic current than the cathodic current. The values of the slopes were found in an irregular manner which indicates that the inhibition was caused by not only adsorption but also a mixed effect of locking active sites and the involvement of some charged species present in the solution (Oubaaqa et al., 2022). With the help of the corrosion current density measurement, it is possible to offer yet another evidence of the influence of BBE on the reduction of corrosion reactions.

TH-3102_146107038

Table 5.2 The obtained parameters from Tafel polarization tests in the HCl and H_2SO_4 media at different BBE concentration.

	Conc. (mg L^{-1})	b_a ($mVdec^{-1}$)	$-b_c$ ($mVdec^{-1}$)	E_{corr} (mV vs AgCl)	i_{corr} (μAcm^{-2})	R_P (Ωcm^{-2})	(μ_P%)
HCl media	0 (Blank) 1(M)HCl	110.98 ± 2.05	66.84 ± 0.80	-457.12 ± -3.32	179.06 ± 7.08	101.17 ± 0.49	0.00 ± 0.00
	50	77.87 ± 1.77	63.05 ± 0.42	-453.94 ± -1.73	66.30 ± 0.91	228.19 ± 1.41	62.97 ± 0.78
	100	79.79 ± 2.75	59.96 ± 1.16	-455.80 ± -2.57	43.46 ± 0.71	342.08 ± 1.15	75.73 ± 0.41
	150	90.53 ± 0.87	61.91 ± 0.33	-454.14 ± -6.35	29.19 ± 0.08	547.1 ± 7.66	83.70 ± 0.12
	200	73.11 ± 0.95	54.25 ± 0.41	-446.08 ± -1.50	19.90 ± 0.05	679.63 ± 21.34	88.89 ± 0.08
H_2SO_4 media	0 (Blank) 0.5 (M) H_2SO_4	93.13 ± 2.26	81.36 ± 1.40	-464.44 ± -3.17	180.25 ± 7.01	104.62 ± 1.25	0.00 ± 0.00
	50	77.95 ± 1.84	62.87 ± 1.11	-454.41 ± -3.73	72.75 ± 1.64	207.76 ± 1.10	59.64 ± 1.17
	100	93.93 ± 2.71	59.55 ± 0.61	-455.41 ± -2.39	48.44 ± 0.62	326.73 ± 4.28	73.13 ± 0.88
	150	84.12 ± 3.77	57.30 ± 1.00	-452.93 ± -1.86	34.48 ± 0.54	429.25 ± 10.32	80.87 ± 0.36
	200	86.53 ± 2.54	57.21 ± 1.32	-445.74 ± -5.52	23.01 ± 0.24	649.92 ± 32.62	87.23 ± 0.70

It can be seen From the Table 5.2 that the values of i_{corr} have decreased greatly when BBE is present in both the acidic media, and the reduction is much more pronounced when higher doses of BBE are present. The low i_{corr} values at high BBE

TH-3102_146107038

concentrations indicate that the corrosion rate was reduced, which is consistent with the notion that the corrosion rate is directly connected to i_{corr}. Additionally, it was also found that the R_P values fell as the BBE concentrations increased. According to these two occurrences of lowering i_{corr} and increasing R_P in both media, a strong barrier protecting the BQ surface from corrosion was likely generated by the BBE, which inhibits the active reaction sites of corrosion from forming. The addition of BBE inhibitor in both media greatly enhances the inhibitory efficiency ($\mu_P\%$) at higher concentrations (Okafor et al., 2010; Prabakaran et al., 2016). The higher concentration might cause the multilayer type of adsorption, which leads to less uncovered area of the surface (Ouakki et al., 2020).

5.3.3 EIS measurements

EIS has been extensively utilized to investigate corrosion, passivation, and other charge transfer processes related to the electrode/electrolyte interface. In the EIS study, Nyquist and Bode plots are showcased to illustrate the impedance response to each frequency. Fig. 5.5 and 5.6 show the Nyquist and Bode plots in HCl and H_2SO_4 media without and with different concentrations of BBE. Because of the BQ steel surface heterogeneity, the semicircle Nyquist plots generated by all of the experiments were slightly depressed in shape. As the shapes and the pattern of the curves are quite similar in the control and inhibited conditions of both media, it is reasonable to conclude that the BBE inhibitors have no influence on the corrosion process. At higher frequencies, these semicircles have large capacitive loops and inductive loops are seen at lower frequencies. The capacitive loop is related to charge transfer in the double layer of the surface, whereas the inductive loop is associated with intermediate products of corrosion. The inductive loop, which is resultant of the relaxation of the intermediate

TH-3102_146107038

products or the adsorption species (SO_4^{2-}, Cl^- and H^+) in the corrosion process, was observed in the absence of an inhibitor (Kadiri et al., 2018; Ouakki et al., 2020). But it was not noticeable in the presence of BBE, which suggests complete inhibitor molecule coverage on the steel surface and is often considered a degradation process for EIS (Zheng et al., 2014). These geometries or the patterns of the Nyquist plot patterns imply that the charge transfer process controlled reactions of the metal-solution interface and the developed resistance is charge transfer resistance (R_{ct}). The diameter of the semicircle (capacitive loop) is the measurement of R_{ct}.

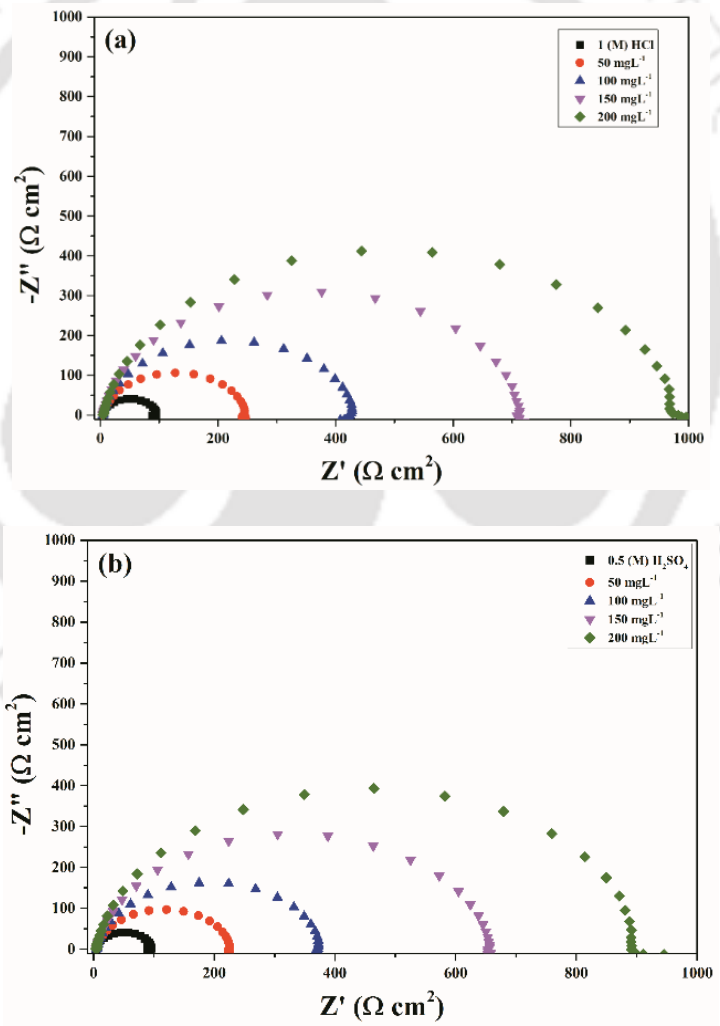

Fig. 5.5 Nyquist plots of BQ steel corrosion without and with applying different concentrations of BBE in (a) HCl and (b) H_2SO_4 media 25° C.

TH-3102_146107038

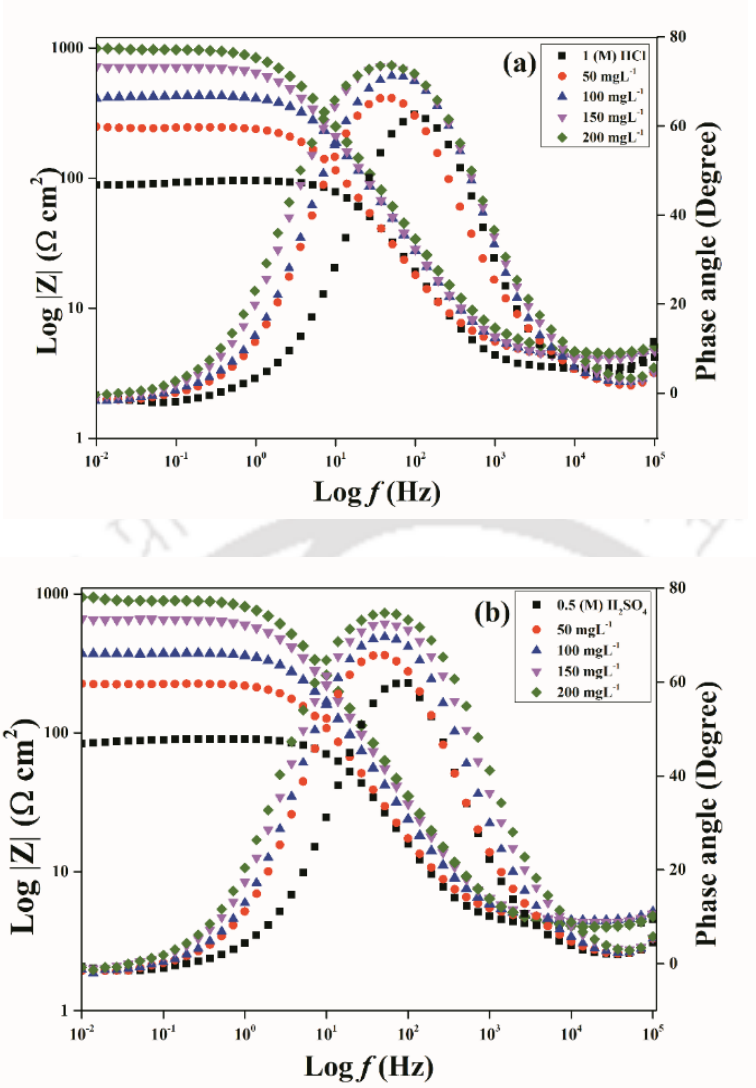

Fig. 5.6 Bode plots for BQ steel without and with different concentrations of BBE in (a) HCl and (b) H_2SO_4 media at 25° C.

The Bode plots (Fig. 5.6 (a) and (b)) in every experiment clearly show the single-time constant in the BQ steel corrosion and are also confirmed by a single narrow peak (Fig. 5.6 (b)), and corrosion was controlled by pure activation kinetic as obtained by polarization curve measurements (Errahmany et al., 2020). Also, the electrochemical property of the surface-electrolyte interface, whether resistive or capacitive, depends on a phase angle of 0° or 90°. As all the phase angle was less than 90° and more than 0°, none of the graphs displayed pure capacitive or resistive behavior. However, a

TH-3102_146107038

strong capacitive response was suggested by increased peak heights at higher inhibitor concentrations. In the phase angle plots, the peak points are not set on a single frequency; hence capacitance changes accordingly. The changes in semicircle diameter of Nyquist plots match with the variations in impedance values in Bode modulus curves of respective BBE concentrations. Fig. 5.5 (a) and (b) demonstrate that when BBE concentration rises, the semicircle diameters increase, suggesting increased charge transfer resistance (R_{ct}). The higher values of $log|z|$ at lower frequencies seen at higher BBE doses indicate that BBE inhibitors were adsorbed on the surface and resistant to both acidic media. The linear relationship can be observed between $\log f$ and $\log z$ with slope close to −1, exhibiting the typical capacitive behavior, therefore existence of adsorption layer (Galai et al., 2020; Mourya et al., 2014a; Saxena et al., 2018a).

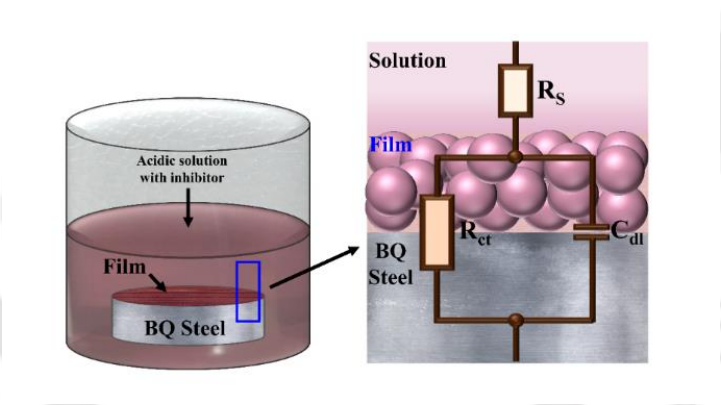

Fig. 5.7 Model of an equivalent circuit for fitting the impedance data points and its physical significance on corrosion BQ steel in the presence of inhibitors.

The resistance mechanism was comprehended by fitting each EIS spectrum to an equivalent circuit (Randles circuit) (Fig. 5.7) and different EIS parameters like R_s, R_{ct} and CPE were calculated. (Fig. 5.7). In the circuit R_s is in a series with R_{ct} and CPE whereas R_{ct} and CPE is parallel to each other. CPE is a substitution for the ideal double-layer capacitance of distributed frequency. It helps to explain the depression of the capacitance semi-circle, which corresponds to the heterogeneity of surface caused

TH-3102_146107038

by surface roughness, impurities, disloctions, grain boundaries, adsorption of inhibitors, formation of porous layers, etc (Galai et al., 2020).

Table 5.3 Impedance parameters for the corrosion of BQ steel in HCl and H_2SO_4 solutions containing different concentrations of BBE.

	Conc (mg L^{-1})	R_S (Ω cm^2)	R_{ct} (Ω cm^2)	CPE parameters		C_{dl} (µF cm^{-2})	$\mu_{R_{ct}}$%
				n	Y_o (µMho cm^{-2})		
HCl media	**0 (Blank) 1 (M) HCl**	3.49 ± 0.001	89.72 ± 1.67	0.93 ± 0.000	137.01 ± 4.94	97.3 ± 0.95	0.00 ± 0.00
	50	4.35 ± 0.001	243.82 ± 2.90	0.89 ± 0.001	186.71 ± 1.50	127.63 ± 0.43	63.20 ± 0.37
	100	4.44 ± 0.001	421.97 ± 4.34	0.92 ± 0.001	101.91 ± 0.19	76.55 ± 0.07	78.74 ± 0.34
	150	4.21 ± 0.001	714.39 ± 30.06	0.91 ± 0.001	104.65 ± 0.40	79.82 ± 0.17	87.44 ± 0.16
	200	4.64 ± 0.001	979.56 ± 28.39	0.90 ± 0.001	93.26 ± 0.24	70.48 ± 0.11	90.84 ± 0.13
H_2SO_4 media	**0 (Blank) 0.5 (M) H_2SO_4**	4.13 ± 0.001	85.082 ± 1.38	0.92 ± 0.000	178.23 ± 8.43	125.46 ± 1.54	0.00 ± 0.00
	50	4.49 ± 0.001	222.96 ± 4.46	0.90 ± 0.001	191.60 ± 3.08	132.57 ± 0.85	61.84 ± 0.66
	100	4.53 ± 0.001	371.05 ± 9.66	0.91 ± 0.001	126.53 ± 0.88	92.00 ± 0.29	77.07 ± 0.21
	150	4.41 ± 0.001	655.68 ± 17.90	0.90 ± 0.001	99.00 ± 0.32	73.14 ± 0.13	87.02 ± 0.27
	200	4.10 ± 0.001	905.64 ± 26.82	0.91 ± 0.001	82.89 ± 0.18	63.94 ± 0.10	90.61 ± 0.20

TH-3102_146107038

Many electrical components like capacitors, resistors, and inductors describe the physical electrochemistry system. The capacitor of the circuit is not an ideal capacitor, particularly when the system is not homogeneous. CPE replaces a capacitor to simulate the homogeneity of the surface (Galai et al., 2020; M'hiri et al., 2016; Srivastava et al., 2018; Verma et al., 2018). The increased BBE concentration leads to larger surface resistance in both acidic media, as seen by the Nyquist and Bode plots, respectively. To understand BQ steel surface behavior in the presence and absence of inhibitors in both acidic media, Table 5.3 shows EIS parameters vary with BBE concentrations. In both the media, R_{ct} increased with BBE concentration, whereas CPE decreased. These changes in R_{ct} indicate formation of a thin protective layer by inhibitor compounds on the metallic BQ surface. This layer blocked the passage of charge from the bulk electrolyte to the surface of BQ, preventing corroding chemicals from reaching active local sites. More significantly, high BBE concentration enhanced layer thickness, minimizing the mass and charge transfer. As more BQ steel surface area wascoated with inhibitor, the chance of corroding components coming into touch with the steel surface was less (Ji et al., 2015; Wang et al., 2019). From Table 5.3 it was also observed that values of n were decreased as the BBE was added in the media. The decrease in the n values indicates increase in non-homogeneity of the steel surface in earlier studies. However the values of n (0.89–0.92) are not equal to 1 but close to 1 which suggest the capacitive characteristic of interface (Alaoui et al., 2016; Ouakki et al., 2020). The maximum inhibition efficiency was found to be nearly 91% for both media at 200 mg L^{-1} when the maximum surface was covered with BBE.

TH-3102_146107038

5.4 Adsorption studies

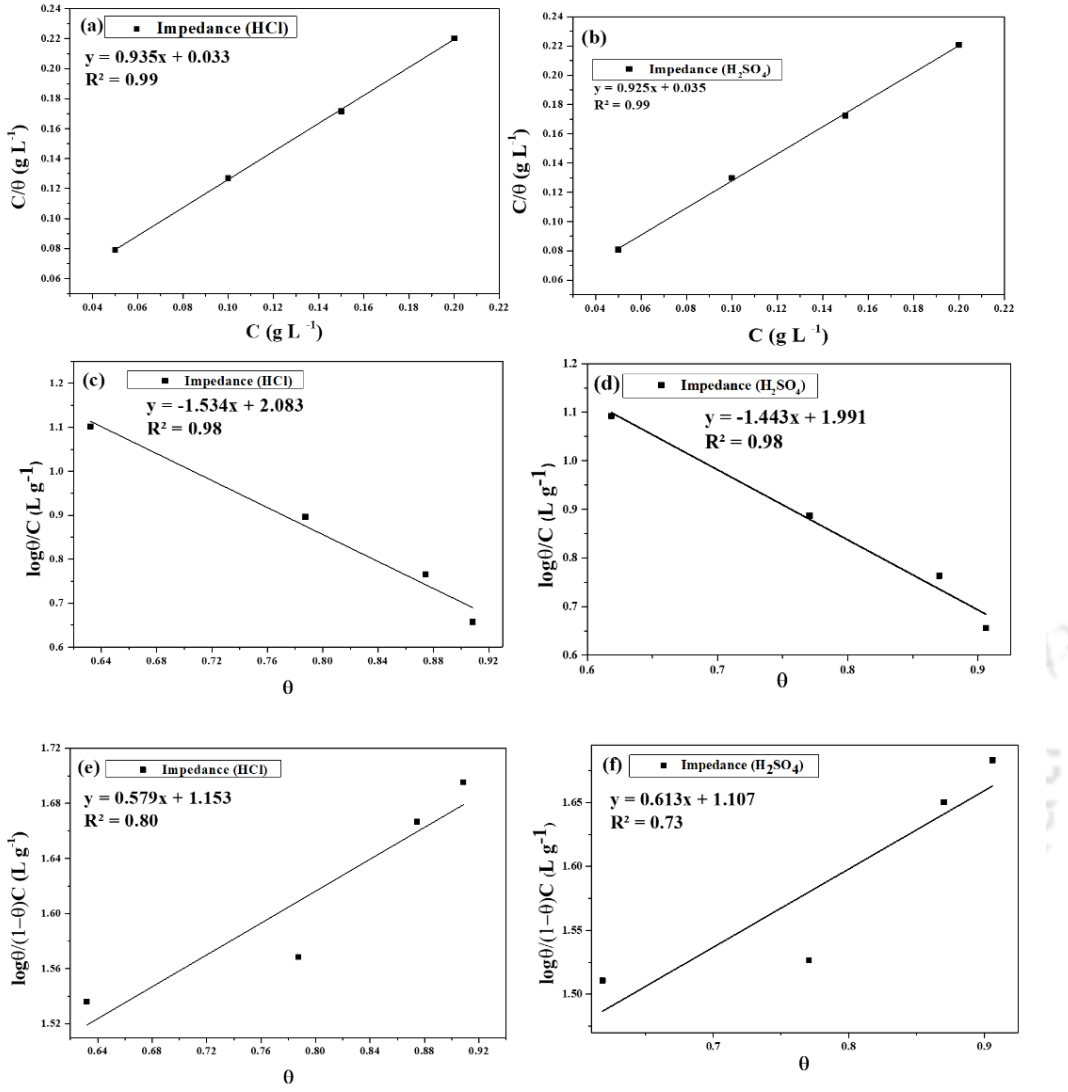

Fig. 5.8 Adsorption isotherm plots for adsorption of BBE on BQ steel in HCl and H_2SO_4: (a, b) Langmuir, (c, d) Temkin, (e, f) Frumkin at 25° C.

The results of the electrochemical already indicated the adsorption of BBE (adsorbate) on the BQ steel surface (adsorbent). But the type of interaction between them needs to be revealed. The kind of adsorption occurring on the surface may be physisorption, chemisorption, or mixed. To assess the type, some conventional adsorption isotherms such as Langmuir (Fig. 5.8 (a) and (b)), Temkin (Fig. 5.8 (c) and

TH-3102_146107038

(d)), and Frumkin isotherms (Figs. 5.8 (e) and (f)), were examined. Each isotherm relates inhibitor concentration (C), surface coverage (θ), and the equilibrium constant (K_{ads}). It was found that the Langmuir model (Fig. 5.8(a) and (b)), which had a regression coefficient (R^2) of 0.99 in both HCl and H_2SO_4 was the best-fitted model. As it follows the Langmuir model, it can be assumed that a monolayer is formed, and the interaction with the inhibitor molecules is not so possible (Thomas et al., 2020).

The Langmuir isotherm can be expressed in the straight-line equation as the given equation:

$$\frac{C}{\theta} = \frac{1}{K_{ads}} + C \qquad \textbf{5.3}$$

Where the value of K_{ads} (L^{g-1}) was acquired by plotting $\frac{C}{\theta}$ (gL^{-1}) vs C (gL^{-1}). K_{ads} is the adsorption equilibrium constant from which the adsorption free energy, also known as standard Gibbs free energy (ΔG°_{ads}) can be calculated using the following expression:

$$\Delta G^{\circ}_{ads} = -RTln(C_{water}K_{ads}) \qquad \textbf{5.4}$$

Where R denotes the universal gas constant (8.314 $Jmol^{-1}K^{-1}$), C_{water} represents the concentration of water (1000 gL^{-1}), and T is the temperature (298.15 K). The derived linear regression coefficient (R^2) from the Langmuir plot, as well as ΔG°_{ads} and K_{ads} are shown in Table 5.4 with the other variables.

Table 5.4. Adsorption isotherm parameters for BBE in HCl and H_2SO_4

Media	R^2	$1/K_{ads}$ ($g\ L^{-1}$)	K_{ads} (Lg^{-1})	$\Delta G°_{ads}$ ($kJmol^{-1}$)
1 M HCl	0.99	0.033	30.74	-25.62
0.5 M H_2SO_4	0.99	0.035	28.28	-25.41

TH-3102_146107038

The resulting negative values of the $\Delta G°_{ads}$ indicated the spontaneous adsorption of the inhibitory molecules on the surface. The earlier studies suggest that $\Delta G°_{ads}$ is an indicator of adsorption type. If, $\Delta G°_{ads} \geq$ -20 kJmol^{-1}, then the adsorption is occurred due to the electrostatic interaction (physisorption) and $\Delta G°_{ads} \leq$ -40 kJmol^{-1}, then the adsorption takes place due to electron sharing or transferring (chemisorption) (Azmi and Soedarsono, 2018; Qiang et al., 2020). Here $\Delta G°_{ads}$ values are -25.62 and -25.41 kJmol^{-1} in HCl and H_2SO_4 solution. These values suggest that the adsorption type is mixed-type adsorption as the values lie between -20 kJmol^{-1} and -40 kJmol^{-1}.

5.5 Characterization of surface

5.5.1 Field Emission Scanning Electron Microscopy (FESEM-EDX)

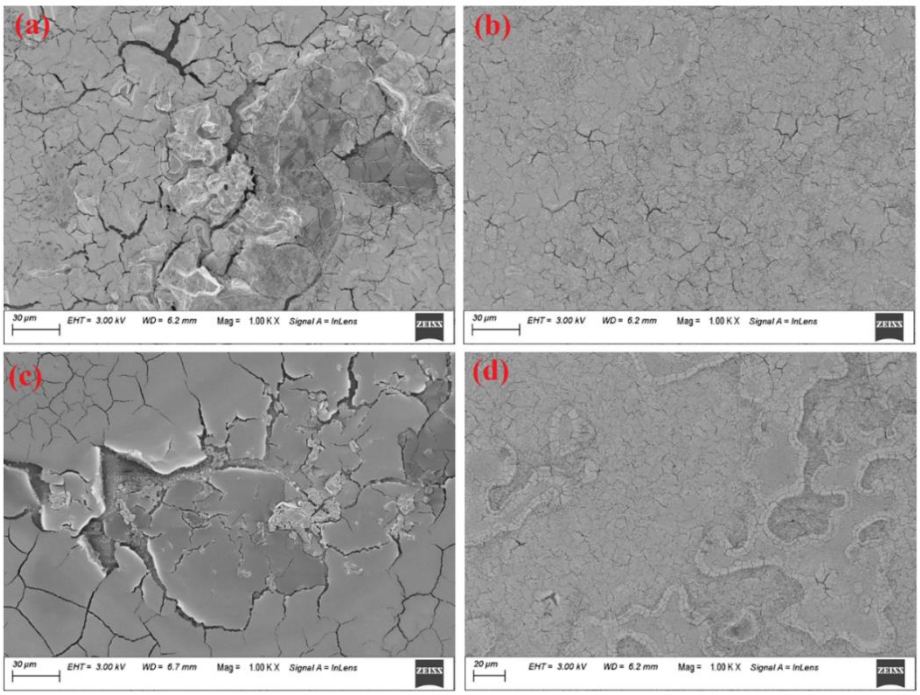

Fig. 5.9 FESEM images for BQ steel surface after immersing for 24 h (a) without, (b) with BBE (200 mgL^{-1}) in 1 M HCl, (c) without BBE, and (d) with BBE (200 mgL^{-1}) in 0.5 M H_2SO_4 at 25° C.

TH-3102_146107038

FESEM tests were performed in HCl and H_2SO_4 media with and without appropriate BBE concentrations to assess surface morphology and validate weight loss and electrochemical interpretations. Fig. 5.9 (a) and (b) demonstrate the difference between the surfaces in 1 (M) HCl solution without and with the addition of BBE inhibitors. Fig. 5.9 (c) and (d) show the untreated and treated surface of BQ in 0.5 (M) H_2SO_4, respectively. The addition of BBE significantly changed the microstructure of the steel surface in both the acidic media. When BBE was absent in the media, the acid corrosion caused fractures and pits on the surface. However, in the presence of BBE, such degraded structures were invisible. The phenolic chemicals in BBE bounde on the steel surface, forming a protective coating that inhibited corrosion processes by blocking active reaction sites. As a result, BBE reduced surface cracks and pits. (Zheng et al., 2014).

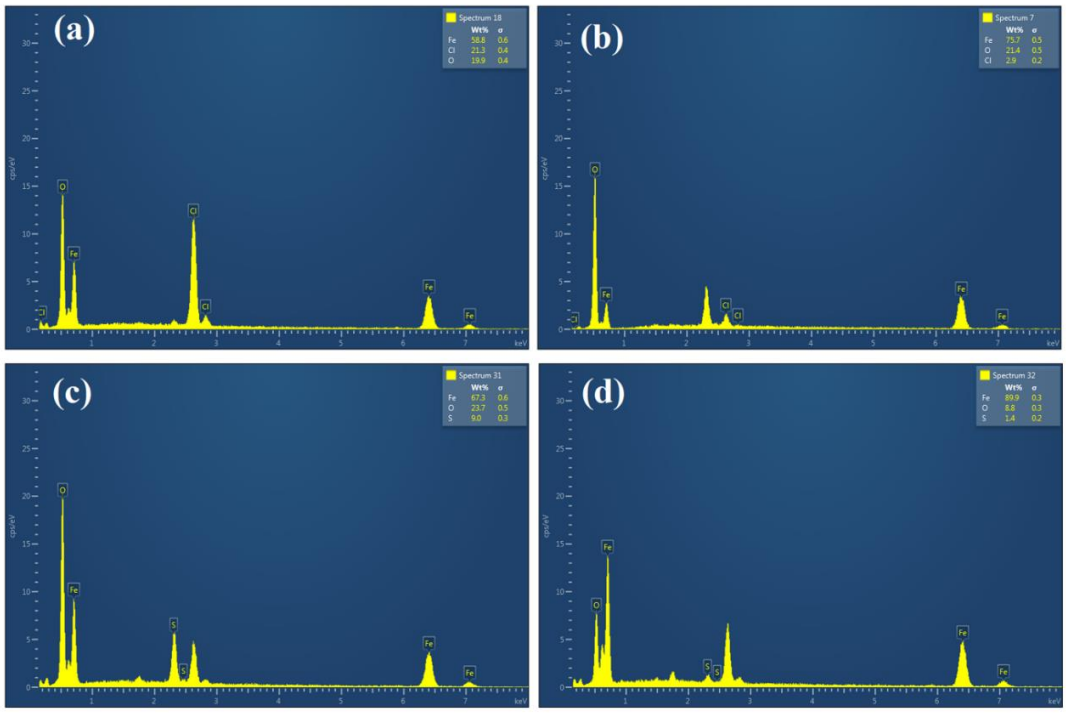

Fig. 5.10 EDX spectra for BQ steel surface after immersing for 12h (a) without, (b) with BBE (200 mgL^{-1}) in 1 M HCl, (c) without, and (d) with BBE (200 mgL^{-1}) in 0.5 M H_2SO_4 at 25° C.

TH-3102_146107038

EDX spectra of BQ steel without and with BBE addition were obtained in both acidic environments to explore the elementary changes in the BQ steel surface. Fig. 5.10 shows the BQ surface EDX spectra with and without the BBE. The EDX spectra in Fig. 5.10 (a) show that the weight percentage of iron (58.8%) and chloride (21.3%) ions are smaller in the absence of BBE than in the presence of BBE (iron: 75.7 %; chloride: 2.9 %) (Fig. 5.10 (b)). In the absence of BBE (Fig. 5.10 (c)), the iron (67.3%) and sulfur (9.0%) weight percentages are lower than in the presence of BBE (iron: 89.9%; sulfur: 1.4 %) (Fig. 5.10 (d)). For various redox reactions to occur, the Fe^{2+} on the surface electrostatically attracted the Cl^-, resulting in the adsorption of Cl^- on the surface. Because SO_4^{2-} was less electronegative than Cl^-, it was less likely to adsorb on the surface of H_2SO_4 than Cl^-. It is believed that this drop in weight % is due to the protective surface generated by BBE inhibitor chemicals on the BQ, making it more resistant to corrosive attacks (Naghi Tehrani et al., 2021).

5.5.2 AFM study

Since all the experiment till now has indicated the adsorption of BBE components on the BQ steel surface, the topological changes of the surface after the addition of BBE is required to be observed. So the 3D AFM micrographs ($20 \times 20\ \mu m^2$) of the BQ steel surface show changes in average surface roughness due to the presence of BBE in both acidic solutions. (Fig. 5.11). A considerable decrease in average surface roughness was seen when an appropriate concentration of BBE was present in both acidic media compared to when BBE was absent. When BBE is present, the average surface roughness of HCl media decreases from 235.57 nm (Fig. 5.11 (a)) to 20.86 nm (Fig. 5.11 (b)). Fig. 5.11 (c) shows that the average roughness of H_2SO_4 in the presence of BBE is 223.36 nm (Fig. 5.11 (c), whereas the average roughness in the absence of

TH-3102_146107038

BBE is 19.34 nm (Fig. 5.11 (d)). So it is observed that there is a significant reduction in the average roughness of BQ samples which were exposed to BBE (Prabakaran et al., 2016; Singh and Quraishi, 2016; Srivastava et al., 2018).

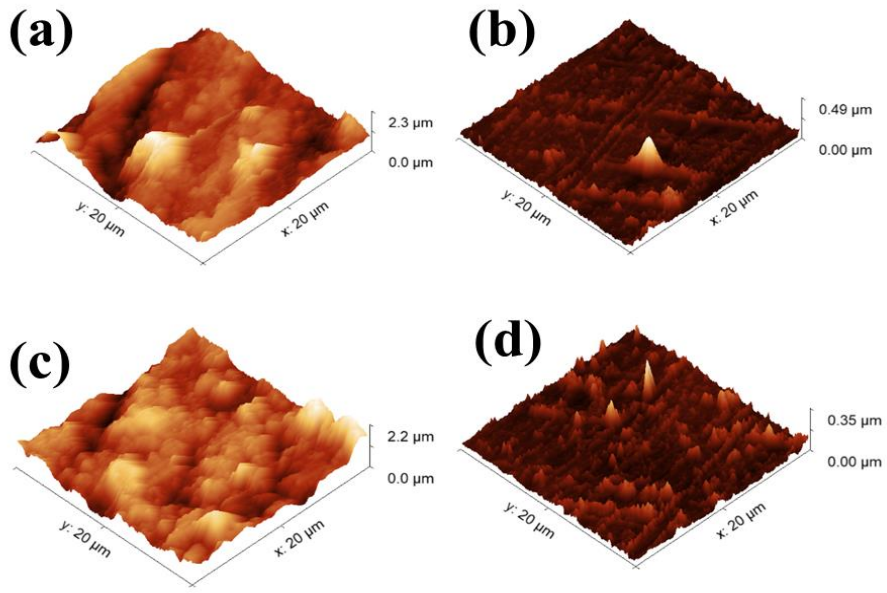

Fig. 5.11 3D AFM images for BQ steel surface after immersing for 3h (a) without, (b) with BBE (200 mgL^{-1}) in 1 M HCl, (c) without BBE, and (d) with BBE (200 mgL^{-1}) in 0.5 M H_2SO_4 at 25° C.

5.6 Theoretical studies by quantum chemical calculations using DFT

Electrochemical analysis revealed corrosion kinetics and basic corrosion inhibition mechanism. The chemical correlation between corrosion protection and inhibitor molecule structures was necessary to comprehend the protection process. Quantum level simulations provided crucial insights into the link between inhibitor molecule structure and inhibition efficiency (Mourya et al., 2014b).

TH-3102_146107038

5.6.1 Quantum chemical parameters

The frontier molecular orbital (FMO) hypothesis is a prominent tool for quantum chemical computations. The FMO hypothesis of reactivity states that the formation of a transition state relies on FMO interactions (HOMO and LUMO). Adsorption and chelation processes use HOMO and LUMO as indicators. Because corrosion inhibition depends on adsorption, HOMO and LUMO measurement is vital for inhibitor efficacy. As a result, the HOMO and LUMO are regarded essential markers in the analysis of any adsorption or chelation process, respectively. A crucial factor in the efficacy of an inhibitor is the measurement of HOMO and LUMO, which is important since corrosion inhibition is based on the concept of adsorption (Mourya et al., 2014a). Because of the abundant electrons in π bonds, benzene rings, and other heteroatoms, HOMO locations are considered electron donors and adsorption sites, while LUMO locations are known as electron acceptors (Ganash, 2018). The capacity of a compound to donate electrons to the d-orbitals of metal is measured by its ionization potential (I), whereas the metal's electron affinity (A) shows the compound's tendency to receive electrons. As a result, these two factors may also serve as a useful signal of a potent inhibitor (Hsissou et al., 2021). All the parameters were determined in the gas phase.

Cyanidin-3-glucoside and peonidin-3-glucoside were detected as significant inhibitory compounds based on LCMS findings, and their optimized structures with FMO are portrayed in Fig 5.12. The electronegativity characteristics and the presence of π electron clouds of the compound are reflected in the colored lobes, which are green and red. The more electronegative areas are depicted by red lobes, while the green lobes represent the less electronegative areas (Nofrizal et al., 2012). The delocalization of electrons from both HOMO-LUMO regions occurs to build an optimum interaction

TH-3102_146107038

involving most of the (Fig. 5.12) (Verma et al., 2018). As a result, substantial atoms of HOMO-LUMO areas make interaction with the BQ steel surface to achieve stable interactions. These interactions are mostly dependent on the ability of different single atoms, phenyl rings, and functional groups either to donate electrons onto the steel surface or from the steel surface (Ganash, 2018). For the C3G and P3G molecules, the energy values of HOMO and LUMO), as well as the related quantum chemical parameters, were determined and already reported in last chapter (Table 4.5).

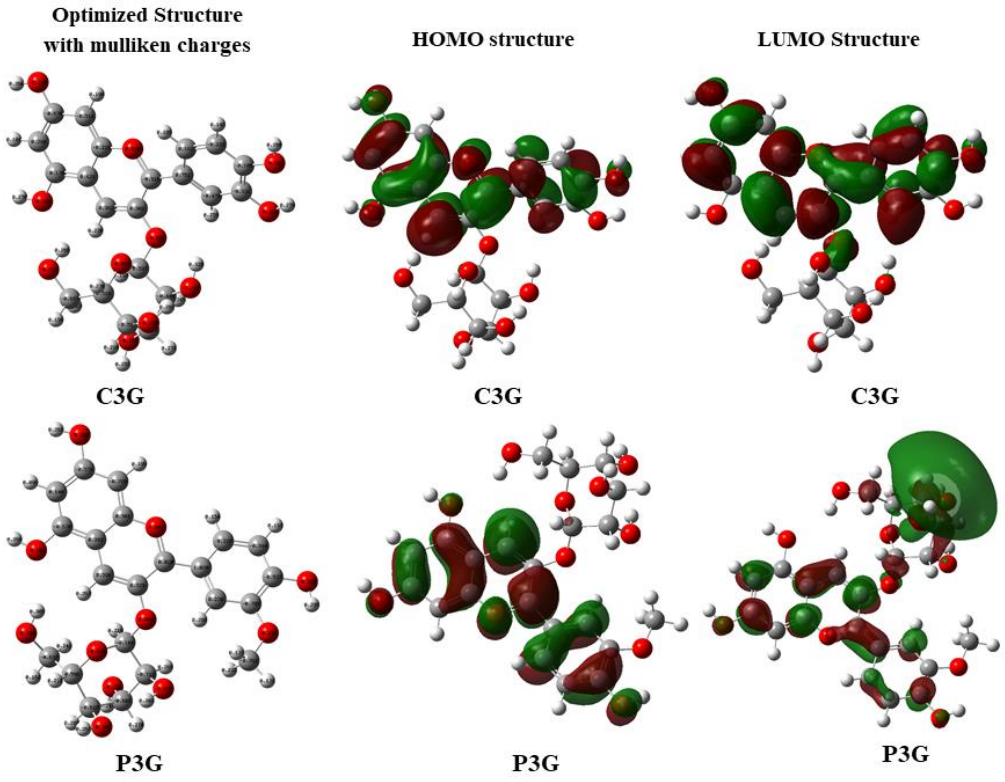

Fig. 5.12 Electron density distribution and Frontier molecular orbitals of detected BBE compounds (C3G and P3G).

In general, it is understood that a higher E_{HOMO} results in a greater inclination for electrons to move to a lower-energy orbital level. Therefore, a higher E_{HOMO} the value indicates a strong interaction between the surface and the molecule, which ultimately results in improved adhesion of the molecule to the surface. Having a lower

TH-3102_146107038

E_{LUMO} value suggests that the molecule is more likely to accept an electron from higher-energy orbitals, resulting in it being an efficient adsorbate on the surface (Liao et al., 2018). The study reveals that both LUMO and HOMO value is higher for P3G than C3G. The energy gap ($\Delta \boldsymbol{E}$) serves as a reactivity and stability indicator in chemical reactions. Because, less energy is needed to transport electrons between orbitals when the molecule interacts with other substances, a low $\Delta \boldsymbol{E}$ value leads the molecule to be more reactive when interacting with other substances. In this study, it was discovered that the $\Delta \boldsymbol{E}$ of P3G is lesser than C3G which helps a to maintain a stable bonding between the surface of BQ and P3G (Verma et al., 2018). Furthermore, its electronegativity (χ), softness (σ), and global hardness (η) were also computed. The C3G molecule has slightly lower hardness (1.567 eV) than C3G (1.605 eV). According to the definition of hardness, it is the resistance of an atom, ion, or molecule to distortion or polarization of its electron cloud when a chemical process is disrupted by a little amount of energy (Hsissou et al., 2021; Verma et al., 2018). Furthermore, for both compounds ΔN (transferable electrons) ≥ 0. So it means they were efficient enough to transfer electrons to the metallic surface. In contrast, P3G (1.471) had a superior electron-donating capacity and inhibition efficiency than C3G (1.376) (Belghiti et al., 2019a).

TH-3102_146107038

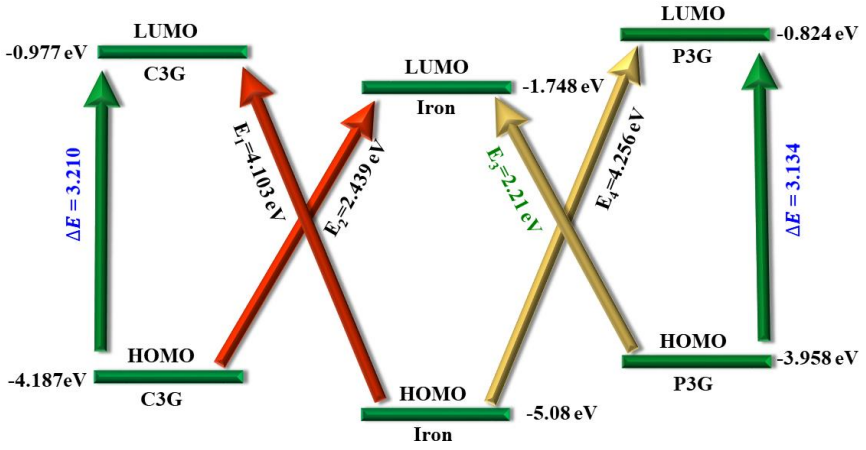

Fig. 5.13 Schematic representation of HOMO and LUMO energy levels of iron, C3G and P3G.

In the last chapter, Fig. 4.13 indicates that the transfer of the electron from HOMO of C3G and P3G to the Fermi level of iron is more favorable than the electron transfer from the Fermi level of iron.to LUMO of molecules as the energy gap between the Fermi level of iron and LUMO of C3G and P3G was higher (2.437 and 2.590 eV) (Bashiri et al., 2017; Singh et al., 2019) . The energy differences between the LUMO of iron and the HOMO of C3G and P3G are also important factors that help to infer the efficiency of the molecules. The presence of methoxy (-OCH_3) group also makes P3G a better inhibitor (Errahmany et al., 2020). From Fig. 5.13, it is exhibited that the E_3 (difference between LUMO of iron and HOMO of P3G), value is lower than E_1, E_2, E_4. This indicate that the electron flows more readily in LUMO of iron from the HOMO of P3G than the HOMO of C3G (Khanra et al., 2018).

The Fukui indices of C3G and P3G Fukui indices were explored to identify local reactivity sites. These indices assist in locating the electrophilic and nucleophilic sites of compounds. In an acidic solution, the BQ surface is either negatively or positively charged due to adsorbed anions on the positively charged surface.

TH-3102_146107038

Table 5.5 Fukui function of atoms cyanidin-3-glucoside and peonidin-3-glucoside.

Detected compound in PRBE	Atom	f_k^+	f_k^-	f_k^2
C3G	C (18)	0.605	-0.131	0.736
	C (5)	0.365	-0.836	1.201
	C(9)	0.308	-0.046	0.354
	H(53)	0.043	0.012	0.031
	C(7)	-0.351	0.748	-1.099
	C(8)	0.056	0.352	-0.297
	C(2)	-0.214	0.343	-0.557
	O(43)	0.004	0.077	-0.074
P3G	C(36)	0.270	0.174	0.097
	C(32)	0.262	0.335	-0.073
	C(8)	0.193	0.073	0.121
	H(47)	0.127	-0.019	0.146
	C(2)	-0.253	0.376	-0.628
	C(32)	0.262	0.335	-0.073
	C(1)	-0.274	0.305	-0.579
	O(44)	-0.005	0.054	-0.059

Sites having large f_k^+ values may stabilize extra electrons, making the molecule more prone to nucleophilic attack. In contrast, when the f_k^- is large, the electrophilic attack occurs (Belghiti et al., 2019b; Ganash, 2018; Liao et al., 2018; Naghi Tehrani et al., 2021; Verma et al., 2018). Few of the atoms with the highest f_k^+ (electrophilic) and f_k^- (nucleophilic) are listed in Table 5.5. The atoms with high f^+ values are electrophilic and the site of nucleophilic attack (back donation from the metal surface to the molecule). Whereas the atoms with high f_k^- values are electron donator or nucleophilic where the electrophilic attack occurs. Table 5.5 also displays the values of a f_k^2 which shows the atoms with $f_k^2 > 0$ are electrophilic, and the atoms with $f_k^2 < 0$ are nucleophilic (Belghiti et al., 2019a; Hsissou et al., 2021; Liao et al., 2018).

TH-3102_146107038

5.7 Mechanism of inhibition

Both media do not exhibit the same anodic shift, as shown by Tafel polarization studies. If the anodic reactions in both mediums are explored, they can be explained. So it is essential to understand the distinctions between anodic reactions in H_2SO_4 and HCl environments.

5.7.1 Anodic reaction

The electro-dissolution of iron in acidic sulfate solution is mainly influenced by the adsorption intermediated $FeOH_{ads}$, which are formed throughout the dissolving process. In HCl media, iron dissolution differs from the dissolution of iron in the H_2SO_4 medium and follows a distinct route. The $(FeCl)_{ads}$ are responsible for anodic dissolution in HCl, whereas the $(FeOH)_{ads}$ are responsible for anodic dissolution in H_2SO_4. When an inhibitor is incorporated into an acidic media, multiple reaction phases may occur depending on the electrolyte and iron dissolution process. As a result, the variation in the anodic curve of Tafel slopes is due to the different anodic dissolution processes. The inhibitors in HCl solution cause certain extra chemical reactions (Section 47) (Galai et al., 2020; Mourya et al., 2013).

5.7.2 Cathodic reaction

In the cathodic reactions, the proton (H^+) and the protonated inhibitor ($InhH^+$) compete for the same active site on the BQ steel surface in order to get adsorbed on the surface of the steel. The Tafel plots (Fig. 5.4) portray that cathodic curves are approximately parallel, indicating the cathodic activation-controlled nature of the reaction. From the activation-controlled nature of the cathodic reactions in the above equations, the first step is likely to be the rate-controlling step (Mourya et al., 2013).

TH-3102_146107038

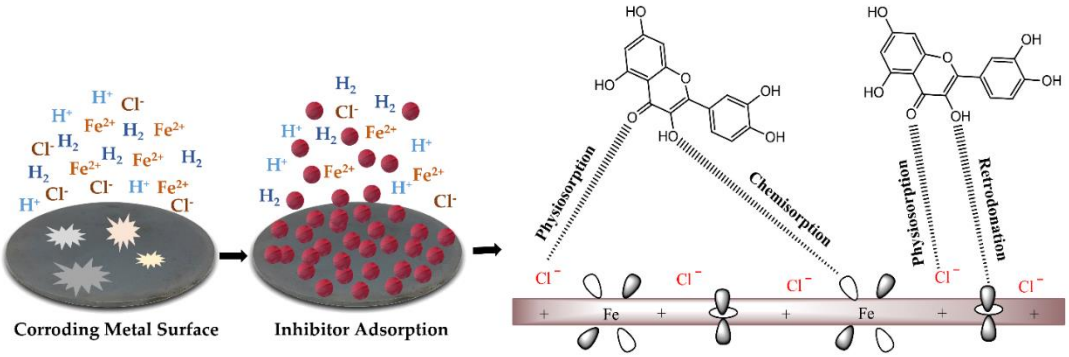

Fig. 5.14 Schematic representation of corrosion inhibition mechanism by inhibitor on steel in acidic medium.

It has already been stated that the anodic reactions release Fe^{2+} and that the cathodic reactions produce H_2 gas throughout the process. When inhibitors are added to acidic environments, they get protonated and adsorb on charged surfaces of BQ steel. Then, the protonated inhibitors engage electrostatically with the Cl^- which has already been adsorbed on the surface, and the interaction between them is referred to as physisorption (Fig. 5.14). At high inhibitor concentrations, the protonated inhibitors may compete with other cationic species to bind on the nucleophilic sites (Al-Moubaraki, 2015). Once they receive electrons from metallic surfaces, the protonated inhibitors revert to their neutral state. Then the lone pair electrons of the heteroatoms in the inhibitory molecules initiate chemical adsorption (Srivastava et al., 2018). As the surface gets completely saturated with electrons, it becomes negatively charged. In order to surplus the excess electrons from the surface, the "d" orbital electrons of iron may get transferred to the empty π (antibonding) orbital of the BBE molecules via the mechanism of retrodonation, which leads to the more strong adsorption of the inhibitor onto the BQ surface (Saxena et al., 2018c, 2018b; Srivastava et al., 2018). Even while the results of adsorption experiments show a strong likelihood of electrostatic connection, the possibility of chemical interaction cannot be discounted. Tiny pits

TH-3102_146107038

appear on the surface of the metal as a result of the Cl^- ions' induction of iron oxidation when they are in close proximity to the iron surface. However, these Cl- ions also serve in drawing the protonated molecules to the surface, where they eventually form a protective coating which was proved by electrochemical studies after one hour of incubation period.

5.8 Summary

It is possible to infer from the current experimental and computational studies that the extract of banana bract, agro-waste, is a viable natural corrosion inhibitor that is both environmentally benign and effective. Experimental studies of corrosion in 1 (M) HCl and 0.5 (M) H_2SO_4 on the BQ steel, as well as theoretical research on the compounds of BBE, were carried out to determine the efficacy of BBE as green corrosion inhibitors. The following findings have been drawn after the completion of all experiments:

1. P3G and C3G were identified as the most abundant compound in BBE by LCMS analysis.
2. The studies of Tafel polarization revealed that the BBE acts as a mixed-type inhibitor on the BQ steel surface. It also disclosed that the corrosion current (i_{corr}) were 179.06 µA cm^{-2} and 180.25 µA cm^{-2} in 1 (M) HCl and 0.5 (M), respectively, in the absence of BBE. The minimum corrosion current (i_{corr}) was found as 19.90 µA cm^{-2} and 23.01 µA cm^{-2} at 200 mg L^{-1} of BBE in 1 (M) HCl and 0.5 (M) H_2SO_4. The polarization resistance (R_P) was also changed from 101.17 to 679.63 Ω cm^2 and from 104.62 to 649.92 Ω cm^{-2} in HCl and H_2SO_4 medium on the addition of BBE.

TH-3102_146107038

3. The protectiveness of BBE was further proved by EIS measurements, as the presence of BBE has reduced the charge-transfer resistance. The charge-transfer resistance (R_{ct}) was found as 89.72 Ωcm^2 and 85.08 Ω cm^2 in 1 (M) HCl and 0.5 (M) H_2SO_4 media without incorporating BBE. Whereas in the presence of BBE (200 mg L^{-1}) R_{ct} was increased in both HCl (979.56Ωcm^2) and H_2SO_4 media (905.64 Ωcm^2). The inhibition efficiency calculated from R_{ct} was found to be a maximum 90.84% and 90.61% after incorporating 200 mg L^{-1}.
4. The corrosion inhibition was caused by adsorption phenomena. The value of K_{ads} (30.74 L g^{-1} in HCl and 28.28 L g^{-1} in H_2SO_4) and $\Delta G°_{ads}$ (-25.62 kJ mol^{-1} in HCl and -25.41 kJ mol^{-1} in H_2SO_4) has also supported thermodynamic favorability of the adsorption. The adsorption of BBE components on the surface of BQ steel followed the Langmuir isotherm. The values of $\Delta G°_{ads}$ indicated the mixed-type adsorption behavior of BBE.
5. The results of the FESEM, EDX, and AFM investigations also revealed the formation of a protective layer of BBE components on BQ steel.
6. In comparison to C3G, P3G exhibited a stronger inhibitory effect because of its lower energy gap.

5.9 References

Al-Moubaraki, A.H., 2015. Corrosion Protection of Mild Steel in Acid Solutions Using Red Cabbage Dye. Chem. Eng. Commun. 202, 1069–1080. https://doi.org/10.1080/00986445.2014.907565

Alaoui, K., El Kacimi, Y., Galai, M., Touir, R., Dahmani, K., Harfi, A., Ebn Touhami, M., 2016. Anti-corrosive properties of polyvinyl-alcohol for carbon steel in hydrochloric acid media: Electrochemical and thermodynamic investigation. J. Mater. Environ. Sci. 7, 2389–2403.

Alexandra Pazmio-Durán, E., Giusti, M.M., Wrolstad, R.E., Glória, M.B.A., 2001.

TH-3102_146107038

Anthocyanins from banana bracts (Musa X paradisiaca) as potential food colorants. Food Chem. 73, 327–332. https://doi.org/10.1016/S0308-8146(00)00305-8

Azmi, M.F., Soedarsono, J.W., 2018. Study of corrosion resistrance of pipeline API 5L X42 using green inhibitor bawang dayak (Eleutherine americanna Merr.) in 1M HCl. IOP Conf. Ser. Earth Environ. Sci. 105. https://doi.org/10.1088/1755-1315/105/1/012061

Begum, Y.A., Deka, S.C., 2017. Stability of spray-dried microencapsulated anthocyanins extracted from culinary banana bract. Int. J. Food Prop. 20, 3135–3148. https://doi.org/10.1080/10942912.2016.1277739

Belghiti, M.E., Echihi, S., Dafali, A., Karzazi, Y., Bakasse, M., Elalaoui-Elabdallaoui, H., Olasunkanmi, L.O., Ebenso, E.E., Tabyaoui, M., 2019a. Computational simulation and statistical analysis on the relationship between corrosion inhibition efficiency and molecular structure of some hydrazine derivatives in phosphoric acid on mild steel surface. Appl. Surf. Sci. 491, 707–722. https://doi.org/10.1016/j.apsusc.2019.04.125

Belghiti, M.E., Echihi, S., Dafali, A., Karzazi, Y., Bakasse, M., Elalaoui-Elabdallaoui, H., Olasunkanmi, L.O., Ebenso, E.E., Tabyaoui, M., 2019b. Computational simulation and statistical analysis on the relationship between corrosion inhibition efficiency and molecular structure of some hydrazine derivatives in phosphoric acid on mild steel surface. Appl. Surf. Sci. https://doi.org/10.1016/j.apsusc.2019.04.125

Errahmany, N., Rbaa, M., Abousalem, A.S., Tazouti, A., Galai, M., Kafssaoui, E.H. El, Touhami, M.E., Lakhrissi, B., Touir, R., 2020. Experimental, DFT calculations and MC simulations concept of novel quinazolinone derivatives as corrosion inhibitor for mild steel in 1.0 M HCl medium. J. Mol. Liq. 312, 113413. https://doi.org/10.1016/j.molliq.2020.113413

Galai, M., Rbaa, M., Ouakki, M., Abousalem, A.S., Ech-chihbi, E., Dahmani, K., Dkhireche, N., Lakhrissi, B., EbnTouhami, M., 2020. Chemically functionalized of 8-hydroxyquinoline derivatives as efficient corrosion inhibition for steel in 1.0 M HCl solution: Experimental and theoretical studies. Surfaces and Interfaces 21, 100695. https://doi.org/10.1016/j.surfin.2020.100695

Ganash, A.A., 2018. Theoretical and experimental studies of dried marjoram leaves

TH-3102_146107038

extract as green inhibitor for corrosion protection of steel substrate in acidic solution. Chem. Eng. Commun. 205, 350–362. https://doi.org/10.1080/00986445.2017.1391096

Haruna, K., Saleh, T.A., 2021. N,N′-Bis-(2-aminoethyl)piperazine functionalized graphene oxide (NAEP-GO) as an effective green corrosion inhibitor for simulated acidizing environment. J. Environ. Chem. Eng. https://doi.org/10.1016/j.jece.2020.104967

Hsissou, R., Abbout, S., Safi, Z., Benhiba, F., Wazzan, N., Guo, L., Nouneh, K., Briche, S., Erramli, H., Ebn Touhami, M., Assouag, M., Elharfi, A., 2021. Synthesis and anticorrosive properties of epoxy polymer for CS in [1 M] HCl solution: Electrochemical, AFM, DFT and MD simulations. Constr. Build. Mater. 270, 121454. https://doi.org/10.1016/j.conbuildmat.2020.121454

Ji, G., Anjum, S., Sundaram, S., Prakash, R., 2015. Musa paradisica peel extract as green corrosion inhibitor for mild steel in HCl solution. Corros. Sci. 90, 107–117. https://doi.org/10.1016/j.corsci.2014.10.002

Kadiri, L., Galai, M., Ouakki, M., Essaadaoui, Y., Ouass, A., Cherkaoui, M., Rifi, E.-H., Lebkiri, A., 2018. Coriandrum Sativum.L Seeds Extract as a Novel Green Corrosion Inhibitor for Mild Steel in 1.0 M Hydrochloric and 0.5 M Sulfuric Solutions. Anal. Bioanal. Electrochem. 10, 249–268.

Khanra, A., Srivastava, M., Rai, M.P., Prakash, R., 2018. Application of Unsaturated Fatty Acid Molecules Derived from Microalgae toward Mild Steel Corrosion Inhibition in HCl Solution: A Novel Approach for Metal-Inhibitor Association. ACS Omega 3, 12369–12382. https://doi.org/10.1021/acsomega.8b01089

Liao, L.L., Mo, S., Luo, H.Q., Li, N.B., 2018. Corrosion protection for mild steel by extract from the waste of lychee fruit in HCl solution: Experimental and theoretical studies. J. Colloid Interface Sci. 520, 41–49. https://doi.org/10.1016/j.jcis.2018.02.071

M'hiri, N., Veys-Renaux, D., Rocca, E., Ioannou, I., Boudhrioua, N.M., Ghoul, M., 2016. Corrosion inhibition of carbon steel in acidic medium by orange peel extract and its main antioxidant compounds. Corros. Sci. 102, 55–62. https://doi.org/10.1016/j.corsci.2015.09.017

Mathew, N.S., Negi, P.S., 2021. Phenolic content and anti-oxidative attributes of various parts of wild banana (Ensete superbum Roxb. Cheesman) plant. J. Food

TH-3102_146107038

Biochem. 45, 1–13. https://doi.org/10.1111/jfbc.13657

Mourya, P., Banerjee, S., Rastogi, R.B., Singh, M.M., 2013. Inhibition of mild steel corrosion in hydrochloric and sulfuric acid media using a thiosemicarbazone derivative. Ind. Eng. Chem. Res. 52, 12733–12747. https://doi.org/10.1021/ie4012497

Mourya, P., Banerjee, S., Singh, M.M., 2014a. Corrosion inhibition of mild steel in acidic solution by Tagetes erecta (Marigold flower) extract as a green inhibitor. Corros. Sci. 85, 352–363. https://doi.org/10.1016/j.corsci.2014.04.036

Mourya, P., Banerjee, S., Singh, M.M., 2014b. Corrosion inhibition of mild steel in acidic solution by Tagetes erecta (Marigold flower) extract as a green inhibitor. Corros. Sci. 85, 352–363. https://doi.org/10.1016/j.corsci.2014.04.036

Naghi Tehrani, M.E.H., Ghahremani, P., Ramezanzadeh, M., Bahlakeh, G., Ramezanzadeh, B., 2021. Theoretical and experimental assessment of a green corrosion inhibitor extracted from Malva sylvestris. J. Environ. Chem. Eng. 9, 105256. https://doi.org/10.1016/j.jece.2021.105256

Nofrizal, S., Rahim, A.A., Saad, B., Bothi Raja, P., Shah, A.M., Yahya, S., 2012. Elucidation of the corrosion inhibition of mild steel in 1.0 M HCl by catechin monomers from commercial green tea extracts. Metall. Mater. Trans. A Phys. Metall. Mater. Sci. 43, 1382–1393. https://doi.org/10.1007/s11661-011-1030-3

Okafor, P.C., Ebenso, E.E., Ekpe, U.J., 2010. Azadirachta Indica Extracts as Corrosion Inhibitor for Mild Steel in Acid Medium. Int. J. Electrochem. Sci 5, 978–993.

Ouakki, M., Galai, M., Rbaa, M., Abousalem, A.S., Lakhrissi, B., Rifi, E.H., Cherkaoui, M., 2020. Investigation of imidazole derivatives as corrosion inhibitors for mild steel in sulfuric acidic environment: experimental and theoretical studies. Ionics (Kiel). 26, 5251–5272. https://doi.org/10.1007/s11581-020-03643-0

Oubaaqa, M., Ouakki, M., Rbaa, M., Benhiba, F., Galai, M., Idouhli, R., Maatallah, M., Jarid, A., Warad, I., Lakhrissi, B., Zarrouk, A., Ebn Touhami, M., 2022. Experimental and theoretical investigation of corrosion inhibition effect of two 8-hydroxyquinoline carbonitrile derivatives on mild steel in 1 M HCl solution. J. Phys. Chem. Solids 169, 110866. https://doi.org/10.1016/j.jpcs.2022.110866

Ove, T.A., Kamal, M.M., Nasim, S.M.N.I., Momin, M.M.I., Mondal, S.C., 2019. Extraction and Quantification of Anthocyanin from Banana Bracts Using Different pH and Solvent Concentration. Int. J. 4, 60–64.

TH-3102_146107038

Prabakaran, M., Kim, S.H., Hemapriya, V., Chung, I.M., 2016. Evaluation of polyphenol composition and anti-corrosion properties of Cryptostegia grandiflora plant extract on mild steel in acidic medium. J. Ind. Eng. Chem. 37, 47–56. https://doi.org/10.1016/j.jiec.2016.03.006

Qiang, Y., Li, H., Lan, X., 2020. Self-assembling anchored film basing on two tetrazole derivatives for application to protect copper in sulfuric acid environment. J. Mater. Sci. Technol. 52, 63–71. https://doi.org/10.1016/j.jmst.2020.04.005

Salinas-Solano, G., Porcayo-Calderon, J., Martinez de la Escalera, L.M., Canto, J., Casales-Diaz, M., Sotelo-Mazon, O., Henao, J., Martinez-Gomez, L., 2018. Development and evaluation of a green corrosion inhibitor based on rice bran oil obtained from agro-industrial waste. Ind. Crops Prod. 119, 111–124. https://doi.org/10.1016/j.indcrop.2018.04.009

Saxena, A., Prasad, D., Haldhar, R., 2018a. Use of Asparagus racemosus extract as green corrosion inhibitor for mild steel in 0.5 M H2SO4. J. Mater. Sci. 53, 8523–8535. https://doi.org/10.1007/s10853-018-2123-9

Saxena, A., Prasad, D., Haldhar, R., 2018b. Investigation of corrosion inhibition effect and adsorption activities of Cuscuta reflexa extract for mild steel in 0.5 M H2SO4. Bioelectrochemistry 124, 156–164. https://doi.org/10.1016/j.bioelechem.2018.07.006

Saxena, A., Prasad, D., Haldhar, R., Singh, G., Kumar, A., 2018c. Use of Saraca ashoka extract as green corrosion inhibitor for mild steel in 0.5 M H2SO4. J. Mol. Liq. 258, 89–97. https://doi.org/10.1016/j.molliq.2018.02.104

Shabani-Nooshabadi, M., Ghandchi, M.S., 2015. Santolina chamaecyparissus extract as a natural source inhibitor for 304 stainless steel corrosion in 3.5% NaCl. J. Ind. Eng. Chem. 31, 231–237. https://doi.org/10.1016/j.jiec.2015.06.028

Shahmoradi, A.R., Ranjbarghanei, M., Javidparvar, A.A., Guo, L., Berdimurodov, E., Ramezanzadeh, B., 2021. Theoretical and surface/electrochemical investigations of walnut fruit green husk extract as effective inhibitor for mild-steel corrosion in 1M HCl electrolyte. J. Mol. Liq. 338, 116550. https://doi.org/10.1016/j.molliq.2021.116550

Singh, P., Quraishi, M.A., 2016. Corrosion inhibition of mild steel using Novel Bis Schiff's Bases as corrosion inhibitor: Electrochemical and Surface measurement. Meas. J. Int. Meas. Confed. 86, 114–124.

TH-3102_146107038

https://doi.org/10.1016/j.measurement.2016.02.052

Srivastava, V., Chauhan, D.S., Joshi, P.G., Maruthapandian, V., Sorour, A.A., Quraishi, M.A., 2018. PEG-Functionalized Chitosan: A Biological Macromolecule as a Novel Corrosion Inhibitor. ChemistrySelect 3, 1990–1998. https://doi.org/10.1002/slct.201701949

Thomas, A., Prajila, M., Shainy, K.M., Joseph, A., 2020. A green approach to corrosion inhibition of mild steel in hydrochloric acid using fruit rind extract of Garcinia indica (Binda). J. Mol. Liq. 312, 113369. https://doi.org/10.1016/j.molliq.2020.113369

Verma, C., Olasunkanmi, L.O., Ebenso, E.E., Quraishi, M.A., 2018. Adsorption characteristics of green 5-arylaminomethylene pyrimidine-2,4,6-triones on mild steel surface in acidic medium: Experimental and computational approach. Results Phys. 8, 657–670. https://doi.org/10.1016/j.rinp.2018.01.008

Wang, Cai, Chen, J., Hu, B., Liu, Z., Wang, Chongbin, Han, J., Su, M., Li, Y., Li, C., 2019. Modified chitosan-oligosaccharide and sodium silicate as efficient sustainable inhibitor for carbon steel against chloride-induced corrosion. J. Clean. Prod. 238, 117823. https://doi.org/10.1016/j.jclepro.2019.117823

Zheng, X., Zhang, S., Li, W., Yin, L., He, J., Wu, J., 2014. Investigation of 1-butyl-3-methyl-1H-benzimidazolium iodide as inhibitor for mild steel in sulfuric acid solution. Corros. Sci. https://doi.org/10.1016/j.corsci.2013.11.053

TH-3102_146107038

TH-3102_146107038

6

Corrosion inhibition by extract of onion peel (kitchen waste)

TH-3102_146107038

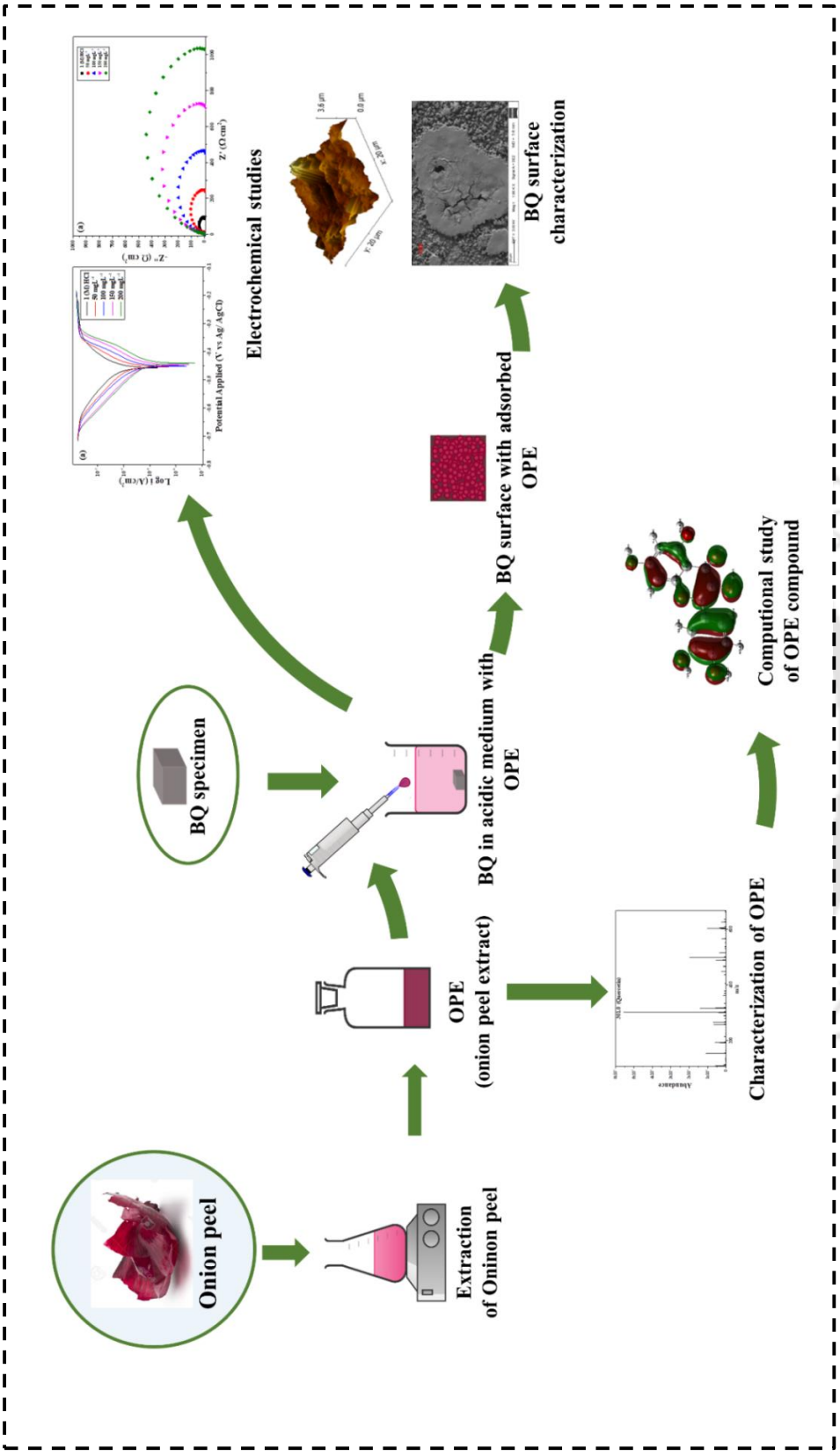

Corrosion inhibition by extract of onion peel (kitchen waste)

TH-3102_146107038

Corrosion inhibition by extract of onion peel (kitchen waste)

In this chapter the findings obtained from corrosion inhibition of boiler quality (BQ) steel by onion waste were discussed. The extract from onion peel was characterized using the conventional extraction method and was characterized using LC-MS. The efficacy of the onion peel extract (OPE) as a green corrosion inhibitor was studied using the weight loss method and a variety of electrochemical techniques, including open circuit potential (OCP), potentiodynamic polarization (PDP), electrochemical impedance spectroscopy (EIS). The Tafel polarization revealed that at 200 mg L^{-1} of onion peel extract (OPE), corrosion current density was reduced maximum in both 1 (M) HCl and 0.5 (M) H_2SO_4 media. From the electrochemical impedance spectroscopy studies, the maximum inhibition efficiencies of 91.30% and 90.71 % were found at 200 mg L^{-1} in 1 (M) HCl and 0.5 (M) H_2SO_4, respectively. The Langmuir isotherm was determined to be the best-fitting model, and the thermodynamic parameter, such as free energy ΔG°_{ads} was computed, which indicated the physisorption of OPE onto the BQ surface. In theoretical investigations, density functional theory DFT was used to determine the adsorption efficiency and reactive sites.

Published Artcle: Pal, A., Das, C., 2022. Novel use of kitchen waste: protection of boiler quality steel from corrosion in acidic media using onion waste. **Chem. Papers**, https://doi.org/10.1007/s11696-022-02549-7

TH-3102_146107038

6.1 Characterization of the compound in OPE

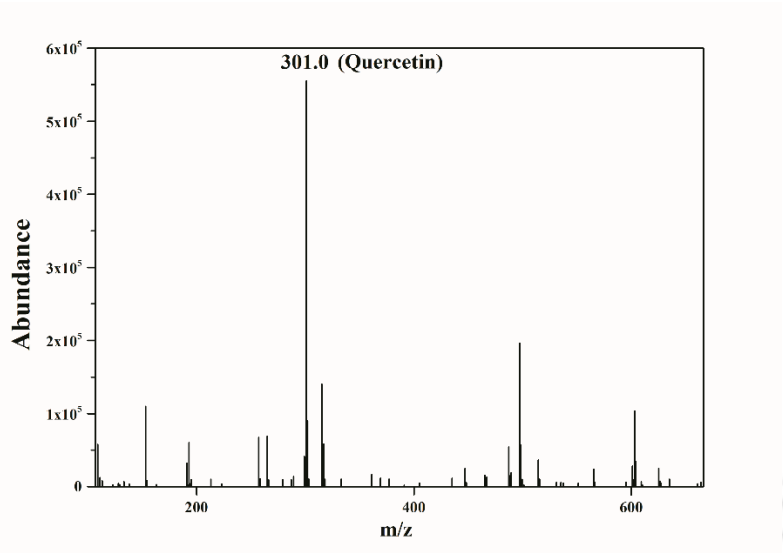

Fig. 6.1 Mass spectra of OPE.

The LC-MS is a potential and widely accepted tool for qualitative and quantitative analysis of the polyphenols in biomass. The qualitative profile of OPE was analyzed by LC-MS, and the chromatogram of the extract is displayed in Fig. 6.1. The mass spectrum of the extract was obtained in negative ionization mode. From the spectrum, it was noticed that maximum intensity was observed for the m/z value of 301.0. From the literature, it was found that in negative ionization mode, the m/z value of 301.0 indicates the presence of quercetin (Celano et al., 2021; Chen et al., 2015). Some early works have also supported the abundance of quercetin in onion peel (Bedrníček et al., 2020; Celano et al., 2021; Singh et al., 2009). The presence of quercetin makes the OPE an efficient inhibitor because of its antioxidant property and ability to make a complex with iron (Bedrníček et al., 2020; Xu et al., 2019).

6.2 Gravimetric analysis

The gravimetric method is an easy and commonly used method for evaluating the inhibitory capability of various compounds. This approach was employed to assess the inhibitory efficiency of OPE, and the results revealed that when specimens were

TH-3102_146107038

immersed in acid solutions, they lost a significant amount of weight. However, the presence of OPE slowed the dissolving of BQ steel in acidic conditions. In both media, the corrosion rate (CR) and inhibition efficiency ($\mu_{CR}\%$) of OPE were determined using Eq. 2.1 and 2.2. To observe the effect of OPE concentration, various OPE concentrations (50 mg L^{-1} to 200 mg L^{-1}) were incorporated in both HCl and H_2SO_4 media. Table 6.1 and Fig. 6.2 clearly indicate that OPE was an effective corrosion inhibitor for BQ steel as the CR decreased and the $\mu_{CR}\%$ increased with increased OPE concentration.

Table 6.1 Variations in corrosion rate and inhibition efficiency of BQ steel at different concentrations of OPE in (a) 1 (M) HCl and (b) 0.5 M H_2SO_4.

	Conc. (mg L^{-1})	$CR \times 10^2$ (mm $year^{-1}$)	μ_{CR} (%)
HCl media	**0 (Blank) 1(M)HCl**	210.13 ± 9.55	0.00 ± 0.00
	50	69.26± 2.91	67.04 ± 1.09
	100	43.24 ± 0.56	79.42 ± 0.38
	150	28.15 ± 0.23	86.61 ± 0.20
	200	21.94 ± 0.31	89.56 ± 0.48
H_2SO_4 media	**0 (Blank) 0.5 (M) H_2SO_4**	213.51 ± 8.12	0.00 ± 0.00
	50	78.33 ± 3.31	63.31 ± 1.18
	100	50.23 ± 1.45	76.48 ± 1.16
	150	37.25 ± 0.89	82.55 ± 1.03
	200	22.31 ± 0.25	89.55 ± 0.60

TH-3102_146107038

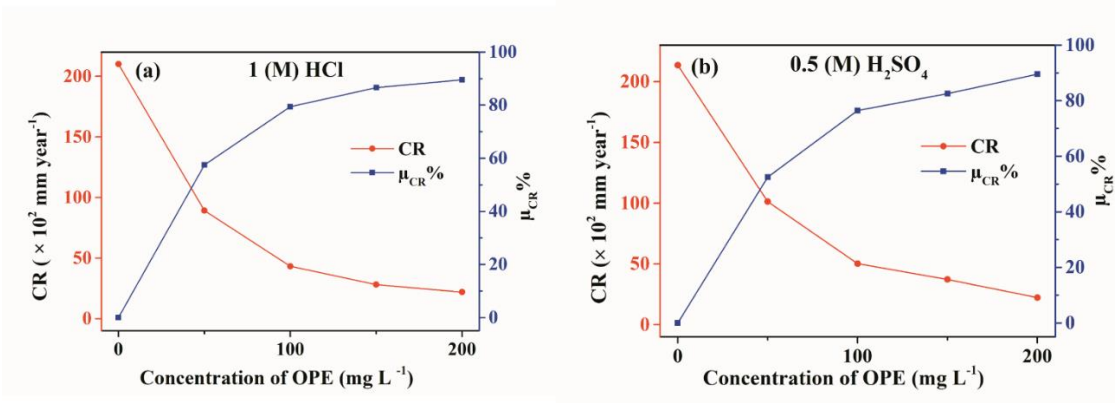

Fig. 6.2 Variations in corrosion rate and inhibition efficiency of BQ steel at different concentrations of OPE in (a) 1 (M) HCl and (b) 0.5 M H_2SO_4.

It is apparent from Fig. 6.2 (a) and (b) that even at the lowest concentrations of OPE, there is considerable efficiency. This increase in OPE inhibition efficiency is due to the redox reaction rate being depleted during corrosion. During the corrosion process, two types of reactions occur that have a substantial impact on the intensity of the corrosion process. These are the anodic reaction, in which iron is oxidized into Fe^{2+} (Eq. 6.1), and the cathodic reaction, which results in hydrogen being reduced into H_2 gas (Eq. 6.2) (Ali Asaad et al., 2018; Mourya et al., 2014). The use of OPE reduces the anodic reaction and cathodic reduction reaction rates, which ultimately result in the reduction of iron oxidation. Table 6.1 shows that the efficiency is roughly comparable in both acidic situations at the highest dosages. In contrast, at 50 mg L^{-1} (lowest), the efficiency of OPE in HCl is slightly higher than in H_2SO_4. As SO_4^{2-} was lesser adsorbable than Cl^-, the surface in SO_4^{2-} media was negatively charged. Adsorption of the protonated organic molecules was more suited for a higher negatively charged surface than a lower negatively charged surface. So at the lower concentration, Cl^- ions made a difference from the SO_4^{2-} as they attracted the protonated inhibitory molecules more aggressively than SO_4^{2-}. The interaction between the anions and the inhibitory

TH-3102_146107038

molecules might be physical or chemical or mixed, which is discussed in the following sections.

Oxidation: $Fe \rightarrow Fe^{2+} + 2e^-$ **6.1**

Reduction: $2H^+ + 2e^- \rightarrow 2(H)_{ads} + H_2$ **6.2**

6.3 Electrochemical measurements

Different electrochemical investigations were required to analyze the corrosion rate and other electrochemical kinetics of BQ steel in a specific electrolytic condition to evaluate the inhibition efficiency. In particular, these investigations are concerned with the manifestation of the inhibition efficiency, corrosion current density, i_{corr}, charge transfer resistance R_{ct}, and many other electrochemical parameters.

6.3.1 OCP measurements

The open-circuit potential (OCP) (E_{oc}) is the developed potential between the electrolyte and the working electrode when no external current is applied. As no external current is applied, OCP is sometimes referred to as zero-current potential. The term OCP is also interchangeable with corrosion potential. OCP is an important parameter in electrochemical operations since it indicates the stability of the system, which is significant for any perturbation-based experiments. The system under investigation should attain a steady state by allowing OCP to be stabilized before proceeding with any subsequent electrochemical studies. Once the OCP has achieved stability, it is assumed that the steady state has been reached, and the perturbation-based experiments can be performed. The time required for establishing a stable OCP might range from a few minutes to several hours, depending on the reaction. For the purpose of experimentation, an automated system records the OCP values over a period of time until the average OCP becomes stable. Once the stability of the system is confirmed,

TH-3102_146107038

then the system is ready for any perturbation-based experiment (Shabani-Nooshabadi and Ghandchi, 2015).

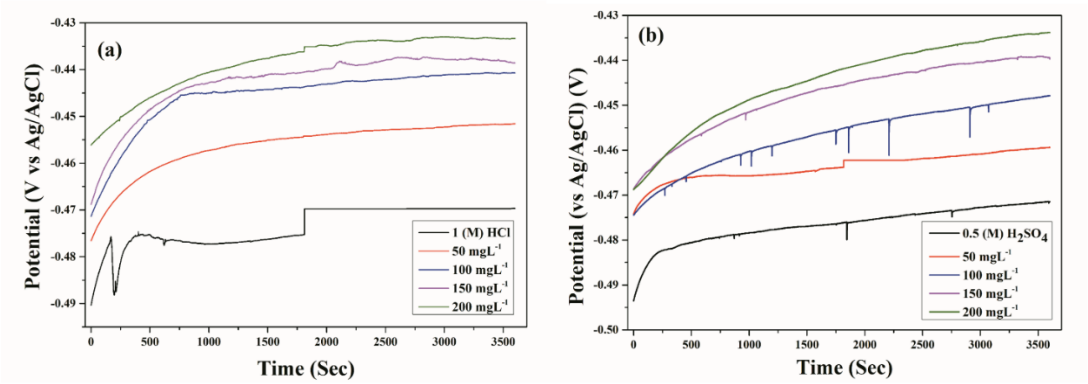

Fig. 6.3 OCP curves for BQ steel without and with different concentrations of OPE in (a) HCl and (b) H_2SO_4.

To achieve stability in the system, the average OCP values were obtained by recording the OCP values for 60 min. Different OPE concentrations were applied in both acidic media and were compared with the control solution. The variations in OCP with regard to time are shown in Fig. 6.3 (a) and (b). It is apparent from the figures that, when inhibitors are present, the OCP tends towards positive values as compared to when inhibitors are absent. More importantly, when the concentrations increase from 50 mgL^{-1} to 200 mgL^{-1}, the plots begin to shift in a more positive direction. The changes of OCP in the positive direction are considered an improvement in the OCP due to the establishment of a stable, protective layer on BQ (Naghi Tehrani et al., 2021; Salinas-Solano et al., 2018; Singh and Quraishi, 2016). The formation of the protective layer was accomplished in two-step processes. At first physical adsorption occurs, and then chemical transformation (polymerization) leads the molecule to adsorb on the surface (Vorobyova and Skiba, 2021).

TH-3102_146107038

6.3.2 Potentiodynamic Polarization tests

Understanding the electrochemical kinetics of surface corrosion necessitates a potentiodynamic polarization or Tafel polarization study. Tafel graphs for OPE in HCl and H_2SO_4 media are shown in Fig. 6.4 (a) and (b), respectively, to illustrate the effects of polarization. The various corrosion parameters, including the density of corrosion current (i_{corr}), corrosion potential (E_{corr}), cathodic (b_c) and anodic (b_a) slopes were obtained using the extrapolation method and are shown in Table 6.2 along with inhibition efficiency (IE).

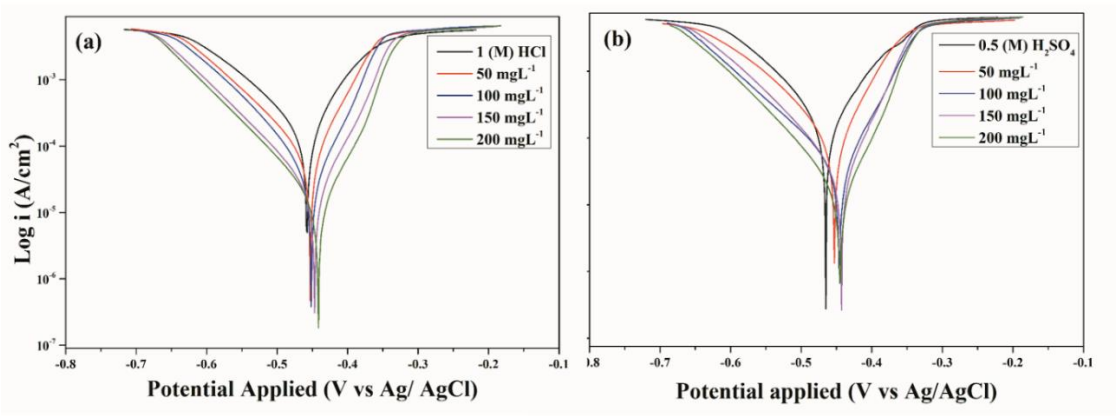

Fig. 6.4 Tafel polarization curves for BQ steel without and with different concentrations of OPE in (a) HCl and (b) H_2SO_4 media.

The potentiodynamic studies show that the OPE reduces the anodic and cathodic currents, indicating a decrease in the corrosion rate. In the absence of OPE, both anodic and cathodic currents increase. This is owing to increased anodic metal dissolution and cathodic hydrogen evolution in both acidic media. It is also noticed that in the presence of OPE, the Tafel curves shift toward positive on anodic sides in both the acidic media. Although the curves shift towards the anodic site, it is not an anodic inhibitor as the shift is less than 85 mV. So, it is considered a mixed-type inhibitor.

TH-3102_146107038

Also, i_{corr} and the Tafel constants b_c and b_a were affected by the addition of inhibitors. So it is clearly seen that OPE acts as a mixed-type of inhibitor (Verma et al., 2018).

Table 6.2 Electrochemical parameters obtained from Tafel polarization at different concentration OPE in HCl and H_2SO_4.

	Conc. (mg L^{-1})	b_a ($mVdec^{-1}$)	$-b_c$ ($mVdec^{-1}$)	E_{corr} (mV vs AgCl)	i_{corr} (μAcm^{-2})	R_P (Ωcm^{-2})	(μ_P%)
HCl media	**0 (Blank) 1 (M) HCl**	110.98 ± 2.05	66.84 ± 0.80	-457.12 ± -3.32	179.06 ± 7.08	101.17 ± 0.49	0.00 ± 0.00
	50	86.54 ± 0.92	58.22 ± 0.21	-454.90 ± -3.69	53.73 ± 0.31	281.33 ± 1.77	69.99 ± 0.24
	100	73.30 ± 0.98	58.59 ± 0.41	-451.70 ± -7.62	35.17 ± 0.07	402.07 ± 4.34	80.36 ± 0.30
	150	92.63 ± 0.89	60.18 ± 0.32	-445.26 ± -6.22	23.21 ± 0.06	682.69 ± 9.56	87.04 ± 0.12
	200	93.55 ± 1.21	65.25 ± 0.49	-440.81 ± -1.48	16.80 ± 0.04	993.68 ± 31.20	90.62 ± 0.08
H_2SO_4 media	**0 (Blank) 0.5 (M) H_2SO_4**	93.13 ± 2.26	81.36 ± 1.40	-464.44 ± -3.17	180.25 ± 7.01	104.62 ± 1.25	0.00 ± 0.00
	50	80.89 ± 2.51	57.27 ± 0.77	-448.61 ± -1.89	61.73 ± 1.40	235.91 ± 3.94	65.75 ± 0.62
	100	99.31 ± 3.03	61.06 ± 0.42	-444.90 ± -9.25	39.01 ± 0.33	420.96 ± 6.15	78.36 ± 0.67
	150	80.47 ± 1.04	54.22 ± 0.83	-441.78 ± -8.14	29.11 ± 0.22	483.23 ± 10.39	83.85 ± 0.62
	200	84.56 ± 5.60	60.21 ± 1.18	-444.30 ± -1.86	17.48 ± 0.16	873.81 ± 12.97	90.30 ± 0.56

It can be seen in Table 6.2 that the b_a is consistently greater than the b_c in every trial, indicating that the inhibitors are more effective at reducing anodic current than the cathodic current. A further demonstration of the impact of OPE on the decrease of corrosion reactions is provided by i_{corr} measurement. In the presence of OPE in both

TH-3102_146107038

HCl and H_2SO_4 environments, the values of i_{corr} was reduced significantly, and the reduction was even more in the presence of higher concentrations of OPE. The low i_{corr} values at high concentrations of OPE suggest that the corrosion rate was decreased, which is consistent with the fact that the corrosion rate is directly related to i_{corr}. Furthermore, it was also found that the R_P values decreased with increasing OPE concentrations. In both acidic media, the decreasing i_{corr} and increasing R_P suggest that the OPE protected the BQ surface from corrosion by establishing a strong barrier that prevents the active reaction site of corrosion from being formed. Additionally, the values of inhibitory efficiency ($\mu_P\%$) indicates that a high concentration of OPE inhibitor significantly increased the $\mu_P\%$ (Okafor et al., 2010; Prabakaran et al., 2016).

6.3.3 EIS measurements

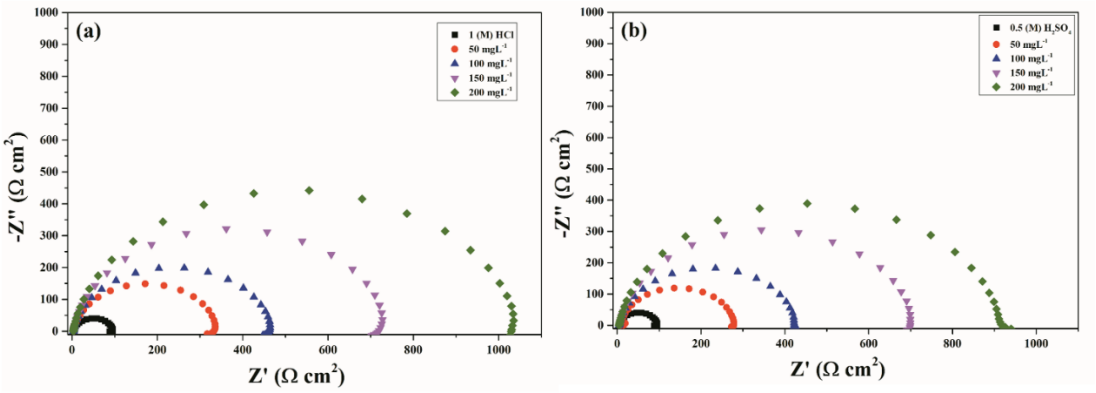

Fig. 6.5 Nyquist plots of BQ corrosion in acidic media without and with different concentration of OPE: (a) HCl and (b) H_2SO_4 media.

TH-3102_146107038

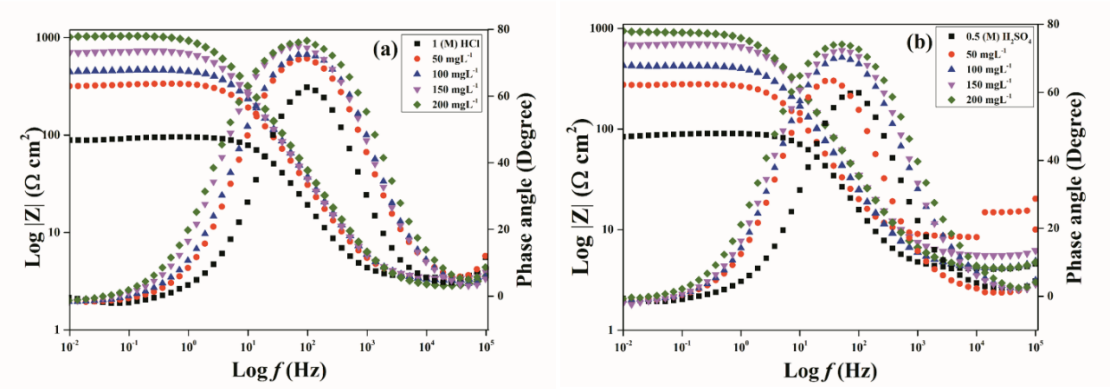

Fig. 6.6 Bode plots of BQ corrosion in acidic media without and with different concentration: (a) HCl and (b) H_2SO_4 media.

EIS is a commonly used method for analyzing corrosion, passivation, and charge transfer processes at the electrode/electrolyte interface. The EIS study uses Nyquist and Bode charts to illustrate the impedance responses to the frequencies. The Nyquist and Bode plots are represented in Fig. 6.5 and Fig. 6.6, respectively, in both HCl and H_2SO_4 media in the absence and presence of different doses of OPE. The Nyquist plots of uninhibited and inhibited solutions have similar patterns. However, the semicircle plots are slightly depressed because of the surface heterogeneity on BQ steel. The shapes and patterns are similar, suggesting that the OPE inhibitors have no effect on the corrosion mechanism in both acidic media. These semicircles are distinguished by the presence of a big capacitive loop at higher frequencies and an inductive loop at lower frequencies. The capacitive loop is usually associated with the charge transfer in the double layer of the surface, and the inductive loop is the resultant of the relaxation of the intermediate products in the corrosion process. The absence of the inductive loop in the presence of OPE is often considered a “degradation” event for EIS, suggesting full coverage by inhibitor molecules on the steel surface (Zheng et al., 2014). These geometries, together with the patterns of Nyquist plots and the Bode plots, imply that the metal-surface interactions were mainly controlled by charge transfer reactions. As

TH-3102_146107038

a result, the generated resistance on the surface was likewise regulated by the charge transfer resistance (R_{ct}). The value R_{ct} is measured by the diameters of the capacitive loops or semicircles. The existence of a single-time constant in the electrochemical process are indicated by semicircle in Nyquist plots and single narrow peak in Bode plots (phase angle plots) (Fig. 6.6 (a) and (b)). The Phase angles of Bode plots (90° or 0°) imply capacitive or resistive characteristics of the surface-solution interface. There was no pure capacitive behavior observed from any of the plots since the phase angles were all less than 90°. But the increased peak heights certainly at higher inhibitor concentrations suggest a stronger capacitive response of the metal solution interface, which is consistent with previous findings. The peak points of the phase angle plots are also not fixed on a single frequency, so the capacitance varies accordingly. The changes in values of impedance with OPE concentration in Bode modulus curves match with the trend of semicircle diameter variation of the Nyquist plots (Mourya et al., 2014; Pal and Das, 2022; Saxena et al., 2018a). The Nyquist plots in Fig. 6.5 (a) and (b) show that the diameters of the semicircles become larger as the OPE concentration is increased, indicating a greater charge transfer resistance (R_{ct}). At higher OPE dose, the higher values of $log|z|$ at lower frequencies indicates resistance in both acidic conditions by adsorbed OPE inhibitors on the surface of the surface.

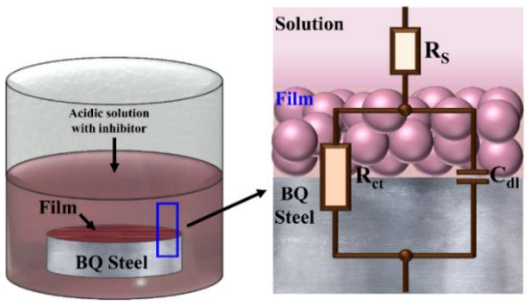

Fig. 6.7 Model of an equivalent circuit for fitting the impedance data points and its physical significance on corrosion BQ steel in the presence of inhibitors.

TH-3102_146107038

Table 6.3 Impedance parameters for the corrosion of BQ steel in HCl and H_2SO_4 solutions containing different concentrations of OPE.

	Conc (mg L^{-1})	R_S (Ω cm^2)	R_{ct} (Ω cm^2)	CPE parameters n	CPE parameters Y_o (µMho cm^{-2})	C_{dl} (µF cm^{-2})	$\mu_{R_{ct}}$%
	0 (Blank) 1 (M) HCl	3.49 ± 0.001	89.72 ± 1.67	0.93 ± 0.001	137.01 ± 4.94	97.3 ± 0.95	0.00 ± 0.00
HCl media	**50**	3.32 ± 0.001	330.23 ± 8.99	0.91 ± 0.001	92.71 ± 0.55	65.52 ± 0.17	72.83 ± 0.29
	100	3.25 ± 0.001	466.58 ± 12.25	0.91 ± 0.001	79.65 ± 0.28	56.64 ± 0.09	80.77 ± 0.40
	150	3.39 ± 0.001	740.04 ± 23.22	0.91 ± 0.001	79.35 ± 0.16	60.3 ± 0.06	87.88 ± 0.18
	200	2.87 ± 0.001	1031.80 ± 20.95	0.91 ± 0.001	67.37 ± 0.10	51.37 ± 0.05	91.30 ± 0.14
	0 (Blank) 0.5 (M) H_2SO_4	4.13 ± 0.001	85.08 ± 1.38	0.92 ± 0.001	178.23 ± 8.43	125.46 ± 1.54	0.00 ± 0.00
H_2SO_4 media	**50**	9.65 ± 0.001	266.95 ± 4.10	0.94 ± 0.001	144.35 ± 1.23	117.82 ± 0.37	68.13 ± 0.29
	100	4.30 ± 0.001	423.44 ± 8.16	0.90 ± 0.001	127.48 ± 0.32	91.13 ± 0.14	79.91 ± 0.38
	150	5.60 ± 0.001	696.44 ± 20.01	0.91 ± 0.001	88.74 ± 0.414	63.34 ± 0.13	87.78 ± 0.16
	200	4.24 ± 0.01	916.18 ± 26.66	0.90 ± 0.001	83.30 ± 0.20	67.23 ± 0.10	90.71 ± 0.20

An equivalent circuit model was used to fit EIS spectra and numerous parameters, including solution resistance (R_s), charge-transfer resistance (R_{ct}), and constant phase element (CPE) were computed to understand how the inhibitor inhibits corrosion on the metal surface (Fig. 6.7). For the fitting, a basic Randles circuit was employed, which is made up of R_s in series with R_{ct} and CPE, a replacement for an

TH-3102_146107038

ideal double-layer capacitance of dispersed frequency with R_{ct} and CPE in parallel. There are many different electrical components, like a capacitor, resistor, and inductor, which help to explain the physical electrochemistry of any solution-surface interface. Conventionally if the surface is not homogeneous, then the capacitor is replaced by a constant phase element (CPE) to simulate the heterogeneity of the surface (M'hiri et al., 2016; Srivastava et al., 2018; Verma et al., 2018).

Both the Nyquist plots and the Bode plots show that in acidic environments, higher OPE concentrations result in increased surface resistance. By showing the variations in impedance parameters at various concentrations of OPE, Table 6.3 draws attention to learn more about the surface behaviors of BQ steel in the presence and absence of inhibitors in both acidic media. In both the HCl and H_2SO_4 medium, it is evident that the values of R_{ct} increased as the concentration of OPE increased. These changes in EIS values suggest that inhibitor chemicals have accumulated at the metal-acid contact, resulting in the formation of a thin protective layer. This layer restricted the charge flow from the bulk electrolyte to the BQ surface by blocking the corroding agents, which induced local sites of corrosion. The thickness of the layer grew as OPE concentration increased, further decreasing corrosion risk. So, the more the BQ steel surface was covered, the less chance of corroding components coming into touch with the steel surface. (Ji et al., 2015; Wang et al., 2019).

6.4 Adsorption studies

The findings of electrochemical experiments already confirmed the occurrence of adsorption on the BQ surface and provided insight into the mechanism of electrochemical interaction between the BQ steel surface and inhibitory compounds. Therefore, it was necessary to understand the kind of adsorption, which might be either

TH-3102_146107038

physisorption, chemisorption, or a combination of the two types. Three widely used adsorption isotherms, Langmuir (Fig. 6.8 (a) and (b)), Temkin (Fig. 6.8 (c) and (d)), and Frumkin (Fig. 6.8 (e) and (f)), were used to determine the type of adsorption. These isotherms establish relationships between inhibitor concentration (C), surface coverage ($\theta = \mu_{R_{ct}} 100^{-1}$), and the adsorption equilibrium constant (K_{ads}). After computing the slopes, intercepts, and regression coefficients (R^2) for all of the isotherms tested, the Langmuir model (Fig. 6.8 (a) and (b)) was shown to have the best fit.

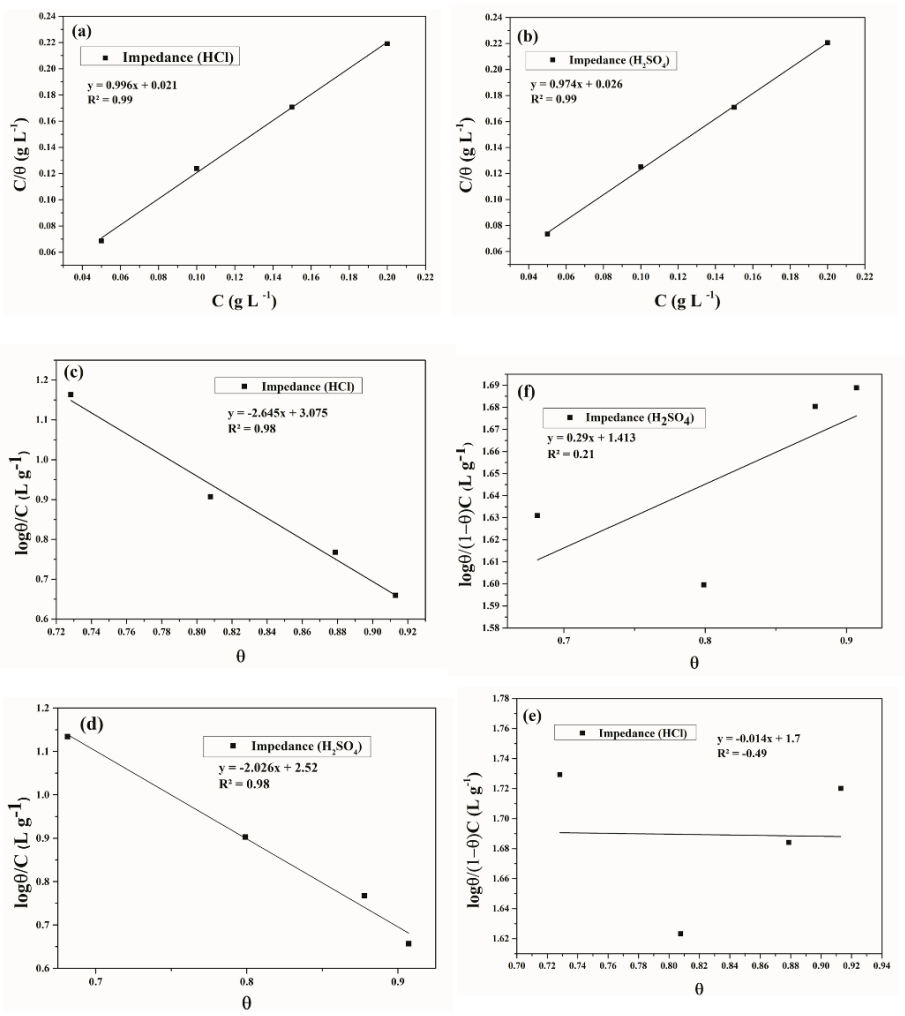

Fig. 6.8 (a, b) Langmuir, (c, d) Temkin, (e, f) Frumkin adsorption isotherm plots using OPE in HCl and H_2SO_4.

TH-3102_146107038

The Langmuir isotherm can be expressed in the straight-line equation as the given equation:

$$\frac{C}{\theta} = \frac{1}{K_{ads}} + C \qquad \textbf{6.3}$$

To obtain the value of K_{ads} (L g^{-1}) $\frac{C}{\theta}$ was plotted against C (gL^{-1})r. K_{ads} is the adsorption equilibrium constant from which the adsorption free energy, also known as standard Gibbs free energy (ΔG°_{ads}) can be calculated using the following expression:

$$\Delta G^{\circ}_{ads} = -RTln(C_{water}K_{ads}) \qquad \textbf{6.4}$$

Where R is the universal gas constant (8.314 Jmol^{-1}K^{-1}), C_{water} represents the concentration of water (1000 gL^{-1}), and T is the temperature (298.15 K). The derived linear regression coefficient (R^2) from the Langmuir plot, as well as ΔG°_{ads} and K_{ads} are shown in Table 6.4 with the other variables.

Table 6.4 Parameters of adsorption isotherm for OPE in HCl and H_2SO_4

Media	R^2	$1/K_{ads}$ (g L^{-1})	K_{ads} (Lg^{-1})	ΔG^0_{ads} (kJmol^{-1})
1 M HCl	0.99	0.021	47.55	-26.70
0.5 M H_2SO_4	0.99	0.026	38.87	-26.19

Earlier studies revealed that the value of ΔG^0_{ads} indicates the nature of adsorption. The negative values of ΔG^0_{ads} indicate the spontaneous adsorption of inhibitory compounds of OPE on the BQ plate. When ΔG^0_{ads} value is around -20 kJmol^{-1} or less negative; then the interaction is only electrostatic, then the adsorption is considered as physisorption. On the other hand, when ΔG^0_{ads} value is equal to or more negative than -40 kJmol^{-1}, then the interaction is associated with charge transfer, i.e., chemisorption (Azmi and Soedarsono, 2018; Verma et al., 2018). The values of ΔG^0_{ads} in Table 6.4 indicate that the adsorption in this study was actually

TH-3102_146107038

physicochemical, as the values in both acidic media lie between -20 $kJmol^{-1}$ and -40 $kJmol^{-1}$.

6.5 Characterization of surface

6.5.1 FESEM-EDX

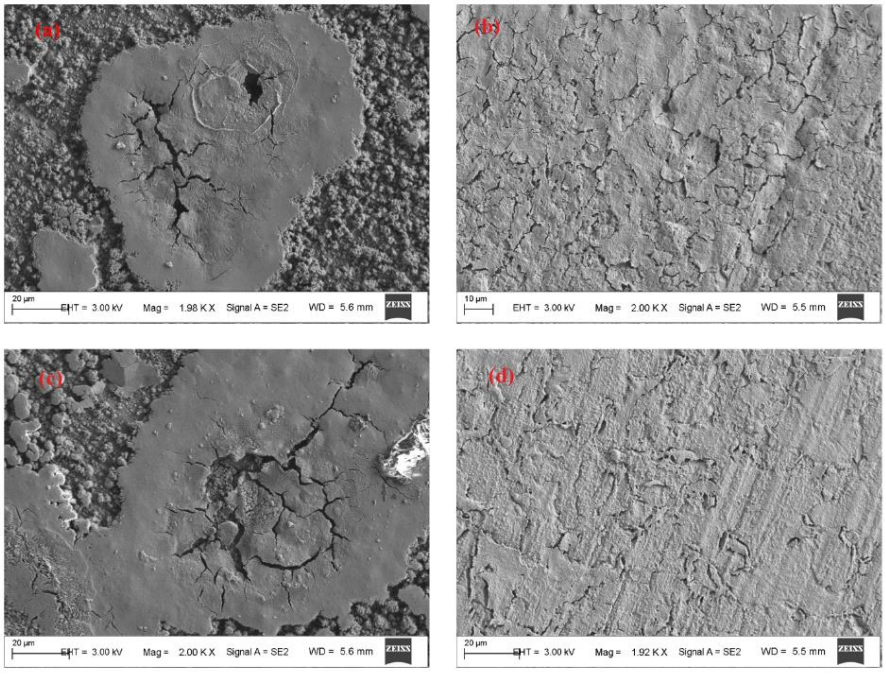

Fig. 6.9 FESEM images of BQ steel sample after corrosion (a) without OPE in 1 M HCl, (b) in the presence of OPE (200 mg L^{-1}) in 1 M HCl, (c) without OPE in 0.5 M H_2SO_4, and (d) in the presence of OPE (200 mg L^{-1}) in 0.5 M H_2SO_4.

The FESEM tests were carried out in both acidic media with and without OPE to assess surface morphology and validate interpretations gained from gravimetric and electrochemical investigations. FESEM pictures in Fig. 6.9 (a) and (b) show the changes on the BQ surface when OPE (200 mgL^{-1}) was applied to the HCl solution. Similarly, Fig. 6.9 (c) and (d) depict the changes on the BQ surface upon applying OPE in 0.5 (M) H_2SO_4 solution. Without OPE, the surface was corroded due to aggressive anodic and cathodic reactions, which produced fractures and pits. Whereas, when OPE

TH-3102_146107038

was incorporated in both acidic media, such severely damaged structures were not visible on the surface. The incorporation of OPE brought a significant change in the microstructure of BQ, which was observed in both acidic media. The adsorption of the phenolic compounds of OPE on the BQ surface developed a protective layer, which then blocked the active reaction sites and slowed down the corrosion response. As a consequence, in the presence of OPE, fewer fractures and pits are visible on the surface (Zheng et al., 2014).

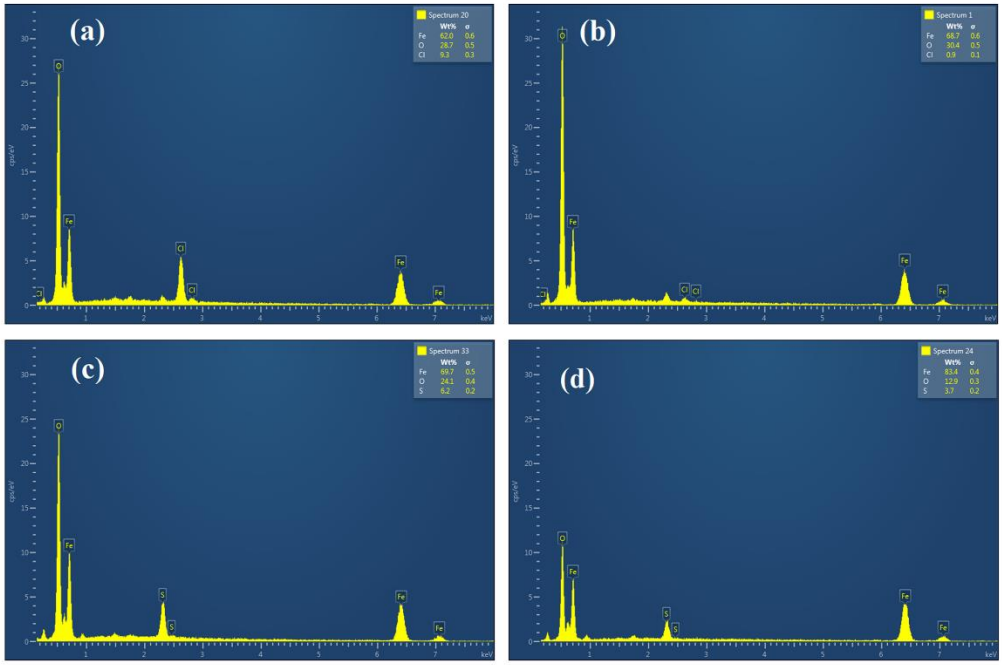

Fig. 6.10 EDX spectra of BQ steel sample after corrosion (a) without OPE in 1 M HCl, (b) in the presence of OPE (200 mg L^{-1}) in 1 M HCl, (c) without OPE in 0.5 M H_2SO_4, and (d) in the presence of OPE (200 mg L^{-1}) in 0.5 M H_2SO_4.

The elementary changes of BQ surface by OPE were investigated using EDX, and the spectrums are shown in Fig. 6.10. Fig. 6.10 (a) demonstrates the lower iron (62.0 %) and higher chloride (9.3 %) weight percentage in the absence of OPE than the iron (68.7 %) and chloride (0.9 %) in the presence of OPE (Fig. 6.10 (b)). Same way, in the case of H_2SO_4 media, the lower iron (69.7 %) and higher sulfur (6.2%) weight

TH-3102_146107038

percentage in the absence of OPE (Fig. 6.10 (c)) than the iron (83.4 %) and sulfur (3.7 %) weight percentage in the presence of OPE (Fig. 6.10 (d)) are observed. For various redox reactions to occur, the Fe^{2+} on the surface electrostatically attracted the Cl^-, resulting in Cl^- being adsorbed on the surface. In contrast, since SO_4^{2-} was less electronegative than Cl^-, the likelihood of sulfur being adsorbed on the surface in the H_2SO_4 medium was lower than that of Cl^-. So the increase in iron weight % indicated that the surface was protected by the inhibitor layer and was more resistant to aggressive attacks by corrosive components (Naghi Tehrani et al., 2021).

6.5.2 AFM study

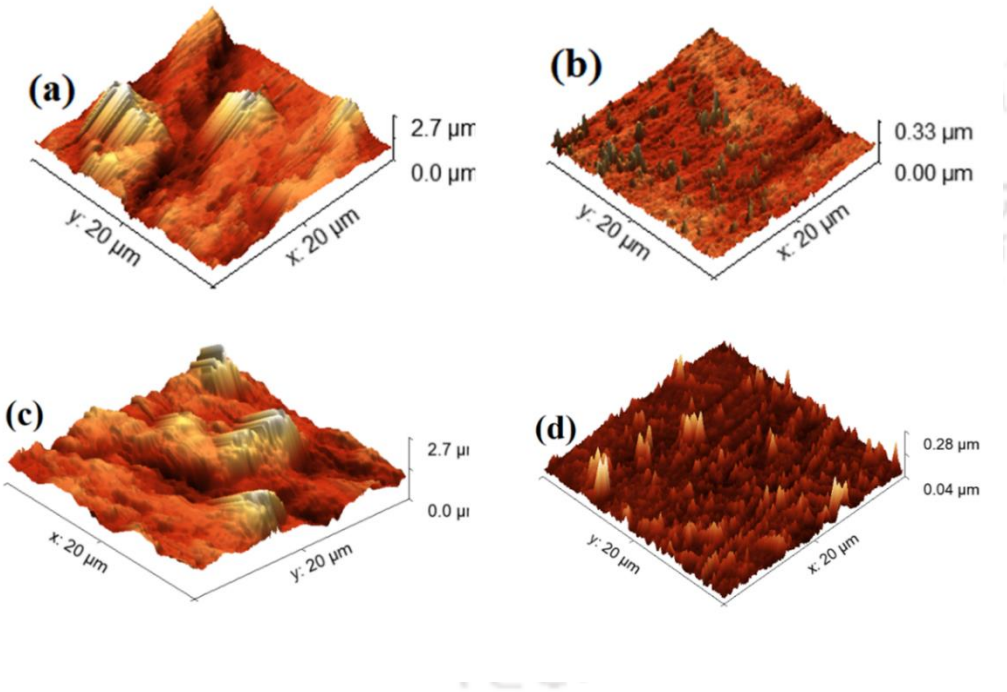

Fig. 6.11 3D AFM images obtained for the surface morphology of BQ steel sample after corrosion (a) without OPE in 1 M HCl, (b) with OPE (200 mg L^{-1}) in 1 M HCl, without OPE in 0.5 M H_2SO_4 (c), and (d) with OPE (200 mg L^{-1}) in 0.5 M H_2SO_4.

TH-3102_146107038

The AFM investigation of a 20 × 20 μm^2 area from the steel surface demonstrated the adsorption of OPE in both HCl and H_2SO_4 solutions. The 3-D AFM images of the steel surfaces show the differences in the average surface roughness between the uninhibited and the inhibited surface in both the acidic solutions (Fig. 6.11). It is apparent from Fig. 6.11 that the presence of OPE (200 mgL^{-1}) made a significant reduction in average surface roughness. In the control HCl media, the average surface roughness was 284.4 nm (Fig. 6.1 (a)), while the addition of OPE reduced the roughness (19.83 nm) (Fig. 6.11(b)). Similarly, in H_2SO_4 media, the average surface roughness was 278.7 nm without OPE (Fig. 6.11 (c)) and 15.17 nm with OPE (Fig. 6.11 (d)). The decrease in roughness was primarily due to the adsorption of the organic compounds in OPE on the surface of the material (Prabakaran et al., 2016; Singh and Quraishi, 2016; Srivastava et al., 2018).

6.6 Theoretical studies by quantum chemical calculations using DFT

The fundamental corrosion prevention mechanism of OPE on BQ steel was examined electrochemically. To know the molecular mechanism of inhibition, one must comprehend the relationship between corrosion inhibition and inhibitory molecule structures. Quantum-level simulations provide crucial insights into the relationship between the structure and inhibition efficiency if inhibitory molecules (Mourya et al., 2014).

6.6.1 Quantum chemical parameters

Molecular orbital theory (FMO) is one of the most widely used approaches for performing quantum chemical computations. As per the FMO theory of chemical reactivity, the formation of a transition state is dependent on the interactions between FMOs (HOMO and LUMO). Therefore, the HOMO and LUMO are considered

TH-3102_146107038

significant indicators to analyze any adsorption or chelation process. As inhibition of corrosion is based on the principle of adsorption, the analysis of HOMO and LUMO is significant with respect to the efficiency of the inhibitor (Mourya et al., 2014). HOMO locations are known to be electron donors and adsorption sites due to the abundance of electrons in π bonds, benzene rings, and also various heteroatoms, while LUMO areas are known to be electron acceptors (Ganash, 2018). It is well known that ionization potential (I) indicates the donation capability of a compound to d-orbitals of the metal and electron affinity (A) indicates the electron acceptance propensity from the metal. So these two parameters can also be a significant indicator of an efficient inhibitor (Hsissou et al., 2021). All the parameters were determined in the gas phase as well as in the aqueous phase since the phenomenon of corrosion occurs mostly in humid conditions.

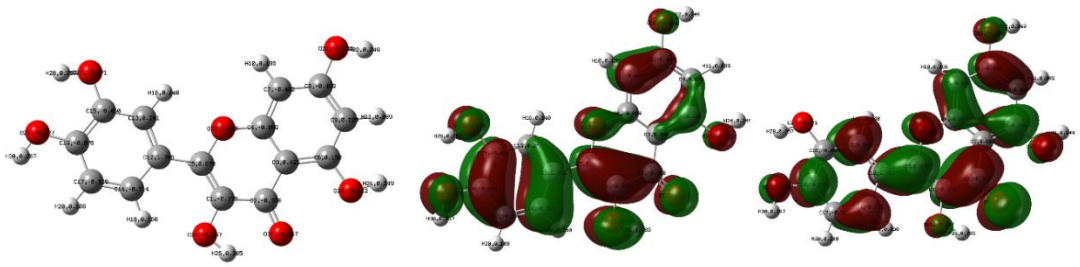

Fig. 6.12 The electron density distribution of quercetin monomer.

Quercetin was identified as a significant inhibitor compound based on LCMS findings. Fig 6.12 shows pictures of the optimized structure and the FMO sites of the detected inhibitory compound from OPE. The electronegativity characteristics and the presence of π electron clouds of the compound are reflected in the colored lobes, which are green and red. The more electronegative areas are depicted by red lobes, while the green lobes represent the less electronegative areas (Nofrizal et al., 2012). The

TH-3102_146107038

delocalization of electrons from both HOMO-LUMO regions is occurred to build an optimum interaction involving most of the areas of the molecule (Fig. 6.12) (Verma et al., 2018). As a result, substantial atoms from such HOMO-LUMO areas make stable interactions with the BQ steel. These interactions are mostly dependent on the ability of different single atoms, phenyl rings, and functional groups of the HOMO-LUMO regions either to donate electrons onto the steel surface or from the steel surface (Ganash, 2018). For the quercetin molecule, the energy values of HOMO and LUMO), as well as the related quantum chemical parameters, were determined and reported in Table 6.5.

Table 6.5 Various quantum parameters of quercetin molecule in gas and aqueous phase.

Inhibitors name	E_{LUMO} (eV)	E_{HOMO} (eV)	ΔE (eV)	I (eV)	A (eV)	χ (eV)	η (eV)	σ ($1eV^{-1}$)	ΔN
Quercetin (gas)	-1.964	-5.744	3.780	5.744	1.964	3.854	1.890	0.529	0.832
Quercetin (aqueous)	-2.186	-5.918	3.732	5.918	2.186	4.052	1.866	0.536	0.790

It is well known that a larger E_{HOMO} shows a greater proclivity to transfer electrons to a lower-energy orbital level. As a result, a larger E_{HOMO} value improves the interaction between the surface and molecule, resulting in better adsorption of the molecule on the surface. Lower E_{LUMO} value indicates that the molecule was more likely to receive an electron from higher-energy orbitals, making it also more efficient to be adsorbed on the surface (Liao et al., 2018). Table 6.5 shows that quercetin has a LUMO value (-1.964 eV) and HOMO value (-5.744 eV). According to the literature, the energy gap (ΔE) is a reactivity and stability indicator. Low ΔE caused the molecule to be more reactive when interacting with another one because it took less energy to

TH-3102_146107038

move electrons from one orbital to another. It was observed that quercetin in the aqueous phase is more reactive than the gas phase as the energy gap (ΔE) in the aqueous phase (3.732 eV) is slightly lower than in the gas phase (3.780 eV) (Table 6.5) (Verma et al., 2018). Furthermore, its electronegativity (χ), softness (σ), and global hardness (η) were also computed. It is observed from Table 6.5 that the quercetin molecule was less hard in the aqueous phase (1.866 eV) than in the gas phase (1.890 eV). When it comes to hardness, it is basically the resistance to distortion or polarization of the electron cloud of atoms, ions, or molecules when a chemical reaction is perturbed by a small amount (Hsissou et al., 2021; Verma et al., 2018). In addition, the fraction of transferable electrons (ΔN) from the inhibitor is higher than zero in both phases, which suggests that the quercetin molecule is efficient enough to transfer the electrons to the metallic surface. However, the value of ΔN is slightly higher in gas phase (0.832) than in the aqueous phase (0.790), but the difference is negligible (Belghiti et al., 2019).

The Fukui indices of quercetin were investigated in order to identify local reactive sites. These indices help to detect the electrophilic and nucleophilic sites of the investigated molecules. Because of the adsorbed anions on the positively charged surface of the BQ, the surface of the BQ may be negatively charged, or it may be positively charged in an acidic medium. The molecule is prone to nucleophilic attacks where f_k^+ values are large as those sites can stabilize supplementary electrons. Conversely, the electrophilic attack is more likely to be initiated at sites where f_k^- values are large (Belghiti et al., 2019; Ganash, 2018; Liao et al., 2018; Naghi Tehrani et al., 2021; Verma et al., 2018).

TH-3102_146107038

Table 6.6 Fukui function with the highest f_k^+, f_k^- and f_k^2, values of some atoms from Quercetin.

Atom	f_k^+	f_k^-	f_k^2
C3	1.321	-1.097	2.418
C9	0.747	-0.830	1.576
C15	0.119	-0.122	0.240
O23	0.001	-0.045	0.045
H28	-0.006	-0.021	0.014
O32	-0.055	-0.038	-0.018
O31	-0.128	-0.064	-0.063
C6	-0.876	0.727	-1.603
C4	-1.108	1.020	-2.127
C1	-1.424	1.439	-2.864

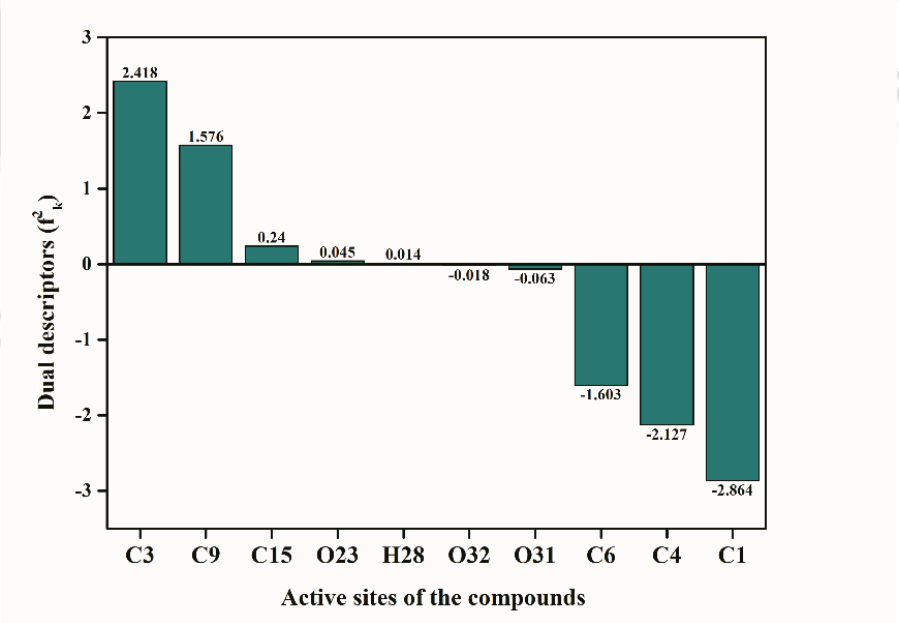

Fig. 6.13 Graphical representation of the dual descriptors of some electrophilic and nucleophilic sites from quercetin.

Table 6.6 lists some of the highest f_k^+ (electrophilic) and f_k^- (nucleophilic) values obtained from these atoms. According to Table 6.6, C3, C9, C15, O23, H28 with the highest f_k^+ values are electrophilic, where the nucleophilic attack occurs (back

TH-3102_146107038

donation from the metal surface to the molecule), whereas C1, C4, C6, O31, and O32 atoms (electron donator or nucleophilic) with f_k^- are the sites for an electrophilic attack. Table 6.6 displays the values of a f_k^2 which shows the atoms with $f_k^2 > 0$ are electrophilic (C3,C9, C15, O23, H28), and the atoms with $f_k^2 < 0$ are nucleophilic (C1, C4, C6, O31, O32) (Hsissou et al., 2021; Liao et al., 2018). The order of the electrophilic sites is C3> C9> C15> O23> H28 and the nucleophilic sites is C1> C4> C6> O31> O32> (Fig. 6.13) (Belghiti et al., 2019).

6.7 Mechanism of inhibition

According to the results of the Tafel polarization experiments, the amplitude of the anodic shifts is not similar in both media. As the anodic dissolution occurs in the absence and presence of an inhibitor, it may be described by the process of anodic dissolution. The anodic processes in H_2SO_4 and HCl environments have separate mechanisms, as discussed below.

6.7.1 Anodic reaction

The electro-dissolution of iron in acidic sulfate solution is mainly influenced by the adsorption intermediated $FeOH_{ads}$, which are formed throughout the dissolving process. The iron dissolution in HCl media differs from the dissolution of iron in the H_2SO_4 medium. The $(FeCl)_{ads}$ are responsible for anodic dissolution in HCl, whereas the $(FeOH)_{ads}$ are responsible for anodic dissolution in H_2SO_4. When the inhibitor is applied to an acidic media, several reaction phases occur depending on the electrolyte and the anodic dissolution mechanism. As a result, the variation in the anodic curve of Tafel slopes is due to the different anodic dissolution processes. The detailed reaction mechanism and the differences in the mechanism are already discussed in section 4.7.

TH-3102_146107038

6.7.2 Cathodic reaction

The cathodic reactions (hydrogen evolution) are mainly influenced by the H^+ and protonated inhibitor ($InhH^+$). These two species compete for the same active site of the BQ steel surface to be adsorbed on the surface. The Tafel plots (Fig. 6.4) portray that cathodic curves are approximately parallel, indicating the cathodic activation-controlled nature of the reaction. From the activation-controlled nature of the cathodic reactions in the above equations, the first step is likely to be the rate-controlling step (Mourya et al., 2013).

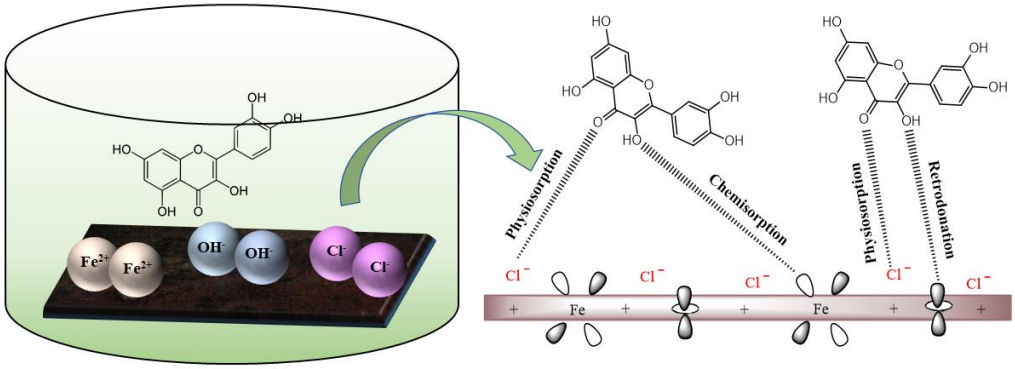

Fig. 6.14 Schematic representation of corrosion inhibition mechanism in acidic medium.

In addition to dissolving Fe^{2+}, the anodic reaction also creates hydrogen gas. Whenever inhibitors are added to an acidic medium, they are protonated and begin to adsorb on the charged surface. The adsorbed Cl^- of the surface attracts the protonated inhibitor (physisorption) (Fig. 6.14). At high inhibitor concentrations, the protonated inhibitors may compete with other cationic species to bind onto nucleophilic sites (Al-Moubaraki, 2015). The protonated inhibitors return to their neutral form once they

TH-3102_146107038

accept electrons from metallic surfaces. Then the lone pair electrons of the heteroatoms in the inhibitory molecules initiate chemical adsorption (Srivastava et al., 2018). As the surface gets completely saturated with electrons, it becomes negatively charged. In order to surplus, the excess electrons from the surface the "d" orbital electrons of iron may get transferred to the empty π (antibonding) orbital of the OPE molecules via the mechanism of retrodonation, which leads to the more strong adsorption of the inhibitor onto the BQ surface (Saxena et al., 2018c, 2018b; Srivastava et al., 2018).

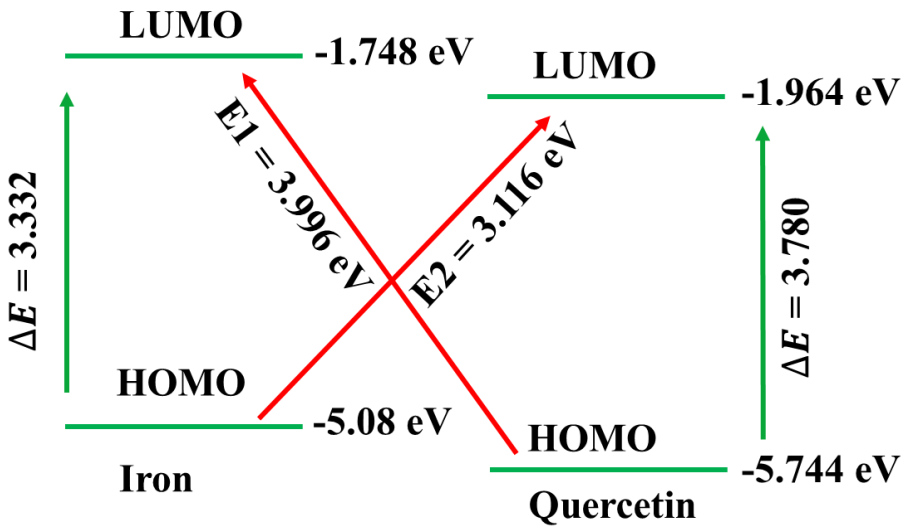

Fig. 6.15 Schematic representation of HOMO and LUMO energy levels of iron and quercetin.

It is also necessary to explore the energy difference between the LUMO of iron and the HOMO of quercetin (E1), as well as the difference between the LUMO of quercetin and the HOMO of iron (E2), to understand the inhibitory function (Fig. 6.15). In Fig. 6.15, it has been observed that the E1 value (3.996 eV) is higher than E2 (3.116 eV) value which suggests the flow of electrons from the iron to quercetin molecule is easier than from the quercetin to iron. So from these pieces of information, it can be concluded that quercetin molecules were attracted to a BQ steel surface by electrostatic

TH-3102_146107038

interactions. Following that, quercetin molecules formed a chemical bond with iron molecules by donating electrons to iron and accepting electrons from iron (back donation) (Khanra et al., 2018; Srivastava et al., 2017).

6.8 Summary

It is possible to infer from the current experimental and computational studies that the OPE, which was isolated from a kitchen waste (onion peel), is a viable green inhibitor that is both environmentally benign and effective. Experimental studies in 1 (M) HCl and 0.5 (M) H_2SO_4 on the BQ surface, as well as theoretical research compound of OPE, were carried out in order to determine the efficacy of OPE as green corrosion inhibitors. The following conclusions have been drawn after doing all of the experiments:

1. Quercetin was identified as the most abundant compound in OPE by LCMS analysis.
2. The studies of Tafel polarization revealed that the OPE acted as a mixed-type inhibitor on the BQ steel surface. It also disclosed that the corrosion current (i_{corr}) were 179.06 µA cm^{-2} and 180.25 µA cm^{-2} in 1 (M) HCl and 0.5 (M), respectively, in the absence of OPE. The minimum corrosion current (i_{corr}) was found as 16.80 µA cm^{-2} and 17.48 µA cm^{-2} at 200 mg L^{-1} of OPE in 1 (M) HCl and 0.5 (M) H_2SO_4. The polarization resistance (R_P) was also changed from 101.17 to 993.68 Ω cm^2 and from 104.62 to 873.81 Ω cm^{-2} in HCl and H_2SO_4 medium on the addition of OPE.
3. The protectiveness of OPE was further proved by EIS measurements, as the presence of OPE has reduced the charge-transfer resistance. The charge-transfer resistance (R_{ct}) was found as 89.72 Ωcm^2 and 85.08 Ω cm^2 in 1 (M) HCl and

TH-3102_146107038

0.5 (M) H_2SO_4 media without incorporating inhibitor. Whereas with OPE (200 mg L^{-1}) R_{ct} was increased in both HCl (1031.80 Ωcm^2) and H_2SO_4 media (916.18 Ωcm^2). The inhibition efficiency calculated R_{ct} was found maximum 91.30% and 90.71% after incorporating 200 mg L^{-1} of OPE in both media.

4. The inhibition of corrosion was caused by adsorption of OPE, as the value of K_{ads} (47.55 L g^{-1} in HCl and 38.87 L g^{-1} in H_2SO_4) and ΔG°_{ads} (-26.7 kJ mol^{-1} in HCl and -26.19 kJ mol^{-1} in H_2SO_4) has also supported. The Langmuir isotherm was identified for OPE adsorption on BQ steel. The K_{ads} and $\Delta G°_{ads}$ values showed thermodynamic adsorption favorability.
5. As shown by investigations in FESEM, EDX, and AFM, the development of a protective layer by OPE on the BQ steel significantly reduced the rate of corrosion.
6. Quantum chemistry calculations revealed that quercetin had a shorter energy gap in the aqueous phase than in the gaseous phase, resulting in a more potent inhibitory effect.

6.9 References

Al-Moubaraki, A.H., 2015. Corrosion Protection of Mild Steel in Acid Solutions Using Red Cabbage Dye. Chem. Eng. Commun. 202, 1069–1080. https://doi.org/10.1080/00986445.2014.907565

Ali Asaad, M., Sarbini, N.N., Sulaiman, A., Ismail, M., Huseien, G.F., Abdul Majid, Z., Bothi Raja, P., 2018. Improved corrosion resistance of mild steel against acid activation: Impact of novel Elaeis guineensis and silver nanoparticles. J. Ind. Eng. Chem. 63, 139–148. https://doi.org/10.1016/j.jiec.2018.02.010

Azmi, M.F., Soedarsono, J.W., 2018. Study of corrosion resistrance of pipeline API 5L X42 using green inhibitor bawang dayak (Eleutherine americanna Merr.) in 1M HCl. IOP Conf. Ser. Earth Environ. Sci. 105. https://doi.org/10.1088/1755-1315/105/1/012061

TH-3102_146107038

Bedrníček, J., Jirotková, D., Kadlec, J., Laknerová, I., Vrchotová, N., Tříska, J., Samková, E., Smetana, P., 2020. Thermal stability and bioavailability of bioactive compounds after baking of bread enriched with different onion by-products. Food Chem. 319. https://doi.org/10.1016/j.foodchem.2020.126562

Belghiti, M.E., Echihi, S., Dafali, A., Karzazi, Y., Bakasse, M., Elalaoui-Elabdallaoui, H., Olasunkanmi, L.O., Ebenso, E.E., Tabyaoui, M., 2019. Computational simulation and statistical analysis on the relationship between corrosion inhibition efficiency and molecular structure of some hydrazine derivatives in phosphoric acid on mild steel surface. Appl. Surf. Sci. 491, 707–722. https://doi.org/10.1016/j.apsusc.2019.04.125

Celano, R., Docimo, T., Piccinelli, A.L., Gazzerro, P., Tucci, M., Di Sanzo, R., Carabetta, S., Campone, L., Russo, M., Rastrelli, L., 2021. Onion peel: Turning a food waste into a resource. Antioxidants 10, 1–18. https://doi.org/10.3390/antiox10020304

Chen, Y., Yu, H., Wu, H., Pan, Y., Wang, K., Jin, Y., Zhang, C., 2015. Characterization and quantification by LC-MS/MS of the chemical components of the heating products of the flavonoids extract in Pollen typhae for transformation rule exploration. Molecules 20, 18352–18366. https://doi.org/10.3390/molecules201018352

Ganash, A.A., 2018. Theoretical and experimental studies of dried marjoram leaves extract as green inhibitor for corrosion protection of steel substrate in acidic solution. Chem. Eng. Commun. 205, 350–362. https://doi.org/10.1080/00986445.2017.1391096

Hsissou, R., Abbout, S., Safi, Z., Benhiba, F., Wazzan, N., Guo, L., Nouneh, K., Briche, S., Erramli, H., Ebn Touhami, M., Assouag, M., Elharfi, A., 2021. Synthesis and anticorrosive properties of epoxy polymer for CS in [1 M] HCl solution: Electrochemical, AFM, DFT and MD simulations. Constr. Build. Mater. 270, 121454. https://doi.org/10.1016/j.conbuildmat.2020.121454

Ji, G., Anjum, S., Sundaram, S., Prakash, R., 2015. Musa paradisica peel extract as green corrosion inhibitor for mild steel in HCl solution. Corros. Sci. 90, 107–117. https://doi.org/10.1016/j.corsci.2014.10.002

Khanra, A., Srivastava, M., Rai, M.P., Prakash, R., 2018. Application of Unsaturated Fatty Acid Molecules Derived from Microalgae toward Mild Steel Corrosion

TH-3102_146107038

Inhibition in HCl Solution: A Novel Approach for Metal-Inhibitor Association. ACS Omega 3, 12369–12382. https://doi.org/10.1021/acsomega.8b01089

Liao, L.L., Mo, S., Luo, H.Q., Li, N.B., 2018. Corrosion protection for mild steel by extract from the waste of lychee fruit in HCl solution: Experimental and theoretical studies. J. Colloid Interface Sci. 520, 41–49. https://doi.org/10.1016/j.jcis.2018.02.071

M'hiri, N., Veys-Renaux, D., Rocca, E., Ioannou, I., Boudhrioua, N.M., Ghoul, M., 2016. Corrosion inhibition of carbon steel in acidic medium by orange peel extract and its main antioxidant compounds. Corros. Sci. 102, 55–62. https://doi.org/10.1016/j.corsci.2015.09.017

Mourya, P., Banerjee, S., Rastogi, R.B., Singh, M.M., 2013. Inhibition of mild steel corrosion in hydrochloric and sulfuric acid media using a thiosemicarbazone derivative. Ind. Eng. Chem. Res. 52, 12733–12747. https://doi.org/10.1021/ie4012497

Mourya, P., Banerjee, S., Singh, M.M., 2014. Corrosion inhibition of mild steel in acidic solution by Tagetes erecta (Marigold flower) extract as a green inhibitor. Corros. Sci. 85, 352–363. https://doi.org/10.1016/j.corsci.2014.04.036

Naghi Tehrani, M.E.H., Ghahremani, P., Ramezanzadeh, M., Bahlakeh, G., Ramezanzadeh, B., 2021. Theoretical and experimental assessment of a green corrosion inhibitor extracted from Malva sylvestris. J. Environ. Chem. Eng. 9, 105256. https://doi.org/10.1016/j.jece.2021.105256

Nofrizal, S., Rahim, A.A., Saad, B., Bothi Raja, P., Shah, A.M., Yahya, S., 2012. Elucidation of the corrosion inhibition of mild steel in 1.0 M HCl by catechin monomers from commercial green tea extracts. Metall. Mater. Trans. A Phys. Metall. Mater. Sci. 43, 1382–1393. https://doi.org/10.1007/s11661-011-1030-3

Okafor, P.C., Ebenso, E.E., Ekpe, U.J., 2010. Azadirachta Indica Extracts as Corrosion Inhibitor for Mild Steel in Acid Medium. Int. J. Electrochem. Sci 5, 978–993.

Pal, A., Das, C., 2022. New eco-friendly anti-corrosion inhibitor of purple rice bran extract for boiler quality steel: Experimental and theoretical investigations. J. Mol. Struct. 1251, 131988. https://doi.org/10.1016/j.molstruc.2021.131988

Prabakaran, M., Kim, S.H., Hemapriya, V., Chung, I.M., 2016. Evaluation of polyphenol composition and anti-corrosion properties of Cryptostegia grandiflora plant extract on mild steel in acidic medium. J. Ind. Eng. Chem. 37, 47–56.

TH-3102_146107038

https://doi.org/10.1016/j.jiec.2016.03.006

Salinas-Solano, G., Porcayo-Calderon, J., Martinez de la Escalera, L.M., Canto, J., Casales-Diaz, M., Sotelo-Mazon, O., Henao, J., Martinez-Gomez, L., 2018. Development and evaluation of a green corrosion inhibitor based on rice bran oil obtained from agro-industrial waste. Ind. Crops Prod. 119, 111–124. https://doi.org/10.1016/j.indcrop.2018.04.009

Saxena, A., Prasad, D., Haldhar, R., 2018a. Use of Asparagus racemosus extract as green corrosion inhibitor for mild steel in 0.5 M H2SO4. J. Mater. Sci. 53, 8523–8535. https://doi.org/10.1007/s10853-018-2123-9

Saxena, A., Prasad, D., Haldhar, R., 2018b. Investigation of corrosion inhibition effect and adsorption activities of Cuscuta reflexa extract for mild steel in 0.5 M H2SO4. Bioelectrochemistry 124, 156–164. https://doi.org/10.1016/j.bioelechem.2018.07.006

Saxena, A., Prasad, D., Haldhar, R., Singh, G., Kumar, A., 2018c. Use of Saraca ashoka extract as green corrosion inhibitor for mild steel in 0.5 M H2SO4. J. Mol. Liq. 258, 89–97. https://doi.org/10.1016/j.molliq.2018.02.104

Shabani-Nooshabadi, M., Ghandchi, M.S., 2015. Santolina chamaecyparissus extract as a natural source inhibitor for 304 stainless steel corrosion in 3.5% NaCl. J. Ind. Eng. Chem. 31, 231–237. https://doi.org/10.1016/j.jiec.2015.06.028

Singh, B.N., Singh, B.R., Singh, R.L., Prakash, D., Singh, D.P., Sarma, B.K., Upadhyay, G., Singh, H.B., 2009. Polyphenolics from various extracts/fractions of red onion (Allium cepa) peel with potent antioxidant and antimutagenic activities. Food Chem. Toxicol. 47, 1161–1167. https://doi.org/10.1016/j.fct.2009.02.004

Singh, P., Quraishi, M.A., 2016. Corrosion inhibition of mild steel using Novel Bis Schiff's Bases as corrosion inhibitor: Electrochemical and Surface measurement. Meas. J. Int. Meas. Confed. 86, 114–124. https://doi.org/10.1016/j.measurement.2016.02.052

Srivastava, M., Tiwari, P., Srivastava, S.K., Prakash, R., Ji, G., 2017. Electrochemical investigation of Irbesartan drug molecules as an inhibitor of mild steel corrosion in 1 M HCl and 0.5 M H2SO4 solutions. J. Mol. Liq. 236, 184–197. https://doi.org/10.1016/j.molliq.2017.04.017

Srivastava, V., Chauhan, D.S., Joshi, P.G., Maruthapandian, V., Sorour, A.A., Quraishi,

TH-3102_146107038

M.A., 2018. PEG-Functionalized Chitosan: A Biological Macromolecule as a Novel Corrosion Inhibitor. ChemistrySelect 3, 1990–1998. https://doi.org/10.1002/slct.201701949

Verma, C., Olasunkanmi, L.O., Ebenso, E.E., Quraishi, M.A., 2018. Adsorption characteristics of green 5-arylaminomethylene pyrimidine-2,4,6-triones on mild steel surface in acidic medium: Experimental and computational approach. Results Phys. 8, 657–670. https://doi.org/10.1016/j.rinp.2018.01.008

Vorobyova, V., Skiba, M., 2021. Peach Pomace Extract as Efficient Sustainable Inhibitor for Carbon Steel Against Chloride-Induced Corrosion. J. Bio- Tribo-Corrosion 7, 1–11. https://doi.org/10.1007/s40735-020-00450-y

Wang, Cai, Chen, J., Hu, B., Liu, Z., Wang, Chongbin, Han, J., Su, M., Li, Y., Li, C., 2019. Modified chitosan-oligosaccharide and sodium silicate as efficient sustainable inhibitor for carbon steel against chloride-induced corrosion. J. Clean. Prod. 238, 117823. https://doi.org/10.1016/j.jclepro.2019.117823

Xu, D., Hu, M.J., Wang, Y.Q., Cui, Y.L., 2019. Antioxidant activities of quercetin and its complexes for medicinal application. Molecules 24. https://doi.org/10.3390/molecules24061123

Zheng, X., Zhang, S., Li, W., Yin, L., He, J., Wu, J., 2014. Investigation of 1-butyl-3-methyl-1H-benzimidazolium iodide as inhibitor for mild steel in sulfuric acid solution. Corros. Sci. https://doi.org/10.1016/j.corsci.2013.11.053.

TH-3102_146107038

7

Overall conclusions and scope for future works

TH-3102_146107038

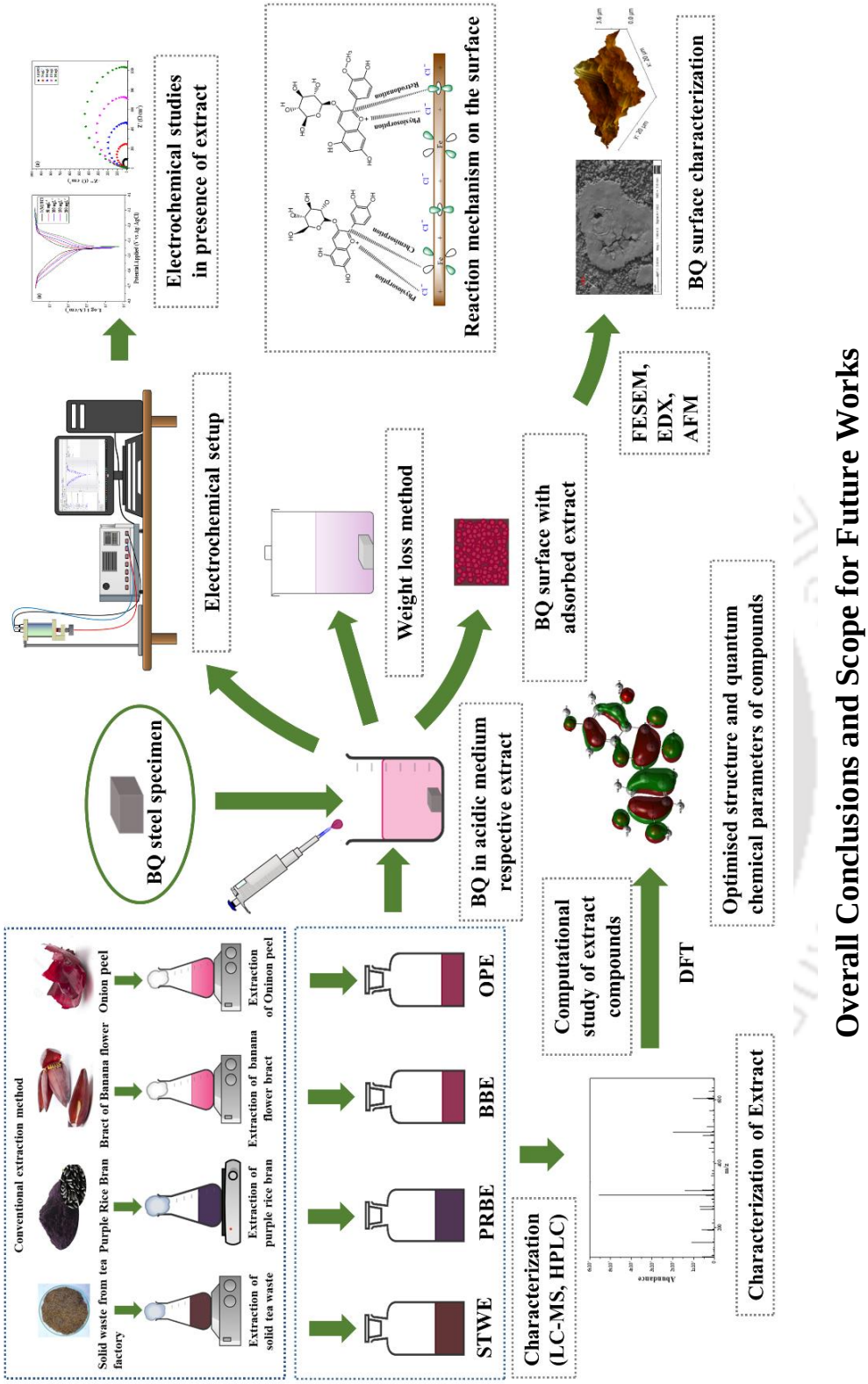

TH-3102_146107038

Overall Conclusions and Scope for Future Works

This chapter summarizes the overall conclusions of the work presented in this thesis, based on all the experimental and theoretical studies done for the four inhibitors. This chapter also provides some useful recommendations for future research in the relevant field.

भारतीय प्रौद्योगिकी संस्थान गुवाहाटी • Indian Institute of Technology Guwahati •

TH-3102_146107038

7.1 Overall conclusions

The work presented in this thesis exhibited the preparation, characterization, and corrosion inhibition efficiency of bio-masses from different waste sources. The preparation of the extract was low-cost and eco-friendly. The attempt to find an eco-friendly approach for corrosion inhibition in acidic media was successful. The results of gravimetric and electro-chemical experiments showed that all four inhibitors (extract) were effective to attain a satisfactory inhibition efficiency. The inhibitors were found as mixed-type inhibitors by thermodynamic parameters. The theoretical studies explored that identified molecules are susceptible enough to be adsorbed on the surface of the iron. From the perspective of thesis novelty, some major conclusions from the study are summarised below.

7.1.1 Overall conclusions on STWE

- Caffeine, catechin, and gallocatechin were detected from the LC-MS data of STWE.
- The corrosion current (i_{corr}) was found the minimum, 25.29 µA cm^{-2} at 500 mg L^{-1} of STWE.
- R_{ct} was found 89.72 Ωcm^{-2} and 923.40 Ωcm^{-2} in the absence and presence of 500 mg L^{-1} STWE.
- A thin barrier was found by confirmed by FESEM, EDX and AFM
- The STWE is a mixed-type inhibitor
- Caffeine has a lower energy gap (ΔE) of 4.976 eV.

7.1.2 Overall conclusions on PRBE

- Cyanidin-3-glucoside (C3G) and Peonidin-3- D-glucoside (P3G) were identified from PRBE.

TH-3102_146107038

- Both anodic and cathodic current were retarded after applying the inhibitor.
- Maximum inhibition efficiencies were found at 91.13% and 87.43% in HCl and H_2SO_4 at 200 mg L^{-1}
- PRBE was found to be a mixed-type inhibitor
- FESEM, EDX, and AFM studies confirmed the presence of a thin layer
- P3G has a lower energy gap compared to C3G, and a higher dipole moment
- PRBE was found to be the most effective inhibitor as 76.35 % efficiency was achieved at 50 mg L-1 of PRBE (Table 7.1 and 7.2).

7.1.3 Overall conclusions on BBE

- The minimum i_{corr} was found as 19.90 µA cm^{-2} and 23.01 µA cm^{-2} at 200 mg L^{-1} of BBE in 1 (M) HCl and 0.5 (M) H_2SO_4.
- In the presence of BBE (200 mg L^{-1}) R_{ct} was increased in both HCl (979.56Ωcm^2) and H_2SO_4 media (905.64 Ωcm^2)
- The inhibition efficiency calculated from R_{ct} was found to be a maximum 90.84% and 90.61% after incorporating 200 mg L^{-1}.
- FESEM, EDX, and AFM investigations revealed the formation of a protective layer of BBE.

7.1.4 Overall conclusions on OPE

- Quercetin was identified in OPE by LCMS analysis
- i_{corr} was found as 16.80 µA cm^{-2} and 17.48 µA cm^{-2} at 200 mg L^{-1} in HCl and H_2SO_4 media.
- R_{ct} was increased in both HCl (1031.80 Ωcm^2) and H_2SO_4 media (916.18 Ωcm^2).
- 91.30% and 90.71% inhibition efficiency were observed after incorporating 200 mg L^{-1} of OPE in both media.

TH-3102_146107038

- OPE was detected as a mixed-type inhibitor.
- FESEM, EDX, and AFM indicated the development of a protective layer by OPE.
- Quercetin had a shorter energy gap in the aqueous phase than in the gaseous phase

Table 7.1 Tafel parameters of all four inhibitors at the lowest and highest concentration.

	Conc (mg L^{-1})	b_a ($mVdec^{-1}$)	$-b_c$ ($mVdec^{-1}$)	E_{corr} (mV vs AgCl)	i_{corr} (μAcm^{-2})	R_P (Ωcm^{-2})	($\mu_{P\%}$)
HCl media (aqueous extract)	**0 (Blank) 1(M)HCl**	103.22 ± 1.81	61.74 ± 0.73	-457.67 ± -3.34	163.51 ± 6.72	102.62 ± 1.54	0.00 ± 0.00
	100 STWE	88.57 ± 1.54	51.98 ± 0.41	-449.27 ± -1.55	35.70 ± 0.37	398.46 ± 4.85	78.17 ± 0.92
	500 STWE	92.12 ± 1.29	62.53 ± 0.52	-445.82 ± -1.73	25.29 ± 0.10	639.61 ± 10.45	84.53 ± 0.00
HCl media (alcoholic extract)	**0 (Blank) 1(M)HCl**	110.98 ± 2.05	66.84 ± 0.80	-457.12 ± 3.32	179.06 ± 7.08	101.17 ± 0.49	0.00 ± 0.00
	50 PRBE	85.27 ± 1.52	58.76 ± 0.45	-449.61 ± -1.54	46.29 ± 0.46	326.42 ± 5.62	**74.15** ± 0.85
	50 BBE	77.87 ± 1.77	63.05 ± 0.42	-453.94 ± -1.73	66.30 ± 0.91	228.19 ± 1.41	62.97 ± 0.78
	50 OPE	86.54 ± 0.92	58.22 ± 0.21	-454.90 ± -3.69	53.73 ± 0.31	281.33 ± 1.77	69.99 ± 0.24
	200 PRBE	79.49 ± 1.97	57.81 ± 0.27	-450.21 ± -2.55	19.48 ± 0.07	746.04 ± 11.73	89.12 ± 0.40
	200 BBE	73.11 ± 0.95	54.25 ± 0.41	-446.08 ± -1.50	19.90 ± 0.05	679.63 ± 21.34	88.89 ± 0.08
	200 OPE	93.55 ± 1.21	65.25 ± 0.49	-440.81 ± -1.48	16.80 ± 0.04	993.68 ± 31.20	90.62 ± 0.08
H_2SO_4 media (alcoholic extract)	**0 (Blank) 0.5 (M) H_2SO_4**	93.13 ± 2.26	81.36 ± 1.40	-464.44 ± -3.17	180.25 ± 7.01	104.62 ± 1.25	0.00 ± 0.00
	50 PRBE	74.70 ± 2.30	52.57 ± 1.07	-444.71 ± -1.77	58.26 ± 1.75	230.01 ± 6.60	**67.68** ± 1.02
	50 BBE	77.95 ± 1.84	62.87 ± 1.11	-454.41 ± -3.73	72.75 ± 1.64	207.76 ± 1.10	59.64 ± 1.17
	50 OPE	80.89 ± 2.51	57.27 ± 0.77	-448.61 ± -1.89	61.73 ± 1.40	235.91 ± 3.94	65.75 ± 0.62
	200 PRBE	85.77 ± 1.30	63.23 ± 0.58	-445.14 ± -1.77	20.07 ± 0.08	787.51 ± 19.02	88.86 ± 0.36
	200 BBE	86.53 ± 2.54	57.21 ± 1.32	-445.74 ± -5.52	23.01 ± 0.24	649.92 ± 32.62	87.23 ± 0.70
	200 OPE	84.56 ± 5.60	60.21 ± 1.18	-444.30 ± -1.86	17.48 ± 0.16	873.81 ± 12.97	90.30 ± 0.56

TH-3102_146107038

Table 7.2 EIS parameters of all four inhibitors at lowest and highest concentration.

	Conc (mg L^{-1})	R_S (Ω cm^2)	R_{ct} (Ω cm^2)	*CPE* parameter		C_{dl} (µF cm^{-2})	$\mu_{R_{ct}}$%
				n	Y_o (µMho cm^{-2})		
HCl media (aqueous extract)	**0 (Blank) 1(M)HCl**	3.49 ± 0.001	89.72 ± 1.67	0.928 ± 0.001	137.01 ± 4.94	96.93 ± 0.94	0.00 ± 0.00
	100	3.28 ± 0.001	438.91 ± 11.94	0.914 ± 0.001	85.65 ± 0.50	63.59 ± 0.17	79.56 ± 0.32
	500	3.35 ± 0.001	923.40 ± 27.71	0.917 ± 0.001	71.72 ± 0.17	56.71 ± 0.09	90.28 ± 0.20
HCl media (alcoholic extract)	**0 (Blank) 1 (M) HCl**	3.49 ± 0.001	89.72 ± 1.670	0.93 ± 0.001	137.01 ± 4.94	97.3 ± 0.95	0.00 ± 0.00
	50 PRBE	3.00 ± 0.001	379.33 ± 5.55	0.91 ± 0.001	92.86 ± 0.24	65.5 ± 0.10	**76.35 ± 0.32**
	50 BBE	4.35 ± 0.001	243.82 ± 2.90	0.89 ± 0.001	186.71 ± 1.50	127.63 ± 0.43	63.20 ± 0.37
	50 OPE	3.32 ± 0.001	330.23 ± 8.99	0.91 ± 0.001	92.71 ± 0.55	65.52 ± 0.17	72.83 ± 0.29
	200 PRBE	4.54 ± 0.006	958.08 ±15.290	0.89 ± 0.001	85.31 ± 1.107	63.5 ± 0.55	90.64 ± 0.19
	200 BBE	4.64 ± 0.001	979.56 ± 28.39	0.90 ± 0.001	93.26 ± 0.24	70.48 ± 0.11	90.84 ± 0.13
	200 OPE	2.87 ± 0.001	1031.80 ± 20.95	0.91 ± 0.001	67.37 ± 0.10	51.37 ± 0.05	91.30 ± 0.14
H_2SO_4 media (alcoholic extract)	**0 (Blank) 0.5 (M) H_2SO_4**	4.13 ± 0.001	85.08 ± 1.38	0.92 ± 0.001	178.23 ± 8.43	125.46 ± 1.54	0.00 ± 0.00
	50 PRBE	5.11 ± 0.001	280.34 ± 6.04	0.92 ± 0.000	142.45 ± 1.38	105.97 ± 0.49	**69.65 ± 0.24**
	50 BBE	4.49 ± 0.001	222.96 ± 4.46	0.90 ± 0.001	191.60 ± 3.08	132.57 ± 0.85	61.84 ± 0.66
	50 OPE	9.65 ± 0.001	266.95 ± 4.10	0.94 ± 0.001	144.35 ± 1.23	117.82 ± 0.37	68.13 ± 0.29
	200 PRBE	2.94 ± 0.001	822.84 ± 17.64	0.90 ± 0.001	68.52 ± 0.08	49.04 ± 0.06	89.66 ± 0.15
	200 BBE	4.10 ± 0.001	905.64 ± 26.82	0.91 ± 0.001	82.89 ± 0.18	63.94 ± 0.10	90.61 ± 0.20
	200 OPE	4.24 ± 0.001	916.18 ± 26.66	0.90 ± 0.001	83.30 ± 0.20	67.23 ± 0.10	90.71 ± 0.20

TH-3102_146107038

Table 7.3 Various quantum parameters of studied molecules.

Inhibitors name	E_{LUMO} (eV)	E_{HOMO} (eV)	ΔE (eV)	I (eV)	A (eV)	χ (eV)	η (eV)	σ ($1eV^{-1}$)	ΔN (eV)
C3G	-0.977	-4.187	3.210	4.187	0.977	2.582	1.605	0.623	1.376
P3G	-0.824	-3.958	**3.134**	3.958	0.824	2.391	1.567	0.638	**1.471**
Quercetin (gas)	-1.964	-5.744	3.780	5.744	1.964	3.854	1.890	0.529	0.171
Quercetin (aqueous)	-2.186	-5.918	3.732	5.918	2.186	4.052	1.866	0.536	0.120
Caffeine	-6.363	-1.387	4.976	6.363	1.387	3.875	2.488	0.402	0.628
Catechin	-5.887	-0.119	5.767	5.887	0.119	3.003	2.884	0.347	0.693
Gallocatechin	-6.081	-0.298	5.783	6.081	0.298	3.189	2.891	0.346	0.659

There are differences in the optimum concentration of the inhibitors because all the inhibitors are bio-extract and contain numerous active compounds having different molecular properties. Since the extracts are the mixture of various compounds, it is also expected to obtain different inhibition efficiency at the same concentration. In addition the differences in effective concentration depend on the solvent of extraction. For example, in the case of STWE, the highest inhibitory concentration was 500 mg L^{-1} whereas for the other three (PRBE, BBE and OPE) it was 200 mg L^{-1}. The main reason behind this is that STWE was extracted using water, and rest three were extracted using ethanol-water mixtures. And this is a well-established theory that an alcohol-water mixture is a better solvent than pure water for more extraction of phenolic compounds. The PRBE was found most efficient at a lower concentration of 50 mg L^{-1} compared to others. But the other inhibitors have also shown some impressive results. The optimum concentration may be higher than some synthetic and commercial inhibitors, but these are totally eco-friendly and biodegradable. In summary, the low-cost, environment-friendly Bio-waste extracts have an impressive efficiency in inhibiting the corrosion of steel in acidic media and can be a substitute for conventional, costly, and toxic

TH-3102_146107038

inhibitors. The obtained data anticipate serving as the reference data for further research in developing or finding a new economically viable and eco-friendly corrosion inhibitor.

7.2 Scope for Future Works

The findings of this work provided a decent number of insights with respect to the preparation, characterization, and applications of bio-waste as a source of eco-friendly corrosion inhibitors. There are undoubtedly several areas that merit further research attention to take this promising research domain to newer heights. A few research areas for future work are proposed as follows:

- The effect of temperature on corrosion inhibition by the inhibitors can be observed.
- XPS and more characterization of the corroded surfaces may explore the new possibilities of research for the products formed during corrosion.
- The inhibition efficiencies of the tested inhibitors can be checked in CO_2 media.
- The anti-corrosive, pH-responsive polyphenolic coating can be developed from the inhibitors.
- Studies on the stability of the extract in acidic media in the presence of the metal surface may show a new direction of industrial application of these extracts as green corrosion inhibitors.

TH-3102_146107038

TH-3102_146107038

List of Publications

TH-3102_146107038

TH-3102_146107038

List of Publication

International Journal Publications

Pal, A., Das, C., 2020. A novel use of solid waste extract from tea factory as corrosion inhibitor in acidic media on boiler quality steel. **Ind. Crops Prod.** https://doi.org/10.1016/j.indcrop.2020.112468, (Elsevier) *Impact factor: 6.449.*

Pal, A., Das, C., 2022. New eco-friendly anti-corrosion inhibitor of purple rice bran extract for boiler quality steel: Experimental and theoretical investigations. **J. Mol. Struct.** 1251, 131988. https://doi.org/10.1016/j.molstruc.2021.131988, (Elsevier) *Impact factor: 3.841.*

Pal, A., Das, C., 2022. Investigations on corrosion inhibition in acidic media for BQ steel using banana flower bract, an eco-friendly novel agro-waste: Experimental and theoretical considerations. **Inorg. Chem. Commun.** 145, 110024. https://doi.org/10.1016/j.inoche.2022.110024, (Elsevier) *Impact factor: 3.428.*

Pal, A., Das, C., 2022. Novel use of kitchen waste: protection of boiler quality steel from corrosion in acidic media using onion waste. **Chem. Papers**, https://doi.org/10.1007/s11696-022-02549-7, (Springer) *Impact factor: 2.146.*

Conferences

Pal, A. and Das, C., 2017. Corrosion resistance system for the steel liner of Hydro-Electric plant in acidic medium at **CORCON**, Mumbai, September 17-20, 2017.

Pal, A. and Das, C., 2019. "The synergistic effect of a metal ion on the corrosion inhibition efficiency of solid tea waste extract in acidic media on boiler quality steel", at 35th National Convention of Chemical Engineers at The Institution of Engineers, (India) [IEI], Guwahati on the theme "**The Food - Energy - Water (FEW) Nexus -- Challenges for Chemical Engineers**" September 6 - 7, 2019.

Pal, A. and Das, C., 2022. The synergistic effect of a nickel ion on the corrosion inhibition efficiency of purple rice bran extract in acidic media at **North-East Research Conclave (NERC)**, IIT Guwahati, May 20 - 22, 2022.

Book Chapters

Pal, A. and Das, C., 2022. The synergistic effect of a nickel ion on the corrosion inhibition efficiency of purple rice bran extract in acidic media, pp 227-235, **Springer Nature.**

Saha D., **Pal, A.**, Das, C. and Pal, S.2022. Effect of Corrosion Behaviour of Microplasma Arc Welded Stainless Steel 316L Thin Sheet in Recent Advances in Manufacturing Processes and Systems pp 339-346, **Springer Nature.**

TH-3102_146107038

TH-3102_146107038